Compound flood hazard assessment of atoll islands

Based on representative scenarios for typhoons and non-typhoon conditions: A Majuro case study

Tije Bakker

TUDelft

Deltares

Compound flood hazard assessment of atoll islands

Based on representative scenarios for typhoons and non-typhoon conditions: A Majuro case study

by

T. M. Bakker

in partial fulfillment of the requirements for the degree of

Master of Science
in Civil Engineering

at the Delft University of Technology,
to be defended publicly on 16 April 2020, at 12:00 AM.

An electronic version of this thesis is available at http://repository.tudelft.nl/.

TUDelft
Delft
University of
Technology

Deltares
Enabling Delta Life

Cover image: aerial view of the narrow southern rim of Majuro Atoll, Republic of the Marshall Islands, with the airport and the Delap, Uliga and Djarrit (DUD) region in the background. Waves from offshore break at the reef (right side of the island), while the lagoon is more sheltered (left side). Image adapted from Kottermair and Jalandoni (2016).

Summary

Small Island Developing States, including many low-lying atoll islands, are among the most vulnerable countries to natural hazards (UNISDR, 2015, p.24, 42), and climate change disproportionately amplifies this vulnerability (IPCC, 2018; UN-Habitat, 2015). Hence, there is a strong need for disaster risk reduction and risk management. Further development and implementation of methodologies for flood hazard assessment of atoll islands contributes to this. The methodology proposed in this research was applied to Majuro; an atoll island and capital of the Republic of the Marshall Islands. More specifically, the flood hazard related to different flood drivers and including compound events (i.e. the combination of coastal flooding and precipitation) was assessed for the densely populated Delap, Uliga, and Djarrit (DUD) region, in the east of Majuro Atoll.

Main flood drivers at Majuro are waves during typhoon events and distantly generated (swell) waves, but precipitation and high water levels (mainly tide) are important as well. The interdependencies in drivers of coastal flooding and precipitation during *'typhoon events'* are fundamentally different than the interdependencies at other moments, here defined as *'non-typhoon events'*. Hence, a distinction was made between the two types of events; the flood hazard related to both types is assessed separately, but according to a similar approach. The main steps of the approach are summarized below:

1. **Collection and analysis of historical data and events** – Historical typhoon track data (IB-TrACS; Knapp et al., 2010), precipitation measurements from local stations, and reanalysis data for offshore wave conditions (ERA5; C3S, 2017) was collected. Offshore water levels were obtained from the Global Tide and Surge Model (GTSM; Muis et al., 2016).

2. **Generation of synthetic events** – To give a full statistical description of all possible combinations of different flood drivers, and to include the spatial variation in events, 1000 years of synthetic events was generated, based on data for historical events. For the generation of synthetic typhoon events, the TCWiSE tool (Hoek, 2017) was used. For the generation of synthetic non-typhoon events, a combination of extreme value analysis of the precipitation rates, and a Non-Parametric Bayesian Network in the software Uninet (UNINET Help, nd) was used. The BEWARE tool (Pearson et al., 2017) and a threshold value for the precipitation were used to select the events relevant for flooding. The tidal water level was based on the GTSM.

The set of synthetic events was concluded to be a reasonably good expansion of the set of historical events, and contains a wider range of (combinations of) conditions. However, simulation of all synthetic events in a model was not feasible. By use of step 3 to 5 below, the number of model simulations was reduced:

3. **Selection of representative events** – Maximum Dissimilarity Algorithm (MDA) was used to select a computationally feasible subset of representative events from the synthetic events. The dissimilarity of the events is maximized based on a selection of parameters that characterize the events, whereby the extremes can be included as well.

4. **Simulation of inundation depths for the representative events** – Delft3D (Lesser et al., 2004) and SWAN (Booij et al., 1997) models were used to transform offshore conditions to nearshore. An XBeach model (Roelvink et al., 2009) was used to simulate inundation depths at the DUD region for each of the representative events. The model included a module for rainfall (first application in XBeach).

5. **Interpolation to obtain the inundation depths for the synthetic events** – Weighted interpolation, based on the same parameters that characterize the events in step (3), was used to approximate the inundation depths for each of the events in 1000 years of synthetic data.

By steps 3 to 5, inundation depths for events could be approximated in a computationally feasible way, while information about the probability of occurrence of each event can be preserved. When compared to simulation of the full set of synthetic events, a reduction in number of simulated events of a factor ±40 for typhoon events, and ±400 for non-typhoon events was obtained. The main steps of the approach seem applicable to many other study areas where a high number of scenarios is needed to include all (combinations of) drivers. However, the selection of data and tools in each of the steps (1-5) was partially tailored to atoll islands.

Based on the inundation depths for 1000 years of synthetic (typhoon and non-typhoon) events, flood maps for different return periods and flood drivers were derived. These provide insight in the flood hazard for the DUD region due to the different flood drivers for different return periods. The main conclusions are summarized below:

- For low return periods, flooding related to non-typhoon events seems to be more important than typhoon related flooding, especially for the more northern parts of the DUD-region. For higher return periods, flood hazard related to both seems to be more similar, although this again varies significantly per location. Although infrequent, typhoons are the most extreme events in terms of wave conditions and precipitation rates, and lead to the most severe flooding.

- Within the DUD region, the relative importance of coastal flooding and precipitation seems to vary significantly per area. Nevertheless, precipitation was concluded to be an important flood driver and exclusion would lead to underestimation of the flood hazard – especially for low-lying areas in the middle of the DUD region and during typhoons. During non-typhoon conditions, coastal flooding was found to be more important for most areas. Compound flooding during non-typhoon conditions seems to be infrequent.

- Analysis of inundation depths for different return periods suggests that for many areas at the DUD region there is a maximum inundation depth, whereafter excess water drains to the ocean – mainly into the lagoon. This might be explained by looking into the specific bathymetry of narrow atoll islands: piling up of water against higher elevation areas is not possible and a cross section gives a *'bathtub'* like bathymetry. In other words: *'the bathtub can be full'*. This may potentially be used as an advantage when taking measures.

Furthermore, the flood maps could be used as a base for assessment of flood risk, climate change impacts and closely related freshwater availability. Especially in relation to the latter, more in-depth understanding of the contributions of precipitation and coastal flooding to the total flood hazard is needed. While both may cause flooding, on the long term infiltration of precipitation seems favourable whilethat of oceanic water is not.

Acknowledgements

Contents

List of Figures

List of Tables

List of Symbols and Abbreviations

Abbreviation	Description
B.C.	Boundary Condition
BEWARE	Bayesian Estimator for Wave Attack in Reef Environments (tool)
BN	Bayesian Network
β	Parameter in Softmax interpolation method
β_b	Beach slope
β_f	Fore reef slope
C_f	Coefficient of friction
CS	Cross Section
DEM	Digital Elevation Model
Dir	Mean wave direction
DRR	Disaster Risk Reduction
DUD	Delap, Uliga and Djarrit (region on Majuro)
ENSO	El Niño–Southern Oscillation
ERA5	Reanalysis data set for wave conditions
GAM	Gamma (distribution)
GEV	Generalized Extreme Value (distribution)
GDP	Gross Domestic Product
GP	Generalized Pareto (distribution)
GTSM	Global Tide and Surge Model
H_s	Significant wave height
IBTrACS	International Best Track Archive for Climate Stewardship (data set)
L_o	Offshore wave length
LOGN	Log-normal (distribution)
MDA	Maximum Dissimilarity Algorithm
MSL	Mean Sea Level
NPBN	Non-Parametric Bayesian Network
RMI	Republic of the Marshall Islands
RMS	Root Mean Square (error)
RP	Return Period
SIDS	Small Island Developing States
SLR	Sea Level Rise
SWAN	Simulating WAves Nearshore (model)
TC	Tropical Cyclone
TCWiSE	Tropical Cyclone Wind Statistical Estimation (tool)
T_p	Peak wave period
WES	Wind Enhanced Scheme
W.F.	Weight Factor
W_{reef}	Reef flat width
z_{beach}	Beach crest elevation above reef flat

1

Introduction

Chapter summary

- Small Island Developing States, including many low-lying atoll islands, are among the most vulnerable countries to natural hazards (UNISDR, 2015, p.24, 42). Climate change disproportionately amplifies this vulnerability (IPCC, 2018; UN-Habitat, 2015), hence there is a strong need in Disaster Risk Reduction (DRR) and risk management. Further development and implementation of methodologies to improve flood hazard assessment of atoll islands contributes to this.

- In a Majuro Atoll (Republic of the Marshall Islands) case study, flood hazard due to compound events (i.e. coastal flooding and precipitation) with different interdependencies and spatial variation is quantified. To make this computationally feasible, this thesis describes a method to select a limited number of scenarios for typhoons and non-typhoon conditions, that combined give a full statistical description of all conditions that can lead to compound flooding.

1.1. **Motivation and background**

On average, annually over 200 million people are affected by natural hazards, of which more than half by flooding (CRED and UNISDR, 2015). Small Island Developing States (SIDS), a diverse group of 58 distinct states including the Marshall Islands (case study of this research), are widely recognized as among the countries most vulnerable to natural hazards, for example by the Sendai Framework for Disaster Risk Reduction (UNISDR, 2015). Given the specific socioeconomic and environmental challenges of SIDS, climate change disproportionately amplifies this vulnerability (IPCC, 2018; UN-Habitat, 2015).

1.1.1. **Vulnerability of small islands**

Two-thirds of the top 25 countries in the world with the highest relative losses due to natural disasters are SIDS (OECD, World Bank, 2016). Over the past decades, the number of reported natural disasters for SIDS has significantly increased (OECD, World Bank, 2016), see Figure 1.1 below.
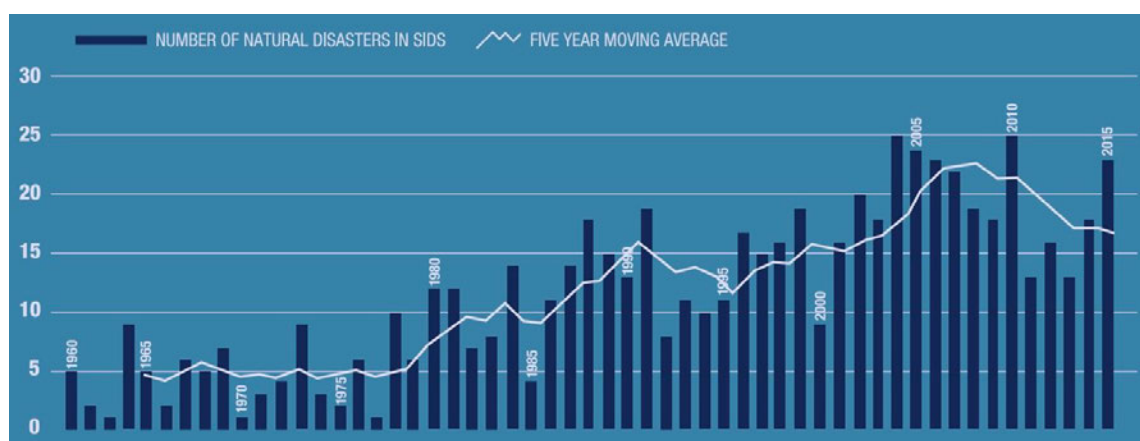
Figure 1.1: Number of major natural disasters in SIDS per year in the 1960-2015 period, Figure adapted from (OECD, World Bank, 2016).

SIDS are often small in land area and population, but with high population density and geographically isolated. This means that domestic markets are small, transportation costs high, natural resources narrow and diversification possibilities in terms of produce and exports limited (CRED and UNISDR, 2015; UN-Habitat, 2015). For a large part this seems to be the case for the Marshall Islands as well. This distinct situation of SIDS is formally recognized in the Sendai Framework for Disaster Risk Reduction, adopted at the Third United Nations World Conference on Disaster Risk Reduction, stating:

> *'Disasters can disproportionately affect Small Island Developing States, owing to their unique and particular vulnerabilities. The effects of disasters, some of which have increased in intensity and have been exacerbated by climate change, impede their progress towards sustainable development. Given the special case of small island developing States, there is a critical need to build resilience and to provide particular support through the implementation of the SIDS Accelerated Modalities of Action (SAMOA) Pathway in the area of disaster risk reduction.' (UNISDR, 2015, p.24, 42).*

This formal recognition comes with world wide attention and has led to numerous programs to cope with the various aspects of Disaster Risk Reduction (DRR). One of the main priorities of the Sendai Framework is *'Understanding disaster risk'* (UNISDR, 2015). As risk can be defined as the combination of hazard, exposure and vulnerability (Kron, 2005), improving the understanding of the hazards contributes to this.

A significant part of SIDS consists of atoll islands. Coral atolls in general have a ring of low-lying, narrow and elongated islands enclosing a lagoon with some openings, and with reef flats on the

ocean side. Atoll islands are mostly in the order of tens of meters to a few kilometers wide, whereby all land is close to the ocean or lagoon. In combination with generally little flood protection, this makes atoll islands especially vulnerable to flooding. The Marshall Islands, formally Republic of the Marshall Islands (RMI) are no exception as 99% of the country has an elevation of less than 5 meters above mean sea level (UN-Habitat, 2015).

1.1.2. An atoll island case study: Majuro

Majuro, subject of this case study and capital of the RMI is home to more than half its population. A general introduction to the RMI and Majuro, and their location in the Pacific Ocean (Figure 1.2) can be found in the Intermezzo below. Majuro Atoll has been frequently used in case studies for other topics, which is closely related to the fact that there is relativity much data available compared to many other atoll islands.

Main focus of this case study is on the Delap, Uliga and Djarrit (DUD) region in the east of Majuro Atoll (See Figure 1.2). This densely populated area is economically important for the RMI (PCRAFI, 2015), and the main government buildings and many public services are located here as well. Besides, the wave climate at the DUD area is particularly interesting, among others due to the predominantly northeasterly waves and sheltering caused by the nearby Arno atoll located ±20 km east of Majuro. Furthermore, the DUD region is exposed to waves from both the north and south.

Intermezzo: The Marshall Islands and Majuro

The Marshall Islands, formally Republic of the Marshall Islands (RMI) consists of roughly 1200 islands spread over 29 atolls, which on their turn are divided over two island chains (Ratak and Ralik). They are located in the Pacific Ocean, roughly 1000 km north of the equator and half way between Australia and Hawaii, with the capital Majuro in the southeast and the Kwajalein Atoll (including Ebeye) approximately in the centre (see Figure 1.2). Stretching almost 2 million km^2, with a total land area of about 180 km^2, the Marshall Islands can be considered as remote and isolated.

Major urban areas at the RMI are the capital Majuro, located on the Majuro Atoll (population of 27,797 (RMI census by SPC, 2012, p.15), and Ebeye (population: 11,408), located on the Kwajalein Atoll. Together these areas house two third of the total population of the RMI (53,158 people) and therefore, they also coincide with the location of main economic activities. Especially the eastern part of the Majuro Atoll, where the Delap, Uliga and Djarrit regions (DUD) are located, is densely populated and economically important (PCRAFI, 2015). Also the main government buildings and many public services are located here.

The other main inhabited area at Majuro Atoll is Laura in the west, and most southern parts are inhabited as well. The lagoon road, between the DUD region and Laura on the southern side of the island is important for accessibility of these areas. Most of the northern islands of the atoll are less densely populated. Laura contains the largest underground freshwater lens of the atoll and therefore is important for freshwater availability. For accessibility, the Marshall Islands International Airport is important, located in the south of Majuro. Large freshwater basins are also located here, where water collected on the airport's runway is stored.

Majuro has a tropical rain forest climate with an average temperature around 27 °C and only small seasonal variations. Annual precipitation rates at Majuro are on average roughly 3200 mm and measurable precipitation events occur on approximately 70% of the days. Northeasterly trade winds are dominant throughout the year with infrequent passing of typhoons. As the nearby Arno Atoll is located roughly 20 km east of Majuro Atoll, especially the western DUD region at Majuro is somewhat sheltered to waves.
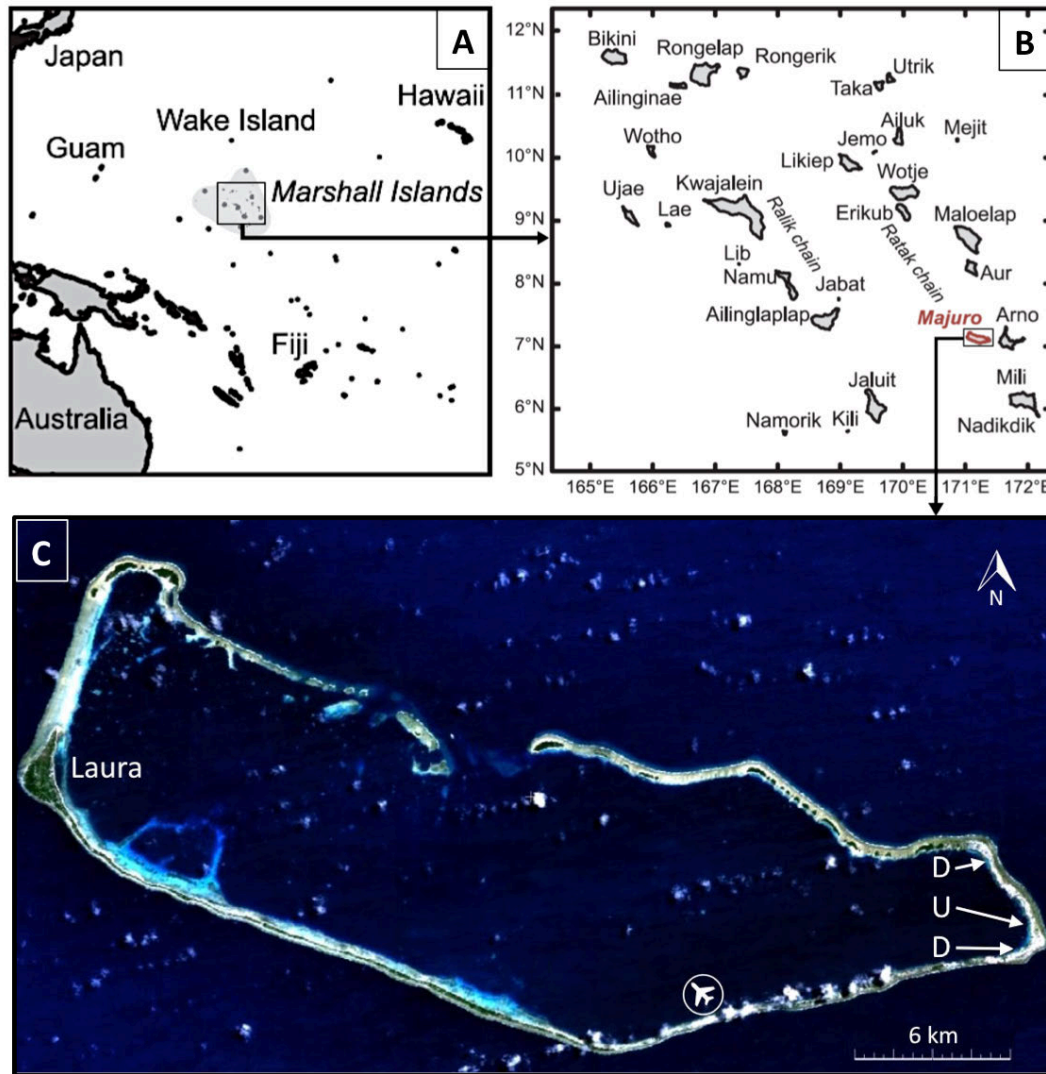
Figure 1.2: *(A) Location of the Marshall Islands in the Pacific Ocean. (B) Location of Majuro Atoll in the Marshall Islands. (C) Overview of Majuro Atoll with in the east the DUD region (Djarrit, Uliga and Delap, from north to south), Laura in the west and Majuro Airport in the south. Parts (A) and (B) adapted from Ford et al. (2013).*

Vulnerability of Majuro

Articles in media, with alarming titles such as *'The Marshall Islands Are Disappearing'* (The New York Times, 2015) and *'Losing paradise: the people displaced by atomic bombs, and now climate change'* (The Guardian, 2015), provide clear examples of the current impacts of climate change on daily life and give insight in the catastrophic consequences that future climate change will have. This is illustrated by Figures 1.3 and 1.4, which show flooding at the ocean and lagoon side of Majuro respectively.

The consequences for people living at the Marshall Islands are urgent. While articles in media give insight in the disruption of human life, various reports provide more insight in the extent of the problems at these Pacific islands. SPC-SOPAC (2012, p.16) gives an overview of the damage at due to natural hazards between 1988 and 2008. In this period, the Marshall Islands faced 18 natural disasters. All were water related, as 9 of these were droughts, 5 tropical storms or typhoons and 4 floods related to waves and high water levels. Excluding droughts, these disasters affected 12,700 people (roughly 20% of the population of the RMI) with an associated reported direct damage of approximately US$ 317 million (roughly 12% of the total GDP at 2008 constant prices).

Although only a minority of the natural disasters reported by (SPC-SOPAC, 2012) were tropical storms or cyclones, these were responsible for the vast majority of population affected (12,000) and more than 99% of reported the economic damage. PCRAFI (2011) gives a lower estimated risk for the Marshall Islands due to tropical storms and typhoons of roughly US$ 3 million annually, of which US$ 650,000 for Majuro Atoll alone. OECD, World Bank (2016) estimates the average annual loss from disasters as percentage of the GDP to be 2.13%, which would be roughly US$ 4.1 million annually based on the 2016 GDP. Furthermore, as disasters such as typhoons are transient events, such long term average damage numbers hide momentary extreme damages. Although the above mentioned numbers seem to be rough estimates, they show that natural hazards – especially typhoons – can have significant impact.

Figure 1.3: *Flooding from the ocean side in Uliga, Majuro: 'King tides and storm surges combined to inundate low-lying areas in the Marshall Islands [...] tossing rocks and debris into roads, backyards and homes.' (The Marshall Islands Journal, 2016b).*

Figure 1.4: *Flooding from the lagoon side in Rita, Majuro: 'Waves pushed by storm winds [...] flooded parts of Majuro, damaging seawalls and structures located close to the lagoon shore.' The Marshall Islands Journal (2016a).*

Drivers of flooding at Majuro

The above mentioned reports based on historical events suggest that typhoons are the most important driver of flooding at the Marshall Islands. However, storms do not have make landfall at Majuro to cause flooding. Swell waves generated by distant storms are also a major flood driver for Pacific islands (Hoeke et al., 2013), especially in combination with high tide. For example, in June 2013, Majuro Airport runway was flooded due to swell related surge during high tide, leading to closure of the airport (PCRAFI, 2015; WSO Majuro, 2013).

Ford et al. (2018) provides further insight in the flood drivers at Majuro; 18 historical inundation events (in a 36 year period) were classified based on physical drivers. Main flood drivers at the ocean side were identified to be oceanic swell waves and storms or typhoons. For the sheltered lagoon side, these were elevated water levels during La Niña phase of El Niño–Southern Oscillation (ENSO), distantly generated swell waves that infiltrate into the lagoon, and wind waves generated in the lagoon. Approximately half of the events were related to local storms or typhoons passing through the area (Smith and Juria, 2019). In some cases, complete overwash of Majuro was reported (Ford et al., 2018).

In a coastal hazard risk assessment by Giardino et al. (2017, 2018) for the nearby atoll island Ebeye, swell waves were found to be the most important source of hazard for the low return periods of the events, while typhoon events are the most important for higher return periods. Flooding due to wind waves (also from the lagoon side) was concluded to be non-negligible. In addition, Giardino et al. (2017, p.130) reported flooding due to precipitation on Ebeye during normal (non-typhoon) conditions. Extreme value analysis of precipitation data for Ebeye and Majuro shows that precipitation rates at Majuro are comparable or even higher than those at Ebeye (see Appendix A.3.2).

Little damage due to precipitation related and swell wave induced floods was reported so far, but frequent flooding with limited depth may on the long term cause damage to roads, houses and other infrastructure, as well as economic and social disruption (SPC-SOPAC, 2012). The difference in reported damage (i.e. typhoons versus swell waves) is most likely explained by under reporting of damage due to smaller flood events, as these occur more frequent and their associated damage per event is much lower. Besides, small flood depths are not necessarily experienced as problematic

by local inhabitants, who have learned to cope with minor flooding events (Giardino et al., 2018).

1.1.3. Impacts of climate change

Effects of climate change such as Sea Level Rise (SLR), more extreme precipitation events and potentially stronger typhoons will let increase risks for SIDS like the Marshall Islands disproportionately (IPCC, 2018). While the Marshall Islands' contribution to climate change in terms of emissions per capita is estimated to be less than half of the world's average (World Bank and CDIAC, 2019), sea level rise rates at the Marshall Islands are above the global average (Slangen et al., 2014).

For most atoll islands, projected SLR rates are higher than measured vertical accretion levels of reef flats (Storlazzi et al., 2018), which will lead to higher water depths on the reef flat and consequently allows for larger waves to reach the shoreline. Although less certain, it is expected that globally on average tropical cyclones will be stronger in terms of wind speed and minimum pressure (IPCC, 2018). This would lead to an additional increase in wave height and water levels. Besides, extreme precipitation events, both during typhoons and non-typhoon conditions are globally expected to increase, although this may vary per location (IPCC, 2018). This may lead to more frequent flooding and higher flood depths.

More regular coastal inundation of the island will also affect underground freshwater lenses due to saltwater intrusion, especially as the specific topography of atoll islands allows for overwash. This may potentially lead to freshwater scarcity and damage the environment, when groundwater becomes toxic to the vegetation present. In addition, higher waves may lead to land loss, as erosion rates will rise under higher wave impact. It is for these reasons that according to Storlazzi et al. (2018), most atoll islands will be uninhabitable by the mid-21st century, see Figure 1.5.
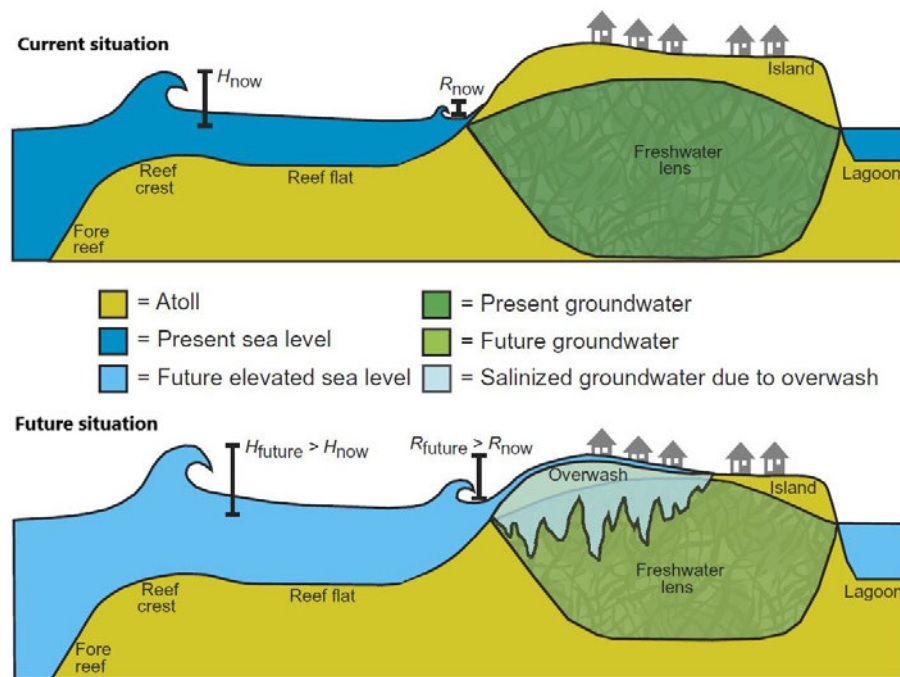
Figure 1.5: Schematic overview of the influence of sea level rise on wave heights, wave-driven runup, and flooding and the resulting impact on underground freshwater lenses, adapted from (Storlazzi et al., 2018).

When the low elevation of atoll islands such as Majuro is taken into consideration, it seems obvious that sea level rise will let risks increase significantly. In an atoll island case study for Ebeye, Giardino et al. (2018) predicted that the future risk (flood and erosion combined) will be increased with a factor 3 or 4 in the year 2100, and that the number of yearly affected people may double. In addition to direct damage caused by such events, indirect consequences, such as further limitation of the possibilities to grow crops due to land loss and salinization (CRED and UNISDR, 2015, p.15)

and a decrease in yield of fishing due to warming oceans (UN-OHRLLS, 2015, p.14) may further limit the possibilities for inhabitants of atoll islands. In general, the economic cost of adaptation to climate change is high in SIDS relative to the size of their economies (UN-OHRLLS, 2015).

Overall, it may be hard to see a bright future in prospects for atoll islands. Besides improving resilience of atoll islands, relocation of inhabitants to less vulnerable areas or even abandonment could become unavoidable in some cases (Storlazzi et al., 2018; UN-OHRLLS, 2015). However, according to McLean and Kench (2015), persistence of many western and central Pacific atoll islands over the next century is likely, and focus should be shifted to persistence of atoll islands and in-country solutions. External migration has raised concerns about the loss of sovereignty (UN-Habitat, 2015) and culture. Especially small islands feature a high degree of resilience through resources from dense social networks, which gives opportunities for climate change adaptation under a social capital approach (Petzold and Ratter, 2015). In summary, improving resilience locally seems very much preferable.

1.2. Problem description and scope

In this section, the knowledge gaps addressed in this thesis are introduced. From the previous section it can be concluded that SIDS, and especially atoll islands such as Majuro are very vulnerable to natural hazards; especially flooding which was responsible for the majority of reported losses. Hence, quantification of flood hazard related for Majuro and more specifically the DUD region is needed. Key in such assessment is to include all relevant (combinations of) flood drivers accurately and in a computationally efficient way.

1.2.1. Flood hazard for the DUD region at Majuro

Some flood hazard, flood risk and damage estimates have been assessed for Majuro (e.g. OECD, World Bank (2016); PCRAFI (2011); SPC-SOPAC (2012), see Section 1.1.2). However, all studies were made on large scale and seem to neglect important drivers of flooding, most notably swell waves, precipitation and combinations of flood drivers. Hence, the flood hazard in Majuro is unknown and therefore, there is a need for a more detailed hazard study including all relevant drivers.

Typhoons are infrequent, but have the largest impact in terms of damage per event, and thus are very important in a flood hazard assessment. Oceanic swell waves can be a major driver of flooding for Pacific islands, especially in combination with high local water levels (Hoeke et al., 2013). Although swell waves are in general lower than waves locally generated by typhoons, swell waves can be more frequent as waves generated in a much larger area can reach the atoll (i.e. the entire Pacific basin). High tidal water levels can contribute to flooding as well. Besides coastal flooding, precipitation can lead to flooding solely, or in combination with coastal flooding lead to compound flooding.

The interdependencies between drivers of precipitation related flooding and coastal flooding are different during typhoons compared to non-typhoon condition. This problem is further elaborated in Section 1.2.2. Another complicating factor is the spatial variation in events. For example, the impact of typhoon passing at the northern or southern side of Majuro can be very different. Hence, key in flood assessment of the DUD region is to capture all relevant (combinations of) flood drivers in a computationally feasible set of scenarios; this problem is further elaborated in Section (1.2.3).

Although certainly relevant, flooding from the lagoon side seems in general less severe than flooding from the ocean side, and falls outside the scope of this thesis. Other events related to coastal flood hazard, such as distant earthquake induced tsunamis, are associated with a much smaller risk (Australian Government Bureau of Meteorology, 2010; Giardino et al., 2018). This is mainly based on the fact that they are infrequent, and in recent history had little impact on the Marshall Islands. For example, the Tohoku tsunami in 2011 did no remarkable damage and had an estimated height lower than 1 m at Majuro, although it could have been higher when it had occurred during high tide (Ford et al., 2014; Giardino et al., 2018). According to PCRAFI (2011), the combined risk due to earthquakes and tsunamis is a factor 30 lower compared to typhoon related risk for the Marshall Islands. Therefore, tsunamis are left out of the analysis.

1.2.2. Compound flooding on atoll islands

To make an accurate compound flood hazard assessment of the DUD region possible, more insight in the interdependencies of different flood drivers relevant for atoll islands is needed. In many existing case studies that assessed compound flood hazard, major rivers and waterways play an important role, and often the topography can vary more in range than on atoll islands. This allows for inland flooding, and flood extents are mainly limited by piling up against areas of higher elevation. Examples are Clear Creek watershed, USA (Torres Dueñas, 2018), Fuzhou City, China, (Lian et al., 2013) and Ravenna, Italy (Bevacqua et al., 2017). This differs for atoll islands such as Majuro, where low-lying and narrow islands allow for overwash and no significant rivers are present. Hence, the specific characteristics of atoll islands require a tailored approach.

Torres Dueñas (2018) showed that for low-lying coastal watersheds, inclusion of compound flooding during typhoon events leads to better results in a flood risk assessment; otherwise the flood depths are underestimated, which leads to an underestimation of the risk. By treating coastal flooding and flooding due to precipitation as separate scenarios, possibly the worst-case scenarios is left out of the analysis. Nevertheless, compound flooding is often not accounted for in flood hazard and risk assessments.

In this case study, compound flooding is limited to the combination of coastal flooding (i.e. flooding by oceanic water) and precipitation related flooding, where coastal flooding can occur due to multiple flood drivers occurring simultaneously (i.e. waves, high tide, storm surge). Compound flooding can be due to drivers that are independent (e.g. high tide coinciding with heavy precipitation), or can be triggered by a common phenomenon (e.g. heavy precipitation and wave impact during a typhoon event). The different flood drivers that combined lead to compound flooding do not necessarily have to be extreme events themselves (IPCC, 2018).

During typhoons, coastal flooding and precipitation related flooding are thus clearly related to the same event. On the other hand, during non-typhoon conditions, coastal flooding and precipitation related flooding can be considered independent, although these events can occur simultaneously as well. To further complicate things, water levels are composed of surge and tidal water levels, where the latter can be considered independent of the other flood drivers. Hence, development and implementation of a methodology to include compound events, tailored to the relevant flood drivers and particular characteristics of atoll islands is needed. Proper representation of the different dependencies between relevant flood drivers is crucial in such method.

1.2.3. Scenario derivation

Accurate flood hazard assessment of Majuro including compound flooding requires that all relevant combinations of flood drivers are properly included in a set of scenarios. To make quantification of the flood hazard possible, the probability of occurrence of each of these scenarios has to be known. An important consequence of the inclusion of compound flooding is that the number of scenarios increases dramatically as different flood drivers can occur simultaneously and interact.

The number of scenarios increases even further when the spatial variation in events is taken into account. For example, no typhoon is the same: characteristics such as wind speeds, precipitation rates and track of the typhoon eye are unique for each event, whereby the consequences of each event can be very different (e.g. the consequences of a typhoon passing at the northern or southern side of an island). Similarly, during non-typhoon conditions the wave conditions at a northern-oriented shoreline can be very different than those at a nearby southern-oriented shoreline.

Often data for historical events is used to include some variation. For example, in Giardino et al. (2018) historical typhoon tracks were used to assess typhoon related flooding at Ebeye. Typhoon track data is collected already for several decades in the Northwestern Pacific (Knapp et al., 2010), but typhoons are not very frequent in the area of Majuro. Hence, currently available data does not include enough historical inundation events for such analysis of Majuro, and many more decades of data would be needed (Smith and Juria, 2019).

Recently, methods have been developed to deal with this problem of data scarcity. Based on historical data, synthetic data covering a much longer period and containing many more events can be created. An example of such tool specifically for typhoons is the Tropical Cyclone Wind Statistical Estimation (TCWiSE) tool (Hoek, 2017), developed at Deltares and among others applied by Richards (2019) in a flood risk assessment. By using a larger data set a more complete overview of the flood hazard can be obtained. However, the modelling of all synthetic typhoon events can become computationally too expensive, as up to thousands of scenarios have to be simulated in models in sufficient detail. In some cases, the used model can be simplified, for example by excluding waves (e.g. Richards (2019); Torres Dueñas (2018)), but for atoll islands waves are actually very relevant and exclusion would lead to unrealistic results.

For non-typhoon conditions, a similar problem occurs. The different flood drivers (i.e. (swell) waves, precipitation, tide) can be considered independent, but this also means that simultaneous occurrence of extreme conditions for the different flood drivers is infrequent (e.g. simultaneous occurrence of high swell waves and an extreme precipitation event). Hence, available historical data is for an insufficiently long period to include all such combinations of flood drivers. Similarly as for typhoons, this can be overcome by generation of a large synthetic data set. As many different combinations can occur, this again leads to a large number of scenarios.

Hence, an important challenge is to make accurate modelling of a set of scenarios computationally feasible. For many atoll islands, further reduction of the computational time per scenario by using a simplified model would lead to oversimplification of the physics of flooding. In this case study, a reduction of the computational time is proposed by reducing the number of scenarios needed to represent all relevant conditions.

1.3. Objectives and research questions

Majuro's high and increasing exposure and vulnerability to flooding in combination with its importance for the Marshall Islands justifies a thorough flood hazard assessment. Hence quantification of the flood hazard including all relevant drivers is strongly needed. As many atoll islands face similar problems, review, improvement and implementation of a methodology that includes all relevant flooding processes and that remains computationally feasible for this type of islands is needed. This leads to the following **objectives**:

A. *Assessment of flood hazard for the DUD region at Majuro Atoll.*

B. *Inclusion of compound events (i.e. coastal flooding and precipitation) in a methodology for flood hazard assessment of atoll islands.*

C. *Selection of a computationally feasible set of scenarios that combined give a full statistical description of all conditions that can lead to compound flooding.*

To include compound events in a methodology for flood hazard assessment of atoll islands (B), a method has to be developed and implemented to make the number of scenarios computationally feasible (C). This will be done based on a case study: a flood hazard assessment of Majuro Atoll (A). To be able to satisfy all objectives, first the following **research questions** are elaborated:

1. *How can the different interdependencies of flood drivers relevant for compound flooding on atoll islands be accounted for in a flood hazard assessment?*

2. *How can the variation in typhoon events be described by a computationally feasible set of scenarios that combined give a full statistical description?*

3. *How can compound flooding due to combinations of multiple flood drivers during non-typhoon conditions be described by a computationally feasible set of scenarios that combined give a full statistical description?*

4. *What are the key drivers of flooding for the DUD region at Majuro Atoll and what is their relative importance for different return periods?*

Insight in the interdependencies of the different flood drivers is needed to derive realistic scenarios, especially given the fundamental difference in the relation between coastal flooding and precipitation during typhoon conditions, compared to non-typhoon conditions. Hence, a computationally feasible number of scenarios should be derived in which these different interdependencies are well represented. Complicating factors here are the spatial variation in events and the limited length of historical records. The inundation depths for each of the scenarios can be simulated by use of numerical models, after which the inundation depths for different return periods can be determined. The outline of the approach to answer these questions is further elaborated in the next Section.

1.4. Methodology

This section provides a short overview of the main elements of the followed approach. Chapter 3 provides a more detailed description of the approach and the used data and numerical models. Although both are closely connected, two main parts can be distinguished in this flood hazard assessment:

1. Derivation of **forcing scenarios** that combined give a full statistical description of all conditions that can lead to compound flooding.

2. Quantification of the **flood hazard** by modelling and combining the inundation depths for the derived scenarios.

Figure 1.6 provides a schematic overview of the approach for the flood hazard assessment, including the main tools and models used in each part. Both parts will be elaborated below.
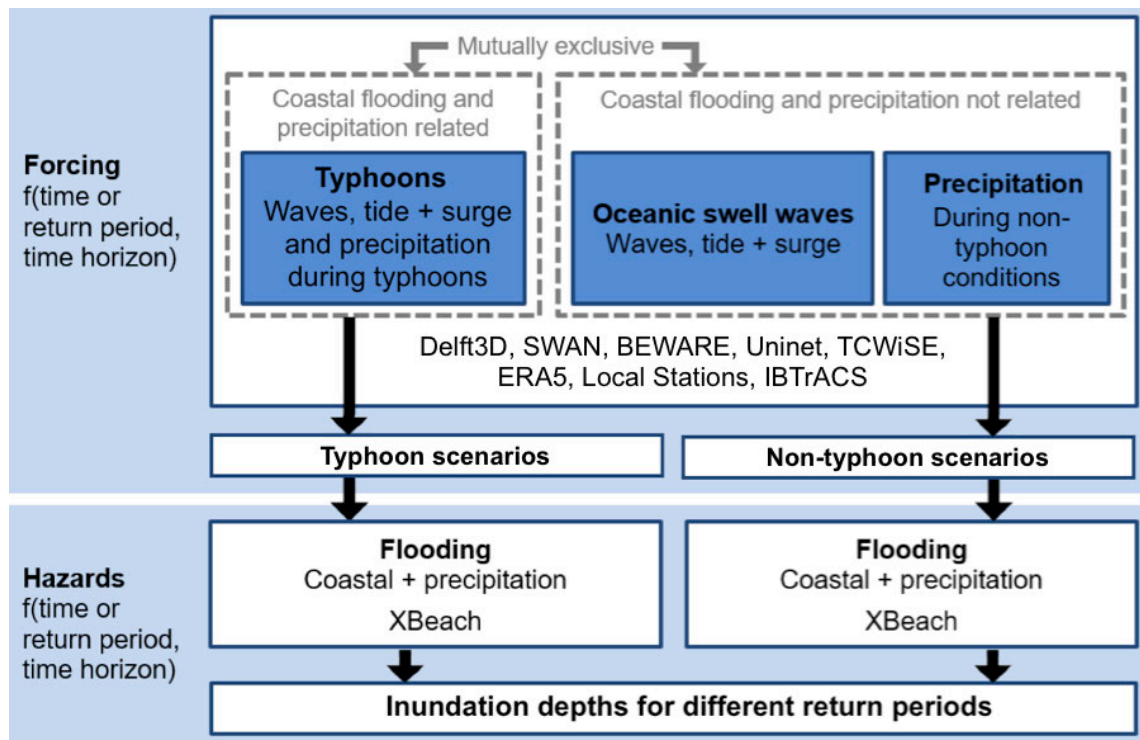
Figure 1.6: Schematic overview of the main elements in the approach for the flood hazard assessment.

1.4.1. Flood drivers

In Section 1.2.1 the main flood drivers for Majuro were identified. Based on flood water source, different types of flooding can be distinguished:

- Coastal flooding – flooding by oceanic water, driven by waves, tides, and (storm) surge;

- Precipitation related flooding – flooding by freshwater (pluvial flooding);

- Compound flooding – the combination of the above.

In contradiction to the tide, wave conditions, surge and precipitation are driven by the weather (e.g. wind, air pressure). Surge at Majuro is mainly related to the local air pressure (see Section 2.2.3), while oceanic swell waves are generated by storms at large distance (Section 2.2.2), hence they are in general not related. On the other hand, during a typhoon both surge and wave conditions are related to the same phenomenon. Similarly, coastal flooding and precipitation during typhoons are much stronger related compared to precipitation and coastal flooding during non-typhoon conditions, such as a swell wave event.

To accurately model these different relations between surge, wave conditions and precipitation, a distinction is made between forcing during typhoon and non-typhoon conditions. Typhoon and non-typhoon conditions are treated as mutually exclusive (in time), this is further elaborated in Section 3.1. By making this distinction in time upfront, the consequential flood hazard can be determined independently for typhoon and non-typhoon conditions, whereafter the results can be recombined. For both types of conditions, a number of scenarios is derived that combined gives a full statistical description of all relevant typhoon and non-typhoon conditions respectively.

1.4.2. Flood hazard quantification

Flood hazard is generally quantified in terms of inundation depth for a certain return period. Several studies describe how multiple hazards or compound flooding can be included in flood hazard or risk assessment. Some background on flood hazard assessments is provided in Section 2.3. By making the distinction between typhoon and non-typhoon conditions, it is possible to assess flood hazard related to these independently. Nevertheless, for both types a similar approach is followed in order to quantify the flood hazard. A flowchart of the main steps, including all tools together with their input and output can be found in Appendix A.1; the main steps are summarized below:

1. Analysis of **historical events**. Different types of data were collected and analyzed: Historical typhoon track data from the International Best Track Archive for Climate Stewardship (IBTrACS; Knapp et al., 2010), precipitation measurements from local stations and ERA5 reanalysis data for offshore wave conditions (C3S, 2017). Offshore water levels were obtained from the Global Tide and Surge Model (GTSM; Muis et al., 2016), see Section 3.2 for a detailed description of the data. For non-typhoon conditions, ERA5 reanalysis data for wave conditions was first transformed from offshore to nearshore by use of a SWAN model (see Section 3.3.2).

2. Generation of a data set of **synthetic events** for a longer period (i.e. 1000 years), based on historical data. By generation of a much larger synthetic data set, the different possibilities and combinations of the relevant parameters are better included. For the typhoons, the Tropical Cyclone Wind Statistical Estimation (TCWiSE; Hoek (2017), see Section 2.2.1) tool was used, see Section 3.4.1. For the non-typhoon conditions, extreme value analysis in combination with a Bayesian Network in the software Uninet (UNINET Help, nd) was used (Section 3.5.3). All events irrelevant for flooding at Majuro were discarded. All typhoons that did not pas through a specified area around Majuro were discarded. For non-typhoon conditions, this was done by use of the Bayesian Estimator for Wave Attack in Reef Environments (BEWARE; Pearson et al., 2017) tool, and a threshold value for precipitation.

3. Selection of **representative events** from the synthetic data by use of Maximum Dissimilarity Algorithm (MDA, explained in Section 2.4.4. The selection was based on relevant parameters of the data set of synthetic events and should represent all possible conditions – including extreme events – as accurate as possible. The representative events are a subset of the synthetic events. The selection of representative events is done separately for the typhoons (see Section 3.4.2) and non-typhoon conditions (Section 3.5.4).

4. Simulation of **inundation depths for representative events** by use of an XBeach model, capable of modelling precipitation. In order to properly include the variation in wave conditions around the DUD region, the wave conditions during each event were specified for different locations around the DUD region. The XBeach model is described in Section 3.3.3.

5. Weighted interpolation is used to obtain the **inundation depths for synthetic events**, based on the representative events. Here, Softmax interpolation is used (described in 2.4.5), with the same parameters and weight factors as in step (3). Hence, interpolation is done separately for the typhoons and non-typhoon events. This is further elaborated in Section 3.4.3 for the typhoons, and Section 3.5.4 for the non-typhoon conditions.

6. Derivation of **flood maps for different flood drivers and return periods**. Based on the inundation depths for 1000 years of synthetic typhoons and synthetic non-typhoon events, inundation depths can be obtained for different return periods. This is done by use of extreme value analysis of the inundation depths. As the drivers of each synthetic event are known, flood maps for different flood drivers can be constructed as well. Additionally, the flood maps for typhoons and non-typhoon conditions can be combined into flood maps for the total flood hazard.

Furthermore, validation of various parts of the approach was done. Most importantly, the used numerical models were tested by use of the historical typhoon Paka (1997), see Section 3.3.4. For the typhoons part, step (3-5) of above were checked and optimized, among others by a second case study (see Section 3.4.3).

1.5. Readers guide

The contents of each chapter are described below:

- *Literature* – Chapter 2. Relevant characteristics of atoll islands and the different types of flood drivers are discussed. Subsequently an overview of methodology for flood hazard assessments is given, and some statistical methods relevant for synthetic data generation and scenario derivation are elaborated.

- *Methodology* – Chapter 3. First the important distinction between typhoon and non-typhoon conditions is made. Subsequently the used data and numerical models are described, where-after the approach to derive the scenarios for typhoon and non-typhoon conditions is elaborated.

- *Results - Scenarios* – Chapter 4. The results of applied methodology for scenario derivation and resulting scenarios are presented. First the scenarios for typhoons and subsequently those for non-typhoon conditions.

- *Results - Flood hazard* – Chapter 5. Based on the modelled scenarios, the resulting flood hazard was quantified. Flood maps are presented for different return periods and flood drivers, related to typhoons and non-typhoon conditions. Subsequently the combined flood maps are presented, again for different return periods.

- *Discussion* – Chapter 6. Here the main results from Chapters 4 (Scenarios) and 5 (Flood hazard) are discussed, together with their limitations and suggestions for improvement and further research.

- *Conclusion and recommendations* – Chapter 7. Here the final conclusions are summarized by answering the research questions from Section 1.3. In addition, the main limitations and some recommendations to overcome these are presented.

Appendix A contains a flowchart of the methodology, and additional information about the processing of the used data. Appendix B elaborates the setup and validation of the numerical models in more detail. Some aspects of the scenario derivation are discussed in more detail in Appendix C, and some additional flood maps for other return periods are presented in Appendix D.

2

Literature

Chapter summary

- This chapter provides an overview of literature relevant for this thesis and some background on the key concepts. First a short overview of some relevant characteristics of atoll islands, coral reefs and freshwater on atoll islands is given, with a focus on*f* Majuro (Section 2.1).

- Main flood drivers were identified to be typhoons and oceanic swell waves, and precipitation and high water levels are important as well. Relevant characteristics of each are discussed, as well as some methods to model these drivers (Section 2.2).

- Methods for compound flood hazard assessment are discussed in Section 2.3. First the key concepts of hazard and closely related risk are elaborated, whereafter methods to combine different hazards and flood drivers are described. Subsequently, the main uncertainties in flood hazard assessment are discussed.

- Section 2.4 gives an introduction to some statistical methods relevant for scenario derivation. Key concepts and terminology of Extreme Value Analysis (EVA), copulas, Bayesian Networks (BNs), Maximum Dissimilarity Algorithm (MDA) and Softmax interpolation are discussed consecutively.

2.1. **Characteristics of atoll islands**

Atoll islands are the islands located on coral atolls and have some distinct characteristics. This section provides a brief general introduction about their formation, some characteristics relevant for flooding, and the closely related risks of land loss and freshwater scarcity. Based on the theory by Darwin (1842), three types of islands with coral reefs can be distinguished: barrier, fringing and atoll reefs, all being the consecutive states of sinking extinct volcanoes in the tropics, see Figure 2.1 below.
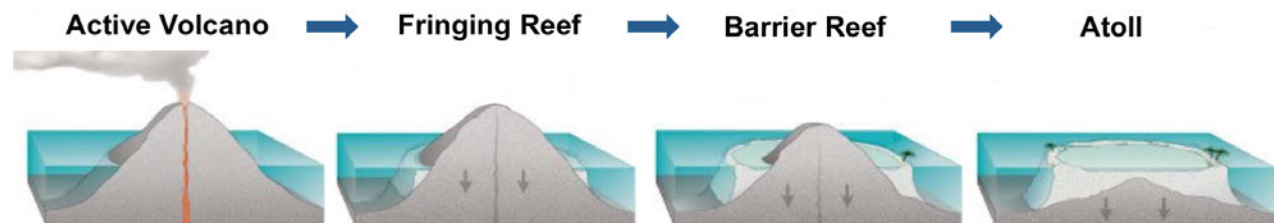
Figure 2.1: Formation of coral atolls according to the theory by Darwin (1842).

As a consequence of this formation process, coral atolls consist of a ring of coral reefs that enclose a relatively shallow lagoon. The low elevation of atoll islands is closely related to this formation process. As corals reefs consist of living coral, they can adapt to (slow) changes in water level (e.g. sea level rise) or compensate for decrease in bottom level, but their rate of growth is limited to a few millimeters per year (Montaggioni, 2005).

Different zones can be identified based on typical atoll geomorphology (Kendall et al., 2012), see Figure 2.2. In general the elevation of atoll islands is highest at the ocean side, lowest in the middle of the island, and again somewhat higher at the bay side. This specific topography of atoll islands has consequences for how flooding occurs; a cross section over the island gives the shape of a *'bathtub'* (see also Figures 3.2 and 3.15), the ocean is always within a few hundred meters distance and significant rivers are absent. Due to their geographical outline, coastlines of atoll islands are relatively long.
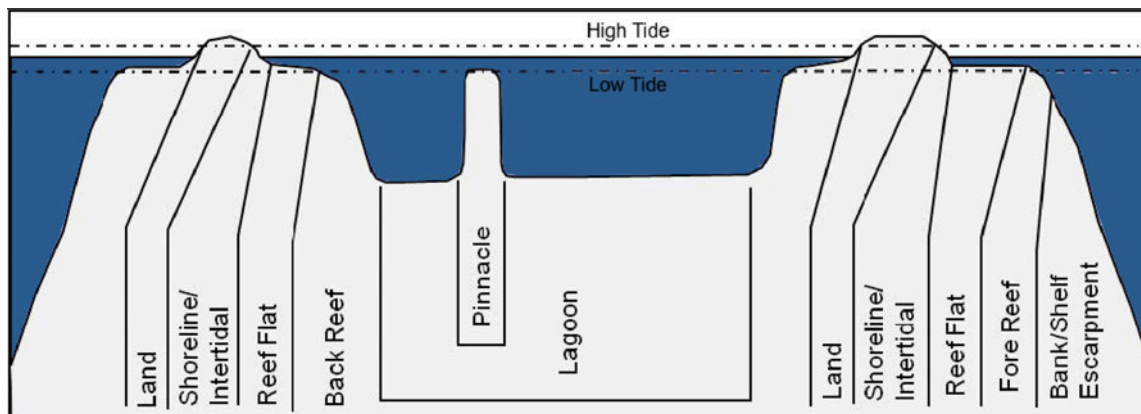
Figure 2.2: Cross section of an atoll with terminology for different zones. Figure adapted from (Kendall et al., 2012).

The reef at the ocean side is often exposed to high wave energy, whereas the coast on the lagoon side is more sheltered. Coral reefs play an important role in flood defence of atoll islands by wave energy dissipation. Both the processes of depth induced wave breaking – mainly on the fore reef – and dissipation due to bottom friction over the reef flat are important (Pearson, 2016). See Figure 2.3 below for an idealized reef profile with key parameters relevant for wave energy dissipation. In reality this is often an oversimplification as the bathymetry may vary significantly per location (Roelvink, 2019; Scott, 2019).
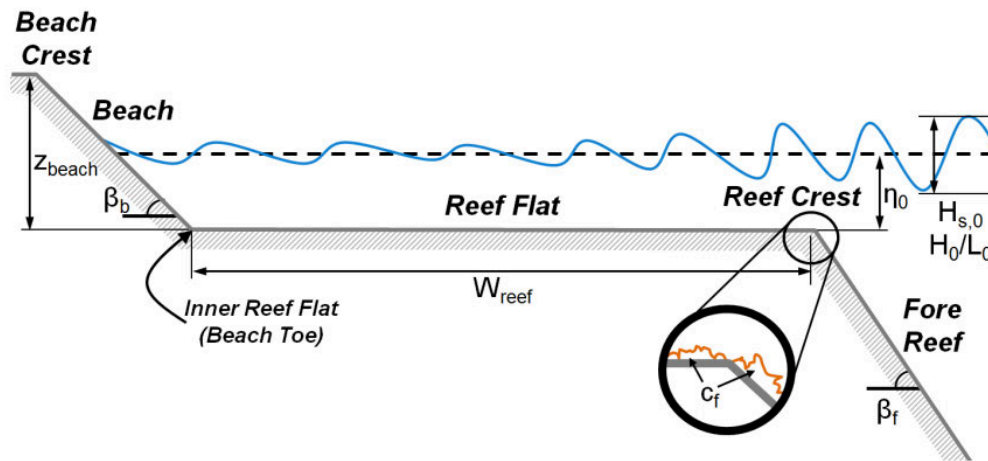
Figure 2.3: *Idealized reef profile with some characteristics relevant for wave dissipation (Pearson, 2016).*

Various studies have been done in relation to morphological changes for Majuro, for example in relation to sea level rise (Ford et al., 2013; Ford and Kench, 2015) and shoreline changes (Sato and Yokoki, 2011; Xue, 2001; Yamano et al., 2006). In addition, human interferences such as dredging or land reclamation affect the morphology. Most notable examples for Majuro are land reclamations for the causeway and around the Airport, and various excavation pits in the reef flat used for sand and aggregate mining.

Majuro case studies have shown that excavation pits in reef flats – depending on their characteristics – can have significant influence on the offshore wave energy that reaches the shoreline (Ford et al., 2013; Klaver, 2018). Construction materials needed for flood protections (i.e. rocks) are in general scarce on atoll islands and supply from other locations is expensive, due to the often remote location of atoll islands. For a large part this seems to be true for Majuro as well, and the existing flood defences are limited to frequently overtopped sea walls.

Freshwater resources and drought
Freshwater availability and drought are major issues on many atoll islands and closely related to coastal flooding and precipitation. Freshwater scarcity is a significant problem on the Marshall Islands. For example, in March 2016, a state of disaster was declared due to severe drought on Majuro (SPC, 2017). Climate change will further emphasize the relations between flooding and freshwater availability. Although the direct consequences of inundation by low water depths may currently be limited in terms of damage, sea level rise and wave-induced degradation of freshwater resources may make atoll islands uninhabitable before flooding does (Storlazzi et al., 2018).

In general, freshwater is only available in underground freshwater lenses and storage facilities, as open water bodies (e.g. rivers and lakes) are mostly absent. Ground water resources of atolls are minimal due to the small surface area and low elevation of the islands Bailey et al. (2010). These lenses are supplied by precipitation from above, and float on deeper saltwater layers, as freshwater has a slightly lower density. Hence, flooding of an area with freshwater lens by oceanic water leads to salinization of the water. This can make water unsuitable for domestic or agricultural use, and can also damage the ecosystem. However, the availability of freshwater is dependent on many factors. Among others, frequency, inundation depth and duration of floods, recharge by precipitation, soil characteristics such as infiltration capacity, extraction rates (via wells), island width and orientation relative to the dominant wind direction play a role (Anthony et al., 1989; Bailey et al., 2009; Barkey and Bailey, 2017; Werner et al., 2017).

At Majuro, capacity of collection and storage facilities is limited and in poor condition (SPC-SOPAC, 2012). A major freshwater storage facility is located at the airport. Here, precipitation is collected at the runway and stored in several basins, from where it is distributed. Besides, many small private storage facilities are used to collect rainwater locally (SPC, 2012). At Majuro, the largest freshwater

lens is located at Laura in the west. This part of the island is relatively wide and on the leeward side of the dominant wind direction, where waves are generally lower and freshwater lenses larger (Bailey et al., 2010). Other smaller freshwater lenses are found mainly at the DUD region, but can be found all over the atoll.

2.2. Flood drivers

In Section 1.2 the main flood hazard forcing events were identified to be typhoons and oceanic swell waves, and precipitation and high water levels are important as well. This section provides a brief description of relevant characteristics and terminology.

2.2.1. Typhoons and tropical storms

Tropical cyclone (TC) is the general term for a strong, cyclonic-scale disturbance that originates over tropical oceans (IPCC, 2018). Tropical cyclones occurring at the Northwestern Pacific Ocean are called typhoons. TCs generally develop in the tropics, but at some distance from the equator. TCs not only threat Majuro or the Marshall islands; the location of SIDS largely coincides with the density of occurrence of tropical cyclones (OECD, World Bank, 2016), see Figure 2.4. As atoll islands are located in the tropics, this especially applies to atoll islands.
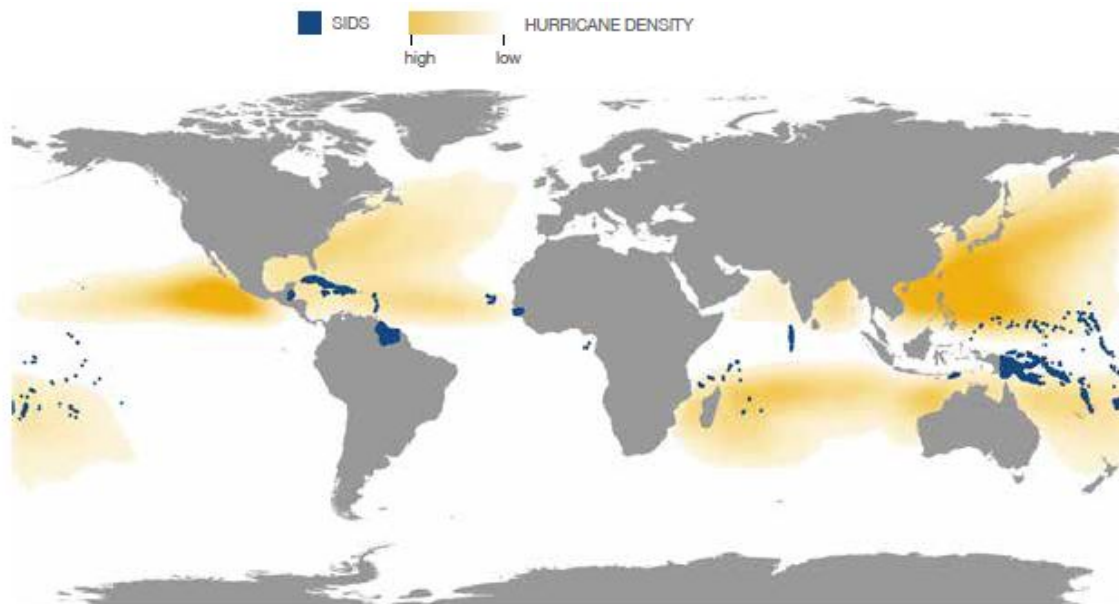
Figure 2.4: Density of tropical cyclones and the location of SIDS (OECD, World Bank, 2016).

While the Northwestern Pacific is the basin with on average the most tropical cyclones per year, the Marshall Islands are in the area where tropical storms and typhoons mainly arise and gain strength. As such are mostly not yet fully developed, but occasionally a stronger typhoon hits the Majuro. For example, Spennemann (1996) mentions a *'devastating typhoon in 1918'*, and more recently, the 1997 typhoon Paka caused US$ 80 million of damage at the Marshall Islands (PCRAFI, 2011, 2015).

Typhoon tracks have been collected world wide for several decades and combined into the International Best Track Archive for Climate Stewardship (IBTrACS; Knapp et al., 2010). The location of the TC eye and the maximum wind speed are available with a time stamp in most cases. In general, a distinction is made between tropical depressions, tropical storms, and tropical cyclones, based on the one-minute averaged surface wind speed. Further distinction can be made by use of the Saffir-Simpson scale, differentiating TCs into five categories based on maximum wind speed. Although this system is probably best known, various other systems are used in different regions. See Table 2.1 below for the Saffir-Simpson scale.

Table 2.1: Overview of the classification of tropical depressions, tropical storms and tropical cyclones (TCs) with associated wind speeds based on the Saffir-Simpson scale (NOAA, 2019).

Storm class	Wind speed m/s	(km/h)	Consequences
Tropical depression	<17	(<62)	-
Tropical storm	18-32	(63-118)	-
TC category 1	33-42	(119-153)	Very dangerous winds will produce some damage
TC category 2	43-49	(154-177)	Extremely dangerous winds will cause extensive damage
TC category 3	50-58	(178-208)	Devastating damage will occur
TC category 4	58-70	(298-251)	Catastrophic damage will occur
TC category 5	>70	(>252)	Catastrophic damage will occur

While the maximum wind speed is the main parameter used for classification of TCs, their impact depends on other characteristics as well. Among others, the distance at which various wind speeds extend outward from the storm center, rainfall patterns, minimum air pressure at sea level, and storm translation speed (forward velocity of the eye), are important for characterizing the impact (Knapp et al., 2010). During typhoons, precipitation rates, surge and wave conditions are strongly related. Generally speaking, typhoons with higher wind speeds also come with a higher air pressure drop and higher precipitation rates, and vice versa.

TC related winds generate waves (see Section 2.2.2) and can lead to wind induced setup, although the latter is very limited in case of Majuro (see Section 2.2.3). Direct damage due to wind falls out of the scope of this thesis. The drop in air pressure can locally lead to higher water levels (surge), but this is limited to the order of a few decimeters (see Section 2.2.3). Within a TC, wind speeds are maximum near the eye wall, while the air pressure drop is maximum in the eye (see Figure 2.5). Precipitation rates vary substantially per typhoon (Bader, 2019), but on average the highest rates can be expected near the eye wall.

The fetch experienced by waves – and thereby the height of the generated waves – is dependent on the wind field within a TC, and the translation speed and direction of the eye. Waves propagating in the same direction as the TC experience a longer fetch than those propagating in the opposite direction (Young, 2003). TCs in the northern hemisphere always rotate counter clockwise, and are infrequent below latitudes of roughly 5°. Generally speaking, TCs move in roughly northwestern direction at lower latitudes. As Majuro is located relatively close to the equator (around 7.1° latitude), this may have important consequences for the waves experienced at Majuro. A schematic overview of a TC is provided in Figure 2.5 below.

Modelling of TCs
Although the spatial variation in air pressure, wind, and precipitation is important, spatial data is often not available. This can be overcome by use of a parametric model for the wind and air pressure fields in TCs, for example the Wind Enhanced Scheme (WES) developed at Deltares (Deltares, 2019). In WES, wind and pressure fields can be generated per time step of track data, based on basic parameters such as maximum wind speed. The model is based on the parametric wind and pressure model by Holland (1980); Holland et al. (2010). Additionally, the relations developed by Nederhoff et al. (2019) can be used to compute TC geometry in more detail. These relations are calibrated specifically for the Northwestern Pacific basin. Examples of applications can be found in Giardino et al. (2018) and Richards (2019).

Precipitation is in general not recorded for historical TC tracks, but sometimes data from local measurement stations is available. Similar as for the wind and pressure fields, various relations exist to estimate the precipitation rates, for example by Jiang et al. (2006); Konrad and Baker Perry (2010); Snaiki and Wu (2018). Recently, Bader (2019) included stochastic rainfall distributions in a probabilistic model approach for compound flooding due to tropical cyclones. This allows for inclusion of the variation in maximum rainfall intensity by random sampling.

Swell radiating out from
intense wind region to the
right of the storm centre

Calm eye of
storm with
minimum air
pressure

Storm
propagation
direction

Eye wall with
maximum
windspeeds

Anti-clockwise
wind direction

Waves generated in this region
propagate in the opposite direction
to the storm and have a short fetch

Waves generated in this region
propagate forward with the storm
and experience an extended fetch

Surface air pressure

Surface wind speed

Figure 2.5: Schematic overview of a translating TC in the northern hemisphere with generated waves. Figure adapted from Young (2003).

Synthetic TC tracks

When historical data for TC is not sufficient, synthetic TC tracks can be constructed based on historical data. Various methods exist to generate such tracks, for example Tropical Cyclone Wind Statistical Estimation Tool (TCWiSE; Hoek, 2017), as used in this thesis. The above mentioned relations for wind and pressure fields by Nederhoff et al. (2019) and precipitation fields by Bader (2019) are implemented in TCWiSE. A schematic overview of the procedure followed to generate a set of TC tracks can be found in Figure 2.6 below. The tool can be used to generate synthetic cyclones from their genesis to termination points with 6-hourly intervals. The maximum sustained wind speed is used to represent the intensity of the event (Hoek, 2017). TCWiSE has been applied for various TC basins, for example for the Northern Atlantic basin by Richards (2019).

An alternative can be found in Sebastian et al. (2017), who developed a method to generate 100 000 synthetic storm events in a case study for the Gulf of Mexico by use of a Bayesian network based on Gaussian copulas. An application can be found in Torres Dueñas (2018), who used these events to determine the local hydraulic boundary conditions for Clear Creek watershed in a compound flood risk assessment.
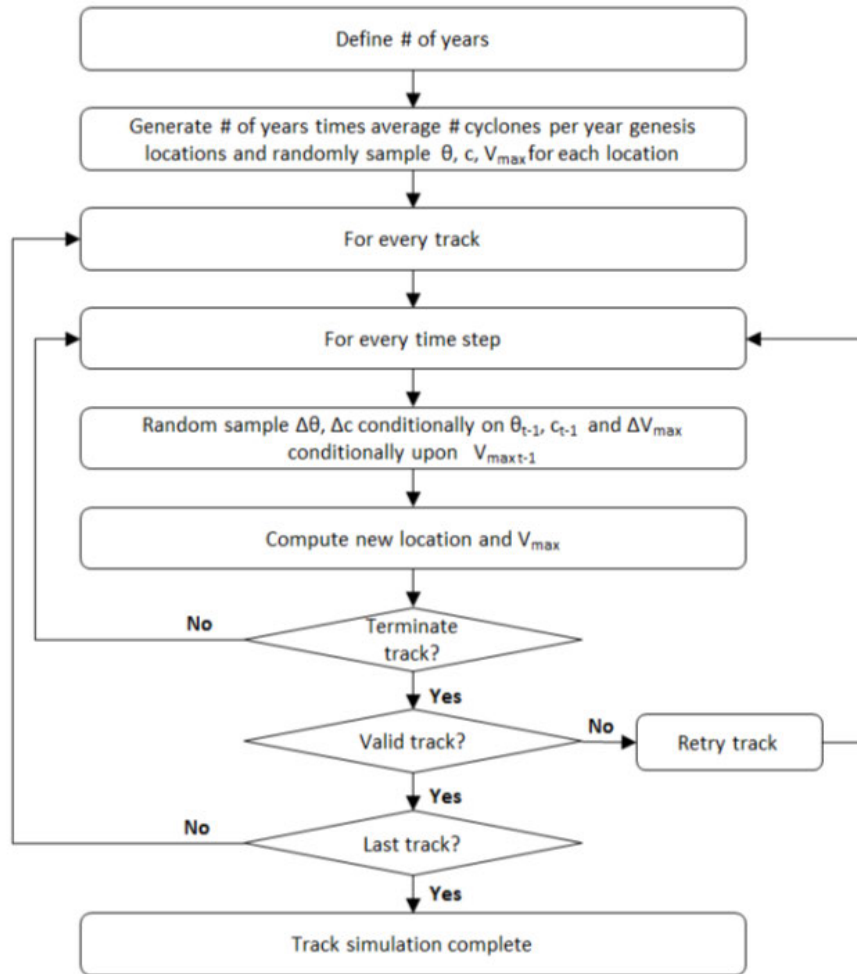
Figure 2.6: *Schematic overview of the synthetic track generation process in TCWiSE (Hoek, 2017).*

2.2.2. Waves

While direct typhoon impact may lead to the highest waves and most extreme impact, waves originating from other sources may actually be more important for inundation at the Marshall Islands for the low return periods Giardino et al. (2018). In this section, some key concepts relevant for understanding flooding due to offshore wave forcing are elaborated.

Both locally generated (wind sea) and swell waves are generated by wind, but a distinction can be made based on wave period (Holthuijsen, 2010), see Figure 2.7. Swell waves arriving at Majuro are generated by winds at large distance. Due to frequency and direction dispersion, only part of the distantly generated waves will arrive at Majuro. The wave energy is shifted towards higher wave periods and the peak is narrower (i.e. the waves are longer and more regular). As a consequence of their generation at large distance, the appearance of swell waves is independent of the local weather and can come with little warning to local residents (Pearson, 2016). Compared to swell waves, locally generated wind sea waves are less regular and have a larger spread in wave period.

Ford et al. (2018) identified distantly generated swell waves as an important driver of historical inundation events at Majuro. In particular, swell waves originating from extratropical regions in the north and south of the Pacific have been drivers of historical inundation events. As Majuro is somewhat sheltered behind Arno Atoll in the east, it can be expected that (swell) wave impact is less from this side. Alves (2006) identified the contributions of several regions to the swell wave climate, among others for the extratropical regions in the pacific. Figure 2.8 provides an overview of the annual mean significant wave height of swell waves originating from these areas.
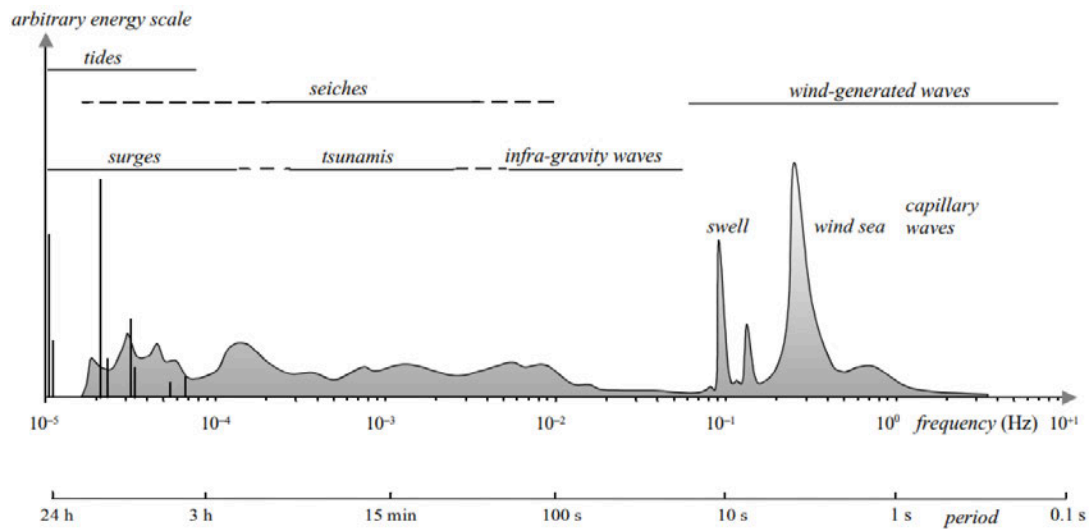
Figure 2.7: Wave energy and period for different types of waves. Figure adapted from Holthuijsen (2010).

The wave climate at Majuro is thus composed of waves from different sources, such as swell generated in different regions and locally generated (wind sea) waves, which may lead to complex wave spectra. Hence, for many Pacific locations, the wave spectrum is inadequately represented by a single set of basic wave parameters such as the significant wave height (H_s), Peak wave period T_p, Mean wave direction (Dir) and directional spread (Hegermiller et al., 2017). In addition, the wave climate may vary significantly per location due to different orientations of the shoreline and with possible sheltering.
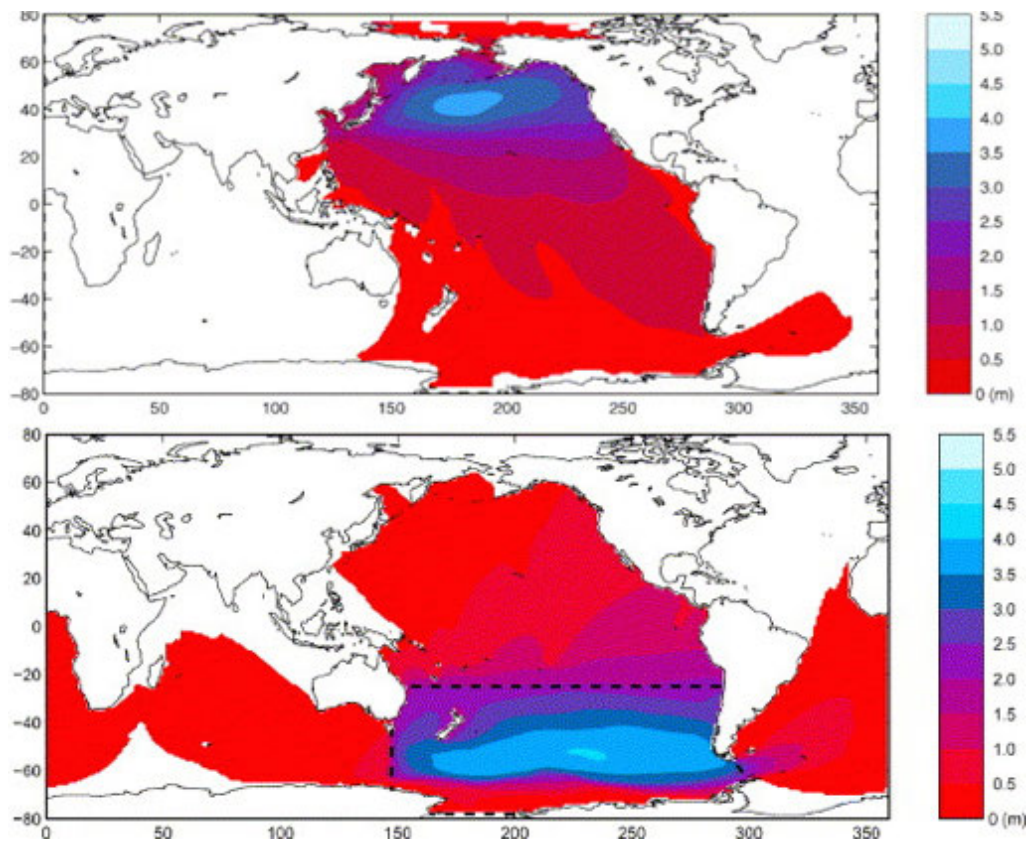
Figure 2.8: Annual mean significant wave height of swell waves from the northern hemisphere (upper part) and southern hemisphere (lower part) extratropical areas. Figure adapted from Alves (2006).

For locally generated offshore (wind sea) waves, the distribution of wave energy over the wave periods can be approximated by a parametric JONSWAP spectrum (Holthuijsen, 2010), based on basic wave parameters. Although this is not necessarily the case for waves during typhoon conditions, distantly generated swell waves, or combinations of different types of waves, the JONSWAP spectrum is also frequently used as an approximation during such types of wave conditions (e.g. Pearson, 2016).

2.2.3. Water levels

Water levels offshore at Majuro are mainly composed of tide and surge. In contradiction to locations with extensive (shallow) continental shelf area, wind induced setup is often less relevant for atoll islands surrounded by the deep ocean such as Majuro. Hence, offshore surge levels can be expected to be inversely proportional to the air pressure drop and thereby the increase in water level is limited to the order of approximately 20 cm.

Historical tidal water levels can be obtained from measurements, but as the tide is composed of tidal constituents with known period (e.g. M_2 and S_2 related to the moon and sun respectively), predictions of the tide can be done as well. On a global scale, such predictions have been done by Muis et al. (2016), who developed the Global Tide and Surge Model (GTSM). Comparison of observed and predicted water levels for locations in the Northwestern Pacific in general showed good results Muis et al. (2016). The GTSM also includes historical surge levels based on hydrodynamic modelling of (reanalysis) wind and air pressure data. However, the extremes – especially during TCs – are underestimated (Muis et al., 2016).

So called *'king tides'* (exceptionally high tides) are often mentioned as a main driver of flooding of atoll islands, especially in relation to swell wave events (Ford et al., 2018; Pearson, 2016). Waves approaching the island from offshore break on the reef and subsequent wave heights on the reef flat are limited, but this wave breaking leads to wave induced setup on the reef flat. Hence, the water level at the shoreline can be seen as the combination of the tide, surge and wave conditions after transformation to wave induced setup, but due to interactions (e.g. the location of depth induced wave breaking depends on the water level, which is composed of tide and surge) these can not be seen as independent contributions to the nearshore water level.

2.3. Compound flood hazard assessment

In this section, first some key concepts related to flood hazard and risk are described. Subsequently, combining multiple hazards, flood drivers and compound events into a hazard assessment is elaborated, and the different types of uncertainties associated with flood hazard assessments are briefly discussed.

2.3.1. Hazard and risk

Risk is in general defined as a combination of hazard and its potential consequences. The conceptual frame work for flood risk assessments by Kron (2005) can be followed, in which the potential consequences can be seen as the combination of exposure and vulnerability:

> *Risk = Hazard x Exposure x Vulnerability*

With:

> *Hazard* – Contains information about the probability and intensity of a possible event (de Moel et al., 2015). It represents the physical phenomenon related to climate change (e.g. sea level rise, storm surges) that has the potential to cause damage and loss to property, infrastructure, livelihoods, service provision and environmental resources (Gallina et al., 2015).

> *Exposure* – Represents the presence of people, livelihoods, environmental services and resources, infrastructure, or economic, social or cultural assets in places that could be adversely affected (Gallina et al., 2015).

Vulnerability – Represents the propensity or predisposition of a community, system, or asset to be adversely affected by a certain hazard. (Gallina et al., 2015).

Flood hazard is often expressed in terms of flood depth with a probability of occurrence. Hence, in order to give a meaningful description of the flood hazard, the probability of occurrence of the forcing event is crucial. Expressing the flood hazard only in terms of flood depth has its limitations. For example, the salinity of the flood water and the time a property is flooded can be even more important factors when assessing the damage to crops.

In flood risk assessments, exposure is generally quantified by land use maps, containing information about what is present at a geographical location (e.g. monetary value or number of people present). Vulnerability in flood risk is mostly described by depth-damage relations (de Moel et al., 2015), for example providing a relation between the water depth and the damage in terms of a percentage of the total monetary value. Hence, flood hazard assessments mainly provide insight into the flood extents and inundation depths, while flood risk assessments can provide additional insight in the human consequences of flooding.

2.3.2. Compound flood and multi-hazard assessments

This section elaborates some key concepts and frameworks in relation to combining different flood drivers. According to IPCC (2018), *compound events* can be defined as:

1. Two or more extreme events occurring simultaneously or successively.

2. Combinations of extreme events with underlying conditions that amplify the impact of the events.

3. Combinations of events that are not themselves extremes, but lead to an extreme event or impact when combined.

Applied to flood events, this means a compound flood event can be due to drivers that are related to the same event (e.g. heavy precipitation and high waves during a typhoon event), or be independent (e.g. high tide and heavy precipitation). The drivers that combined lead to compound flooding do not necessarily have to be extreme themselves (e.g. high but not extreme waves in combination with high tide and precipitation). In this study, the term *'compound flooding'* is only used for the combination of coastal flooding and precipitation related flooding, where coastal flooding can be due to waves and high water levels. These can be caused by multiple flood drivers, and can occur simultaneously (e.g. distantly generated swell waves and locally generated wind waves).

Multi-hazard refers to the totality of relevant hazardous events threatening the same exposed elements or hazardous events occurring at the same time or shortly following each other in a defined administrative area (Gallina et al., 2015). Key steps in a *multi-hazard assessment* are defining what the different hazardous events are and the schematization of the interdependencies and (combined) probabilities of occurrence in a set of scenarios (Marzocchi et al., 2012). To understand the relations between different hazards in compound events that lead to extreme impacts, a framework such as by Leonard et al. (2014) can be used.

In multi-hazard assessments, often the different hazards are treated as independent (Gallina et al., 2015; Leonard et al., 2014; Moftakhari et al., 2017), but hereby the worst case scenario is left out and flood depths could be underestimated. On the other hand, sometimes a worst case scenario is used. This gives a more conservative estimate of the flood depths, but information on the probability of occurrence is lacking. Hence, a set of scenarios should cover all possible combinations of intensities of the hazards (Marzocchi et al., 2012), with known probability of occurrence.

2.3.3. Uncertainties in flood hazard assessment

To identify which elements in a flood hazard assessment are most crucial, the main uncertainties in such assessment are briefly elaborated in this section. Different types of uncertainties can be distinguished (de Moel et al., 2015):

- *Aleatory uncertainty* – results from variability of the process under study. It refers to quantities that are inherently variable in time, space, or populations of individuals or objects (Merz and Thieken, 2009). For example, the randomness of events.

- *Epistemic uncertainty* – results from incomplete knowledge and is related to our inability to understand, measure and describe the system under investigation (Merz and Thieken, 2009).

- *Ontological uncertainty* – Refers to factors missing in the analysis (i.e. incompleteness) (de Moel et al., 2015).

An example of aleatory uncertainty is that it is unknown whether a storm with a return period of 100 years will hit Majuro in 20 or 100 years, although it is statistically described and on average will hit once every 100 years. It is not possible to make a better estimate of when exactly such storm will hit by improving knowledge, only the estimation of the return period can be improved. Section 2.4 elaborates some methods that will be used to decrease the aleatory uncertainty.

Epistemic uncertainties can among others be related to inaccuracies in data or the used model. Vousdoukas et al. (2018) identified the main sources of epistemic uncertainty due to the upscaling of coastal flood risk assessments in a case study for Faro, Portugal. The most important hazard related uncertainties were found in the inclusion and interaction of different hydraulic components leading to extreme sea level, the Digital Elevation Model (DEM) and flood defence information. In particular the way waves are included was of importance for the extreme sea level. In a small islands case study for São Tomé and Príncipe, Parodi (2019) concluded that for the current time horizon, the most important flood hazard related uncertainty was in the DEM data, followed by the significant wave height.

Although the studies mentioned above are for different situations than the one considered in this thesis (i.e. different data sources, models, etc.), it demonstrates that the uncertainty is largely dependent on the available data. For Majuro, relatively good DEM data is available, which means it can be expected that the uncertainty related to this is somewhat lower in this study. Wave conditions and wave transformation require more attention. The approach of this study is focused on both the reduction of aleatory and epistemic uncertainty. By including a larger number and wider range of events, reduction of aleatory uncertainty is obtained. By subsequent scenario selection, computationally more expensive models can be used, whereby epistemic uncertainty can be reduced as well. Hence, the number of scenarios selected and the complexity of the models used should match.

2.4. Scenario derivation and associated statistics

This Section briefly elaborates some methods used in this thesis for the derivation of scenarios. First, parametric distributions used to describe (extreme values of) variables are introduced. The dependence structure of multiple variables can be described by copulas; only the (bivariate) joint normal copula will be used in this thesis, hence the focus is on this type. This is further extended to Bayesian Networks, which can be used to describe the dependence structure of more variables. Finally, the selection of representative scenarios by Maximum Dissimilarity Algorithm and the used Softmax function for non-linear interpolation are elaborated.

2.4.1. Extreme value analysis

In general only limited historical data is available, and more extreme events may not be well present in such data (i.e. large aleatory uncertainty, see Section 2.3.3). To make inclusion of more extreme events possible – also those that have not yet happened in history, parametric distributions in an extreme value analysis can be used.

According to the definition by (IPCC, 2012) *'Extreme events comprise a facet of climate variability under stable or changing climate conditions. They are defined as the occurrence of a value of a weather or climate variable above (or below) a threshold value near the upper (or lower) ends ("tails") of the range of observed values of the variable.'* Different approaches exist to select extreme events, most

widely used are those of taking the maximum value of a variable per unit time (e.g. yearly maxima), and peak over threshold approach (i.e. all events above a certain threshold value).

Subsequently the probabilities of occurrence have to be determined, whereafter the distributions can be fitted to the data and subsequently used to describe the probability of occurrence of less frequent events. Numerous types of extreme value distributions exist, well known examples are the Generalized Extreme Value (GEV) and Generalized Pareto (GP) distributions. For the GEV the Langbein correction (Takeuchi, 1984) can be applied to values for lower return periods, whereby those values can be approximated more realistically, similarly to the peak over threshold approach.

2.4.2. Multivariate dependence modelling with copulas

In compound flooding the probabilities of occurrence of combinations of multiple variables are relevant (e.g. precipitation and offshore water level), while extreme value distributions can only be used to approximate extreme events for one variable. To model the dependence structure of multiple variables, copulas can be used. In this thesis only bivariate copulas are used; these can be used to represent the joint distribution of two variables.

According to the theorem by Sklar (1959) the bivariate joint cumulative distribution function H(x,y) of any pair (X,Y) of continuous random variables can be written as:

$$H(x,y) = C(F(x), G(y)) \tag{2.1}$$

Where F(x) and G(y) are the univariate marginal distributions and C:$[0,1]^2 \rightarrow [0,1]$ represents the copula. Hence, any bivariate distribution H can be expressed in terms of a suitable copula C, and a pair of suitable margins F(x) and G(y) (Genest and Favre, 2007). Although numerous different types of copulas exist, only the joint normal (Gaussian) copula is used in this thesis.

Further introduction to the use of copulas in multivariate modelling in hydrology and climate research can be found in Genest and Favre (2007) and Schölzel and Friederichs (2008) respectively. Practical guidelines for multivariate analysis and design in coastal and offshore engineering can be found in Salvadori et al. (2014).

2.4.3. Bayesian Networks

A Bayesian Network (BN) is a probabilistic graphical model that represents a set of random variables and their conditional interdependencies (Sperotto et al., 2017). A BN consists of a directed acyclic graph and a set of conditional distributions. Each variable in the graph is represented by a node while the direct dependence relationships are represented by arcs (Hanea et al., 2015). Nodes without predecessors are called parent nodes; a predecessor is named a child.

A specific type of BN is the Non-Parametric Bayesian Network (NPBN). A distinguishing feature of the NPBN is that continuous distributions can be used, which makes them more suitable to cope with extreme value distributions for example. In NPBNs, the joint distribution is specified via the marginal distributions (nodes) and the multivariate dependence structure (arcs) in terms of a nonparametric measure of dependence (Hanea et al., 2015).

In this thesis, the software package Uninet (UNINET Help, nd) is used to set up a BN (see Section 3.5.3). Here, the nodes can be specified as either discrete or continues functions. The arcs are parameterized by Spearman's rank correlation coefficient and represented by joint normal copulas (UNINET Help, nd) that only require this parameter. An example of an application of a NPBN with joint normal copulas in modelling compound flood hazard can be found in Couasnon et al. (2018).

2.4.4. Representative scenario selection by MDA

One way of making assessment of a large set of scenarios computationally feasible is cluster analysis, whereafter each cluster can be represented by only one scenario. Numerous different methods for clustering exist; analysis of some clustering and selection methods in relation to the study of multivariate wave climate can be found in Camus et al. (2011). One of the methods analysed in

that study is Maximum Dissimilarity Algorithm (MDA); the method used in this thesis.

Based on parameters that characterize a set of events, MDA can be used to select a representative subset, guaranteeing that all possible states in the original set are represented and thus also the most extreme events (Camus et al., 2011). Examples of applications of MDA in a coastal setting can be found in Antolínez et al. (2018) and Anderson et al. (2019), who selected a number of representative forcing conditions from a set of joint oceanic and atmospheric conditions. An example of a cluster analysis application in a different context is the clustering of airplane trajectories around an airport (e.g. Gariel et al., 2011), which seems in some perspective similar to clustering of typhoon tracks.

In MDA, the first point in the parameter space has to be defined upfront, whereafter the algorithm consecutively selects the events with the largest combined distance to the previously selected events combined (i.e by Pythagoras theorem). The used distances between events are calculated in normalized parameter space. The principle of MDA is illustrated in figure 2.9 below. Examples of 1 parameter (1D) and 2 parameter (2D) cases are shown, but larger numbers of parameters can be used just as well, although visualisation becomes complicated.

Alternatively, one could for example select representative scenarios by discretizing all parameters and select all combinations as representative scenarios. An example of this can be found in the compound flood risk assessment by Torres Dueñas (2018), where a grid was applied to the 2 parameter space (storm surge and river run off). Subsequently, the values for both parameters of the centre of each grid cell were selected as representative events, whereby 400 scenarios were selected.

Hence, for larger numbers of parameters this number of scenarios increases dramatically and will become computationally unfeasible. While in the case study by Torres Dueñas (2018) two parameters could be used to characterize the compound flooding, this is hardly possible for atoll islands. Coastal flooding cannot be well-represented by only one parameter such as storm surge, as both waves and tide play an important role. Wave conditions in particular can vary significantly around the island. In addition, computationally expensive models have to be used to simulate wave induced flooding, which further limits the number of representative scenarios that can be simulated.
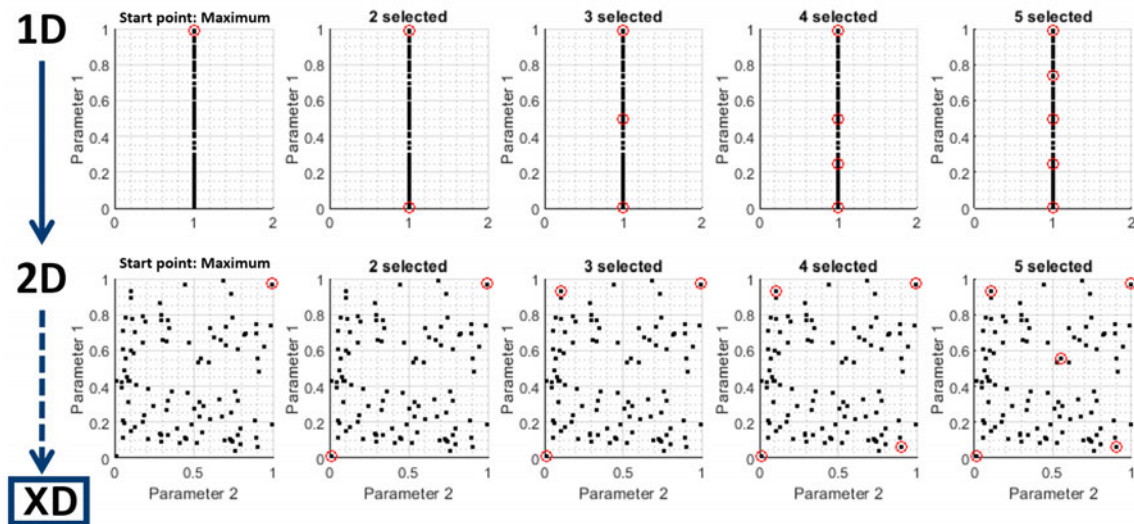
Figure 2.9: Principle of the maximum dissimilarity algorithm. The upper part shows a 1 parameter (1D) case where consecutively 5 representative points are selected (from left to right). In the lower part, the same is done but now for a 2 parameter (2D) case. Similarly, the method could be applied to more parameter (XD) cases.

2.4.5. **Non-linear interpolation with Softmax**

While MDA can be used to select representative scenarios, it does not provide any information on the frequency of occurrence of each scenario. Hence, this information can be obtained by translating the information about the representative scenarios back to all scenarios. To approximate the information in all scenarios, interpolation can be used. One interpolation method that could be used for this is the Softmax function, which maps a vector of inputs to a probability distribution (Goodfellow et al., 2016; Scott, 2019).

When applied to the scenarios, the distances in parameter space between the different scenarios – calculated during MDA to select the representative scenarios – can be used as input vector in the Softmax function to obtain the probabilities. Softmax returns a probability ranging between 0 and 1 for each of the representative scenarios, and the sum of the probabilities for all representative scenarios is 1. Hence, these probabilities can be used as Weight Factors (W.F.) to approximate the variable of interest (e.g. a water level) of a scenario, based on the representative scenarios. See the schematic overview in Figure 2.10. The following Softmax function is used (Scott, 2019):

$$S(x)_i = \frac{exp(-\beta * d_i)}{\sum_{j=1}^{n} exp(-\beta * x_j)} \tag{2.2}$$

Where S(x) is the probability of matching (or W.F.) of representative scenario i, d_i is the distance between the approximated scenario and representative scenario i, x_j is the distance between the representative scenario and approximated scenario j, B is the stiffness parameter, and n is the number of representative scenarios (Scott, 2019).
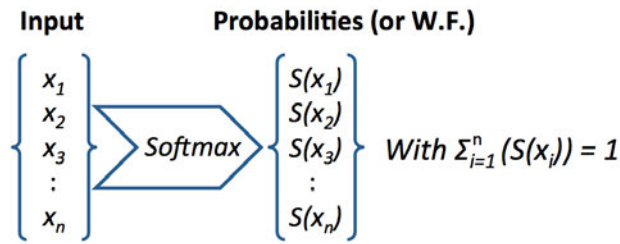
Figure 2.10: Schematic overview of interpolation with Softmax. Figure adapted from (Scott, 2019).

Alternatively, other interpolation methods could be used such as linear interpolation or more advanced radial basis functions. Linear interpolation is expected to lead to worse results though, as the distances in the parameter space can not be weighted. On the other hand, radial basis function seems more promising. These have been applied successfully to interpolate to a larger data set, for example by Rueda et al. (2019). Hence, other methods may potentially lead to better results, but implementation was unfeasible within the scope of this thesis. Application of Softmax interpolation and the influence of the β parameter are further explained in Section 3.4.3.

3

Methodology

<div style="border:1px solid black; padding:10px;">

Chapter summary

- To be able to quantify the flood hazard for Majuro, inundation depths were determined for a number of scenarios that combined give a full statistical description of all conditions that can lead to flooding. Main flood drivers are typhoons and distantly generated (swell) waves, but precipitation and high water levels are important as well. To be able to account for the fundamentally different relation between coastal flooding and precipitation during typhoon events compared to non-typhoon conditions, both conditions were treated as mutually exclusive in time (Section 3.1). By distinguishing typhoon and non-typhoon conditions, the flood hazard related to both can be determined independently, whereafter they can be combined to obtain the flood maps for combined flood hazard.

- Various data types were collected and analyzed. An overview of the used data is provided in Section 3.2, and includes historical data for bathymetry, precipitation, wave conditions, water levels and typhoon tracks. The used Delft3D, SWAN and Beach models are described in Section 3.3.

- The scenario selection for typhoon conditions is elaborated in Section 3.4. To account for the spatial variation in typhoon events and make assessment of flood hazard for larger return periods possible, 1000 years of synthetic typhoons was generated by use of the TCWiSE tool. These tracks include wind, air pressure and precipitation fields. To make numerical modelling of corresponding water levels and wave feasible, 50 representative tracks (scenarios) are selected by use of maximum dissimilarity. Subsequently, the inundation depths for each of the representative scenarios were simulated with Delft3D and XBeach, whereafter interpolation with Softmax was used to get the inundation depths for the full synthetic data set.

- The scenario selection for non-typhoon conditions is elaborated in Section 3.5. First historical data was first transformed to nearshore conditions with the SWAN model. Subsequently synthetic data was generated based on historical data by use of extreme value analysis and Uninet. Only those events that could potentially lead to flooding were selected by use of BE-WARE and a threshold for the cumulative precipitation per day. Just as for the typhoon conditions, maximum dissimilarity is used again to select 50 scenarios whereafter the inundation depths for each of representative scenarios were simulated in XBeach. Interpolation with Softmax was used to get the inundation depths for the full synthetic data set.

</div>

3.1. Distinguishing typhoon and non-typhoon conditions

In this section, first the important distinction between typhoon and non-typhoon conditions is made. A more in-depth description of the used data, modelling approach, and the actual selection of the scenarios for both typhoon and non-typhoon conditions is provided in the remainder of this chapter.

Two situations can be distinguished based on the different relation between coastal flooding and precipitation:

- *Typhoon conditions* – precipitation and coastal flooding are caused by the same driver and strongly related. Infrequent but large consequences.

- *Non-typhoon conditions* – precipitation and coastal flooding are caused by different drivers and not or weakly related. More frequent but limited consequences.

Hence this distinction allows for a different approach of typhoon and non-typhoon conditions. This is not only useful to include compound flooding in a correct way, but also makes inclusion of the spatial variation in typhoon events (i.e. typhoon tracks) possible, which will be further elaborated in Section 3.4.

To be able to model both in a statistically correct way, a distinctions between typhoon and non-typhoon conditions is made in time:

- *Typhoon conditions* – all time frames during which a tropical storm or typhoon is present within an area around Majuro chosen such that it can potentially directly affect Majuro.

- *Non-typhoon conditions* – all other time frames.

The choice for the exact boundaries of the area of influence of a typhoon is rather arbitrary. A larger area will lead to more time with typhoon conditions, while a too small area will mean that typhoon conditions pollute the non-typhoon conditions data, and violate the assumption of independence of precipitation related and coastal flooding for such conditions. In addition, a slightly larger area is favourable to include sufficient historical typhoon track data. As typhoons are not very frequent, a relatively larger area can be chosen, but this consideration should be made independently for each case.

Based on the consideration mentioned in above, the area for distinguishing between typhoon and non-typhoon conditions chosen to be box in between 5°S and 15°N, and 160° and 180°E. The boundaries of this area coincide with those of the Delft3D model, which was already partially developed in an Ebeye case study by Giardino et al. (2017, 2018). Nevertheless the choice is somewhat arbitrary; a circular with Majuro as centre area may seems a logical choice as well. The distance of Majuro to the boundaries of this box is in the order of 1000 km (although Majuro is not exactly in the middle of this box), whereas the largest radius of a typhoon ever recorded (Typhoon Tip in 1979, Northwestern Pacific) was in the same order of magnitude.

By making this distinction, the implicit assumption is made that during typhoon conditions, typhoon induced waves are dominant over swell waves making swell less relevant. This seems a reasonable assumption for two reasons:

1. Flooding due to typhoons is in general associated with higher inundation depths and consequential damage than flooding due to swell wave event.

2. In case that non-typhoon related swell waves or precipitation would occur and be dominant or significantly contribute to inundation during typhoon conditions, only a small part of the time series used for the non-typhoon conditions will be excluded. Hence, even in this case, the error made in determining the non-typhoon conditions would be small.

In spite of that, a few remarks have to be made. In making the distinction between typhoon and non-typhoon conditions, it is implicitly assumed that all typhoons and tropical storms are present in this data set. The classification of a storm as *'tropical storm'* or *'typhoon'* is based on certain distinct characteristics, but these criteria have their limitations and are not always strictly applied for milder storms. Classification of typhoons based on maximum wind speed (e.g. the Saffir-Simpson scale) is used, and although the classification of a storm as tropical storm or typhoon is useful and they have certain distinct characteristics, the criteria for classification, for example based on the Saffir-Simpson scale have limited physical base (see Section 2.2.1).

Besides, also during non typhoon conditions, precipitation and coastal flooding for example due to swell waves is not necessary completely independent, as seasonal effects (e.g. storm season during winter or El Niño) can play a role as well. This is left out of the scope of this thesis.

3.2. Data description

Different types of data are needed to carry out the flood hazard assessment. The following data has been collected:

- Bathymetry and topography

- Precipitation

- Waves conditions

- Water levels – surge and tide

- Historical typhoon tracks

These are described in the remainder of this Section. Figure 3.1 gives an overview of the locations of the used stations.
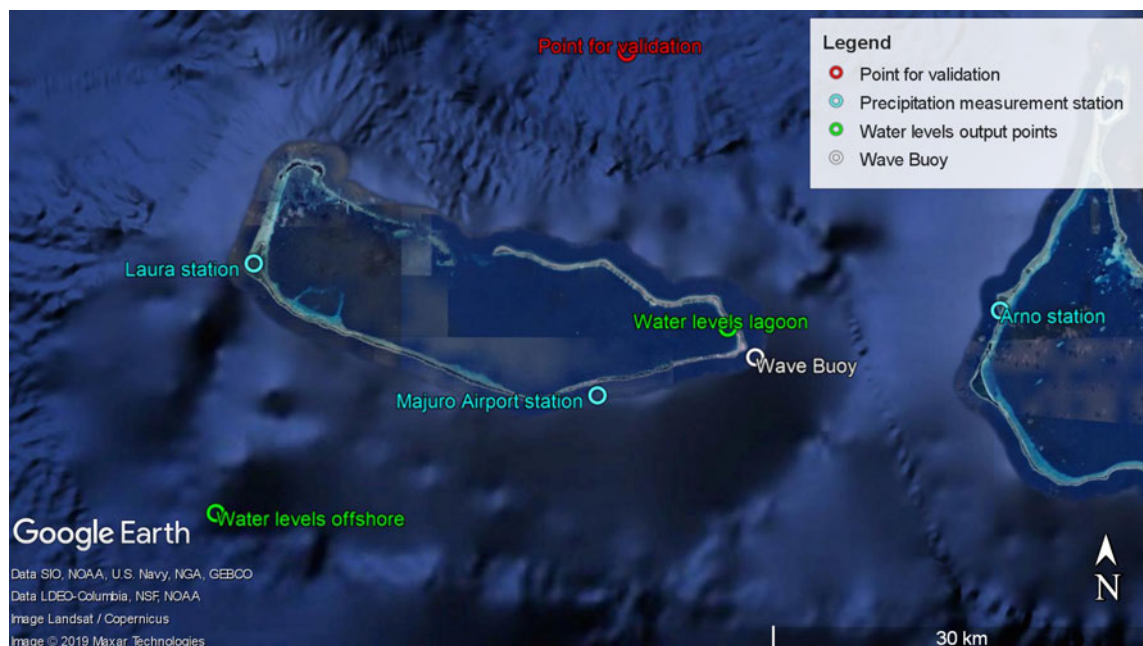
Figure 3.1: Overview of the locations of the used stations and other locations for which data is used. In addition, the location used for validation of water levels during typhoon conditions is shown.

3.2.1. Bathymetry and topography

In the large scale Delft3D and SWAN models and more local XBeach model, the bathymetry had to be specified. Different data sources were available for different areas, with different spatial resolution. All data was transformed to the WGS84 coordinate system.

- GEBCO 2008 global bathymetric data set with a horizontal resolution of 0.067°.

- Bathymetric data of the Republic of the Marshall Islands and Vicinity by Hein et al. (2007) or the area between 3°- 17°N, and 153°- 175°E with a horizontal resolution of 0.01°.

- Detailed topobathymetric depth elevation model for Majuro Atoll by Palaseanu-Lovejoy et al. (2017), with a horizontal resolution of 1 m, see Figure 3.2.
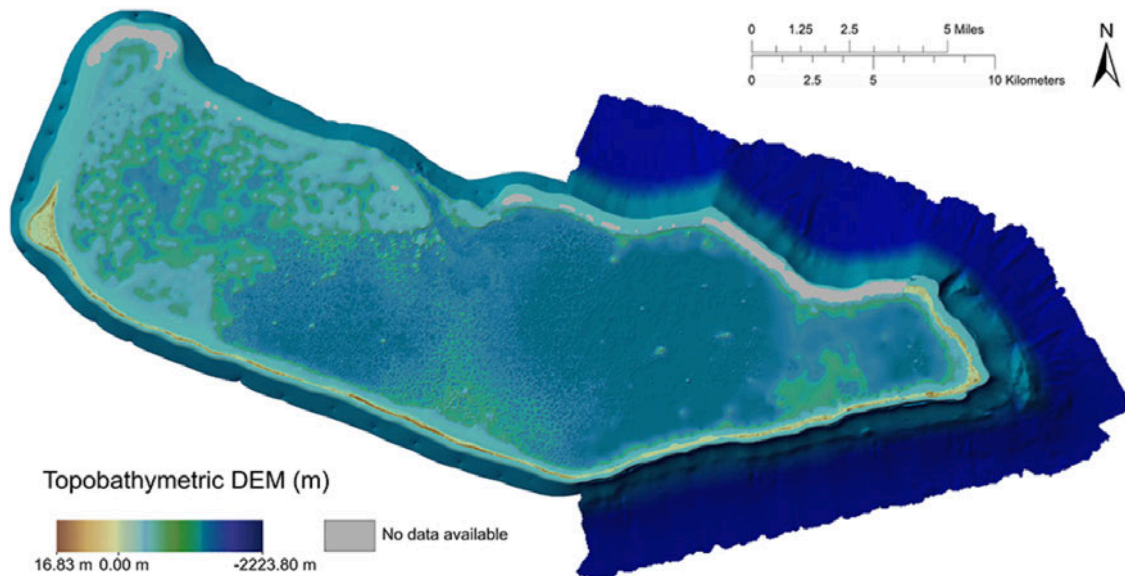
Figure 3.2: *Overview of the detailed topobathymetric digital elevation model adapted from Palaseanu-Lovejoy et al. (2017). All elevations are relative to local mean sea level.*

The local Mean Sea Level (MSL) as used in the detailed bathymetry for Majuro is used as reference level. In the figure, atoll features as described in Section 2.1 such as the bathtub like shape of the island topography can be recognized. Especially at Laura in the West the higher elevation areas can be observed near the shoreline, while the more central areas are of relatively lower elevation. The ocean side is clearly higher than the middle of the island, while the lagoon side as again somewhat higher. Some cross sections of the DUD region are presented in Figure 3.15. Also the shallower lagoon, the reef flat with elevation around Mean Sea level around the island, and steep slope towards the shelf depth of roughly 2 km are clearly visible.

3.2.2. Precipitation

Different weather stations measure precipitation rates at Majuro Atoll and nearby atoll islands, since different moments in history and with different frequency. An overview of precipitation measurements from weather stations is available via PACRAIN (Comprehensive Pacific Rainfall Database) by Greene et al. (2008), which aims to provide an integral rainfall database with data from all available stations in the Tropical Pacific Ocean, see http://pacrain.ou.edu/. Additionally, some data was obtained directly via NOAA (National Oceanic and Atmospheric Administration), see https://www.ncdc.noaa.gov/.

Majuro WBAS Airport, Laura and Arno stations are located on or near Majuro Atoll and all provide multiple decades of rainfall data, although with some interruptions. In addition, data from the Kwajalein weather station (located near Ebeye) is used for comparison with the Majuro data. See an overview of the data sources and used stations below:

- *Majuro WBAS Airport* – Majuro Atoll (7.06497°N; 171.27203°E), daily measurements from 1954-05-01 till 2019-03-12, Hourly measurements from 1984-02-01 till 2005-12-31. Data downloaded from NOAA website on 2019-03-15.

- *Laura* – Majuro Atoll (7.13611°N; 171.04111°E), daily measurements from 1990-08-01 till 2018-12-31. Data downloaded from NOAA website on 2019-03-15.

- *Arno* – Arno Atoll (7.07250°N; 171.55444°E), daily measurements from 1991-03-01 till 2018-11-30. Data downloaded from NOAA website on 2019-03-15.

- *Kwajalein (near Ebeye)* – Kwajalein Atoll (8.71670°N; 167.73300°E), daily measurements from 1952-04-16 till 2019-01-19. Data downloaded from PACRAIN website on 13-3-2019.

See Figure 3.1 for an overview of the locations of the weather stations. A comparison of the data and extreme value analysis of the daily precipitation rates was done for the different stations, see Appendix A.3.2.

Extreme precipitation rates at Majuro are higher compared to Kwajalein, while the precipitation rates do not differ too much over Majuro Atoll. Precipitation rates at Majuro WBAS Airport station are estimated to be slightly higher than those measured at Kwajalein, but the difference is minimal and well within the 95% confidence bands.

Precipitation rates at Laura and Arno seem to be slightly lower, but the available data for these stations is actually so limited that a good comparison is not possible. All differences are well within the confidence bands. Based on this comparison it seems a reasonable assumption that precipitation rates are spatially homogeneous for the DUD region, see Appendix A.3 for the details.

Majuro WBAS Airport station is the only station in the vicinity of Majuro with a sufficiently long time series for a sufficiently reliable extreme value analysis for the higher return periods (i.e. 50 years and longer). In addition, this station is relatively central on the Majuro and the only station for which hourly data is available. Therefore, the data of this station only was used to determine the daily precipitation rates for different return periods. Figure 3.3 below gives an overview of the daily rates for this station.
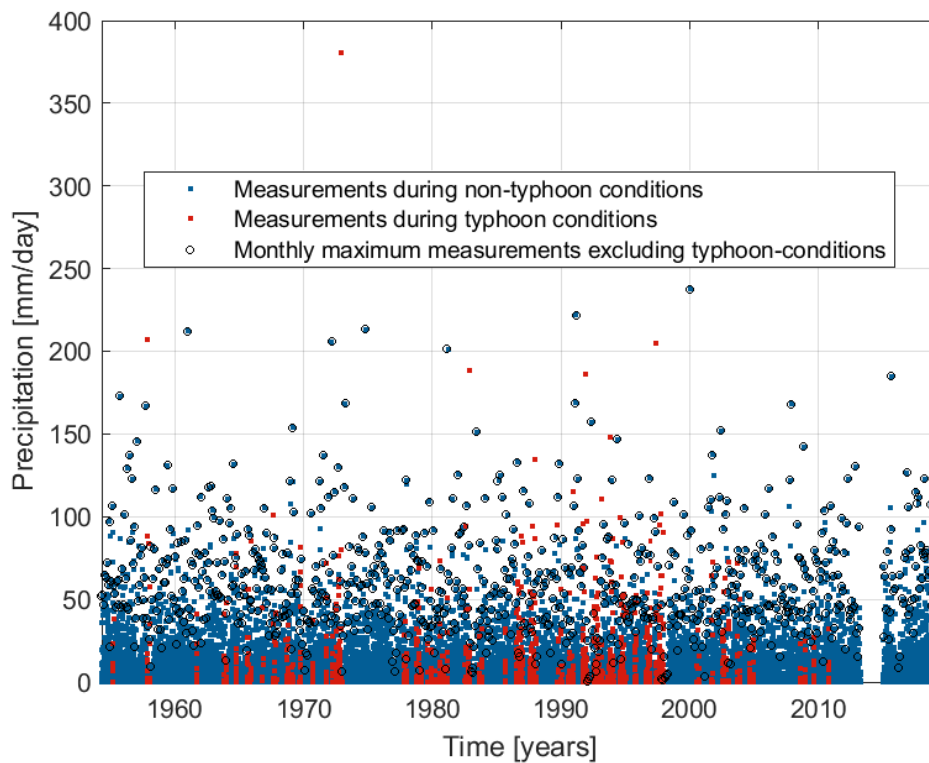
Figure 3.3: *All daily measurements for Majuro WBAS Airport station. Measurements during typhoon conditions are filtered out of the data set, after which the monthly maximum daily precipitation rates are determined.*

A relatively large part of the days with high measured precipitation rates seems to be during typhoon events – this includes the most extreme measurement. All data for days during typhoon conditions is excluded for the non-typhoon conditions. The precipitation rates for different return periods were determined based on an extreme value analysis. For the daily data, the monthly maximum precipitation rates were selected. In addition, an equal number of days with the highest precipitation rates is selected, as multiple extreme events can occur in the same month while in other months only less significant events took place. The threshold value used for this was 49.5 mm/day, see Figure 3.4 below.
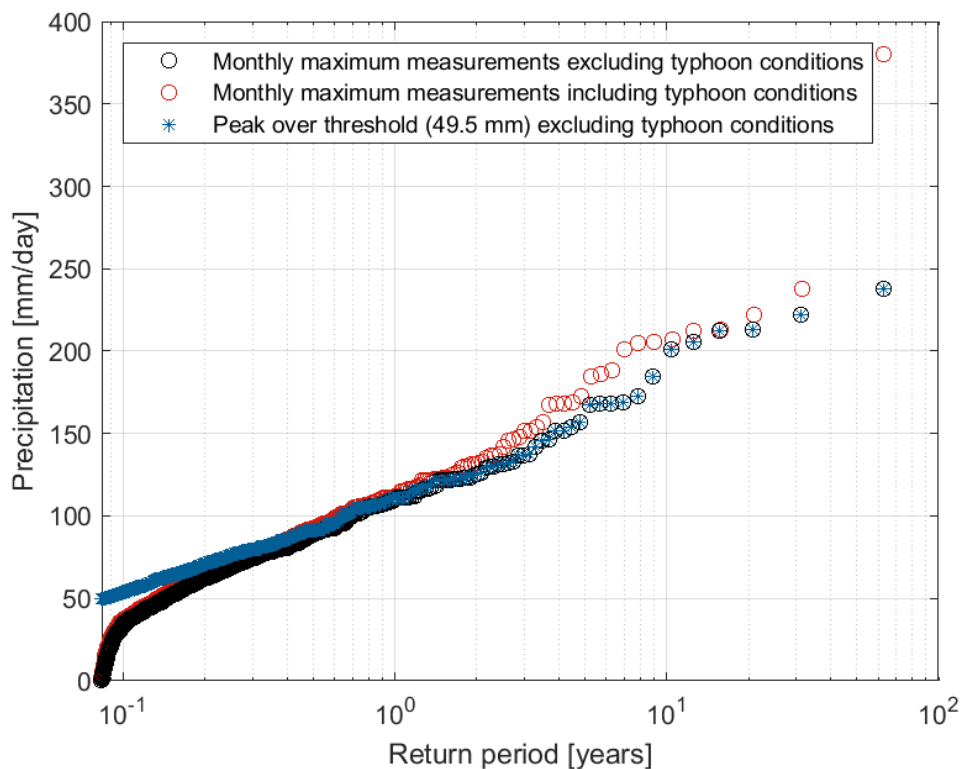
Figure 3.4: Comparison of the extreme daily precipitation rates based on different approaches.

Comparison of the monthly maximum measurements with the same number of measurements as selected by the peak over threshold approach shows that some months had multiple extreme events while others had none. Hence, when only the monthly maximum rates would be used this leads to an underestimation of the rates for the low return periods. This is partially caused by excluding the data for typhoon conditions. By doing so, some months have only a few days with non-typhoon conditions left and hence very low maximum daily precipitation rates.

Precipitation during typhoon conditions
Figure 3.5 gives an overview of the measured precipitation rates at Majuro (WBAS Airport Station) during typhoon conditions. Clearly, daily precipitation rates during most historical typhoons were significant, often in the order of 50-100 mm per day, with an extreme of 380 mm on one day. As a typhoon event can affect Majuro for multiple days, total precipitation rates during such an event can be even more significant.
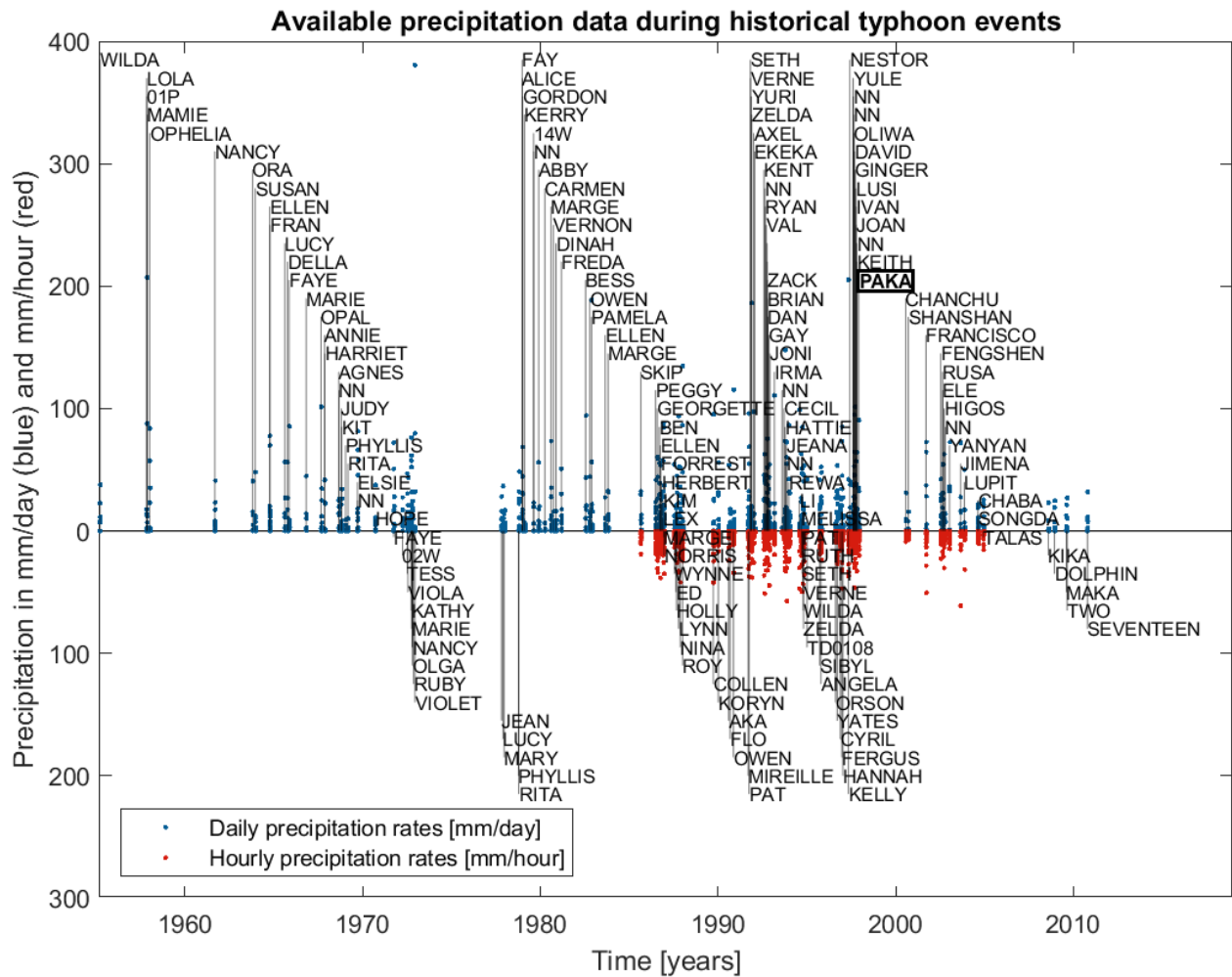
Figure 3.5: *Overview of precipitation rates at Majuro WBAS Airport Station during historical typhoon events. Typhoon Paka (1997) is highlighted as it is used for various purposes in this study.*

3.2.3. **Wave conditions**

Wave conditions are described by the significant wave height (H_s), peak period (T_p) and mean wave direction. Both reanalysis data (ERA5) and some measurements from a local wave buoy are available:

- Local wave buoy measurements at 7.0835°N; 171.3918°E, southeast of Majuro and with local water depth 553 m. Data is collected by PacIOOS (Pacific Islands Ocean Observing System, see http://www.pacioos.hawaii.edu/) with a Datawell directional buoy and available for about half of the 2010-2019 period.

- ERA5 data for the 01-01-1979 till 31-12-2018 period, hourly data with a spatial resolution of 0.5 degrees (C3S, 2017).

See Appendix A.2 for the wave roses of all locations with used data. No local measurements were available for periods with significant typhoon impact at Majuro. Besides, wind and wave conditions during typhoons are not well represented in the ERA5 data set. The wave roses of the local measurements and the nearest ERA5 point were compared and differ significantly, see Appendix A.2.
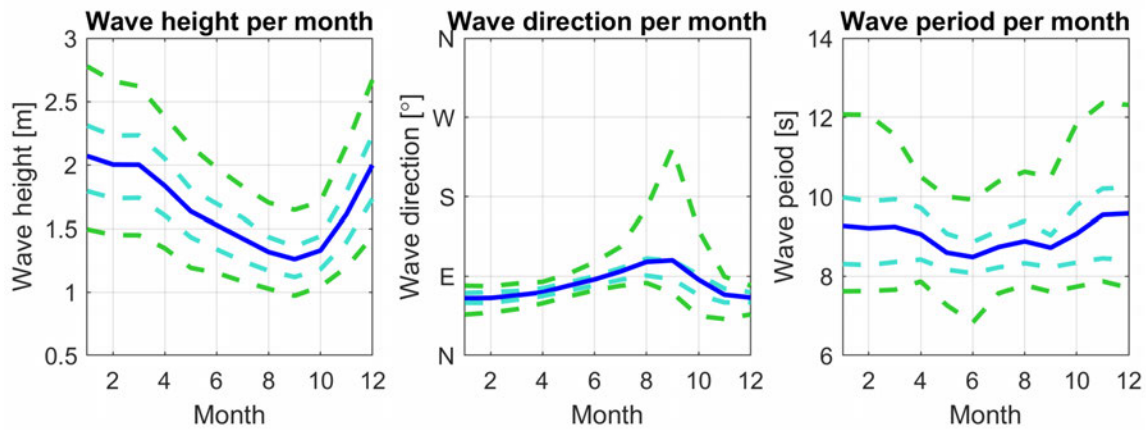
Figure 3.6: *ERA5 monthly offshore significant wave height H_s (left), direction (middle) and Peak period T_p (right) representative for the location 7.5 N 171.5 E (northeast of Majuro). Plotted are the median values per month in solid blue, the 25/75%-percentiles in dashed turquoise lines and the 5/95%-percentiles in dashed green lines.*

3.2.4. Water levels

Water levels are composed of tide and surge. The tide at Majuro is semi-diurnal, with clear diurnal inequalities and a spring tide range of approximately 1.6 m (Ford et al., 2018). The contribution of surge to the water level is limited to roughly 10 cm at most. Different data types and sources were used:

- A measurement station located at the Uliga dock inside the lagoon (7.083°N; 171.392°E). Data is collected by PacIOOS with a pressure sensor mounted to the sea floor at 2 m depth and water levels are recorded every 4 minutes. Records since 1968 are available.

- Data from a Global Tide and Surge Model (GTSM; Muis et al., 2016) based on ERA5 data. 2 output points are located near Majuro, for both locations data with an interval of 10 minutes is available for the 01-01-1979 till 31-12-2017 period. Both tide and surge levels are provided, which can be summed to obtain the total water levels. The locations of the output points are:
  - At 7.1045°N; 171.3721°E, near the location of the measurement station inside the lagoon.
  - At 6.9727°N; 171.0059°E, approximately 17 km south-southwest of Majuro.

See Figure 3.1 for the locations of these measurement stations and output points. Besides the normal tidal variation, variations on other time scales are clearly present in the data based on the GTSM. Figure 3.7 below shows the annual variation in water levels.
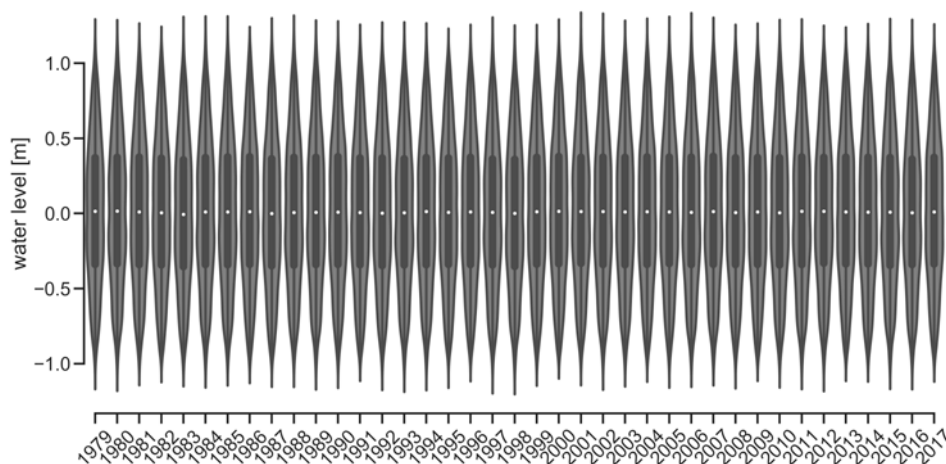
Figure 3.7: *Yearly variation in total water levels based on the Global Tide and Surge Model (GTSM), offshore of Majuro (6.9727° N; 171.0059° E). Each vertical bar represents one year and the width of the bar is a measure for the frequency of occurrence of the corresponding water level on the vertical axis in that year.*

Yearly variations are mainly caused by the El Niño Southern Oscillation (ENSO), with lower water levels during the El Niño phase and higher water levels during the La Niña phase (Ford et al., 2018). Based on historical records, sea level rise was estimated to be around 3.3 mm/year (Ford et al., 2018).

Besides, based on the data from the GTSM water levels vary seasonally, with the highest water levels around February and a second peak around September, see Figure 3.8 below. This is more or less in agreement with the analysis of historical water level inside the lagoon by Ford et al. (2018), where it was concluded that the highest water levels (or *'king tides'*) typically occur between January and March.
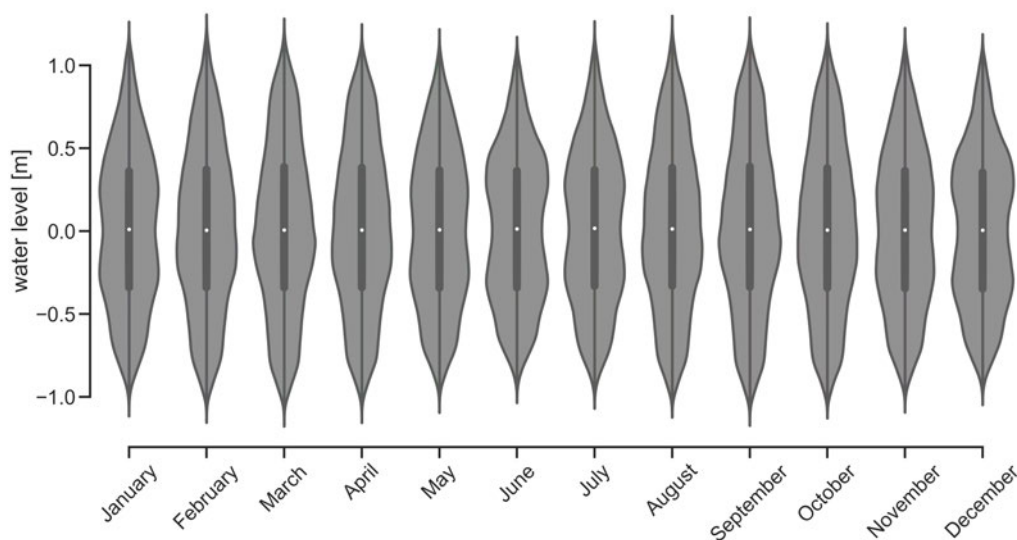
Figure 3.8: *Monthly variation in total water levels based on the Global Tide and Surge Model (GTSM), offshore at Majuro (6.9727° N; 171.0059° E). Each vertical bar represents one month and the width of the bar is a measure for the frequency of occurrence of the corresponding water level on the vertical axis in that month.*

3.2.5. Historical typhoon tracks

International Best Track Archive for Climate Stewardship (IBTrACS Knapp et al., 2018, 2010) combines information from numerous tropical cyclone datasets and is the most complete global set of historical tropical cyclones available. The subset JTWC-WP was used, which contains 71 years of typhoon tracks for the Northwestern Pacific basin. Hence, this subset seems best applicable for Majuro, although other subsets may contain some typhoons that were not included in this set but hit the area of interest. For example, typhoons in the southern hemisphere that hit the area of interest were not included in the JTWC-WP subset. Data was collected from https://www.ncdc.noaa.gov/ibtracs/index.php?name=ibtracs-data, accessed on 3-6-2019.

Among others, the data set contains information about the location and maximum wind speed with time stamp for historical typhoons and tropical storms. Figure 3.9 provides an overview of the available typhoon tracks for the Northwestern Pacific with maximum wind speeds. Majuro is located in an area where typhoons are relatively infrequent compared to other regions in the NW-Pacific basin. In general, cyclogenesis occurs around the Marshall Islands and hence are in general relatively weak in terms of maximum wind speeds. Further analysis of the typhoon tracks is elaborated in Section 3.4.
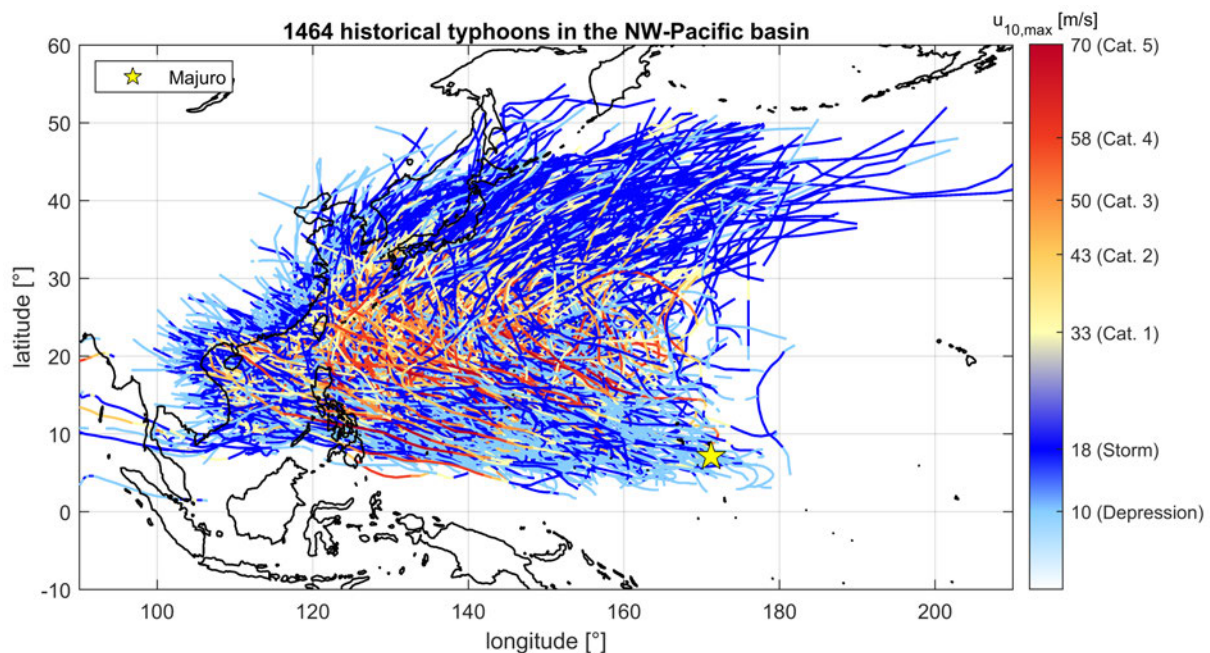
Figure 3.9: Historical typhoon tracks in the NW-Pacific basin, as in the subset JTWC-WP of the International Best Track Archive for Climate Stewardship (IBTrACS) data set. The categories 1-5 are based on the Saffir-Simpson scale.

3.3. Numerical models

A wide range of numerical models is available, with different ranges of applications. First the modelling approach is discussed, whereafter the used models (Delft3D, SWAN and XBeach) are elaborated. Subsequently validation of the models – although limited possible – is discussed and a short overview of the computational times of the models is provided.

3.3.1. Model selection

While different sets of scenarios have to be derived – and different methods are used to do so – the physical processes that have to be included in the simulation are similar for typhoon and non-typhoon conditions. Typhoons and tropical storms come with high wind speeds, an area with low (air) pressure and high precipitation rates. High wind speeds lead to large waves, while low pressure contributes to storm surge as well. Although not related to the typhoon, an high tide can occur simultaneously and contribute to the nearshore water level as well.

During non-typhoon conditions, distantly generated oceanic swell waves are expected to be the most important flood driver, but also more locally generated waves are included in the flood hazard assessment. Also during non-typhoon conditions, heavy precipitation events do occur and cause flooding. High tide contributes to flooding, reportedly especially during swell wave events. Although swell waves, precipitation and high tide can all occur simultaneously, they all have different drivers (i.e. distant storms, local weather conditions and astronomical respectively).

As such, the approaches for the simulation of these scenarios in numerical models can be similar. Key processes that have to be included as boundary conditions to obtain the inundation depths at Majuro are:

- Wave conditions – at different locations around the DUD region. Key parameters are the significant wave height (H_s), peak period (T_p) and mean wave direction.

- Water levels – being the combination of tide and surge

- Precipitation rates

To model the inundation depths on the DUD region, an XBeach model is chosen. This model seems to be best capable of including all relevant processes, especially as XBeach is capable of 2D modelling of wave transformation over reef flats. Precipitation rates can be applied as a boundary condition as well, whereby compound flooding can be modelled. While being most suitable for modelling inundation depths, the XBeach model is relatively computationally expensive, hence only the DUD region could be modelled. In addition, the water depth in the XBeach may not become too large. Therefore, the boundaries of the XBeach model offshore are located at the 20 m depth contour. A disadvantage of XBeach is that wave conditions can only be specified at one side of the model; in this case only at the ocean side as an approximation. Water levels can be specified at all sides. The XBeach model is further described in Section 3.3.3.

Various data sources have to be used to specify the boundary conditions. However, data is specified in various formats, for different time frames, with different frequencies and for different locations, mostly not directly in the DUD region as modelled in XBeach. For transformation of these conditions to the boundaries of the XBeach model, large scale Delft3D and SWAN models are better suitable. These computationally less expensive models can be used to model water levels and wave conditions in deeper water, but are not capable of wave transformation over coral reefs. In Delft3D model, wave conditions, water levels, air pressure and wind fields varying in space and time can be applied as boundary conditions, while SWAN is only used for the wave conditions. The setup of the Delft3D and SWAN models and the different configurations are further elaborated in the next Section (3.3.2). Figure 3.10 provides a schematic overview of the inputs and outputs for all models.
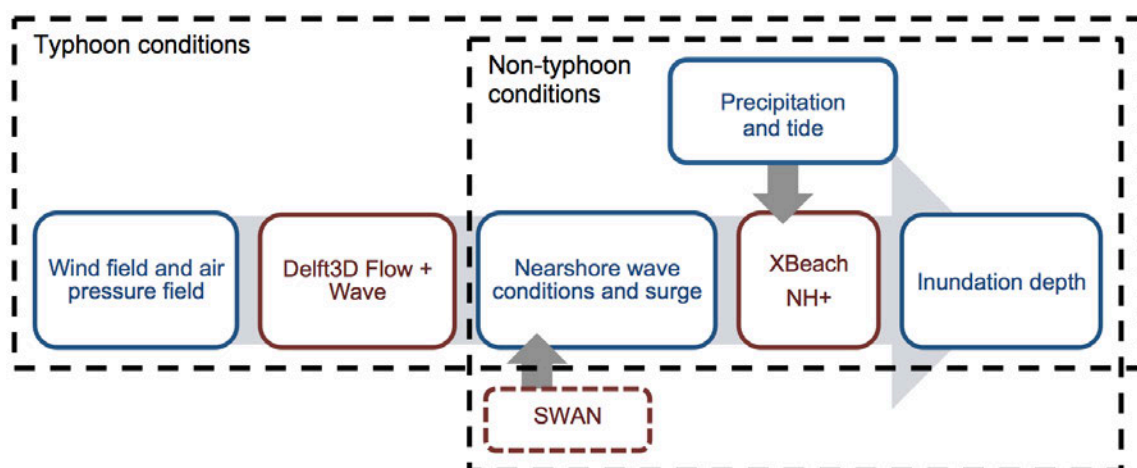
Figure 3.10: Overview of the used model train with the inputs and outputs per scenario of the Delft3D and XBeach models. The SWAN model is actually not used to model each of the scenarios, but to transform the historical data to nearshore conditions, and after some intermediate steps, the scenarios are derived directly as nearshore conditions (see Section 3.4).

3.3.2. Delft3D and SWAN models

Delft3D is modelling suite for hydrodynamic modelling, sediment transport and morphology and water quality for fluvial, estuarine and coastal environments (Lesser et al., 2004). The core of the suite is the hydrodynamics module Delft3D-FLOW. SWAN (Simulating WAves Nearshore; Booij et al., 1997) is a model for wave propagation and transformation. SWAN is included in the Delft3D suite as the Delft3D-WAVE module, which can be coupled with the Delft3D-FLOW module.

The following versions of Delft3D modules were used:

- FLOW2D3D Version 6.02.07.6118, May 2016.
- Delft3D-WAVE Version 3.05.01.6118, May 2016.

Used configurations

The Delft3D and SWAN models are used to determine the offshore wave and water level conditions around Majuro and inside the lagoon. Three different configurations are used, each wih a different

purpose:

- *SWAN only* – Used for transformation of non-typhoon wave conditions to offshore wave conditions near Majuro. Only the nested grids were use, where the coarsest of the 2 nested grids was extended to the ERA5 output points, such that wave and wind conditions from the ERA5 data could be used as boundary conditions. No additional boundary conditions to force the model were applied.

- *Delft3D-FLOW only* – Basic setup to verify the method used for typhoon scenario selection and interpolation as described in Section 3.4. Each of the historical and synthetic typhoons is simulated individually by use of spider web grids, containing the time-varying wind and pressure fields. The model has a run time in the order of 1 hour.

- *Delft3D-FLOW + WAVE coupled model* – Including a nested grid for the Majuro and Arno atolls area, and an additional nested grid for Majuro Atoll. This more advanced and computationally expensive setup is used for more detailed modelling of the representative typhoons and includes waves. Each these selected typhoons is simulated individually by use of spider web grids, containing the time-varying wind and pressure fields. The model has a run-time in the order of 1 day.

For all setups, standard default parameters and open boundaries were used unless specified otherwise.

Numerical grids

Different grids are used. The large scale grid for the Marshall Islands area was developed by Giardino et al. (2017, 2018). Two additional smaller grids were made, see the overview of the grids below:

- *Marshall Islands area* – This main grid covers the area between 160°- 180°E and 5°S - 15°N and has a grid cell size of 0.1°x 0.1° (±11 x 11 km). The area of the model domain is the same as the area used for distinguishing typhoon and non-typhoon condition (Section 3.1).

- *Grid of Majuro and Arno* – This subgrid is nested in the main grid (Marshall Islands area) and a factor 5 finer, with a grid cell size of 0.02°x 0.02° (±2.2 x 2.2 km). The grid is specified for the 6.7°- 7.6°N and 170.7°- 172.3°E box area.

- *Grid of Majuro* – This subgrid is nested in the Majuro and Arno grid and a factor 10 finer, with a grid cell size of 0.002°x 0.002° (±220 x 220 m). The grid is specified for the 7.04°- 7.24°N and 171.2°- 171.4°E box area.

By including Arno Atoll in the Majuro and Arno grid, possible sheltering of eastern parts of Majuro and the conditions in the lagoon are better included. In addition, this grid is needed as an intermediate step as the direct transition to the Majuro grid may give problems at the boundaries. The boundaries of the nested grids are shown in Figure 3.11.

Bathymetry

For all grids, a bathymetry was specified based on available data. A value for the bottom level is assigned to each grid cell. Data of the different sources described in 3.2.1 was combined according to the following principles:

- In order to make the transitions between the grids as smooth as possible, first the bottom level was specified for the smallest grid (Majuro) These bottom levels were used for the middle grid (Majuro and Arno), and those were subsequently used in the large scale grid (Marshall Islands).

- Data with the higher resolution was preferred over data with lower resolution.

- When multiple data points were available, grid cell averaging was used.

- At the locations of boundaries of the data, some smoothening was done to make sure discrepancies in the different data sources would not lead to unrealistic transitions.

The resulting bathymetry is shown in Figures 3.11 (Marshall Islands grid), 3.12 (Majuro and Arno grid), and 3.13 (Majuro grid) below.
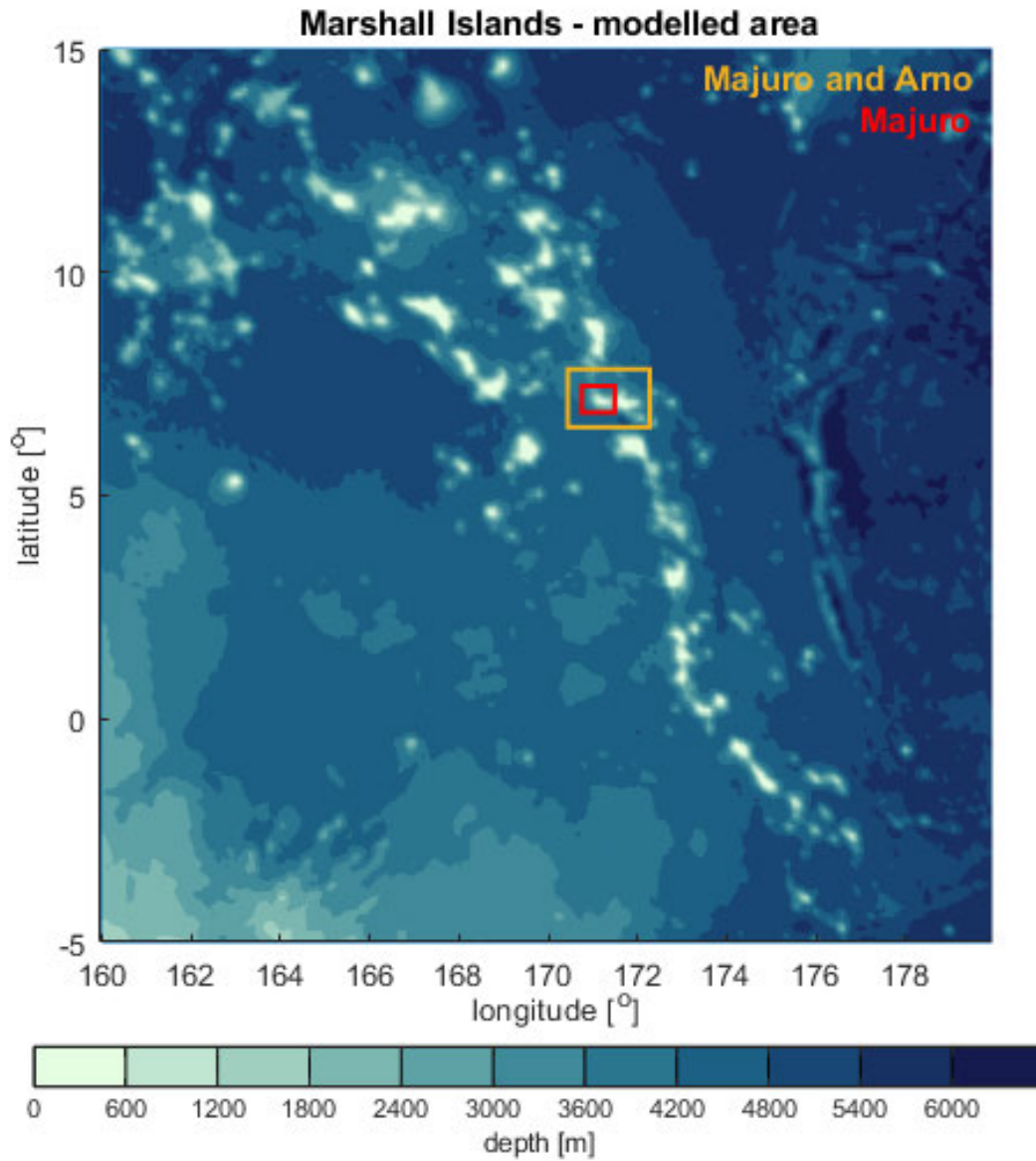
Figure 3.11: *Overview of the bathymetry used for the Delft3D model, with the boundaries nested grids for Majuro and Arno in yellow, see Figure 3.12, and for Majuro in red, see Figure 3.13.*
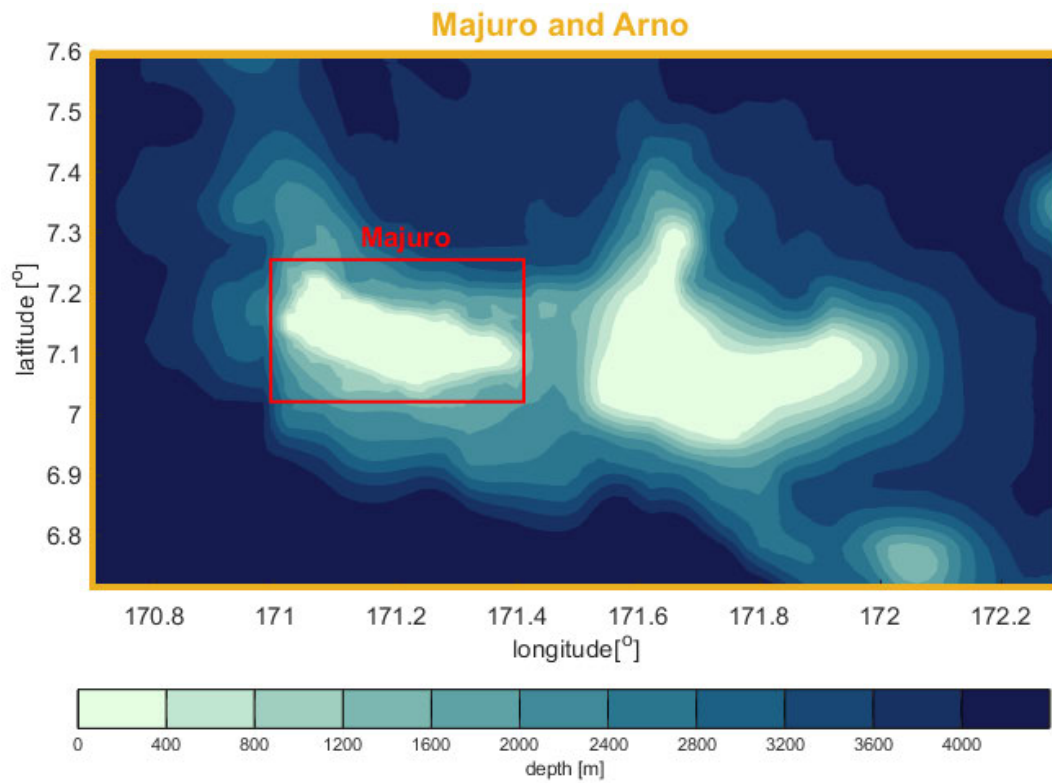
Figure 3.12: *Overview of the bathymetry used in the Majuro and Arno grid for the Delft3D model, which was nested in the large scale model of the Marshall Islands area. The Majuro grid area (shown in red) is subsequently nested in the grid for this area.*
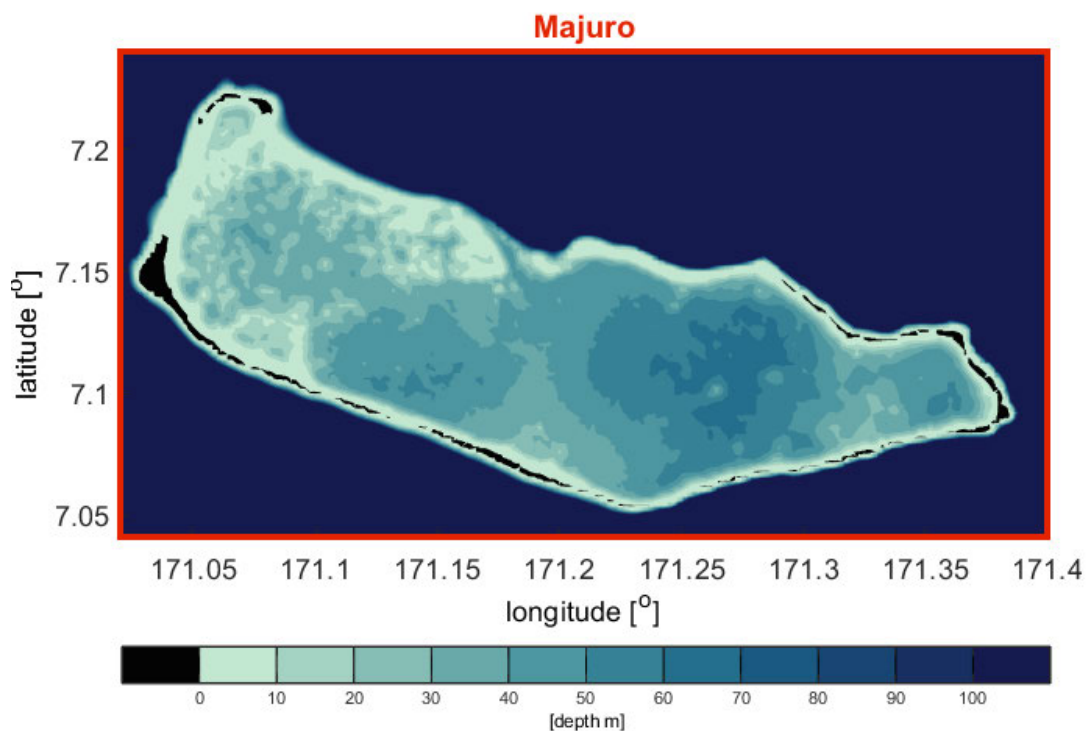
Figure 3.13: *Overview of the bathymetry used in the most detailed grid (Majuro) for the Delft3D model, which was nested in the Majuro and Arno grid. The scale of the depth is focused on the lagoon and as such, all depths larger than 100 m are shown in one color. Figure 3.12 provides more insight in the bathymetry for depths larger than 100 m.*

3.3.3. XBeach model of the DUD region

XBeach is an open source model for wave propagation, mean flow, sediment transport and morphological changes of the nearshore area (Roelvink et al., 2009). XBeach was originally developed for sandy coasts, but has been applied to fringing and atoll reefs as well. The model includes the hydrodynamic processes of short wave transformation (refraction, shoaling and breaking), long (infragravity) wave transformation (generation, propagation and dissipation), wave-induced setup and unsteady currents and can be used to simulate overwash and inundation (Hoonhout, 2015). Different modes of XBeach are available: Stationary mode, Surfbeat mode and Non-hydrostatic (NH) mode. These modes resolve waves of decreasing time-scales with increasing computational costs. Further details can be found in the XBeach manual by Hoonhout (2015). XBeach version 1.23.5526 was used. This version has the new option to include rainfall.

Used configuration

A 2DH non-hydrostatic (NH), wave-resolving version of XBeach with a curvilinear grid was used to model wave transformation and inundation depths for the DUD region at Majuro. Short waves dominate the bottom stresses on the fore reef and near the reef crest (Van Dongeren et al., 2013). Hence, the computationally expensive NH version of XBeach is needed. In the NH version, incident-band (short wave) runup and overwash are included, which is especially important on steep slopes (Hoonhout, 2015). In the vertical, a second layer was used (i.e. the NH+ option) to allow for a larger water depth (i.e. approximately 20 m). This was needed due to the steep slope of the fore reef.

The boundary at the ocean side of the model was set at a depth of approximately 20 m. The model is extended with a few grid cells to the ocean side, where a constant water depth of 20 m is applied to make sure that waves can propagate into the model before breaking. Inside the lagoon, the boundary is set at a depth of approximately 5 m, to ensure that overwash of the island can be included. Here no boundary condition other than a water level is applied.

Bottom friction plays an important role as waves propagate across the reef flat towards the shore (Pearson, 2016) and is often parameterized by a Coefficient of friction C_f. Various studies have been done into the modelling of bottom roughness on coral reefs. For example, in a study to wave runup on atoll reefs for Kwajalein Atoll, Quataert et al. (2015) used a spatially varying bottom friction, where a value of $C_f = 0.01$ on the reef flat in combination with $C_f = 0.4$ on the fore reef gave good results. Veldt (2019) used a spatially homogeneous value of $C_f = 0.02$ in a study to the effect of wave directional spread on coastal hazards at coastlines fronted by a coral reef. For BEWARE (Pearson, 2016), values in the range of 0.01-0.1 were included.

Based on the above mentioned reports, a spatially homogeneous bottom friction coefficient C_f of 0.02 across the whole model domain was assumed. Nevertheless, a spatially varying bottom friction may lead to more accurate results and this could potentially be based on the ecosystems mapping report by (Kendall et al., 2012), but this falls out of the scope of this thesis.

Boundary conditions

Specification of the Boundary Conditions (B.C.) of the XBeach model is crucial in order to simulate the inundation depths. Water levels were specified at all sides of the model, while wave conditions were only specified at the ocean side of the model. In order to capture the spatial variation in wave condition around the DUD region, wave conditions were specified for 5 different locations at the ocean side, see Figure 3.14. In addition, representative cross sections were defined for the full Majuro Atoll. The five locations for the B.C. at the ocean side were chosen such, that they coincide with the ocean side of representative cross sections C-G, see figure 3.14 (other cross sections not shown). The wave conditions specified at these locations are applied at the nearest domain boundary in XBeach. The representative cross section are used in the scenario selection method for the non-typhoon conditions (Section 3.5) and to check the model performance (Section 3.3.4).

For the simulation of typhoon scenarios, wave conditions at the XBeach model boundary were obtained from the Delft3D model. For the non-typhoon scenarios, the SWAN model was used to obtain the wave conditions at these locations, but additional steps were taken to get the actual wave conditions and water levels as used in the scenarios. This is further elaborated in Section

3.5. Wave conditions were specified as a series of parametric JONSWAP spectra (see Section 2.2.2), with the parameters significant wave height, peak period, and mean wave direction. For the typhoon scenarios, the directional spreading could be based on the Delft3D output as well; for the non-typhoon conditions the default value of 10 was used. Other than that the standard default values were used and wave conditions were specified with an interval of 30 minutes.

Water levels at the boundaries are composed of tide and surge, of which the later was mainly related to the air pressure and limited to the order of 10 cm. Hence, little variation in water level along the model boundary on the ocean side was expected and a constant water level along the boundary on the ocean side was applied. For simplicity, the same water level was assumed at the other boundaries. Water levels at the boundary are composed of surge and tide, and these are assumed to be independent. This seems a reasonable approach as the surge level at the offshore boundary is almost completely related to the air pressure, and no (wind or wave) induced setup is expected at the model boundary. As such, the tidal water level is not expected to significantly influence the (already low) surge levels.

Surge levels for typhoons were obtained by use of the Delft3D model. The approach to obtain the offshore surge levels for the non-typhoon conditions is elaborated in Section 3.5. As the tide was not included in the Delft3D model nor the SWAN model, a random time series for the tide was constructed by selecting a random time frame from a 1000 year period. Subsequently, the associated predicted offshore tidal water levels were obtained from the GTSM (Section 3.2.4). This tidal water level was added to the surge level, to obtain the total water level at the boundary. Water levels were specified with an interval of 30 minutes.

Numerical grid and bathymetry
The curvilinear grid and bathymetry were constructed based on the following principles:

- In cross shore direction, the cell size is based on the depth and the smallest wave that should be well represented. In longshore direction, an approximately 5-10x larger grid cell size was allowed. Different grid sizes were compared, see Appendix B for the details.

- At the boundaries, a margin of a few grid cells with a continuous depth of 20 m at the ocean side, and 5 m at the lagoon side was used, to allow waves to travel undisturbed into the domain and prevent boundary effects.

- Bathymetry was based on the detailed DEM model by Palaseanu-Lovejoy et al. (2017) as described in Section 3.2.1.

The grid size is one of the most important factors in the computational efficiency of the model. In principle, a smaller grid cell leads to a more accurate simulation of the inundation depths, but a too small grid was computationally not feasible. Different grid sizes have been tested in order to find a good balance between computational efficiency and accurate prediction of the simulated inundation depths. The hour with peak wave conditions during typhoon Paka (see Section 3.3.4) was simulated.

The boundary conditions (wave conditions and water level) were obtained from the simulation of Paka in the Delft3D model, no precipitation was included. Grids with a cross shore grid cell size of 2, 4 and 8 m were tested (i.e. a refinement factor of 2 and 4 was applied to the 8 m grid, in both cross shore and longshore directions). In addition, another test with the 8 m grid, only refined by a factor 2 in the longshore direction was done. Maximum water levels and significant wave height were compared for cross sections C and G (see Figure 3.14). Besides, the maximum inundation depths were compared for the 8, 4 and 2 m grids. Details and results can be found in Appendix B.2.3.

The 4 m grid was concluded to be the best option. The models with 8 m grids were significantly faster, but inundation depths were largely underestimated. On the other hand, the 4 m grid underestimated the inundation depths compared to the 2 m grid, but the difference was smaller and

the 2 m grid was computationally unfeasible. See Figure 3.14 for an overview of used the XBeach model with the bathymetry.
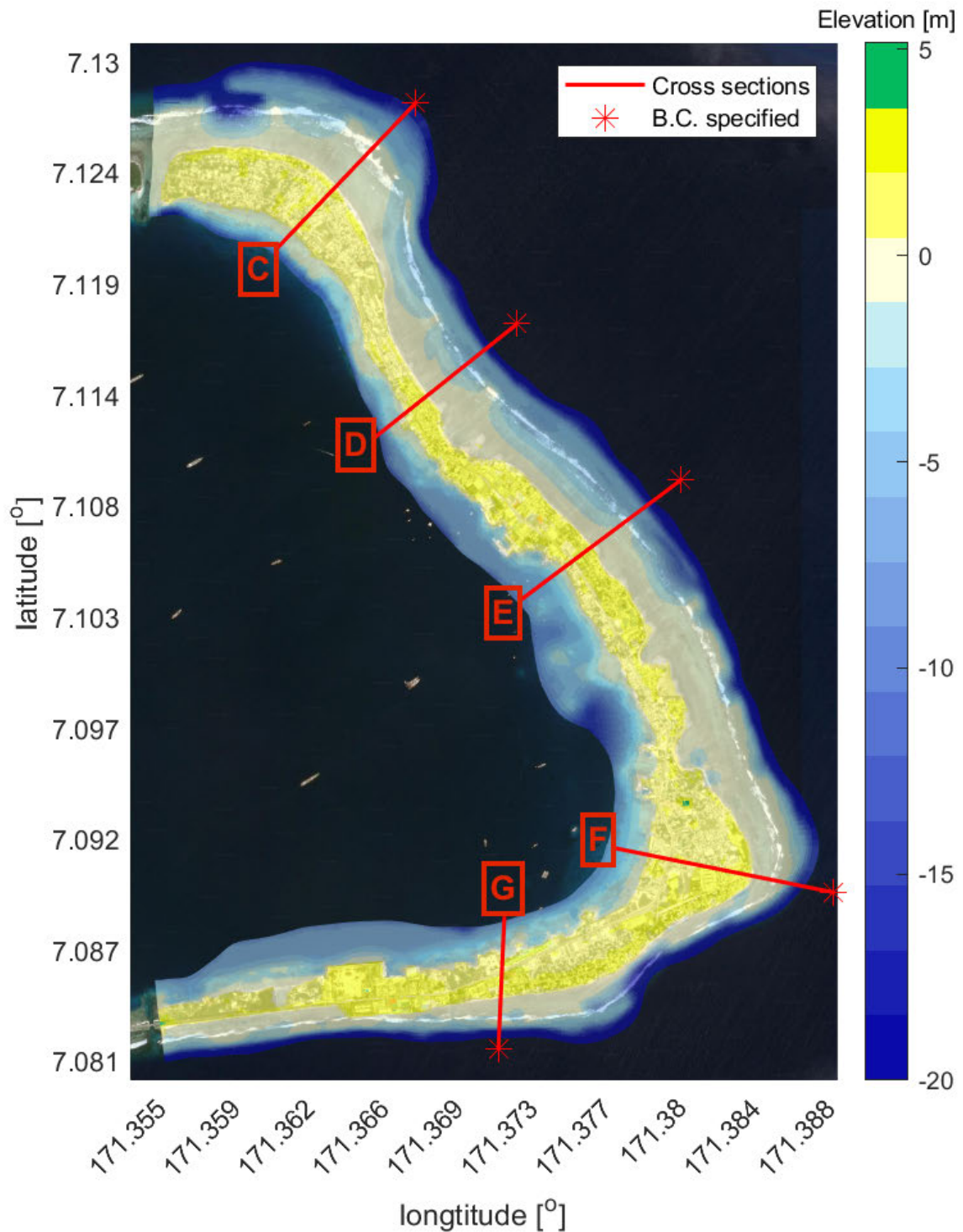
Figure 3.14: *Overview of the XBeach model of the DUD region with cross sections C-G. The B.C. for waves were obtained from the Delft3D and SWAN models and specified in the XBeach model at the ocean side points of the cross sections . In XBeach, these conditions are applied to the nearest point at the model boundary. Underlying satellite image: ©2019 CNES/Airbus, 17-3-2017 via Google Maps.*
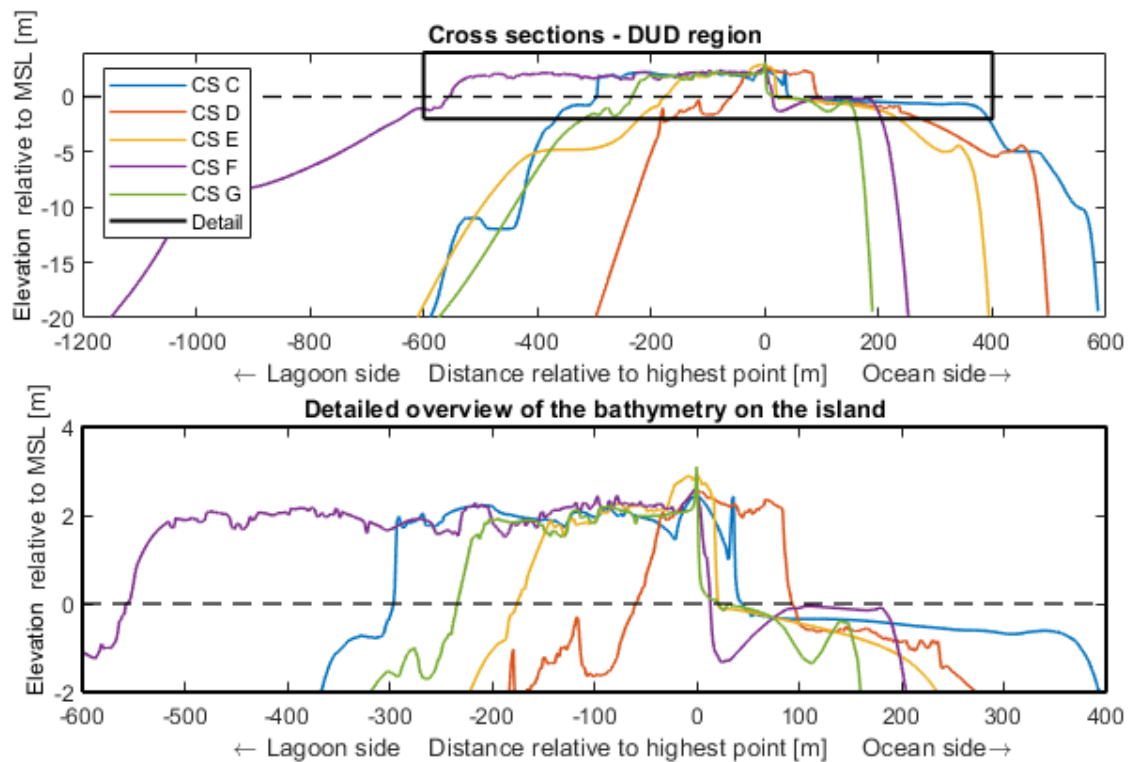
Figure 3.15: Elevation relative to Mean Sea Level (MSL) in cross sections C-G. The upper part shows the full Cross Sections (CS) of Figure 3.14; the lower part shows the island in more detail. All distances are relative to the highest point in that cross section, which is found at the ocean side of the island in all cross sections.

Precipitation

To be able to model compound flooding, rainfall was added to the XBeach model as an optional boundary condition. Precipitation rates can vary in space and/or over time and have to be specified in mm/hour. Validation of the function to include precipitation in XBeach is elaborated in the next Section. For the simulation of the typhoon and non-typhoon scenarios, spatially homogeneous rainfall rates were specified with an interval of 30 and 60 minutes respectively.

3.3.4. Model validation and computational efficiency by typhoon Paka

To increase confidence in the output of the used numerical models, some checks and validation of the used models was done. In addition, the computational times of the different model setups are discussed, as often the balance between computational time and accuracy is key in the setup of the models. Both the Delft3D and XBeach software have been widely used for many different locations, environments and purposes. Nevertheless each case is different and validation is an important step, especially considered the atoll environment with a coral reef and the inclusion of precipitation in this case study.

The most suitable method for validation would most likely be the comparison of water levels or wave conditions in data for historical typhoons with the model simulation output. While a wave buoy is present near Majuro and water levels are recorded inside the lagoon, unfortunately no data was available for periods with significant typhoon impact.

Typhoon Paka

To get some insight in the performance of the models in simulating water levels, wave conditions, precipitation and subsequent flooding, typhoon Paka (1997) was simulated. Typhoon Paka seems a logical candidate as it was relatively strong around Majuro, being often named as the most recent heavy storm that hit Majuro. Paka caused an estimated US$ 1 million of damage (Ford et al., 2018) just at Majuro. Paka developed as a tropical depression around 28 October 1997, about 3000 km east of Majuro and passed the dateline (and eastern boundary of the Delft3D model) on December

7. It further intensified to a strong tropical storm before passing over Majuro Atoll on December 10 and became a category 1 typhoon shortly after. After passing the Marshall Islands, Paka continued to the west and became a category 5 typhoon around 14 December 1997, see Figure 3.16 for a satellite image of Paka.

A maximum water level of 0.54 m was measured inside the lagoon and offshore, at 7.6°N, 171.6°, the maximum significant wave height was estimated to be 4.11 m, based on WAVEWATCH III hindcast (Ford et al., 2018). However, it is likely that wave conditions during energetic storms (such as Paka) are underestimated (Cox et al., 2011) and hence larger simulated wave heights should be expected. Few hours after passing Majuro, Paka was classified as a category 1 typhoon and hit Ailinglaplap Atoll (±280 km west of Majuro Atoll), where it caused an estimated US$ 80 million of damage and affected 70% of the houses (PCRAFI, 2011, 2015).

Delft3D and SWAN models
In Section 3.3.2 different setups of the Delft3D and SWAN model are described. Typhoon Paka was simulated in the Delft3D-FLOW + WAVE configuration, as the Delft3D-FLOW and SWAN model can be seen as the two parts that combined are the FLOW + WAVE model. The capability of the model to simulate water levels based on air pressure and wind fields was validated, and simulated wave conditions were assessed qualitatively.

Water levels and wave conditions were compared for the offshore location of the wave buoy (see Figure 3.1 for this location). See Figure 3.16 for the air pressure and wind conditions as applied in the Delft3D model during the passing of Majuro. At the location of the wave buoy, the simulated water levels are indeed proportional to the inverse of the air pressure drop. Maximum simulated wave heights offshore at the location of the wave buoy are in the order of 6.9 m. As expected this is significantly higher than the 4.11 m mentioned in the previous section. See Appendix B for further details.
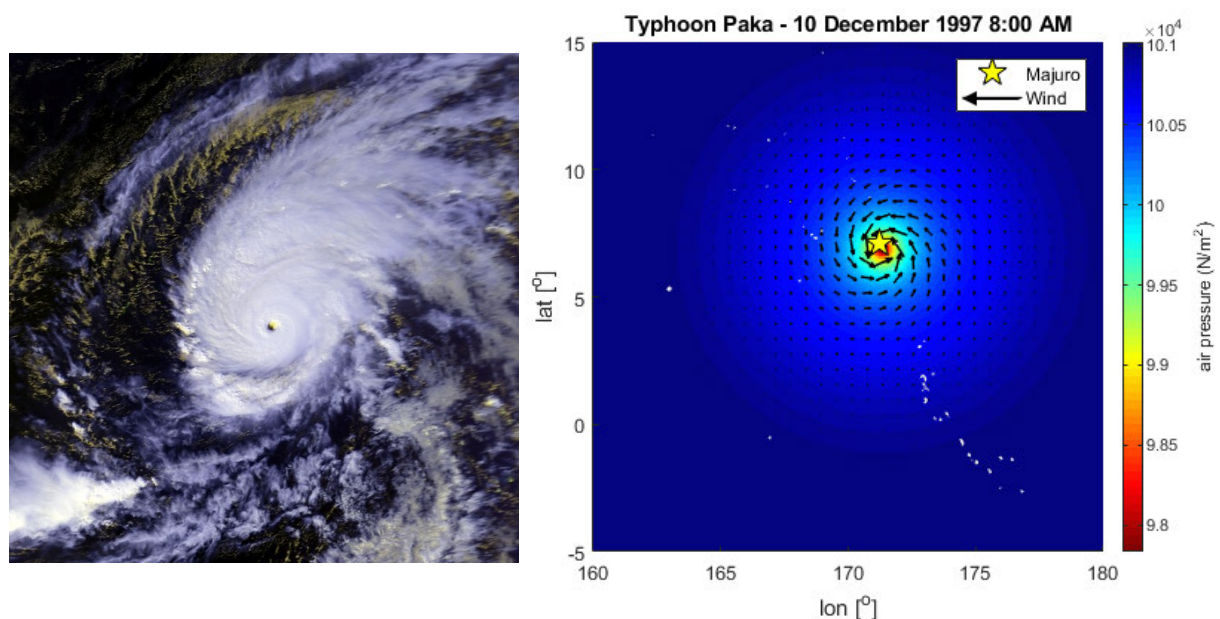
Figure 3.16: Left: Satellite image of Typhoon Paka on 15 December 1997 after becoming a category 5 typhoon, 5 days after passing Majuro (image in public domain). Right: Overview of the air pressure field and wind field (black vectors) around peak strength for the DUD region at Majuro as applied in the Delft3D model. The black vectors give the (mean) direction of the wind and the magnitude of the vector is a measure for the magnitude of the wind speed.

As described in Section 3.3.2, some parts of the Delft3D model have been reused from a model developed by Giardino et al. (2017, 2018). This model was originally used in an Ebeye (Kwajalein atoll) case study. In that study, similar problems with data scarcity in the validation were overcome

by validation with another case study (Hawaii, Hurricane Iniki, 1992), where a similar setup was used. See Giardino et al. (2017, 2018) for further details. Hence, when the same setup is followed in this Majuro case study, the setup could be considered as similar to that used in the Ebeye study, and thereby indirectly to the validated Hawaii study.

Although the overall setups of the Ebeye and Majuro models are very similar, there are some differences as well. The Ebeye model did not include the two nested grids for Majuro and Arno (Figure 3.12), and Majuro (Figure 3.13). Besides, the bathymetry in the Ebeye study was partially based on different data, as the detailed topobathymetric depth elevation model for Majuro by Palaseanu-Lovejoy et al. (2017) was not used.

XBeach model with precipitation

Validation of the XBeach model partially encounters the same problem as that of the Delft3D model described above: there are no measurements for wave conditions available. However, hourly precipitation measurements from Majuro Airport station were available for typhoon Paka. Hence partially the same approach was used; water depths, wave conditions and inundation depths during typhoon Paka were simulated, and the results were evaluated only qualitatively.

To validate the newly build in function to add rainfall in XBeach, a number of tests have been done. First, 3 simple tests were done on a small XBeach model of 10 x 10 grid cells of 1 by 1 m each, without any waves or water levels applied at the boundaries. For all the model boundaries, the type *'Wall'* was selected, whereby no water could flow out of the domain. Precipitation rates were kept spatially homogeneous and a constant precipitation rate and two time varying rates were simulated for a 1 hour period. For all simulations the cumulative precipitation after 1 hour was 100 mm. For all 3 tests, the water level in the domain was 100 mm as well after one hour and hence the rainfall function was concluded to preform as expected in this test. See Appendix B.2.1 for the details and an overview of the applied rainfall rates and corresponding water levels over time.

For a second test, the XBeach model of the DUD region was used. Hourly precipitation measurements from Majuro Airport station were available for typhoon Paka. To validate the inclusion of precipitation, 3 different cases were simulated: (1) Coastal flooding only, (2) Precipitation only, and (3) Compound flooding; coastal flooding and precipitation combined. Clearly, the simulation of compound flooding should lead to the highest water levels. Although the test was only done for Typhoon Paka, the test also provides some insight in the relative importance of rainfall and coastal flooding during a compound flood event. The boundary conditions of these simulations can be found in Appendix B.2.2. The flood extents can be found in Section 5.1.1.

Computational efficiency

An overview of the tested model setups with their estimated run time is given in table 3.1 below. Simulated times vary per scenario (e.g. the duration of typhoons is different) and run times may vary as well, depending on the simulated conditions.

Table 3.1: Overview of the run times per model. The shown times are estimated values and vary per simulated case.

Model	Simulated time [days]	Estimated run time [hours]	Description
Delft3D			**On 1 node / 4 cores**
FLOW	14	1	Large grid only
FLOW+WAVE	14	30	Including nested grids and waves
XBeach			**On 2 nodes / 8 cores**
Grid 2 m	1	240	With grid size on reef in cross shore direction of ~2 m
Grid 4 m	1	90	With grid size on reef in cross shore direction of ~4 m
Grid 4 / 8 m	1	50	Grid size in cross shore of 8 m grid, in longshore of the 4 m grid
Grid 8 m	1	40	With grid size on reef in cross shore direction of ~8 m
Grid 4 m Precipitation	1	20	Grid 4 m with only precipitation simulated (no waves and no varying WL)
Grid 4 m Compound	1	100	Grid 4 m with prcipitation, waves and varying water levels

3.4. Scenario derivation for typhoon conditions

To be able to quantify the flood hazard during typhoon conditions, a computationally feasible number of scenarios has to be derived that combined give a good representation of all possible typhoon events that can lead to flooding. A number of steps is followed to derive such a set of scenarios:

1. Based on the 71 years of **historical typhoons** (see Section 3.2.5), 1000 years of synthetic data is generated by use of TCWiSE, see Section 3.4.1. The synthetic data set includes a wider range of typhoons (i.e. in terms of track location and wind speeds).

2. As modelling of inundation depths for all **synthetic typhoons** is computationally unfeasible, 50 representative typhoons are selected by use of Maximum Dissimilarity Algorithm (MDA), see Section 3.4.2. Subsequently, for each of these representative typhoons, the Delft3D and XBeach models can be used to get the corresponding inundation depths in the DUD region of Majuro.

3. Based on the inundation depths for the **representative typhoons** only, it is not possible to give return periods of certain inundation depths. Therefore, the inundation depths for all synthetic typhoons are estimated based on the representative typhoons, by use of Softmax, see Section 3.4.3. Hereby, estimated maximum inundation depths for all synthetic typhoon tracks were obtained.

Figure 3.17 below provides a schematic overview of these steps. As an example, the maximum inundation depth at a certain point is used on the vertical axis, but this could be any other relevant parameter. Historical data does not include the more extreme cases that can occur due to the limited period for which data is available. By use of TCWiSE, a much larger range of wind speeds is obtained, but simulation is computationally unfeasible. By maximum dissimilarity a limited number of scenarios is selected, that covers the whole range of wind speeds, but with unknown return periods. Subsequently, after interpolation with Softmax the water levels for 1000 year of typhoons can be approximated, but now only 50 typhoons had to be simulated which was computationally feasible. For each set of events (i.e. historical, synthetic and representative) the above described limiting factor is indicated in red in Figure 3.17.
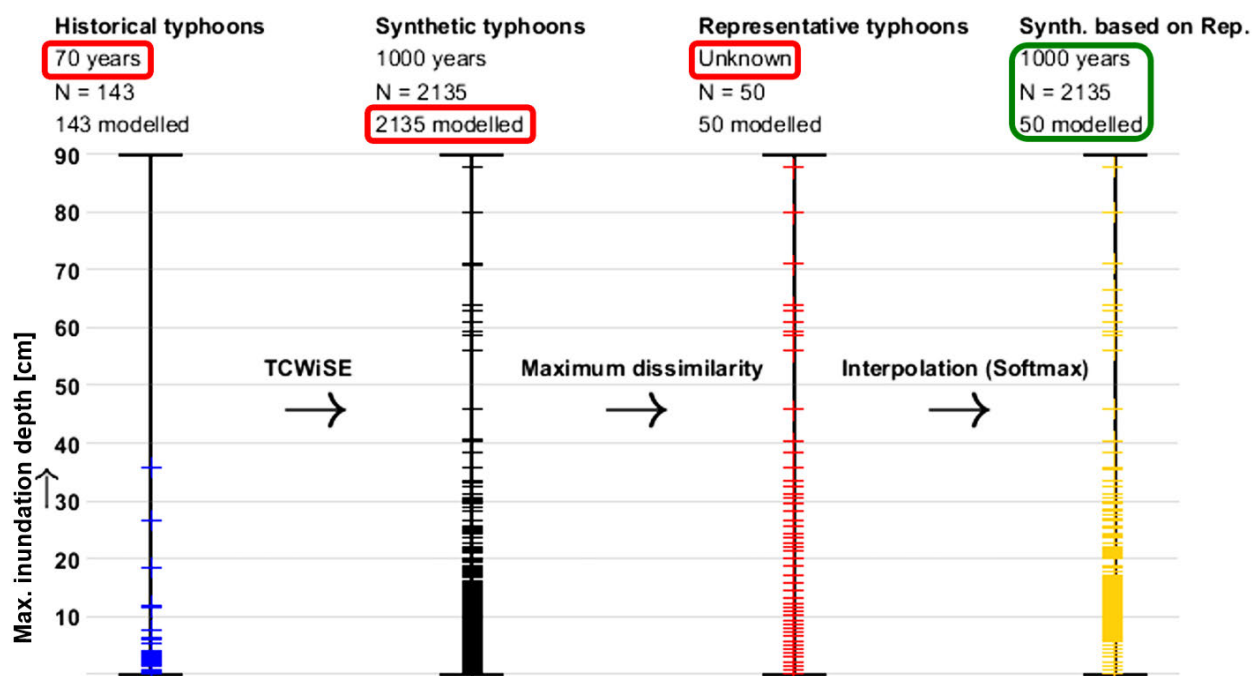
Figure 3.17: *Methodology for typhoon scenario selection. As an example, a (fictional) maximum inundation depth is used on the vertical axis, but any other relevant parameter (e.g. maximum wind speed or forward velocity of the typhoon) could be used.*

To validate that the derived inundation depths based on the selection and interpolation methods are realistic, water levels and wave characteristics determined after interpolation were compared with those based on simulated synthetic tracks. However, following from Table 3.1 in the previous Section, simulation of wave conditions for all synthetic typhoons around Majuro was computationally unfeasible within the scope of this thesis.

Hence for this purpose a second case study was used: Charchenga station, located at the Bay of Bengal in Bangladesh, in the Northern Indian Ocean TC Basin. For this location, simulated water levels and wave conditions for a large set of synthetic typhoons was already available at Deltares (Leijnse et al., 2019, in preparation), making optimization of the interpolation method possible (see Section 3.4.3). A brief description of this study and models used to derive the data for wave conditions and water levels as used in this thesis can be found in Appendix B.3.

While simulation of waves was unfeasible, simulation of only the surge levels for all synthetic typhoons near Majuro was actually feasible as this can be done by use of the relatively fast Delft3D-FLOW model. Hereby it could be verified that the results from the Bangladesh case can also be applied to Majuro (Section 3.4.3).

3.4.1. Synthetic typhoon tracks with TCWiSE

Based on historical typhoon track data for the whole Northwestern Pacific region, 1000 year of typhoon tracks was generated with use of the TCWiSE tool (Hoek, 2017), as described in Section 2.2.1. Typhoon tracks consist of 6 hourly data for:

- Date and time;

- Location of the eye – latitude and longitude coordinate;

- Maximum wind speed of the typhoon.

Genesis and termination locations, wind speeds and tracks of historical and synthetic typhoon tracks were compared. Subsequently, only the typhoons that hit the area of interest – the area as defined in section 3.1 to distinguish typhoon and non-typhoon conditions and the domain of the Delft3D model – were selected. All other typhoon tracks were discarded.

Secondly, TCWiSE was used to obtain 6 hourly wind, air pressure and precipitation fields for the selected tracks, based on the typhoon location and maximum wind speeds. TCWiSE returns wind, air pressure and precipitation fields for spiderweb grids that can be directly used in Delft3D.

3.4.2. Selection of representative typhoons

Representative typhoons were selected from the data set of synthetic typhoons by use of MDA (described in Section 2.4.4). First, relevant parameters to characterize the typhoon were selected. Subsequently the data was normalized and different sets of weight factors were selected.

Selected parameters

To describe the typhoon track, 4 categories of relevant typhoon characteristics were distinguished based on Section 2.2.1. Subsequently, for each of these categories relevant parameters were selected:

- **Full typhoon track** – These parameters are the latitude and longitude coordinates of the start and end points, as well as the latitude and longitude coordinates of points after 1/3 and 2/3 of the duration, see Figure 3.18. In addition, the duration of the full typhoon is included. These parameters are related to the full typhoon track, while the parameters for the other categories are related to the area of interest only.

- **Maximum wind speed** – For each of the typhoon tracks, the maximum wind speed (in space) is defined every 6 hours. Here, the minimum, median and maximum in time of the maximum wind speed in taken. Only the data in the area of interest is used, to prevent the inclusion of

irrelevant wind speeds at large distance of Majuro. Besides, the latitude and longitude coordinates and the distance to Majuro of the point with the maximum wind speed are included, see Figure 3.18.

- **Forward velocity** – Based on the 6 hourly locations of the typhoon, the forward velocity of the typhoon eye is calculated. The minimum, median and maximum in time of the forward velocity are included. Only the data in the area of interest is used.

- **Minimum distance** – For each of the tracks, the minimum distance to Majuro is calculated, Besides, the latitude and longitude coordinates, and the maximum wind speed (in space) of this point are included, see Figure 3.18.

An overview of the above described parameters in all 4 categories can be found in Table 3.2. For some parameters, the choice for the selected category is rather arbitrary as it is actually on the edge of 2 categories (e.g. maximum wind speed at the location with the minimum distance of the typhoon track to Majuro), but they are put in one of the categories anyway to make the use of weight factors per category possible (described below).
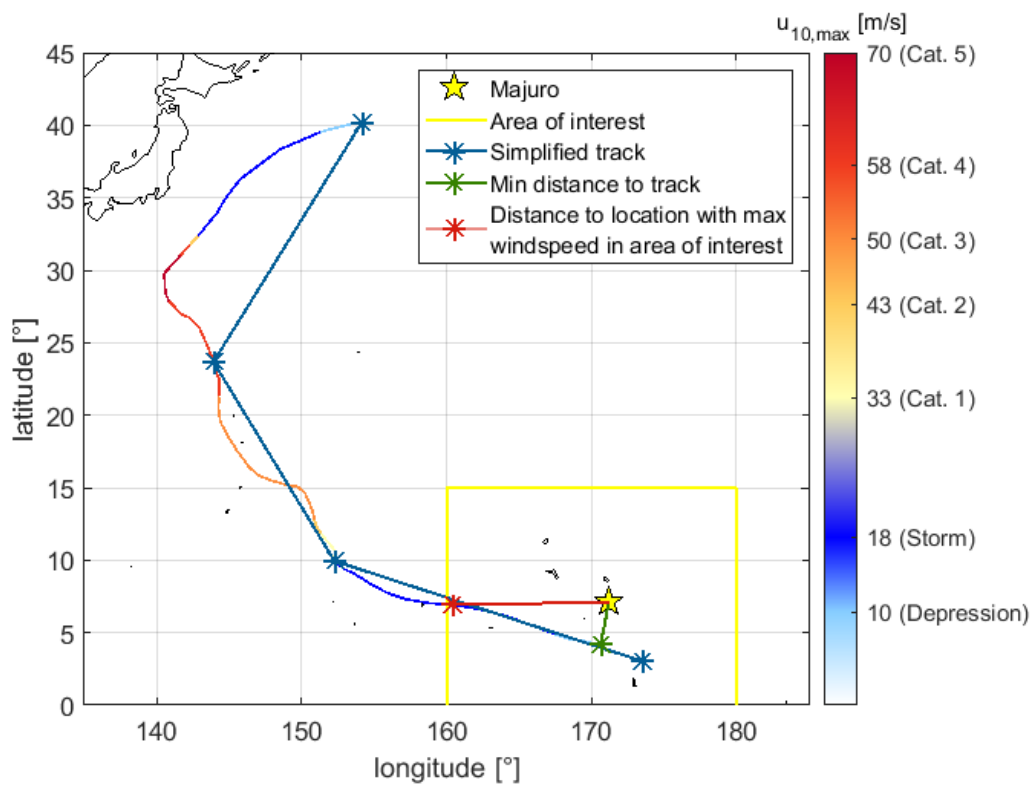
Figure 3.18: *Overview of the used parameters per typhoon track. For the simplified track, the latitude and longitude coordinates of the marked points were used. For the minimum distance to the track and the max, the latitude and longitude coordinates and the distance to Majuro (line) were used.*

Normalization of the data

For each of the typhoons in the synthetic data set, all selected parameters were calculated. Subsequently, for each of the parameters, the data was normalized. In MDA, the distance in the parameter space between all typhoons is calculated, and in the selection process of representative typhoons, each time the typhoon with the maximum distance in the parameter space to the previously selected typhoons is selected (see Section 2.4.4). Hence, if the data would not be normalized, in the calculation of the distance in parameter space, the parameters will not get the same weight.

For example, the longitude coordinates of the starting point are in the order of 170 degrees, while the latitude coordinates of the starting point are in the order of 10 degrees. Hence, if one would calculate

the distance between the starting points of different typhoons, the variation in latitude almost completely determines the variation in distance, while longitude may vary just as much. This problem is overcome by normalization of the data, whereby the minimum value of each parameter is defined as 0 and the maximum as 1.

Weight factors

After normalization, all parameters have the same weight in MDA. However, some characteristics of the typhoon track are described by more parameters than others, which may lead to an unbalanced set of parameters where too much weight is given to some characteristics of the typhoon track. For example, the full track is represented by 9 parameters (i.e. 8 for the location and 1 for the duration), while the characteristics of the minimum distance category are represented by only 4. In case all parameters will have the same weight factor, the difference in location of the full typhoon track is best represented, while actually the local conditions near Majuro may be more important. Hence, weight factors are used to compensate for this.

3 different sets of Weight Factors (W.F.) were tested and compared, in the following order:

- **No W.F.** – all parameters get a weight factor of 1.

- **W.F. per category** – all categories of parameters get a weight factor of 1. However, some parameters that were considered more important in a category got more weight than others in the same category.

- **Final W.F.** – all weight factors per parameter as in the *'weight factor per category'* are used, but a weight factor of 2 was used for the category *'minimum distance'*, as these parameters are most important for the conditions at Majuro.

An overview of the weight factors per parameter can be found in Table 3.2 below. The resulting selected tracks for the 3 different sets of weight factors are compared in Section 4.1.2.
For MDA, the first typhoon track (or starting point in the parameter space) has to be selected and specified. For all 3 sets, the typhoon was selected that was expected to have the most impact at Majuro (i.e. has the lowest minimum distance of all the typhoon tracks to Majuro) and has the highest velocity at that location. These were combined according to formula 3.1 below:

$$\max \sqrt{-1.5 * (Min\ distance)^2 + (Max\ wind\ speed\ at\ location\ of\ min\ distance)^2} \qquad (3.1)$$

The 2 parameters used above were found to be the most important for the conditions at Majuro, and again somewhat more weight was given to the minimum distance (in agreement with the weight factors).

Table 3.2: Overview of the used parameters per typhoon track with Weight Factors (W.F.) as used for the selection of representative typhoon scenarios. The weight factors for each of the 3 tested sets are presented: (1) No W.F. applied, (2) W.F. of 1 per parameter category and (3) Final set of W.F. with more weight to minimum distance category.

Parameter	No W.F.	W.F. per cat.	Final W.F.
Lat coordinate of startpoint	1	1/10	1/10
Lon coordinate of startpoint	1	1/10	1/10
Lat coordinate of point at 1/3 of duration	1	1/10	1/10
Lon coordinate of point at 1/3 of duration	1	1/10	1/10
Lat coordinate of point at 2/3 of duration	1	1/10	1/10
Lon coordinate of point at 2/3 of duration	1	1/10	1/10
Lat coordinate of endpoint	1	1/10	1/10
Lon coordinate of endpoint	1	1/10	1/10
Duration	1	1/5	1/5
Total for full typhoon track category	**9**	**1**	**1**
Minimum max windspeed in area of interest	1	1/9	1/9
Median max windspeed in area of interest	1	1/9	1/9
Maximum windspeed in area of interest	1	1/3	1/3
Lon coordinate of maximum max windspeed in area of interest	1	1/9	1/9
Lat coordinate of maximum max windspeed in area of interest	1	1/9	1/9
Distance of location with maximum windspeed in area of interest to Majuro	1	2/9	2/9
Total for maximum windspeed category	**6**	**1**	**1**
Minimum forward velocity in area of interest	1	1/2	1/2
Median forward velocity in area of interest	1	1/4	1/4
Maximum forward velocity in area of interest	1	1/4	1/4
Total for forward velocity category	**3**	**1**	**1**
Minimum distance of track to Majuro	1	2/7	4/7
Lat coordinate of minimum distance of track to Majuro	1	1/7	2/7
Lon coordinate of minimum distance of track to Majuro	1	1/7	2/7
Maximum windspeed at the location with minimum distance of track to Majuro	1	3/7	6/7
Total for minimum distance category	**4**	**1**	**2**

3.4.3. Interpolation with Softmax

To get the water levels for all synthetic typhoons, interpolation is needed. Here, weighted interpolation by use of the Softmax function as described in Section 2.4.5 is used. Again, the distance between the normalized parameters as calculated in the previous section for the scenario selection is used. When obtaining the water level for a synthetic track based on the representative tracks, more weight is given to tracks with the lowest distance in the parameter space. Interpolation is done for the inundation depth in each of the grid cells in the XBeach model independently. Subsequently, the inundation depths for different return periods can be determined per grid cell by extreme value analysis, to generate flood maps.

In the Softmax function, a parameter β is present. A higher value of β means relatively more weight is given to the closest representative typhoon, while a lower value of β means more typhoons are used in the interpolation. Figure 3.19 below shows the concept of Softmax interpolation based on 2 parameters (i.e. latitude and longitude coordinates of the starting point of the typhoon), for different values of β. In the actual interpolation, all 22 parameters with the weight factors as described in Table 3.2 are used.
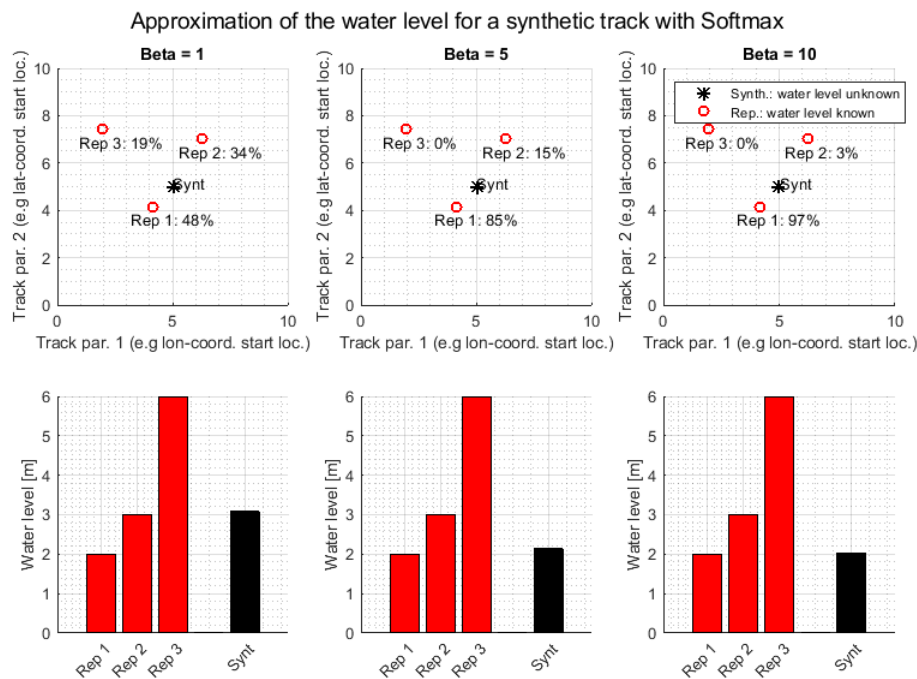
Figure 3.19: *Concept of weighted interpolation by use of Softmax and the influence of the Beta factor. This example shows a simplified case where the water level for 1 synthetic typhoon is determined based on 2 parameters (2D) and 3 representative typhoons. For the actual interpolation, 50 representative typhoons and 22 parameters are used to estimate the water levels in each of the 2135 synthetic typhoons that were not modelled.*

Estimating β by wave conditions and surge levels for Charchenga Station (Bangladesh)

The β factor clearly has a significant influence on the estimated inundation depths. Hence the choice of the value for β is based on an additional case study where simulated water levels and wave heights for a set of synthetic Tropical Cyclones was already available: Charchenga Station in Bangladesh. The required data for this location was already available at Deltares (Leijnse et al., 2019, in preparation) and this case study is described in Appendix B.3.

β values of 1 to 100 were tested to find the optimal value. The influence of the number of representative TCs used is assessed as well. In addition, after finding the optimal β, the interpolation was done based on historical TCs instead of the representative TCs, to validate that making the selection indeed leads to a better estimate of all inundation depths. The results can be found in Section 4.1.3.

In many perspectives the Charchenga Station case study is similar to the Majuro case. For this area a large set of synthetic typhoons was generated by use of TCWiSE and water levels and wave heights were simulated for all synthetic TCs individually by use of a Delft3D-FM model coupled with SWAN (Leijnse et al., 2019, in preparation). However, there are some important differences as well. Charchenga station is not located on an island surrounded by the deep ocean such as Majuro. Tropical Cyclones mainly come from one side (i.e. the ocean) and a large shelf is present at Bay of Bengal, which allows for much higher surge levels. Hence, additional checks are needed when results for Charchenga station are translated back to the Majuro case study.

Verification by surge levels for Majuro

To verify that the interpolation method with the value of β derived in the Bangladesh case also works for the Majuro case study, water levels were simulated for all synthetic typhoons. This was done by use of the large scale Delft3D-FLOW model without the nested grids, see Section 3.3.2 for the used configuration. Subsequently, derived surge levels offshore for the synthetic typhoon tracks could be compared with the surge levels based on the representative tracks and interpolation. This was done for an offshore location, north of Majuro, see figure 3.1 for the location.

3.5. **Scenario derivation for non-typhoon conditions**

To derive a set of representative scenarios for non-typhoon conditions, a similar approach was used as for the typhoon conditions (see Figure 3.17). However, there are some important differences as well. An overview of the main steps is given below:

1. Offshore wave conditions in **historical data** (ERA5 data, see section 3.2.3) are translated to the location of the oceanic boundary of the XBeach model by use of the SWAN model (Section 3.5.1). Extreme value analysis of precipitation data was done (Section 3.5.2). All data for periods with typhoon conditions was excluded from the historical data sets.

2. Based on the nearshore historical data, 1000 years of **synthetic data** for wave conditions and surge is generated by use of a Bayesian Network (BN) in Uninet. Subsequently, BEWARE is used to select only those events that can potentially lead to flooding. In addition, 1000 years of synthetic precipitation data is generated by sampling from the extreme value distribution. Precipitation was assumed to be independent of the wave and surge conditions. This is further elaborated in Section 3.5.3.

3. **Representative scenarios** are selected from the data set of synthetic events that can potentially lead to flooding, again by use of maximum dissimilarity (Section 3.5.4). These scenarios were simulated in XBeach, and the maximum inundation depths per event were determined.

4. The inundation depths for all synthetic events that can potentially lead to flooding were again determined by **interpolation with Softmax** (Section 3.5.4).

5. Inundation depths for different return periods were determined per grid cell by extreme value analysis. Subsequently **flood maps** were made.

Thus the same steps are followed as for the typhoons, but partially in different order:

- The moments that offshore conditions are transformed to nearshore conditions (i.e. by SWAN and Delft3D models) is different. For the typhoon conditions, this is done before the generation of synthetic data and selection of representative scenarios, while for the non-typhoon scenarios this is done after those steps.

- For the non-typhoon conditions, an event is defined as 1 day, while for the typhoon conditions an event has the duration of the typhoon, although in the XBeach model only the peak ±24 hour is modelled. Hence, the duration of events, and the moments that relevant events are selected differ.

During non-typhoon conditions, main flood drivers were identified to be (oceanic swell) waves and precipitation, but water levels (i.e. mainly tide and little surge) are important as well. Extreme values distributions were determined for daily data (i.e. cumulative precipitation, maximum wave height and period, mean wave direction, maximum surge), as only daily data was available for all the required parameters. Hence, generated synthetic data is also per day.

In spite of that, the variation over a day is important as well, especially as there can be a time lag between maximum precipitation rate and maximum surge level. As a consequence of using daily values, the variation over a day is not present in the synthetic data. For precipitation rates, these are approximated by using a standard event based on analysis of historical events. Wave conditions and surge levels vary more slowly and were assumed constant over the full day. In order to be consistent with typhoon conditions, a random tide is used.

3.5.1. **Nearshore conditions**

The SWAN model was used to transform the ERA5 wave data (Section 3.2.3 to the nearshore wave conditions. The 5 locations where the B.C. of the XBeach model were specified as output points for the SWAN model. Nearshore surge levels were assumed to uniform along the oceanic boundary of the XBeach model (as for the typhoon conditions) and the data in the offshore ERA5 output point near Majuro was used, see Section 3.2.4. Time frames during typhoon conditions were excluded

from the data.

Subsequently, Generalized Extreme Value (GEV), Gumbel, Weibull, Gamma, Log-Normal and Normal distributions were fitted to the daily maxima of the significant wave height at each of the locations independently, and to the surge levels, see Appendix A.2.2.

3.5.2. Precipitation

For precipitation during non-typhoon conditions, daily precipitation rates for different return periods were determined by use of extreme value analysis, see Figure 3.4. Various extreme value distributions were fitted and compared. Generalized Extreme Value (GEV), Gamma distribution and Log-Normal distributions were fitted to the annual maximum precipitation rates, see Appendix A.3.1. The GEV distribution was selected as best fit to the annual maximum precipitation rates, but seems to underestimate the precipitation rates for low return periods.

Hence, the Generalized Pareto (GP) distribution was fitted to all data points above the threshold value of 49.5 mm/day, derived in Section 3.2.2. Besides, the Langbein correction (see Section 2.4.1) was applied to the GEV distribution for return periods < 10 years, to prevent underestimation of the precipitation rates for lower return periods, and both were compared. The results can be found in Section 4.2.2.

Variation over a day and standard event

In the above section, daily precipitation rates were determined. However, at Majuro precipitation events are often very momentary, and this influences the inundation depths. If all the precipitation of a certain day falls in a very short period of time (e.g. in an hour), inundation depths will be higher than if the precipitation is evenly spread over the day. Therefore, insight is needed in the distribution of precipitation over a day, after which these can be schematized into a standard event.

The hourly precipitation rates measured at Majuro WBAS airport station is the best available data for this, as higher frequency measurements were not available. As daily measurements during non-typhoon conditions were used to determine the daily rates for different return periods, the distribution over a day during non-typhoon conditions is needed. Hence first all hourly data on days with typhoon conditions is filtered out. Peak precipitation is not always in the same hour of the day. Therefore, for each day, the hour with the highest precipitation rate [mm/hour] is selected as hour zero, and all other hours of that day are added before and after.

As especially the events with high precipitation rates are important for flooding, those should be well represented by a standard event. To prevent an disproportional influence of days with little precipitation, a threshold value was chosen for the cumulative precipitation on a day. The influence of the threshold is elaborated in Appendix A.3.3. Again value for the threshold of 49.5 mm was chosen, whereby on average one event per month was included. By doing so, sufficient data was included to get a realistic average, while the most extreme events are represented as well. See Figure 3.20 below.
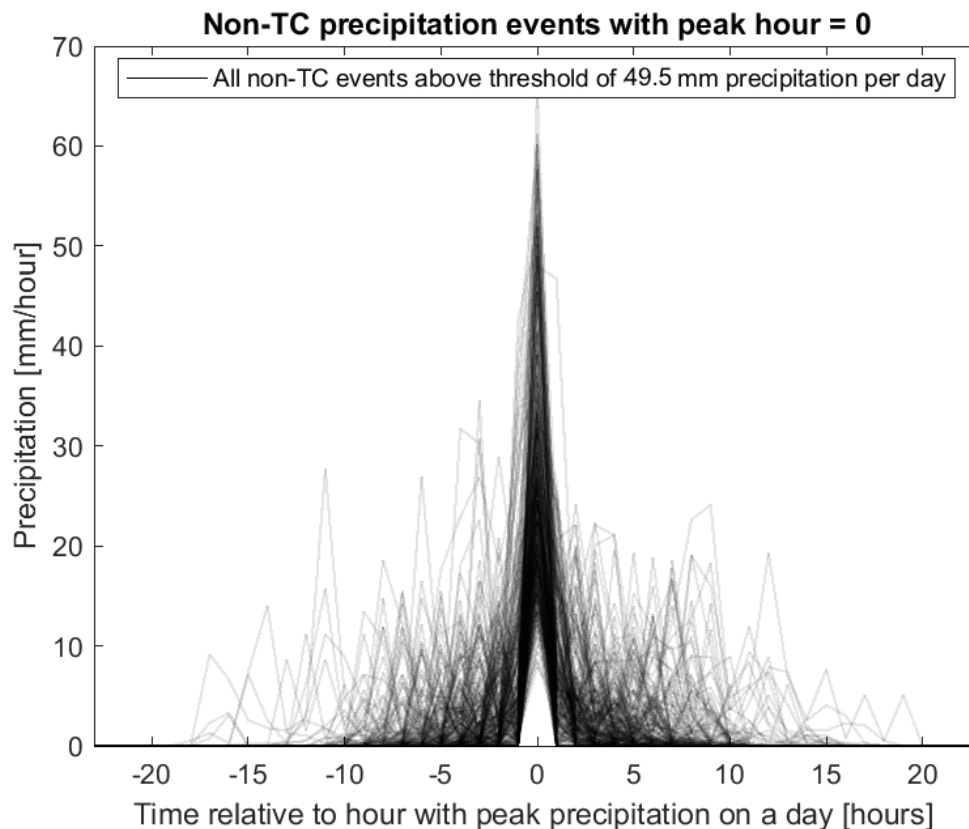
Figure 3.20: *Precipitation distribution over a day, only the days with a cumulative precipitation above the threshold value of 49.5 mm/day are included. The value of the threshold was chosen such, that on average one event per month is included. Clearly, non-typhoon precipitation events are very momentary.*

Subsequently, for all days the events were normalized to the hour with peak precipitation, standard deviations were determined as well for each hour. Only the middle 24 hours were selected. Finally, the distribution over the day was determined as fraction of the total. See Appendix A.3.3 for more details.

3.5.3. Synthetic data generation

Based on the historical data, 1000 years of synthetic data was generated in order to include the full range of conditions that can potentially lead to flooding. Each event was defined as one day, and there are 365250 days in 1000 years. In the historical data, 7.8% of the days was filtered out as being typhoon conditions, meaning 92.2% of the days consisted of non-typhoon conditions. Hence, in 1000 years of typhoon conditions, 336747 days with non-typhoon conditions are present.

Therefore, 336747 synthetic events were generated. For wave conditions and surge, this was done by use of a Bayesian Network in the software Uninet (described below). Precipitation during non-typhoon conditions and tide were assumed to be independent of the surge and wave conditions and were determined separately. Subsequently BEWARE was used to select only those events that can potentially lead to flooding.

Precipitation was not included in the Uninet and assumed to be independent from the wave conditions and surge. In reality some correlation between precipitation rates and for example surge levels may be found as both are to some extent related to the local air pressure, but specification of the GEV with Langbein correction or GP distribution in Uninet was not possible. Daily precipitation rates could be sampled directly from the fitted distribution based on the peak over threshold approach (see Section 3.5.2). However, these sampled events occur on average ones every month. Only on 2.92% of the days such precipitation event was present, these days were selected ran-

domly. For all other days, cumulative precipitation rates are lower and these were not included in the analysis for flooding.

For the tide, a random time series was constructed by selecting a 1000 year period and obtain the associated predicted offshore water levels from the Global Tide and Surge Model (Section 3.2.4), and could thereby be specified with a 30 min interval. This tidal water level was subsequently added to the surge level at the boundary that was derived by Uninet.

Uninet

Uninet is a stand alone program used for stochastic modelling and multivariate data mining by use of Bayesian Networks (BNs). A distinguishing feature of Uninet is that nodes may be assigned arbitrary as continuous or discrete distributions (UNINET Help, nd). Uninet version 2.97.9 was used.

In Uninet, first the set of variables with their marginal distributions have to be specified, these are the nodes. Subsequently, the connections between the nodes have to be specified to capture the conditional relations. Probabilistic influence between different nodes is represented as conditional rank correlation. The joint probability density for the probabilistic nodes is built by use of Joint Normal copulas, to realize the dependence relations. Only Joint Normal copulas can be used in Uninet. Finally, Monte Carlo sampling of the entire joint distributions can be done to obtain a synthetic data set. For further details, the reader is referred to the manual for Uninet (UNINET Help, nd).

Historical data for wave conditions and surge was uploaded to Uninet whereafter distributions were specified per parameter. In agreement with Section 3.5.1, Weibull distributions were selected for the significant wave height (H_s) for locations C-G, and a Normal distribution was selected for the surge. For the peak wave period (T_p) and Mean Wave Direction (Dir), empirical distributions were selected.

For each location where wave conditions were specified, the H_s, peak wave period and mean wave direction were connected. H_s of each location was connected to the H_s of the nearest location(s). The same was done for the mean wave direction. The surge was connected to H_s at all locations. Subsequently, the 336747 samples were generated with the BN in Uninet. Historical and synthetic data were compared to validate that the generated synthetic events are realistic. See Section 4.2.3 for the resulting network and synthetic data 4.2.3.

Runup based on BEWARE

Bayesian Estimator for Wave Attack in Reef Environments (BEWARE; Pearson, 2016; Pearson et al., 2017) tool is a Bayesian Network based tool that was built by use of pre-computed XBeach model simulations. Hereby, it is several orders of magnitude faster than running numerical models such as XBeach itself. It can be used to estimate various parameters at the shoreline in reef environments, based on simplified reef profiles and offshore wave conditions and water levels. See Figure 3.21 below for an overview of the used configuration.

BEWARE was used to give a value of the most probable (binned) value of the runup ($R_{2\%}$ at the shoreline, based on the conditions at the boundary of the XBeach model. BEWARE returns binned values (e.g. -4 to 0 or 0 to 1, etc.), the bins can as well be found in Figure 3.21.
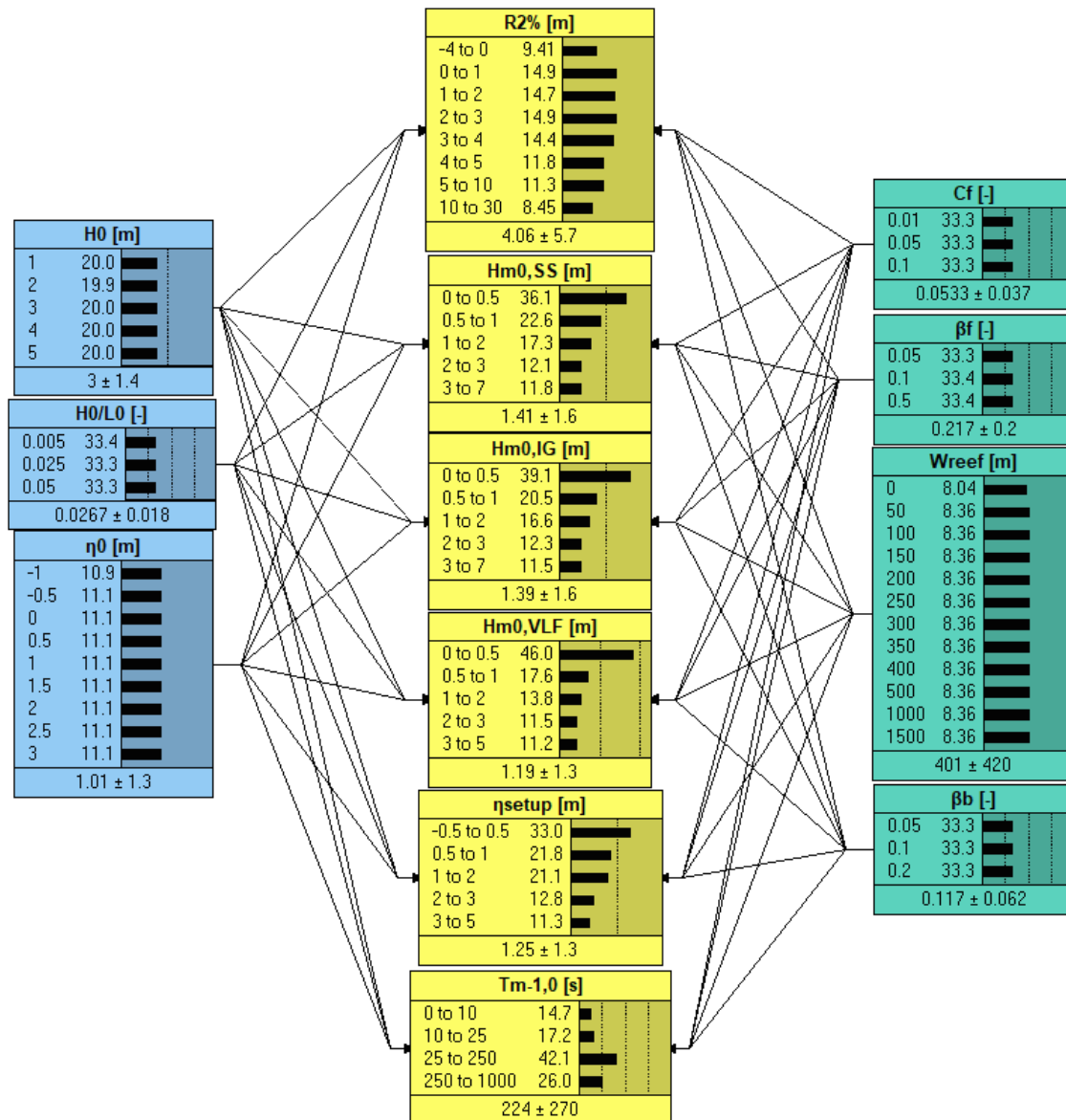
Figure 3.21: *Overview of the used configuration of BEWARE (Pearson, 2016; Pearson et al., 2017). Parameters that characterize the offshore wave conditions (i.e. significant wave height H0 and wave steepness H0/L0) and water level η relative to the reef flat are shown in blue. Parameters that characterize the reef (i.e. bottom firction Cf, Fore reef slope βf, Width of reef flat Wreef and beach slope βb) are shown in green. Runup (R2%, in yellow) is the parameter that was used to predict if the conditions can potentially lead to flooding. Other parameters in yellow were not used.*

Estimated runup levels were determined for all synthetic events, for each of the cross sections C-G as specified in Figure 3.14. To be able to estimate the reef parameters as used in BEWARE, simplified reef profiles were made for cross sections C-G, see Figure 3.22.

In all cross sections, reefs flats were approximately 0.5 m below MSL. Hence, a water level of 0.5 m had to be added to the offshore water levels in BEWARE. The resulting $R_{2\%}$ values are also relative to the level of the reef flat. Hence, half a meter should be subtracted of those estimates to get the $R_{2\%}$ relative to MSL. Reef width and fore reef and beach slopes vary per cross section, see Table 3.3 below. For bottom friction, a C_f of 0.02 was used for all cross sections (same as in the XBeach model).
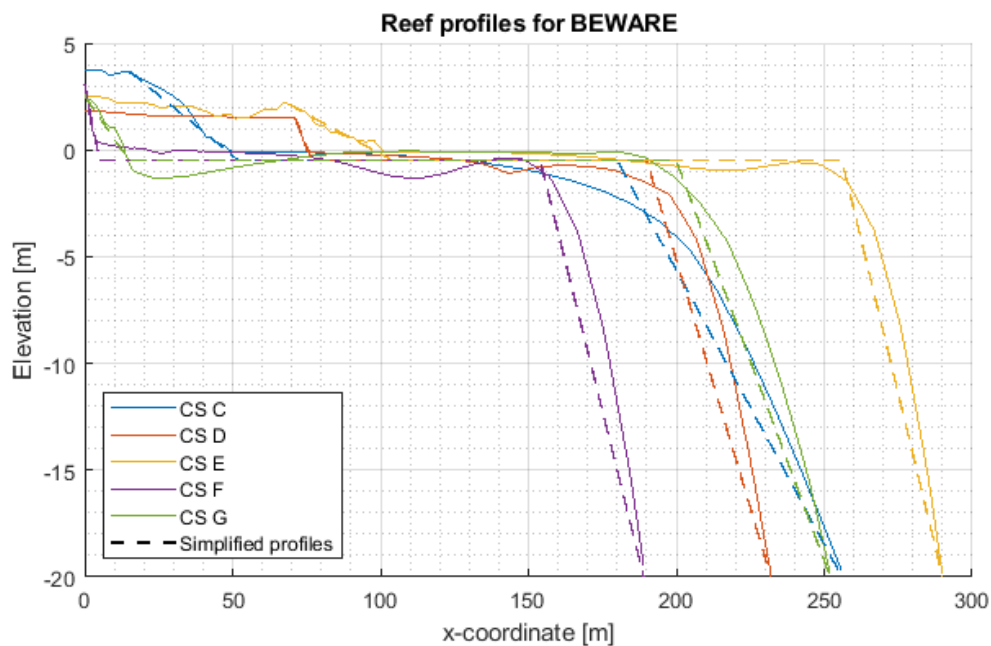
Figure 3.22: *Simplified reef profiles for the reefs in cross sections C-G as used in BEWARE.*

Table 3.3: *Overview of the parameters as used in BEWARE, based on the simplified cross sections C-G. Besides, the beach crest level is included (relative to MSL), which is used to determine the runup level for which potential flooding can occur.*

Cross section	Beach crest level [m]	Beach slope [-]	Reef flat width [m]	Fore reef slope [-]
C	3.7	0.25658	128	0.11351
D	1.5	0.46429	113	0.33333
E	2.14	0.57353	152	0.07543
F	3.11	0.55714	149	0.722
G	2.5	0.375	185	0.2

Selection of potential flood conditions

Based on the runup estimates in BEWARE, only the offshore conditions that may actually lead to coastal flooding could be selected. Only those events with an estimated $R_{2\%}$ > 3.5 m (relative to MSL) **or** cumulative precipitation above 49.5 mm **or** both were selected. Although this value of 3.5 m as threshold for the $R_{2\%}$ seems relatively high, it was chosen such that again on average about one event per month was included, just as with the precipitation. These events form the synthetic data set of events that can potentially lead to flooding.

The same approach with BEWARE to select the events that can potentially lead to flooding was applied to the historical data, to make comparison of the historical events, synthetic events and representative events possible.

3.5.4. Scenario selection and interpolation

Just as for the typhoon conditions, 50 representative scenarios were selected from the synthetic data. Scenario selection and interpolation were done in the same way as for the typhoon conditions in Section 3.4.2, but different parameters and weight factors were used. 3 categories of parameters were distinguished:

- **Precipitation** – here only the cumulative precipitation per day was used.

- **Water level** – here only the maximum total water level was used, being the combination of the maximum water levels due to tide and surge.

- **Wave conditions** – here the maximum significant wave height, peak period, and mean wave direction parameters, for all 5 locations (C-G) were used.

In this case, only a weight factor of 1 per category was used, as a good representation of all categories in the representative scenarios is important. In the wave conditions category, the significant wave height was considered to be more important than the peak wave period and mean wave direction. An overview of the used parameters and weight factors can be found in Figure 3.4 below.

For the starting point again one of the events that was expected to lead to the most severe flooding was selected. For the non-typhoon conditions, the event with the combined maximum of the normalized cumulative precipitation per day and maximum offshore water level per day was used. The resulting scenarios and a comparison of the historical, synthetic and representative events can be found in Section 4.2.4

Interpolation with Softmax was done according to the same method as for the typhoon conditions, as can be found in Section 3.4.3, but now the parameters with weight factor as described in Table 3.4 were used. For the β parameters, the same value as found for the typhoon conditions was used. Flood maps for different return periods were also derived according to the same approach.

Table 3.4: Overview of the used parameters per non-typhoon scenario with Weight Factors (W.F.) as used for the selection of representative scenarios.

Parameter	W.F. per cat.
Cumulative precipitation per day	1
Total for precipitation category	1
Maximum offshore water level per day	1
Total for water level category	1
Maximum Hs per day at C	1/10
Maximum Hs per day at D	1/10
Maximum Hs per day at E	1/10
Maximum Hs per day at F	1/10
Maximum Hs per day at G	1/10
Maximum Tp per day at C	1/20
Maximum Tp per day at D	1/20
Maximum Tp per day at E	1/20
Maximum Tp per day at F	1/20
Maximum Tp per day at G	1/20
Mean Dir per day at C	1/20
Mean Dir per day at D	1/20
Mean Dir per day at E	1/20
Mean Dir per day at F	1/20
Mean Dir per day at G	1/20
Total for wave conditions category	1

4

Results – Scenarios

Chapter summary

- In this chapter the results of the synthetic data generation, scenario selection, and interpolation methods are presented. For the typhoon conditions, first the synthetic typhoons derived by use of the TCWiSE tool are presented. Subsequently, the results for the 3 different configurations, used to select 50 representative typhoons are presented and compared. The influence of the number of representative typhoons, and the influence of the β parameter for interpolation by Softmax were assessed by use of a Bangladesh case study. The resulting combination of selection and interpolation methods was verified by use of the water levels for Majuro. Finally, the resulting set of representative typhoon scenarios – for which the inundation depths were simulated in XBeach – is presented in combination with the optimized parameter for Softmax interpolation.

- For the non-typhoon conditions, first the nearshore wave conditions based on SWAN are presented. Subsequently the synthetic data is elaborated, as generated by use of the results of the precipitation analysis in combination with the Bayesian Network made in Uninet. By use of BEWARE and a threshold for the precipitation, only the events that potentially may lead to flooding are selected. From this set of events, subsequently the 50 representative events were selected. For these 50, the inundation depths were simulated in XBeach.

4.1. Typhoon conditions

In this Section, the results of the different steps taken to select a set of representative scenarios for the typhoons are presented, according to the method described in Section 3.4.

4.1.1. Synthetic typhoons

Based on 71 years of historical typhoon track data, a synthetic data set with a time series of 1000 years of typhoon tracks was created for the whole Northwestern Pacific basin by use of TCWiSE. Each typhoon track contains 6 hourly data for the location (latitude, longitude), maximum wind speed and a timestamp. See Figure 4.1 below for the resulting tracks.
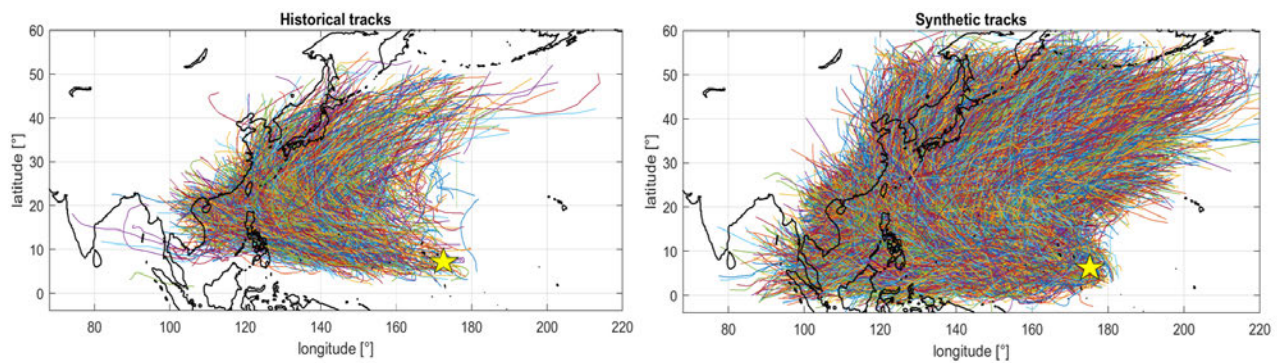
Figure 4.1: Left: 1464 historical typhoon tracks (71 years of data) in the Northwestern Pacific basin used as input in TCWiSE. Right: 20822 synthetic typhoon tracks (1000 years of data) for the Northwestern Pacific basin as derived by use of TCWiSE.

The synthetic typhoon tracks in general seem realistic in terms of track location, duration and distribution over the area compared to the historical data. However, a number of tracks crosses the equator by a few degrees into the southern hemisphere, which is not observed in the historical data and physically not realistic. As cyclogenesis often occurs around Majuro, also the density of the genesis locations of the historical and synthetic typhoons is compared, see Figure 4.2 below. The genesis locations seem to be largely similar.
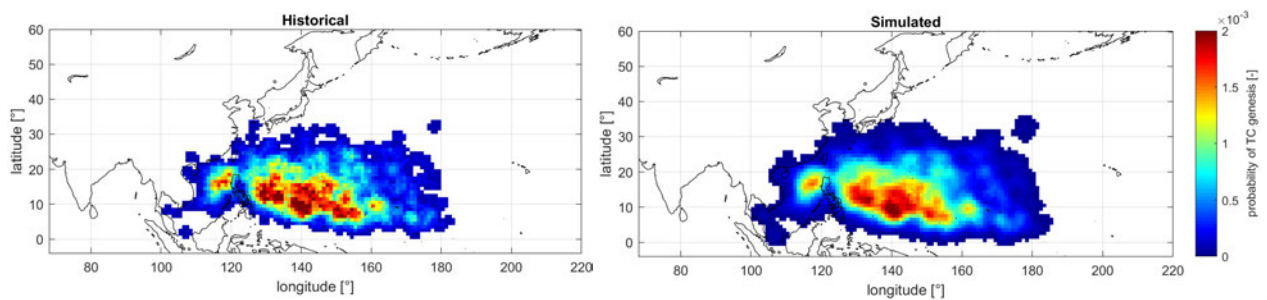
Figure 4.2: Left: Genesis location density of the historical typhoon tracks. Right: Genesis location density of the synthetic typhoon tracks.

A large part of the synthetic typhoons is not directly relevant for flood hazard at Majuro. Only those typhoons that hit the area of interest, as defined in Section 3.1, were selected for the remainder of the analysis. This resulted in a set of 146 historical typhoon tracks and 2135 synthetic typhoon tracks, see Figures 4.3 and 4.4 below.

Generally speaking, typhoons that pass Majuro move in northwestern direction and gain strength while they move in that direction. Cyclogenesis of a significant part of the selected typhoons takes place northwest of Majuro, whereafter they move in northwestern direction and thus not directly pass Majuro.
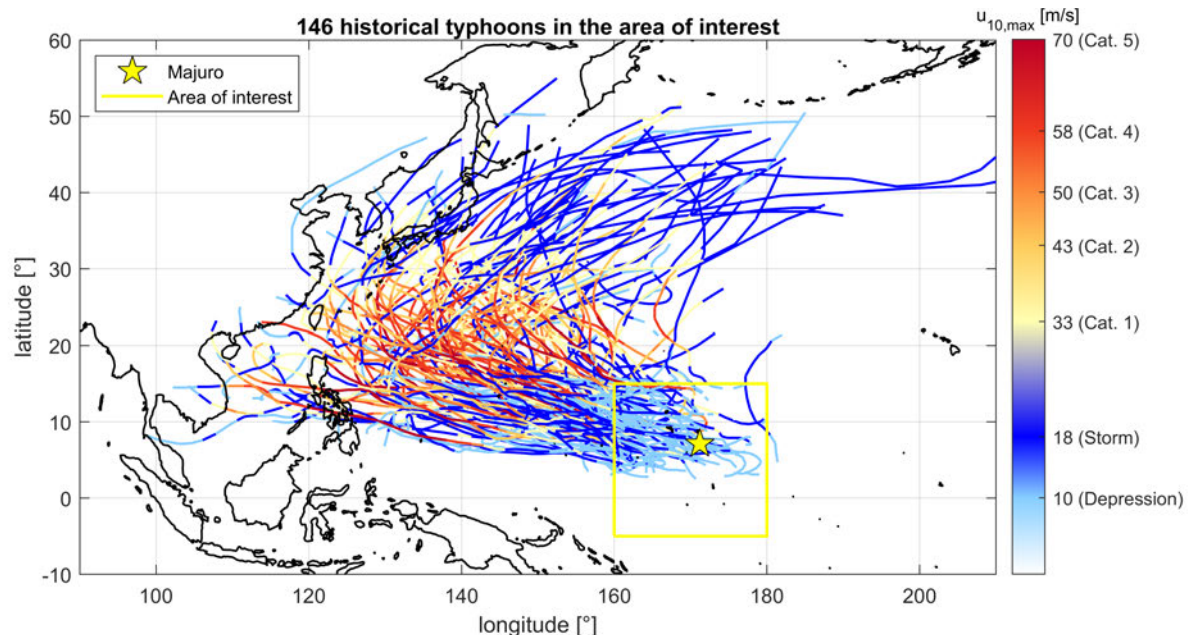
Figure 4.3: *The tracks of the historical typhoons that hit the area of interest (yellow box area). Only these historical tracks are used in the remainder of the analysis.*
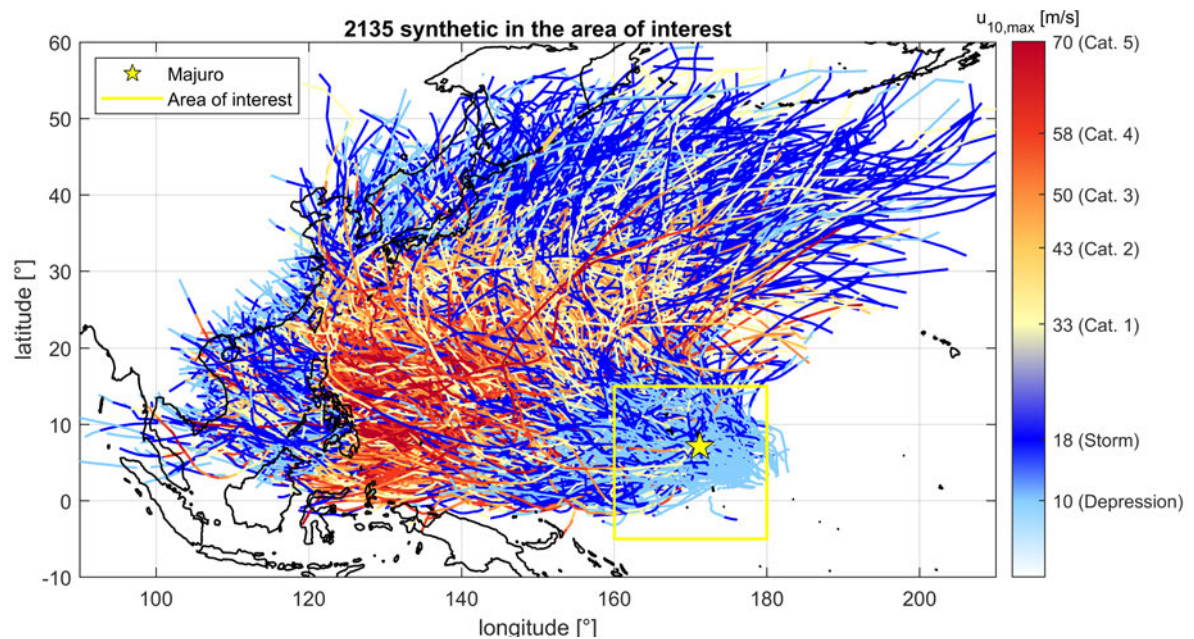
Figure 4.4: *The tracks of the synthetic typhoons that hit the area of interest (yellow box area). Only these synthetic tracks are used in the remainder of the analysis.*

Where the tracks consist only one value for the maximum wind speed at each point on the track, spatially varying wind, air pressure and precipitation fields are needed in the the area of interest as input for models. For those typhoons that hit the area, spiderweb grids with spatially varying fields were made, again by use of TCWiSE. Figure 4.5 gives an overview of the maximum wind speeds in the area based on the wind speeds in the spiderweb grids, for 71 years of historical typhoons and 1000 years of synthetic typhoons.

The larger synthetic data set clearly represents the spatial variation better, although the individual tracks of the typhoons are still visible as strong typhoons are relatively rare in this area. The

maximum wind speeds for the synthetic typhoons are higher, as these are based on 1000 years of data instead of 71. Typhoons are more frequent and more intense in the northwestern part of the area of interest.
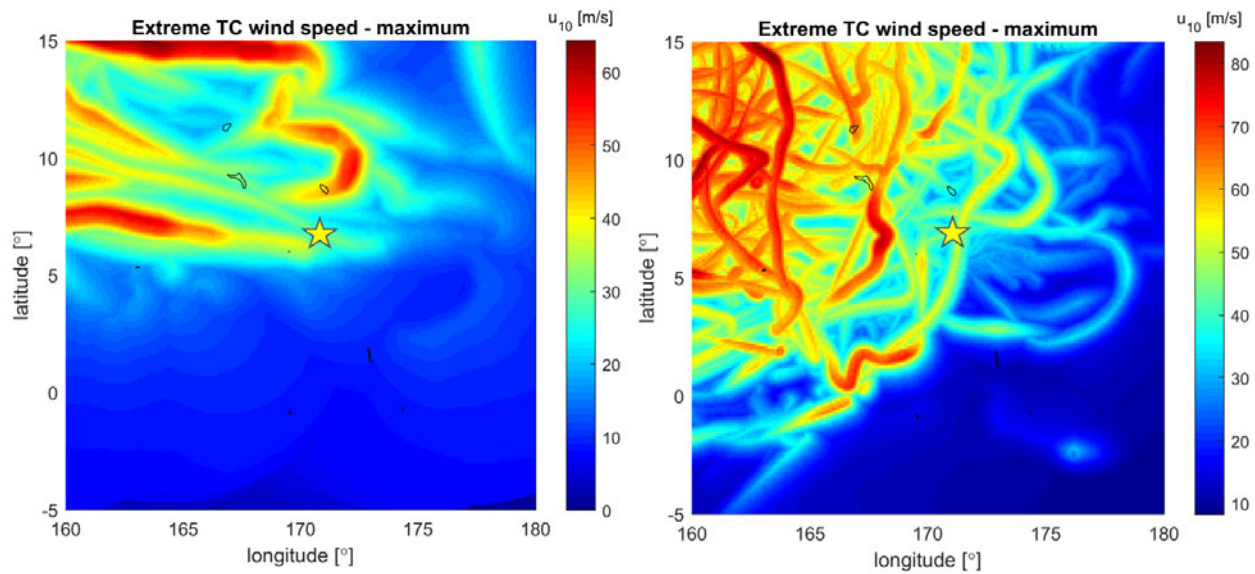
Figure 4.5: *Maximum wind speeds in the area around Majuro for the historical (left) and synthetic (right) typhoons.*

4.1.2. Selection of representative typhoons

As the simulation of inundation depths at Majuro for all synthetic typhoons was not feasible, representative typhoons were selected. In this Section, the resulting sets of representative typhoon scenarios are presented and compared for 3 different sets of weight factors:

A. No weight factors – see Figure 4.6.

B. Weight per parameter category – see Figure 4.7.

C. More weight to local parameters. – see Figure 4.8.

Only the typhoon tracks and maximum wind speed in the area of interest versus the minimum distance between Majuro and the typhoon track are presented and can thereby be compared, while the representative typhoons are selected by use of 22 parameters. Only these (combination of) parameters are shown, as they combined give a good impression of distribution of selected representative tracks over the parameter space. Additional combinations of the used parameters can be found in Appendix C.1. See Section 3.4.2 for an overview and description of all parameters and the weight factors for case A, B and C.

The distribution of data over the parameter space and the marginals of the historical and synthetic data should be similar, as the synthetic data should be a longer realization of the current typhoon climate. In contradiction, distribution of data over the parameter space and the marginals of the representative typhoons should be more uniform, to represent all possible scenarios.

Following from Figures 4.6, 4.7 and 4.8 below, the synthetic data is indeed very similar to the historical data, although the marginals for minimum distances is slightly differ. Clearly, for all 3 sets of weight factors, the representative typhoons are much more equally distributed over the area (left side of the figures) than the historical typhoons. The same applies to the maximum wind speed and minimum distance parameters (right side of the figures below).
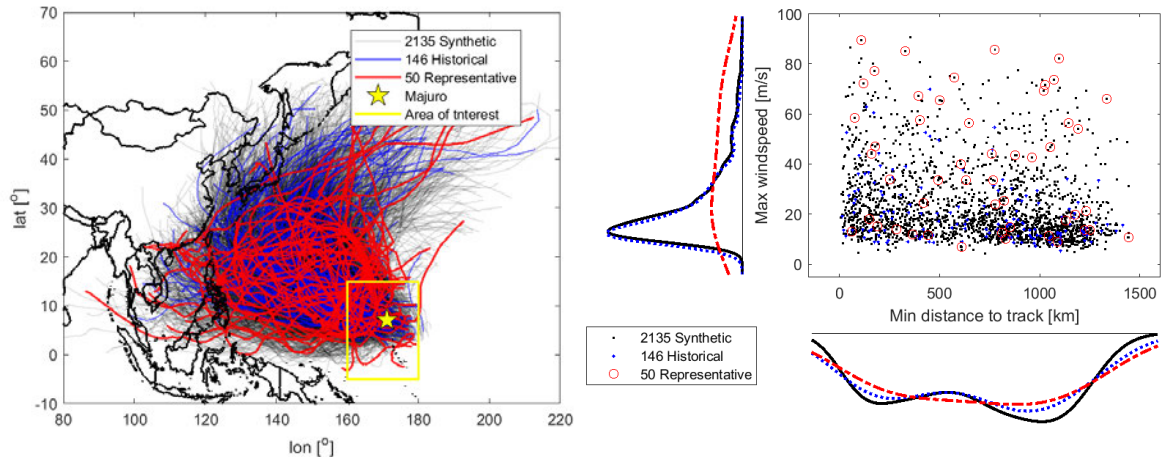
Figure 4.6: *Overview of the historical, synthetic and selected representative typhoon tracks based on the case A. No weight factors. The typhoon tracks (left) and maximum wind speed versus the minimum distance to Majuro (right) are shown.*
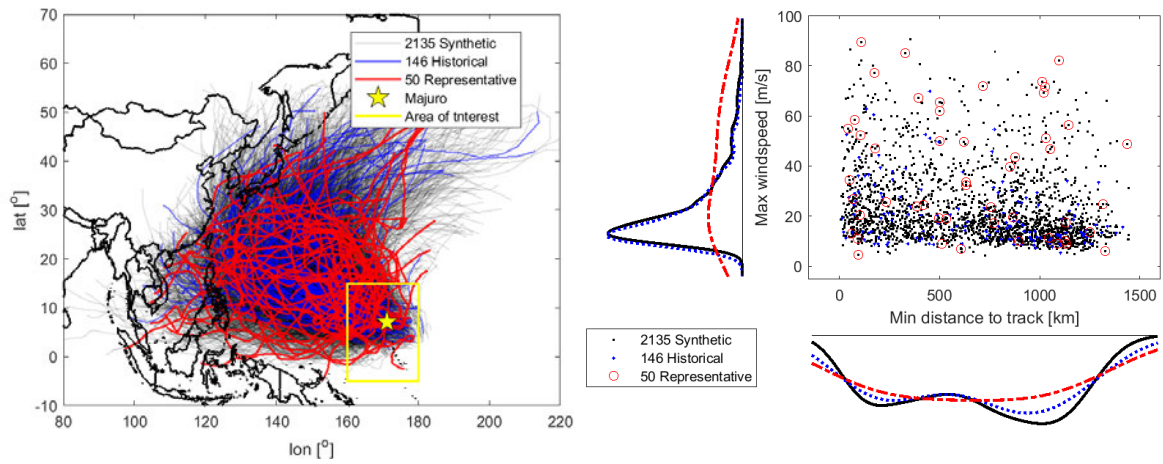
Figure 4.7: *Overview of the historical, synthetic and selected representative typhoon tracks based on the case B. Weight factor per parameter category. The typhoon tracks (left) and maximum wind speed versus the minimum distance to Majuro (right) are shown.*
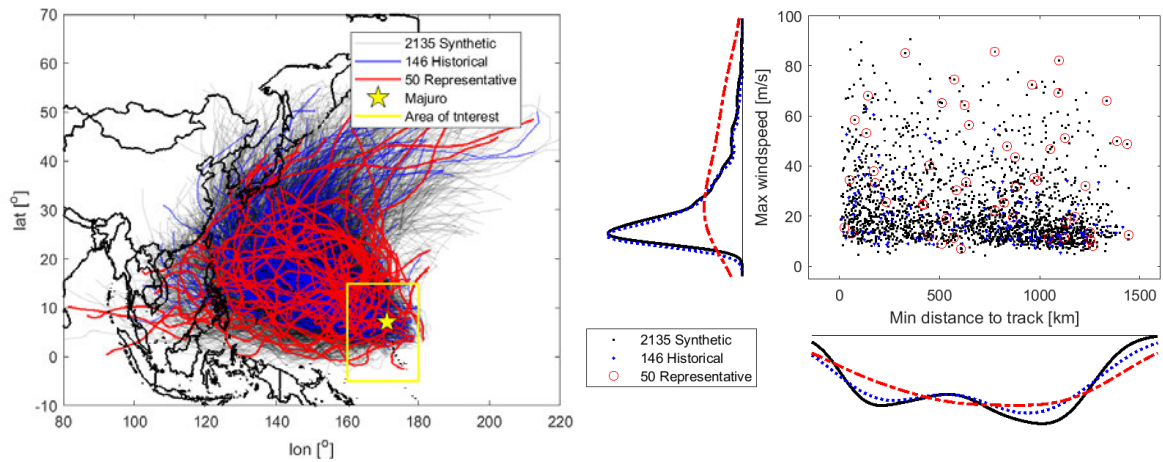
Figure 4.8: *Overview of the historical, synthetic and selected representative typhoon tracks based on the case C. More weight to local parameters. The typhoon tracks (left) and maximum wind speed versus the minimum distance to Majuro (right) are shown.*

By definition, the used maximum dissimilarity algorithm (see Section 2.4.4) makes a selection of representative events that are the most uniformly distributed as possible over the distances in the 22 normalized and weighted parameter space. As only the distribution over a part of the used parameters are shown for comparison – instead of the full 22 parameter case – the actual distribution can be expected to deviate from the uniform distribution. This makes comparison based on only a few parameters complicated.

Nevertheless, the marginals and distribution in 2D parameter space of the representative should be (much) more uniformly distributed than those of the historical and synthetic events. Besides, the most extreme events should be selected to make interpolation possible. If the event that leads to the highest inundation depths is not included, the inundation depths of this event can not be obtained by interpolation. This is also partially covered by selection of one of the most extreme events as a starting point for the selection method, whereby it is already included.

Hence, different considerations play a role in selecting the best set of weight factors and parameters. On the one hand, somewhat more representative events with higher maximum wind speed and lower minimum distance may be favourable, to cover the more extreme events properly. On the other hand, a more uniform distribution will make interpolation to all synthetic events easier.

C – More weight to local parameters was selected as the best set of representative typhoons, based on these considerations mentioned above. The difference with A and especially with B is limited, but in the area of interest the spread of the typhoon tracks over the area is better for C. An advantage of B is that the point with the maximum wind speed and minimum distance to the track was selected as representative event (upper left point in the right side of the figures). This was not the case for C, while this is one of the most extreme typhoons and passes close by Majuro. This is not necessarily the track that causes the most flooding, as this maximum distance may also be at the boundary of the area of interest. Besides, the distribution over the combined maximum wind speed and minimum distance to the track seems to be more uniform for C, compared to B, but the differences are small. The choice for set C will be verified in Section 4.1.4.

Number of representative typhoons
In this thesis only 50 representative typhoons could be simulated for computational time reasons, but the method could also be used to select other numbers of representative typhoons. With 50 representative typhoons as shown above, the full parameter space seems to be already quite well represented and the extremes for the shown combinations of parameters are mostly included. By making a comparison between 50, 100 and 146 representative typhoons, the influence of this number on the representation of all typhoons is illustrated. See Figure 4.9. By using 146, a good comparison with the 146 historical typhoons can be made.

When higher numbers of representative typhoons are selected, the parameter space in between is more or less filled evenly, as in agreement with Figure 2.9. It should be noticed that when selecting a higher number of typhoons, for example 100 instead of 50, the first 50 are still included in this selection. For this reason, the tracks and markers of the first 50 coincide with those for 100 and 146 in Figure 4.9.

It can be expected that by using a larger number of representative typhoons, all synthetic typhoons are better represented. However, the larger the number of representative typhoons, the less further improvement can be obtained by increasing the number of representative typhoons. The question is how well 50 representative typhoons actually represent all 2135 synthetic typhoons, and how increasing or decreasing the number of representative typhoons will influence this. This is elaborated below by use of a Bangladesh case study.
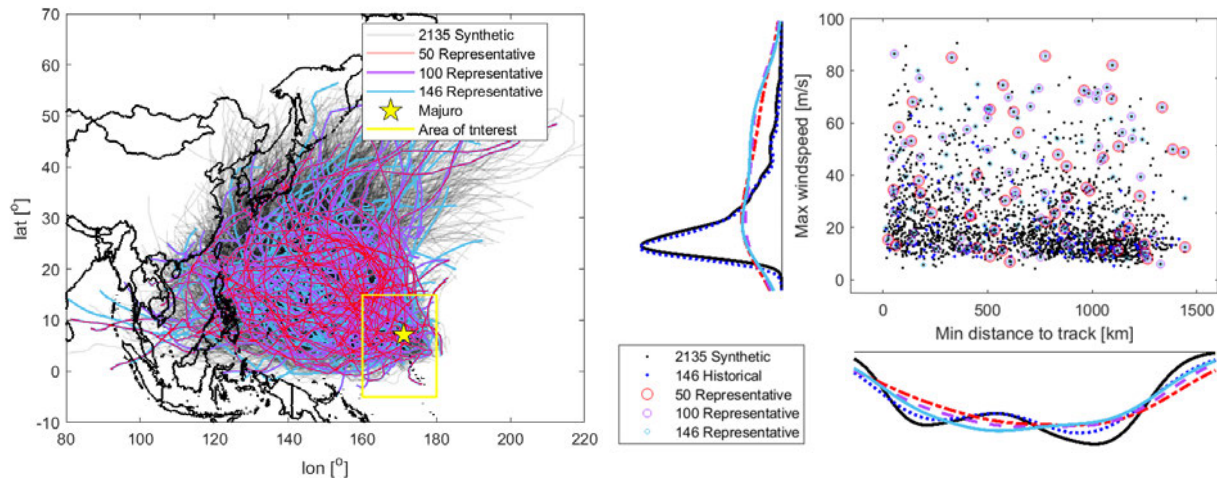
Figure 4.9: *Comparison of different numbers of representative typhoons. In addition, the historical typhoons can be compared with the same number of selected representative typhoons.*

.

When comparing the 146 representative typhoons of Figure 4.9 with the 146 historical typhoons of Figure 4.8, the representative typhoons are much more evenly distributed over the parameter space than the 146 historical typhoons. In fact even the 50 representative typhoons already better represent the full parameter space than 146 historical. Hence, by simulating water levels for 50 representative typhoons instead of 146 historical historical typhoons, one would most likely already include a broader range of outcomes. This will be validated by use of a Bangladesh case study below.

Representative tracks for Bangladesh case

For computational time reasons it was not possible to simulate wave conditions around Majuro for all synthetic typhoons within the scope of this thesis. For reasons explained in Section 4.1.3, this data is needed to assess the influence of the number of representative typhoons and for optimization of the interpolation method. Hence, data from a second case study that was already available was used: Charchenga Station in Bangladesh. To make this possible, the method to select a set of representative typhoons was also applied to the tropical cyclones in the Northern Indian Ocean Basin as used in that case study. Further information about the Bangladesh case can be found in Section 3.4.3 and Appendix B.3.

Just as for the Majuro case study, the area of interest was chosen such that it coincides with the used area for the Delft3D model (see Appendix B.3). Distances of the TC tracks were calculated with respect to Charchenga station, as for this location water levels and wave conditions were available. An important difference with Majuro is the larger size of the area of interest. Hereby TCs that pass relatively far of Charchenga were included as well. To partially prevent this, representative TCs were only selected from those TCs that pass within 15 degrees (±1650 km) of Charchenga station.

For the Northern Indian Ocean Basin, 42 years of TC track data was available, which includes 90 historical TCs for the area of interest. Besides, 1000 years of synthetic TCs (2098 TCs in the area of interest) was available, created by TCWiSE (Leijnse et al., 2019). Again, 50 TCs were selected based on the same parameters and weight factors as for Majuro. Historical, synthetic and selected representative TCs can all be found in Figure 4.10.

The selected representative TC tracks are again well spread over the area. However, as a consequence of the larger area of interest, some of the selected tracks do not get in the proximity of Charchenga Station. A remarkable feature is the lower boundary for the max wind speed in the data for Bangladesh (Figure 4.10, right). Possibly the less strong historical TCs were not recorded for part of the area of interest. Nevertheless, the representative TCs are more uniformly distributed than the synthetic tracks and seem to be a good representation of all synthetic tracks.
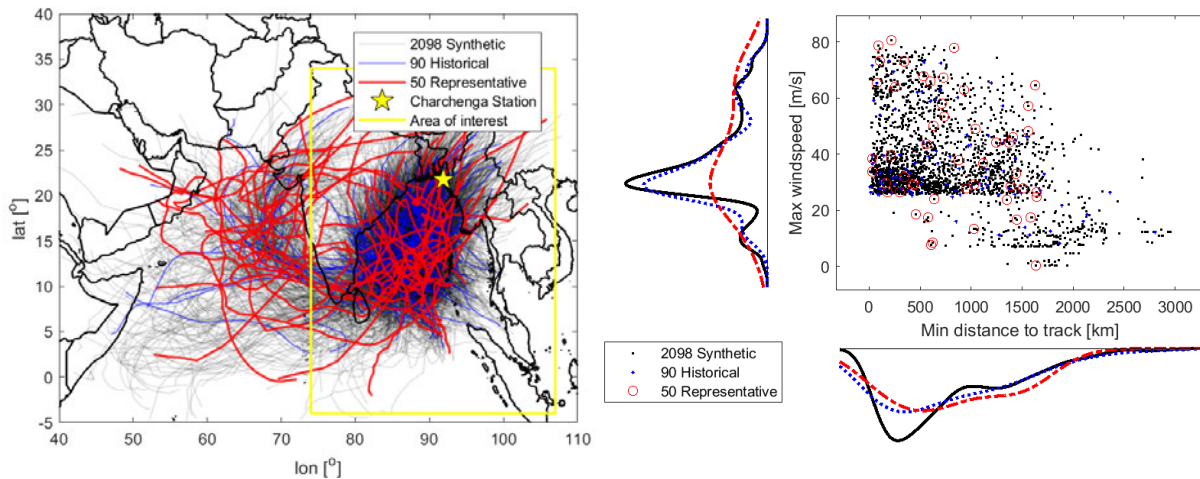
Figure 4.10: Selected representative tropical cyclones for Bangladesh case study.

4.1.3. Interpolation with Softmax

To make estimation of inundation depths for different return periods at Majuro possible, not only the maximum inundation depths for the 50 representative TCs that were simulated have to be known, but actually those for all 2135 synthetic tracks (i.e. 1000 years of typhoon conditions). These inundation depths were approximated by interpolation with use of Softmax. The optimization of the β parameter in this interpolation method is done by use of data for the Charchenga case

Optimization is done by selecting a number of representative TCs for Charchenga Station (described in Appendix B.3) with known maximum water depth. Subsequently, the water levels for all synthetic typhoons are estimated by interpolation, for different values of β (1-100). As in fact not only the water levels for the representative TCs are known in this case, but also those for all other synthetic TCs, the estimated water levels based on interpolation can be compared with the *'true'* simulated water levels. Subsequently, the Spearman rank correlation coefficient, bias, Root Mean Square (RMS) error and Scatter Index were calculated.

The above described procedure was not only done for 50 representative TCs, but for all numbers of representative typhoons between 1-1500. Besides, these errors were not only calculated based on the maximum water levels, but also for the maximum significant wave height. For both the maximum water levels and maximum significant wave height per TC in Charchenga Station, the resulting errors for all above mentioned combinations of β and numbers of representative TCs can be found in Figure 4.11.

Following from these Figures, higher numbers of representative TCs give more accurate results after interpolation. This can be expected as the exact water levels are simply known for a larger part of the synthetic TCs, and as interpolation is done based on a larger number of known water levels. Remarkably, only about 20 representative TCs are needed before results start to improve for most presented errors. For 50 representative TCs these errors are already significantly reduced, although more representative TCs lead to better results.

The optimum value of β differs per number of representative TCs. Following from Figure 3.19, more weight is given to the closer representative TCs (in the used parameter space) for higher β values. For a relatively large number of representative TCs, the distance (in the used parameter space) of each synthetic TC to the most similar representative TCs becomes relatively low. Hence, for a larger number of representative TCs, a larger value of β is favourable, as the closest TC is indeed similar. On the other hand, for a lower number of representative TCs, the closest representative TC may actually be not that similar, and combining multiple representative TCs to approximate a synthetic TC is favourable.
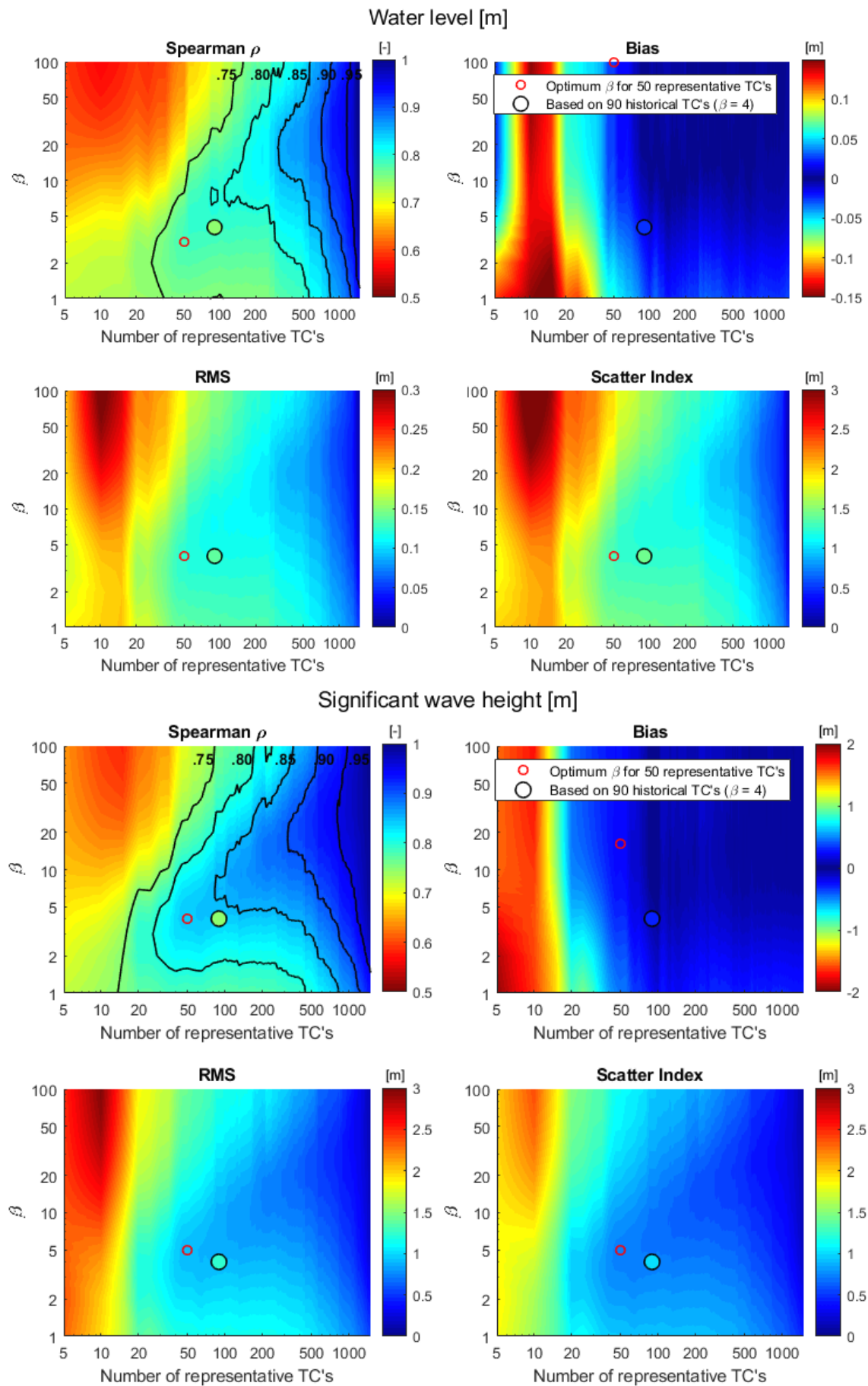
Figure 4.11: *Errors made by estimating the maximum water levels (upper) and significant wave height (lower) with Softmax interpolation, for different numbers of representative TCs and different values of the β parameter in Softmax. Errors are on a log-log scale. The optimum for 50 representative TCs is marked, and the errors that would be made when using 90 historical TCs as representative for the interpolation are shown as well.*

For both maximum water levels and significant wave heights, interpolation based on 90 representative TCs leads to better results than based on 90 historical TCs. This confirms the conclusion from the previous Section (4.1.2) that the representative tracks are indeed a better representation of all synthetic tracks than the historical. For 50 representative TCs, a value for β around 5 gives the lowest error in most cases. Only for the bias, (much) higher values of β give better results, but the influence of β is small in this case. For more than 50 representative typhoons, the bias is anyway low. Hence, a value for β **of 5 was chosen**.

4.1.4. Verification

Based on the 50 representative typhoons selected for Majuro (Section 4.1.2) and Softmax interpolation with the optimized β parameter (β = 5) from the previous Section, the weight factors for interpolation for all 2135 synthetic typhoons can be derived. This resulted in a 50 x 2135 matrix; for all combination of 2135 synthetic and 50 representative typhoons. In this Section, the resulting approximation of synthetic tracks and corresponding water levels for Majuro is verified.

Approximation of synthetic tracks

To illustrate how the approximation of a synthetic tracks based on representative tracks works, 2 synthetic tracks (tracks 876 and 2024) were randomly selected, see 4.12. Synthetic track 876 is for 30.154% represented by one of the representative tracks and for smaller fractions by the other 49 representative tracks. Apparently, synthetic track 2024 is better represented by one of the representative tracks, as it is approximated for 50.5154% by just one of the representative tracks. This seems reasonable, as both track 2024 and the most similar representative track are indeed similar tracks (especially in the area of interest) and have similar minimum distance to Majuro. However, the maximum wind speed is not so similar, hence other tracks with wind speeds more similar to those of track 2024 are used as well.
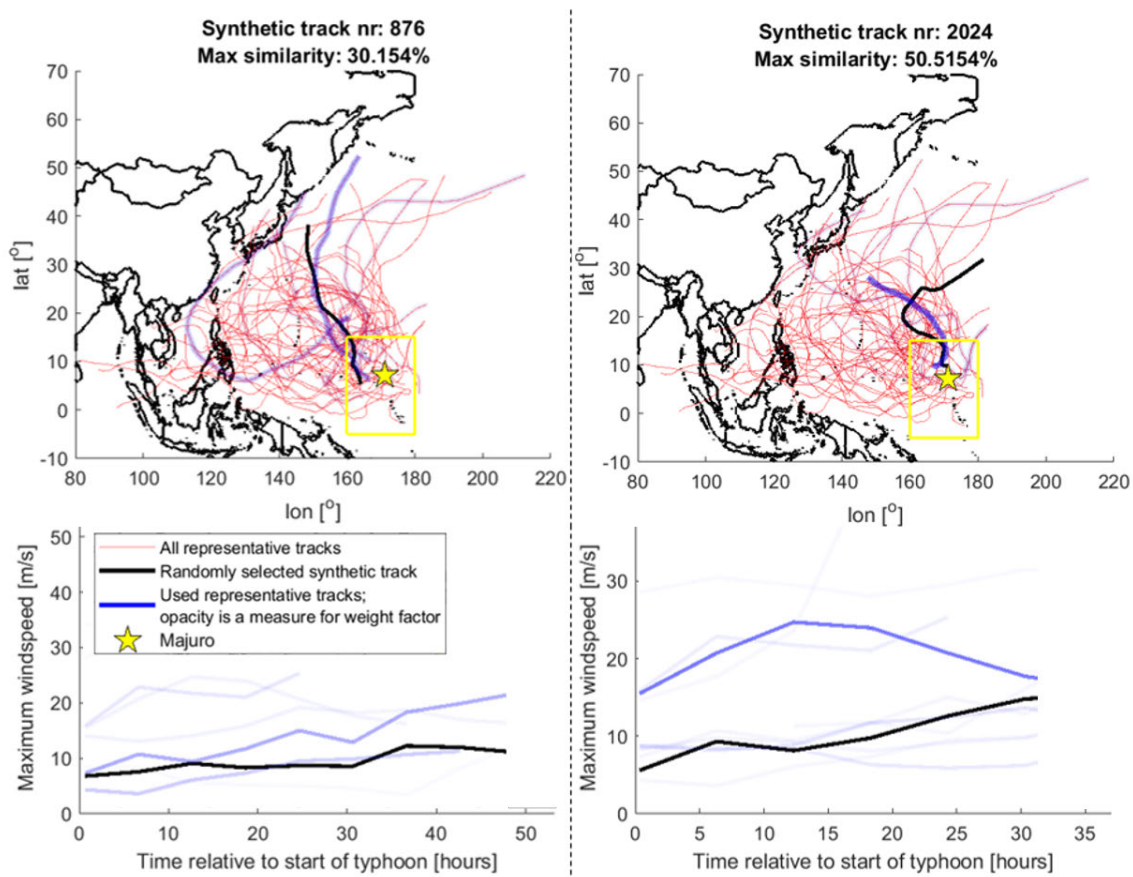
Figure 4.12: *Example of the approximation of 2 randomly selected synthetic tracks by use of representative tracks and interpolation with Softmax. For the maximum wind speed (lower part), only the used representative tracks for the period that the typhoon was in the area of interest are shown.*

Verification based on water levels near Majuro

To verify that maximum water levels corresponding to the synthetic typhoons at Majuro can indeed be well approximated, water levels (only surge) were simulated for all 2135 synthetic typhoons by use of the Delft3D-FLOW model (see Section 3.3.2). For each typhoon, the maximum water level in a point just north of Majuro was obtained (see Figure 3.1 for this location). As simulation of wave conditions for all synthetic typhoons was computationally unfeasible, no significant wave heights could be compared.

The simulated maximum water levels were compared with the water levels approximated by use of the selected 50 representative typhoons and interpolation. This was done by calculating the return periods for simulated water levels and the approximated water levels independently, see Figure 4.13. In addition, maximum simulated water levels of historical typhoons were added to make comparison possible. Note the jump in estimated water levels around a return period of 100 years for the synthetic typhoons. This is most likely caused by the fact that even in 1000 years of synthetic typhoons, only a limited number of typhoons with high air pressure drop passes close to Majuro (see Figure 4.5 for the closely related maximum wind speeds).
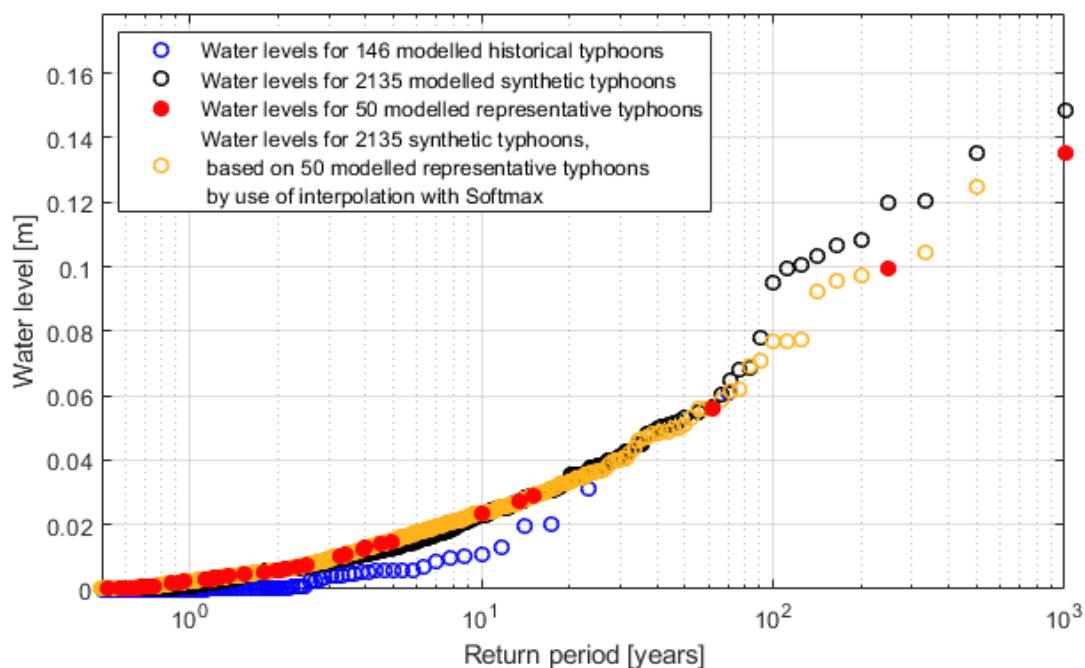
Figure 4.13: *Comparison of maximum water levels for all historical typhoons, synthetic typhoons and approximated synthetic based on 50 representative and interpolation, for an offshore location north of Majuro.*

The water levels for different return periods could be reasonably well estimated, although for individual typhoons the approximated water levels may deviate from those simulated. Simulated water levels offshore at Majuro are limited to only 15 cm. Hence the error in these simulated water levels could be significant as well, although in Appendix B.1.1 it is shown that for another offshore location the water levels as a consequence of drop in air pressure could be accurately simulated.

For the higher water return periods (> 100 years), the approximated water levels are slightly lower than those simulated. This is mainly caused by the fact that the synthetic typhoon that caused the highest water levels was not selected as a representative. As interpolation is used to estimate the water levels, this makes it impossible to get the highest water level correct if it was not simulated. It can be expected that for higher numbers of typhoons, the results are better. Hence, the comparison of above is also made based on 200 representative typhoons. A β factor of 10 was used here, as in agreement with Figure 4.11, see Figure 4.14 for the result.

By using 200 representative typhoons, more extreme events are included and also the tail is well

represented (i.e. water levels for return periods > 100 years). Almost all extreme typhoons are selected as representative now. This is still a reduction factor of more than 10 in the number of scenarios compared to modelling all synthetic typhoons (i.e. 200 versus 2135). For the return periods below 10 years, approximated water levels seem to be slightly larger than the simulated water levels, although the difference is small. This is likely related to the larger value of β, whereby more weight is given to the closest (in 22 parameter space) representative typhoon.
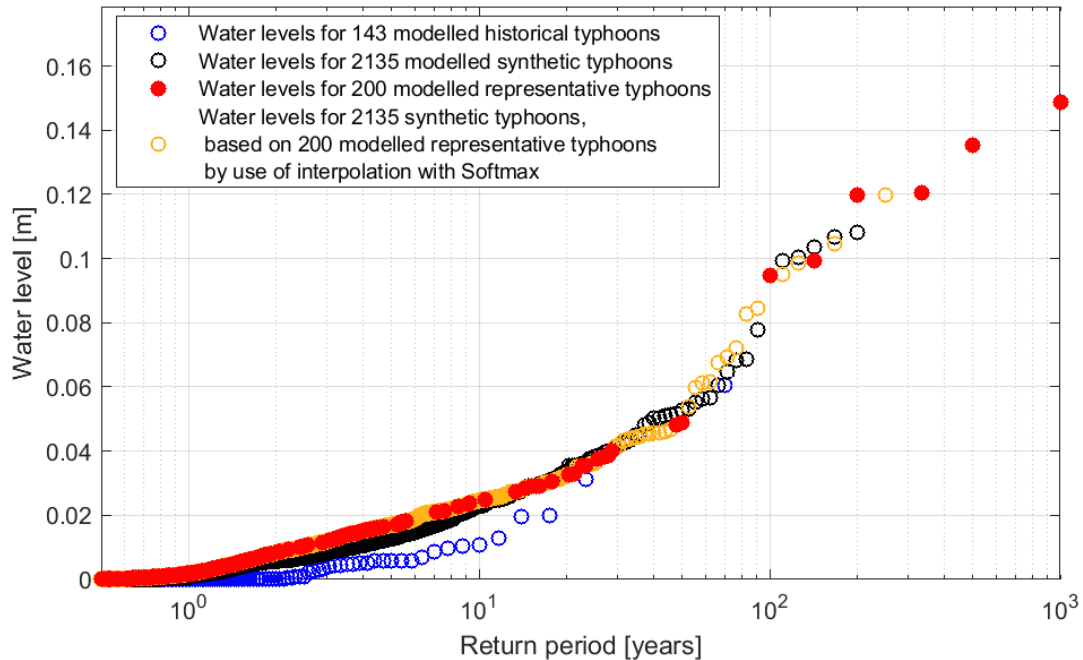
Figure 4.14: *Comparison of maximum water levels for all historical typhoons, synthetic typhoons and approximated synthetic based on 200 representative and interpolation, for an offshore location north of Majuro.*

Similar figures were made for the maximum water levels and significant wave height at Charchenga Station, these can be found in Appendix C.2. By 50 representative typhoons the values for high return periods were underestimated, but for 200 those were again well represented.

4.1.5. Final typhoon scenarios
By using 50 representative typhoons in combination with Softmax interpolation with β=5, water levels for 1000 years of typhoon conditions can be reasonably well approximated. This is especially the case for water levels for return periods < 100 years; for the more extreme cases the effect of errors in individual typhoons becomes more important. By increasing the number of representative typhoons – for example to 200 – the more extreme typhoons are better represented. However, for computational time reasons the simulation of only 50 typhoons was feasible. In any case, uncertainties for return periods > 100 years seem significant due to the use of synthetic typhoons.

Figure 4.15 gives an overview of the selected 50 representative typhoon tracks in the area of interest – and Delft3D model domain. Wave conditions and surge levels for all 50 representative typhoons were simulated by use the Delft3D-FLOW+WAVE model. As simulation of the full period that a typhoon is present in the area of interest is computationally not feasible, only the 24h around the peak precipitation and wave conditions were simulated in XBeach. These time frames were selected manually. Typhoons with cumulative precipitation rates below approximately 20 mm and a maximum wave height below 1 m at all of the 5 locations where the boundary conditions were specified were not simulated in XBeach. For these, an inundation depth of 0 m in the whole DUD region was assumed. By doing so, only 33 out of 50 typhoons had to be simulated in XBeach and about 1/3 reduction in computation time was obtained.

An example of the resulting significant wave heights, water levels and precipitation rates, applied as

boundary conditions in the XBeach model is shown in Figure 4.16. This is one of the most extreme typhoons that was simulated. Based on the simulated inundation depths for all representative typhoons, inundation depths for all synthetic typhoons were approximated by Softmax with a β factor of 5, whereby flood maps for different return periods could be derived. These flood maps for typhoon related flood hazard can be found Section 5.1.
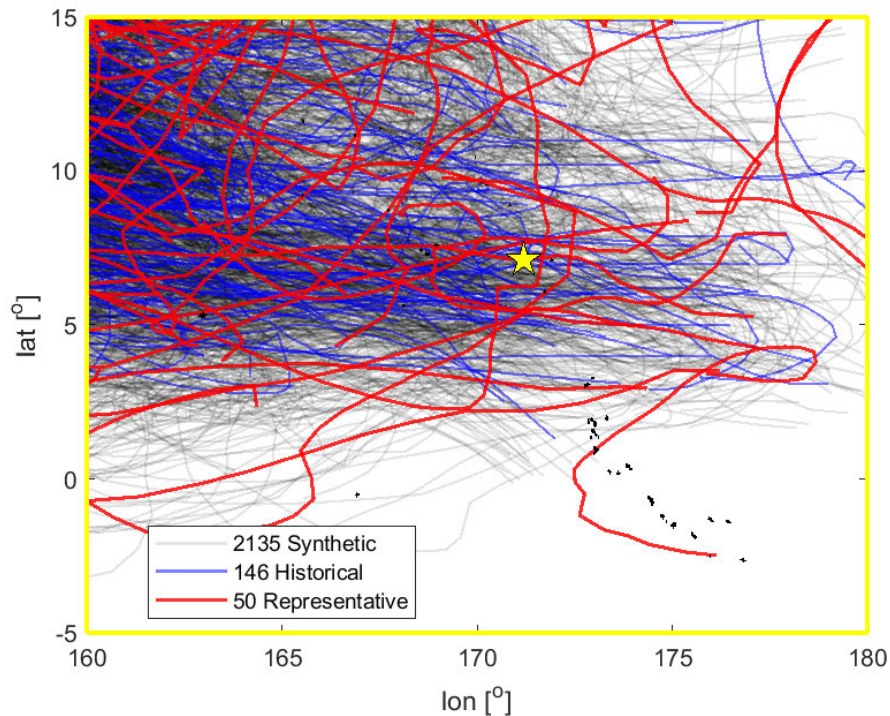
Figure 4.15: *Overview of the final 50 selected representative tracks in the area of interest (and Delft3D model domain). Besides, all synthetic and historical typhoons are plotted. The location of Majuro is marked with a yellow star.*
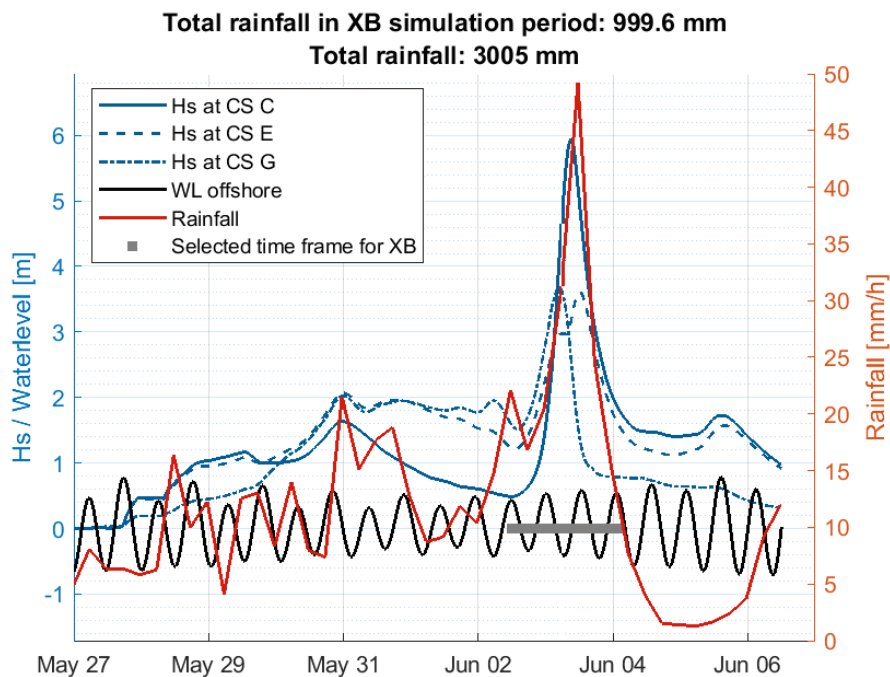
Figure 4.16: *Delft3D results for one of the most extreme representative typhoons that was simulated. The grey marked time frame was subsequently used as boundary condition for the XBeach model.*

4.2. Non-typhoon conditions

In this Section, the results of the different steps taken to select a set of representative scenarios for the non-typhoon conditions are presented, according to the method described in Section 3.5.

4.2.1. Nearshore wave conditions and surge

First the historical nearshore wave conditions are presented. These are based on offshore ERA5 re-analysis data and translated by use of the SWAN model. Subsequently, extreme value distributions were fitted to the wave conditions and surge levels. Finally, the Bayesian Network is elaborated, used to model the interdependencies in the wave conditions for locations C-G and the surge levels.

Nearshore wave conditions by use of SWAN

Historical offshore wave conditions were translated to the locations where the boundary conditions for the XBeach model were specified (approximately at the 20 m depth contours). ERA5 wave data (see Section 3.2.3) was used, and transformed to nearshore by use of the SWAN model (described in Section 3.3.2). Wave roses for locations C-G around the DUD region and other locations around Majuro can be found in figure 4.17 below.
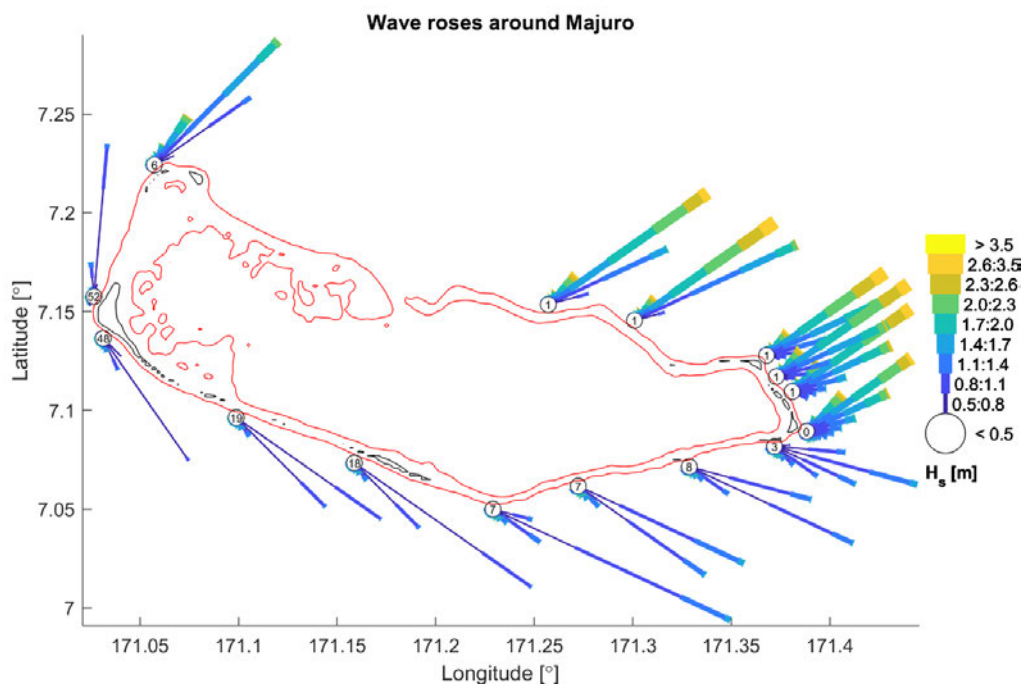
Figure 4.17: *Wave roses around Majuro on the 20 m depth contour line, based on ERA5 data and transformed by use of the SWAN model. The 20 m depth contour lines are shown in red. Wave directions are presented in nautical convention.*

Extreme value analysis of wave conditions and surge levels

Extreme value distributions were fitted to the wave conditions (SWAN output data from the previous Section) at each of the 5 locations (C-G) around the DUD region. Generalized Extreme Value (GEV), Gumbel, Weibull, Gamma, Log-Normal and Normal distributions were fitted to the daily maxima of the significant wave height. This was done for each of the locations independently. A comparison of the fitted distributions can be found in Appendix A.2.2, the results are summarized below.

For the significant wave height (H_s), the Weibull distribution gave the best fit for most locations. Only for the most southern location (G) the wave heights were somewhat underestimated for higher return periods. Hence, for consistency the Weibull distribution was used for the H_s at all locations. A similar approach was followed for the surge levels, here the Normal distribution gave the best fit. For the peak wave period (T_p) and mean wave direction (Dir) at each of the 5 locations, empirical distribution functions were used. For T_p these were based on the daily maxima and for Dir (specified per hour in the SWAN output) the daily mean value was used.

Bayesian Network to model interdependencies of wave conditions and surge levels

Besides the extreme value distributions for individual parameters, the interdependencies between these variables have to be known in order to make generation of a realistic synthetic data set possible. The interdependencies in wave conditions and surge levels are modelled by use of a Bayesian Network (BN, see Section 2.4.3) in the software Uninet (described in Section 3.5.3). Generation of the actual synthetic data set is described in Section 4.2.3.

The above described historical data (SWAN output), with fitted distributions for the wave conditions at locations C-G and the offshore surge levels, was used to describe the variables (nodes). Variables describing the wave conditions (H_s, T_p and Dir) are connected at each of the locations. In addition, variables H_s and Dir were connected to their equivalent at neighbouring locations. Joint normal copulas were used to model the dependence relations (connections or arcs) between the variables (nodes). The resulting Bayesian Network can be found in Figure 4.18 below.
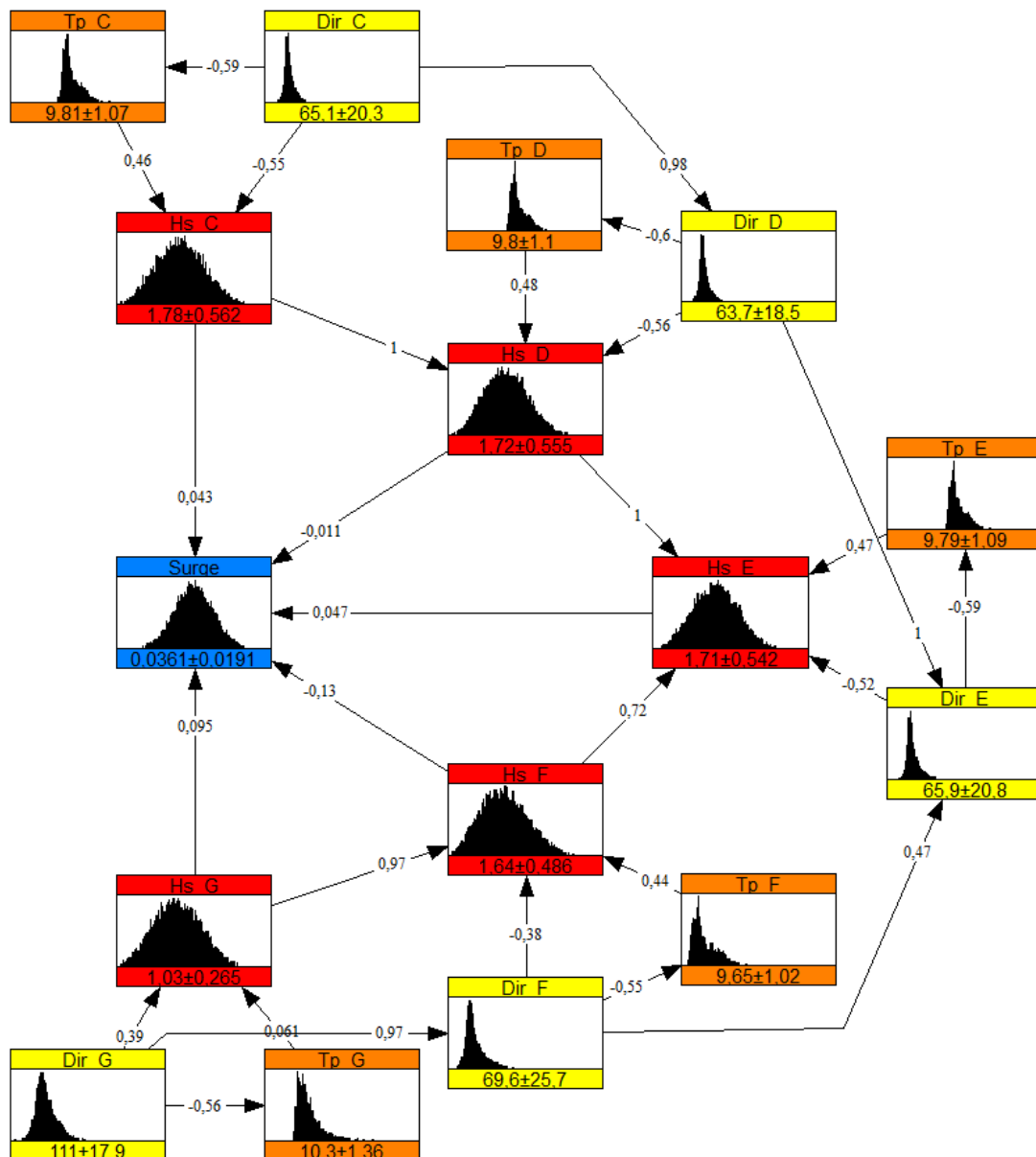
Figure 4.18: *Bayesian Network for wave conditions at different locations (C-G) and surge levels. The significant wave height (Hs) and surge are in meters, the peak wave period (Tp) is in seconds and the mean wave direction (Dir) is in degrees to north (nautical convention). Mean values and standard deviation are shown for each parameter, and the dependence relations (connecting arrows or arcs) are shown with the rank correlation coefficients.*

Based on Figure 4.17 it was concluded that the wave conditions at the northern side (location C) and southern side (location G) of the DUD region differ significantly, while the locations in between seem to be combinations of these. For this reason, the wave conditions of location D and E were assumed to be dependent on their northern neighbouring location and the wave conditions of E and F were assumed to be dependent on their southern neighbouring location. Surge was only connected to H_s at all locations. By making these connections, it was assumed that all other connections were also reasonably well represented. This is checked in Section 4.2.3.

Clearly, the wave conditions at C, D and E are very similar and strongly related. Wave conditions at F and G are strongly related as well, but apparently those at E and F are much less related and the wave climate there is somewhat different. This is in line with the wave roses in Figure 4.17 at the locations of of C-G (see Figure 3.14 for these locations); C-E are mainly prone to waves from the northeast, G mainly to waves from the southeast, and F is in between those regimes. Based on the very low values of the rank correlation coefficients, offshore surge levels are very weekly related to the wave conditions.

4.2.2. Precipitation

In this Section the results of the precipitation analysis of the data for Majuro WBAS Airport Station is presented. Daily precipitation rates were determined for different return periods based on an extreme value analysis and a standard event was constructed to allow for modelling of the distribution of precipitation over a day.

Daily precipitation rates

Daily data was selected based on a peak over threshold approach, where the threshold was chosen such that on average the precipitation rate of one day per month was used. Different distributions were fitted through the data. The Generalized Pareto (GP) and Generalized Extreme Value (GEV) distribution with Langbein correction for return periods below 10 years were compared, see Figure 4.19 below.
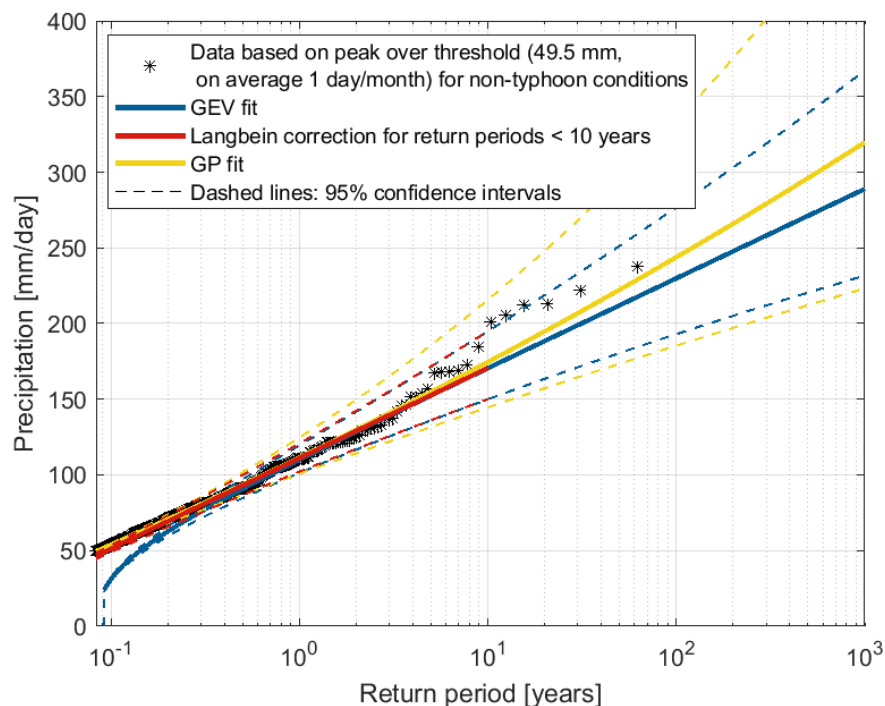
Figure 4.19: *Generalized Pareto (GP) and Generalized Extreme Value (GEV) distributions fitted to measured daily precipitation rates at Majuro WBAS Airport Station. A peak over threshold was used to select on average one event per month.*

Although both are similar, the GP distribution gives a slightly better fit than the GEV distribution. This is especially the case for higher return periods, but both seem to slightly underestimate these

more extreme precipitation rates. Nevertheless the fitted GP distribution was selected as best model. Precipitation rates for the synthetic data set were sampled from this distribution.

Hourly precipitation rates
In order to make inclusion of the variation in rainfall rates over a day possible, a standard rainfall event was derived. This standard event specifies what fraction of the total precipitation falls in each hour of the day. A detailed description of the derivation of this standard event can be found in Appendix A.3. The resulting distribution over the day can be found in Figure 4.20 below.
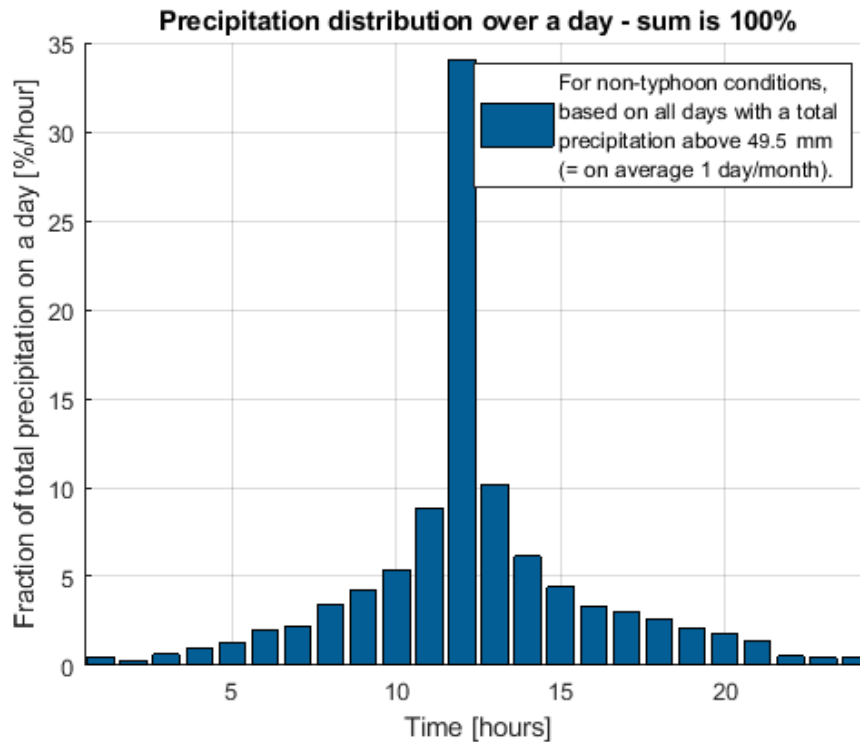
Figure 4.20: Standard event for the distribution of precipitation over a day at Majuro, based on measured hourly precipitation rates at Majuro WBAS Airport Station.

4.2.3. Synthetic data generation
To make inclusion of extremer events and compound flooding possible, synthetic data was generated for 1000 years (336747 days or events) of non-typhoon conditions that can potentially lead to flooding. This data consists of wave conditions at 5 locations, water levels (the combination of surge and tide) and precipitation rates. First, the following synthetic data was generated:

A. Wave conditions and surge levels were generated by sampling from the Bayesian Network (BN) described in Section 4.2.1. This data consists of daily maximum significant wave height, maximum peak period, mean wave direction and maximum surge level. Wave conditions were specified for 5 locations.

B. Random tidal water levels were generated by use of the Global Tide and Surge Model (see Section 3.2.4). Tidal water levels were obtained for every 30 minutes.

C. Cumulative daily precipitation rates were generated by sampling from the GP distribution in Figure 4.19. Only for 2.92% of the days, precipitation rates were above the threshold of 49.5 mm and sampled. For all other days, precipitation was assumed irrelevant for flooding and set to 0 mm. Hourly rates were determined by use of the standard event in Figure 4.20.

Subsequently, the synthetic data from A-C was combined randomly to obtain a full description of each of the synthetic events. By doing so, the tidal water level and precipitation rates are assumed

to be independent from each other, and from the wave conditions and surge. On the other hand, the relations between the wave conditions at different locations and the surge level are accounted for by sampling from the full BN. Lastly, the daily maximum surge was added to the tidal water level to obtain the total water level. The result is a data set with 336474 synthetic events.

Comparison of historical and synthetic wave conditions and surge levels

To validate that the used BN is capable of generating a realistic data set of synthetic events, a comparison is done with historical data for combinations of variables. For the synthetic data to be a good expansion of the historical data set, ideally the distributions should be the same. However, the range of the synthetic data should be larger, as the data set is larger. Only a selection of the combinations of variables was shown, see Figure 4.21 below.
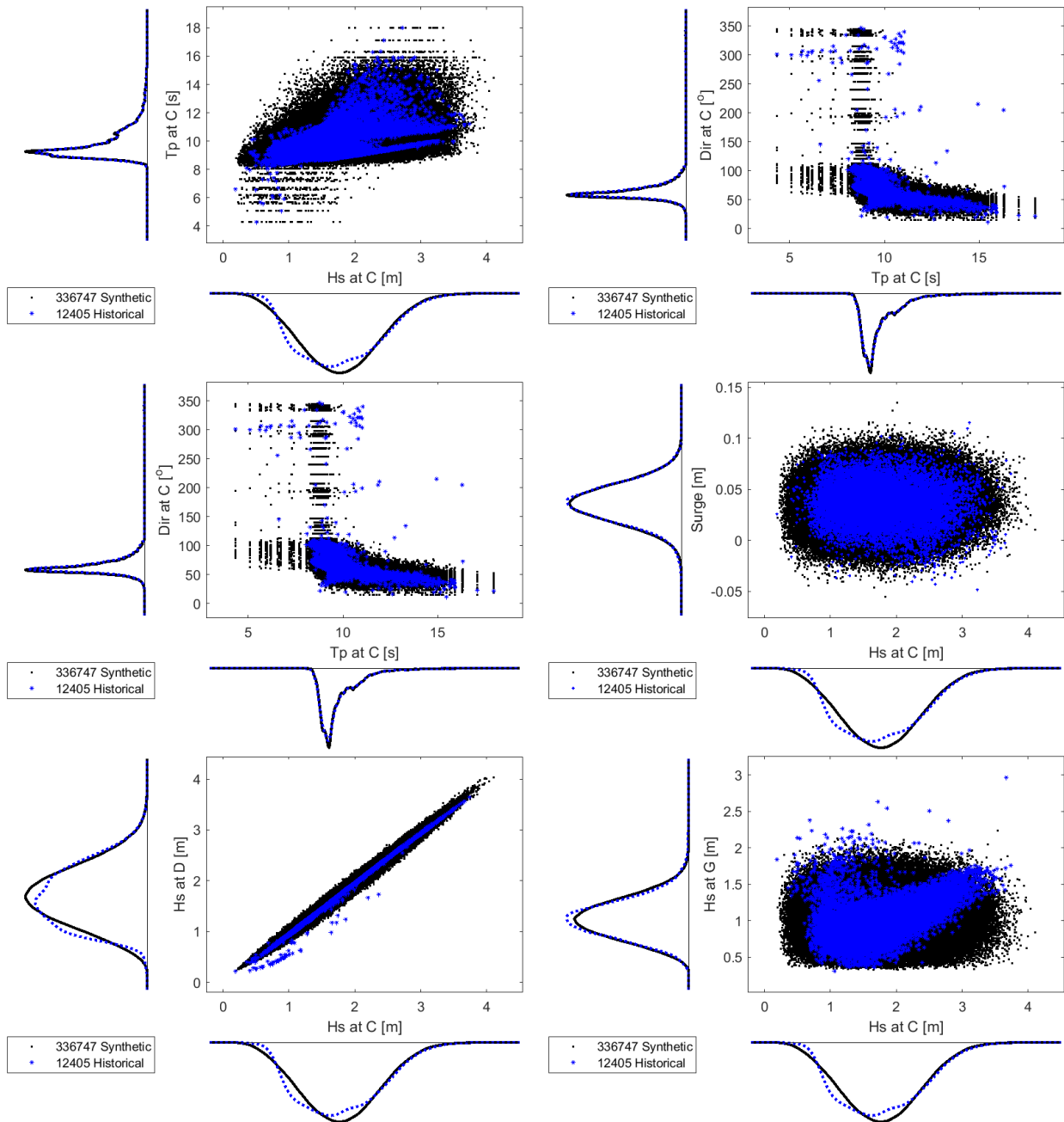
Figure 4.21: *Comparison of the historical data with the synthetic data as generated by sampling from the Bayesian Network in Uninet. Different combinations of parameters are shown together with the marginals of these parameters.*

Selecting synthetic events that can potentially lead to flooding based on BEWARE
The synthetic data in general seem to be reasonably well in agreement with the historical data, but with the advantage of being for a much longer period whereby more extreme cases are available. As a major part of the synthetic events now consists of events that will not lead to flooding, a selection is made by use of BEWARE and a threshold for precipitation. A description of the used setup for BEWARE is given in Section 3.5.3. Estimated runup levels ($R_{2\%}$) were determined in each of the 5 cross sections, for all synthetic and historical events. The fraction of the estimated runup in each bin can be found in Table 4.1 below.

Table 4.1: Overview of the fraction of the events per runup bin based on BEWARE for Cross Sections (CS) C-G. Runup ($R_{2\%}$) is given in meters relative to the reef flat, which is located at -0.5 m relative to MSL in all (simplified) cross sections.

R2% Bin	CS C Historical	CS C Synthetic	CS D Historical	CS D Synthetic	CS E Historical	CS E Synthetic	CS F Historical	CS F Synthetic	CS G Historical	CS G Synthetic
-4 to 0	0.00%	0.00%	0.00%	0.00%	0.00%	0.00%	0.00%	0.00%	0.00%	0.00%
0 to 1	0.02%	0.00%	0.01%	0.00%	0.01%	0.00%	0.01%	0.00%	0.01%	0.00%
1 to 2	26.79%	25.69%	25.42%	26.26%	27.85%	28.24%	28.48%	29.63%	51.40%	55.86%
2 to 3	64.28%	64.63%	57.37%	48.47%	59.22%	52.94%	56.28%	45.67%	48.26%	43.86%
3 to 4	8.88%	9.48%	16.88%	23.76%	12.71%	18.00%	15.16%	24.27%	0.33%	0.27%
4 to 5	0.03%	0.13%	0.01%	0.01%	0.18%	0.70%	0.01%	0.02%	0.00%	0.00%
5 to 10	0.00%	0.07%	0.31%	1.50%	0.03%	0.13%	0.06%	0.42%	0.00%	0.00%
10 to 30	0.00%	0.00%	0.00%	0.00%	0.00%	0.00%	0.00%	0.00%	0.00%	0.00%

Estimated runup values for the synthetic events are slightly higher than for the historical events, except for CS G. This can be explained by looking at the marginals for H_s in figure 4.21 and the fits of Weibull distributions to the historical data for the H_s in Appendix A. The Weibull distributions slightly overestimate H_s, except for location G where they are actually underestimated. Hence, on average slightly higher values of H_s are present in the synthetic data set, which leads to higher estimated runup, except for location G.

Only those synthetic events for which at least at one location the estimated $R_{2\%}$ was above 4 m (3.5 m relative to MSL) *or* cumulative precipitation above 49.5 mm *or* both were selected. Hereby, only the events that may potentially lead to coastal, precipitation related or compound flooding were retained. This resulted in a data set of 19619 synthetic events that can potentially lead to flooding. The same procedure was applied to the historical events, which resulted in 404 historical events that can potentially lead to flooding. The resulting events that potentially can lead to flooding are presented in Figure 4.22 in the next Section.

While the historical data set contains only one event out of 404 that satisfies both thresholds and may potentially lead to compound flooding, the synthetic data set includes 258 of such events out of 19619. Both the total number of synthetic events that may potentially lead to flooding and the part that may cause compound flooding are somewhat higher than can be expected, when looking at the average number of events per year. For the historical events about 11 events per year were selected, versus about 20 per year for the synthetic. This seems a consequence of the binned output of BEWARE in combination with slightly larger wave heights in the synthetic data, whereby a relatively larger part of the synthetic events was selected as *'potentially causing flooding'*.

By using the thresholds for runup and precipitation, the number of events irrelevant for flooding that is simulated in XBeach is strongly reduced. Only the more extreme events are now represented, and a reduction in the number of synthetic events by a factor 17 was obtained.

4.2.4. Scenario selection
In this Section the selected set of representative scenarios for non-typhoon conditions is presented. 50 representative events were selected by maximum dissimilarity according to the procedure described in Section 3.5.4. Only the combinations of H_s at C, H_s at G, Water Level (WL) and precipitation are shown, see Figure 4.22 below.
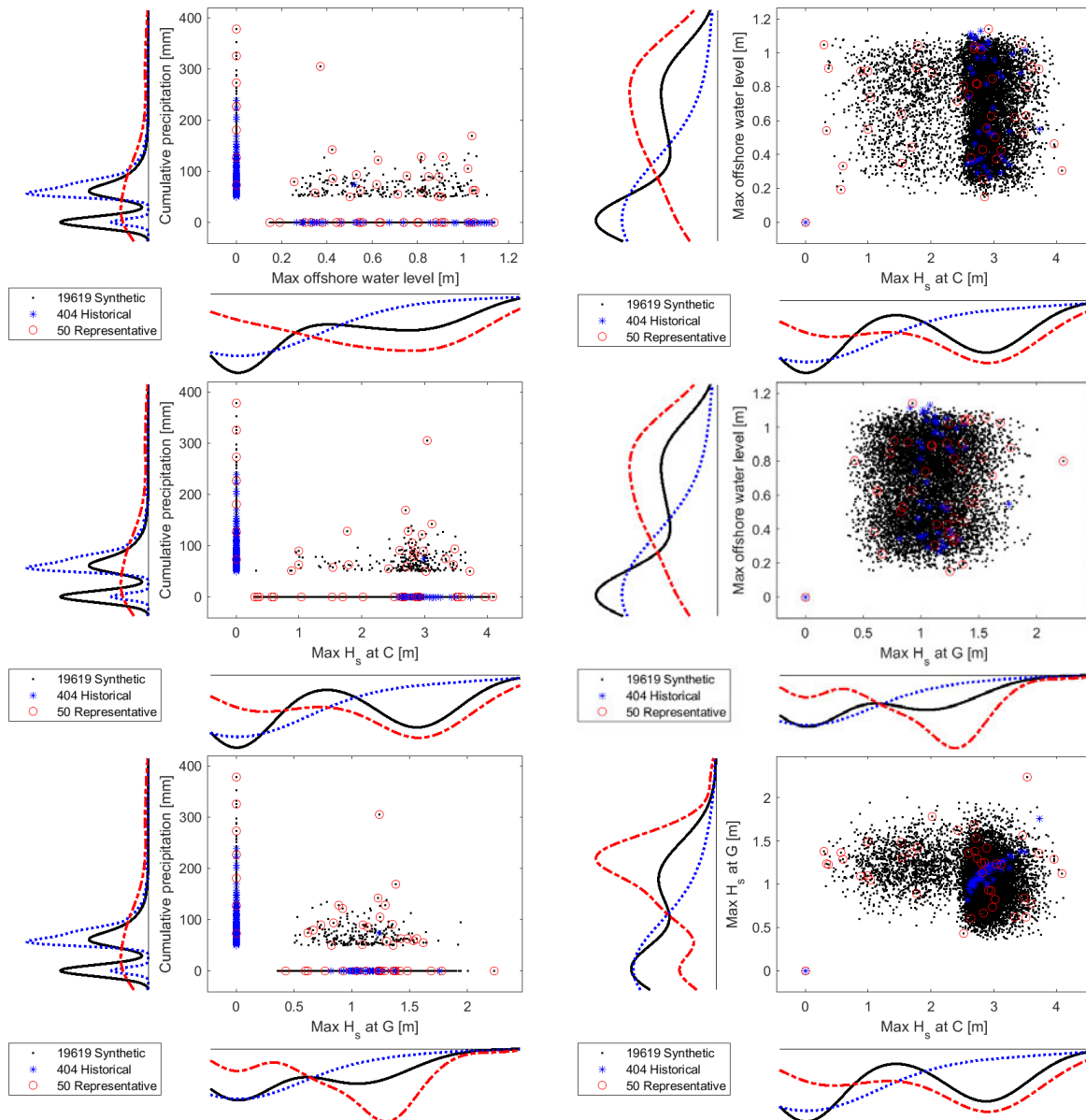
Figure 4.22: *Generated synthetic data and historical data that can potentially lead to flooding and the selected representative events for non-typhoon conditions.*

In general, the selected representative events are well spread over the synthetic events. A remarkable consequence of the 2 thresholds used is that now 3 categories of events can be identified in the events that may potentially lead to flooding:

- Events for which only precipitation is relevant, as estimated runup is below the threshold. For these events, water levels and wave conditions are not relevant and all excluded from the model simulations (i.e. the parameters are set to 0). These events are clearly visible in the left figures as those with a maximum offshore water level of 0. In the figures on the right, these are all located in the lower left point (0,0), as no water levels and wave conditions are applied. For flooding due to precipitation solely, the used maximum dissimilarity algorithm selected 7 representative events out of 10587 synthetic events that may potentially lead to flooding.

- Events where only coastal flooding (i.e. water levels and waves) are relevant, as cumulative precipitation is below the threshold. For these events, precipitation was excluded from the model simulations (i.e. set to 0). These events are clearly visible in the upper left figure as those with 0 precipitation. For coastal flooding, the used maximum dissimilarity algorithm

selected 20 representative events out of 9290 synthetic events that may potentially lead to flooding.

- Events where both precipitation and coastal flooding are relevant and which may potentially lead to compound flooding. In the left figures, these an be found in the upper right cloud of points, as they have non zero values for both variables. For compound flooding, the used maximum dissimilarity algorithm selected 27 representative events out of 258 synthetic events that may potentially lead to flooding.

For each of these categories, the most extreme cases are selected for the set of representative events. The number of selected representative events per category is well in line with the complexity of the flood drivers for each category. For flooding due to precipitation, only the cumulative precipitation is relevant. For coastal flooding, water levels and wave conditions for different locations are all relevant. Hence, more scenarios are needed to represent all combinations. For compound flooding, even more scenarios are needed to represent all possible combinations, as now also precipitation is relevant.

Interpolation with Softmax

Just as for the typhoon conditions, interpolation by use of Softmax was used to obtain the inundation depths for all 19619 synthetic events. Unfortunately, optimization nor validation of the value for the β parameter used in the interpolation was possible, as no alternative data set was available (as was the case for typhoon conditions). For this reason, a comparison of the ratios of the number of representative events over the number of synthetic events, and the corresponding β values was done. For the typhoons this was 50/2135, while for non-typhoon conditions this is 50/19619.

Based on Section 4.1.3 this would mean a somewhat smaller β factor (about 2) should be chosen. On the other hand, it can be expected that the maximum difference in combined parameter space for non-typhoon conditions is actually smaller than for the typhoon conditions, whereby a slightly larger value for β may give better results. Hence, also for the non-typhoon conditions a β **factor of 5 was chosen**. Although this is expected to be in the right order of magnitude, future validation is strongly recommended when a suitable data set would become available.

4.2.5. Final non-typhoon scenarios

In summary, 1000 years of synthetic events (19619 events) was generated for non-typhoon conditions that may potentially lead to flooding. 50 representative events were selected that combined represent flooding due to precipitation solely (7), coastal flooding (20) and compound flooding (27). All 50 events were simulated in XBeach, an example of the boundary conditions as applied in XBeach for one of the representative compound flood events is shown in Figure 4.23 below. This is one of the most extreme events.

The shape of the standard precipitation event is the same for all events and precipitation rates are defined every hour. Water levels consist of the tide and maximum surge and are defined every 30 minutes. For the significant wave height and peak wave period, the maximum value is applied as constant value for the full simulated period. The same applies to the mean wave direction. Although the significant wave height is expected to vary less over a day than the water level and precipitation, this is a somewhat conservative approach. Inclusion of the variation over a day could be further improved by deriving for example a standard event, but this falls outside the scope of this thesis.

After simulation of the inundation depths for all representative scenarios in XBeach, inundation depths for all 19619 synthetic events are approximated by Softmax interpolation (with β = 5). Subsequently flood maps were created for different return periods, these can be found in Section 5.2.
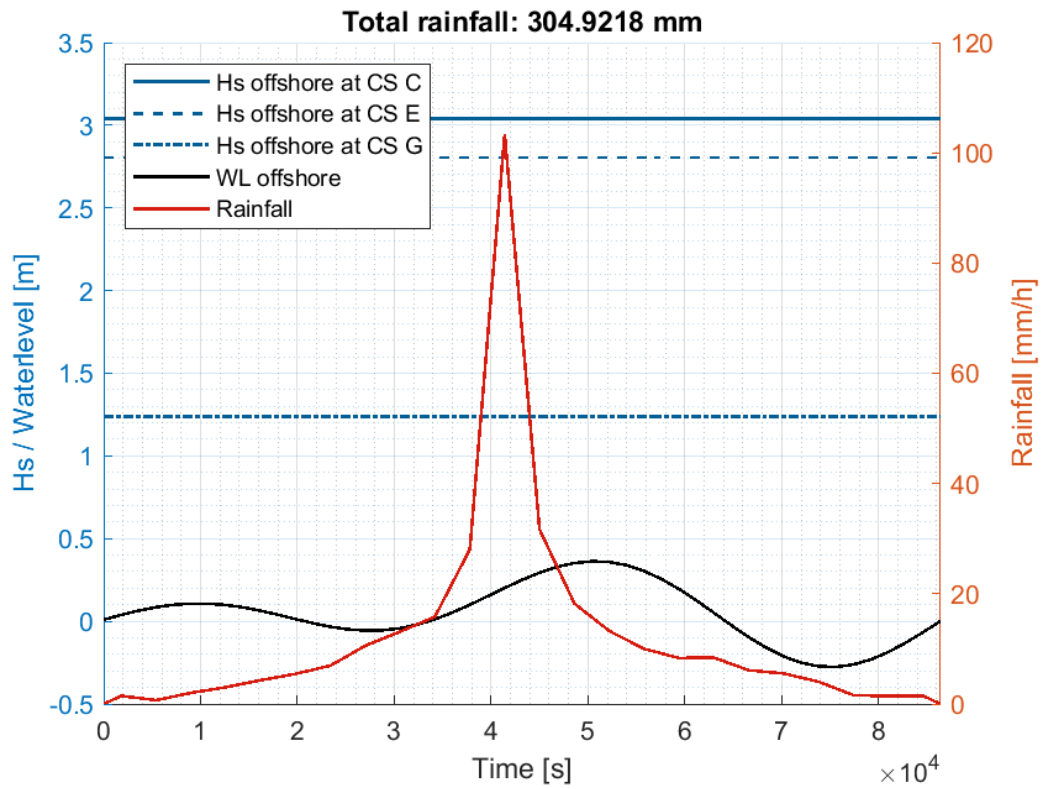
Figure 4.23: *Example of the boundary conditions as applied in XBeach for a representative event that may potentially lead to compound flooding during non-typhoon conditions. The example is for one of the most extreme cases and the total simulation period is 24 hours.*

<div style="text-align: right;">

5

</div>

Results – Flood hazard

Chapter summary

- In this chapter the results of the flood hazard assessment of the DUD region are presented. To get some insight in the influence of different flood drivers, simulated flood extents related to coastal flooding, precipitation, and compound flooding are presented for historical typhoon Paka (1997). Subsequently, the flood maps corresponding to typhoon conditions are presented for return periods of 5 and 50 years (Section 5.1).

- Similarly, the flood maps corresponding to non-typhoon conditions are presented in Section 5.2. To gain additional insight in the relevant flood drivers for different areas, flood maps for non-typhoon conditions were made for the scenarios with only precipitation and only coastal flooding respectively.

- Finally, the combined flood maps for the total flood hazard are presented in Section 5.3. An overview of the flood extents due to different flood drivers and for different return periods is provided here as well.

5.1. Typhoon related flood hazard

In this Section, first the maps with the flood extents for coastal, precipitation related and compound flooding for typhoon Paka are presented. Subsequently, the flood maps for the typhoon conditions are presented for different return periods.

5.1.1. XBeach simulations for typhoon Paka

To get insight in the influence of different flood drivers, and to validate that the rainfall function in XBeach also works for the model of the DUD region, 3 separate simulations were done:

- Precipitation only – no waves and water level variations applied (i.e. water level set to MSL)

- Coastal Flooding – waves and water levels applied, no precipitation

- Compound flooding – waves, water levels and precipitation applied.

The resulting flood extents can be found in Figure 5.1 below. Only areas with inundation depths above 5 cm are marked as flooded. A description of typhoon Paka can be found in Section 3.3.4 and an overview of the boundary conditions applied to the XBeach model can be found in Appendix B.2.2.

As can be observed in Figure 5.1, flood hazard for different areas is related to different drivers. Areas on the ocean side are most prone to coastal flooding (in blue) and overwash to the lagoon can be observed at various locations. On the other hand, some areas are only flooded due to precipitation (in red). Especially areas in the middle of the island are mainly flooded by precipitation. These are in general low-lying areas surrounded by higher elevation areas.

Some additional areas are only flooded when combining coastal flooding and precipitation in the same simulation. These are marked in green as compound flooding in Figure 5.1. Hence, when precipitation and coastal flooding would be assessed individually, the flood extents would be underestimated. A map with the simulated inundation depths for compound flooding due to typhoon Paka can be found in Appendix D.1.

5.1.2. Typhoon related flood hazard for different return periods

The flood hazard maps with estimated inundation depths related to typhoons are presented for Return Periods (RP) of 5 and 50 years in Figures 5.2 and 5.3 respectively. Only inundation depths above 5 cm are shown.

Flooded areas largely correspond with those areas flooded by typhoon Paka (Figure 5.1), although relatively more flooding can be observed in the northern part of the DUD region. This can be expected as Paka caused relatively high waves on the southern side (see Appendix B.2.2). In addition, precipitation seems to be important as a significant part of the inundated areas corresponds with the areas inundated by precipitation during typhoon Paka, for example the area around (7.108°N; 171.373°E). This seems to be especially the case for a return period of 5 years.

For a RP of 50 year, the flooded areas are slightly larger and inundation depths somewhat higher, although the difference for many areas is limited compared to those those for a 5 year RP. Some additional areas are flooded, especially areas near the coastline, for example around (7.124°N; 171.357°E).
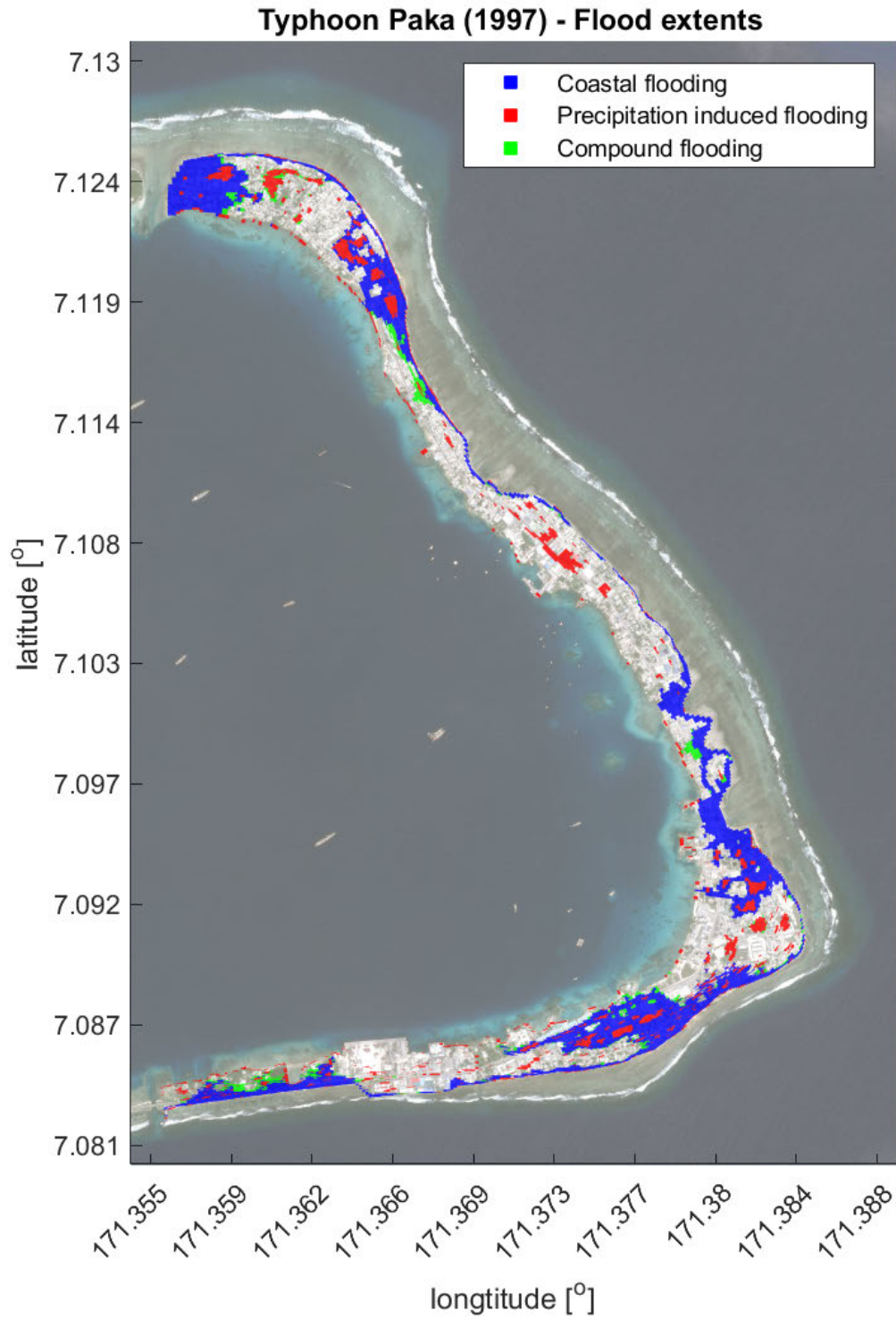
Figure 5.1: *Comparison of the flood extents related to coastal flooding, precipitation and compound flooding for typhoon Paka (1997). Areas that were not flooded due to precipitation or coastal flooding individually but due to the combination are marked as compound flooding. Underlying satellite image: ©2019 CNES/Airbus, 17-3-2017 via Google Maps.*
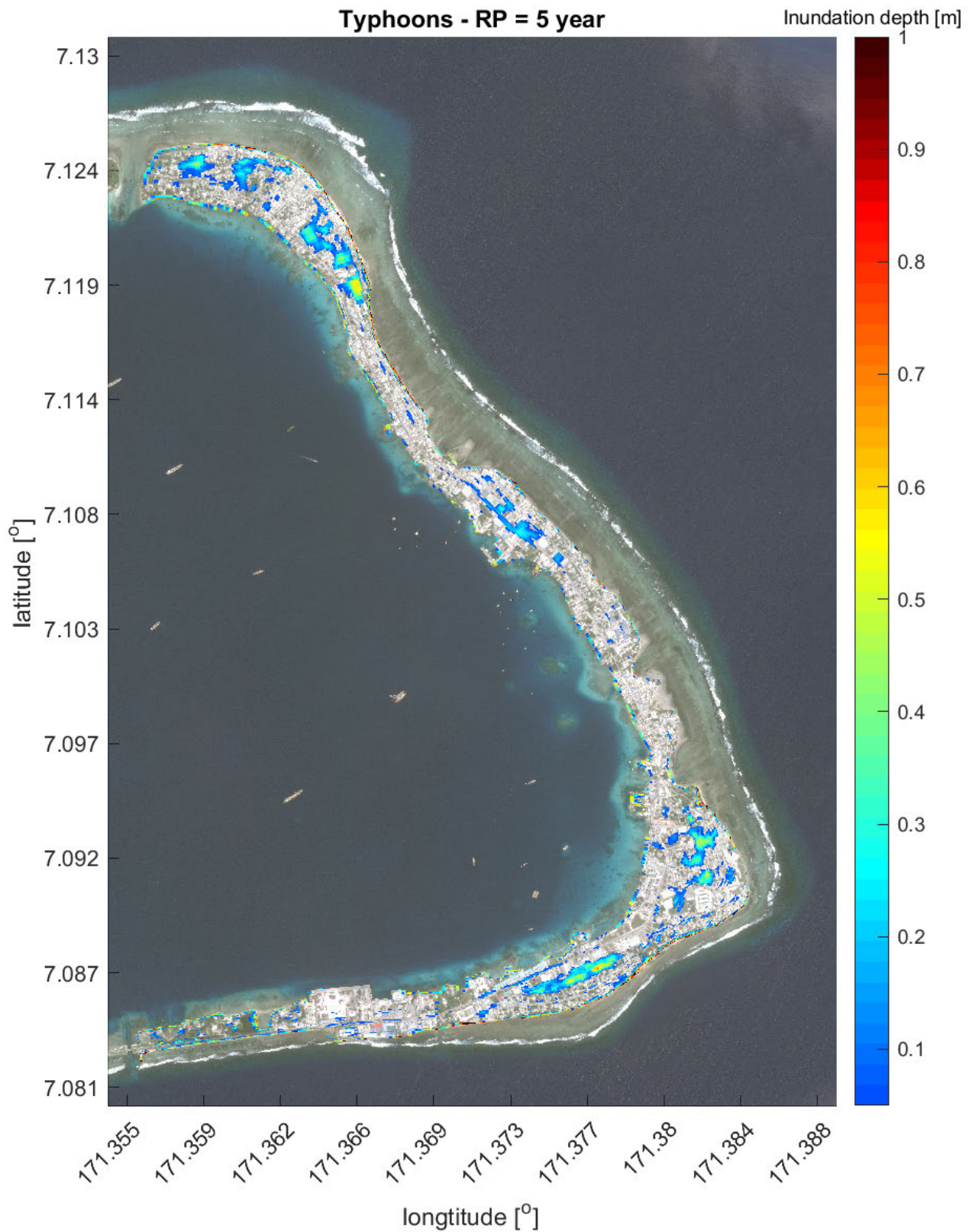
Figure 5.2: *Estimated inundation depths due to typhoons with a return period of 5 year. Underlying satellite image: ©2019 CNES/Airbus, 17-3-2017 via Google Maps.*
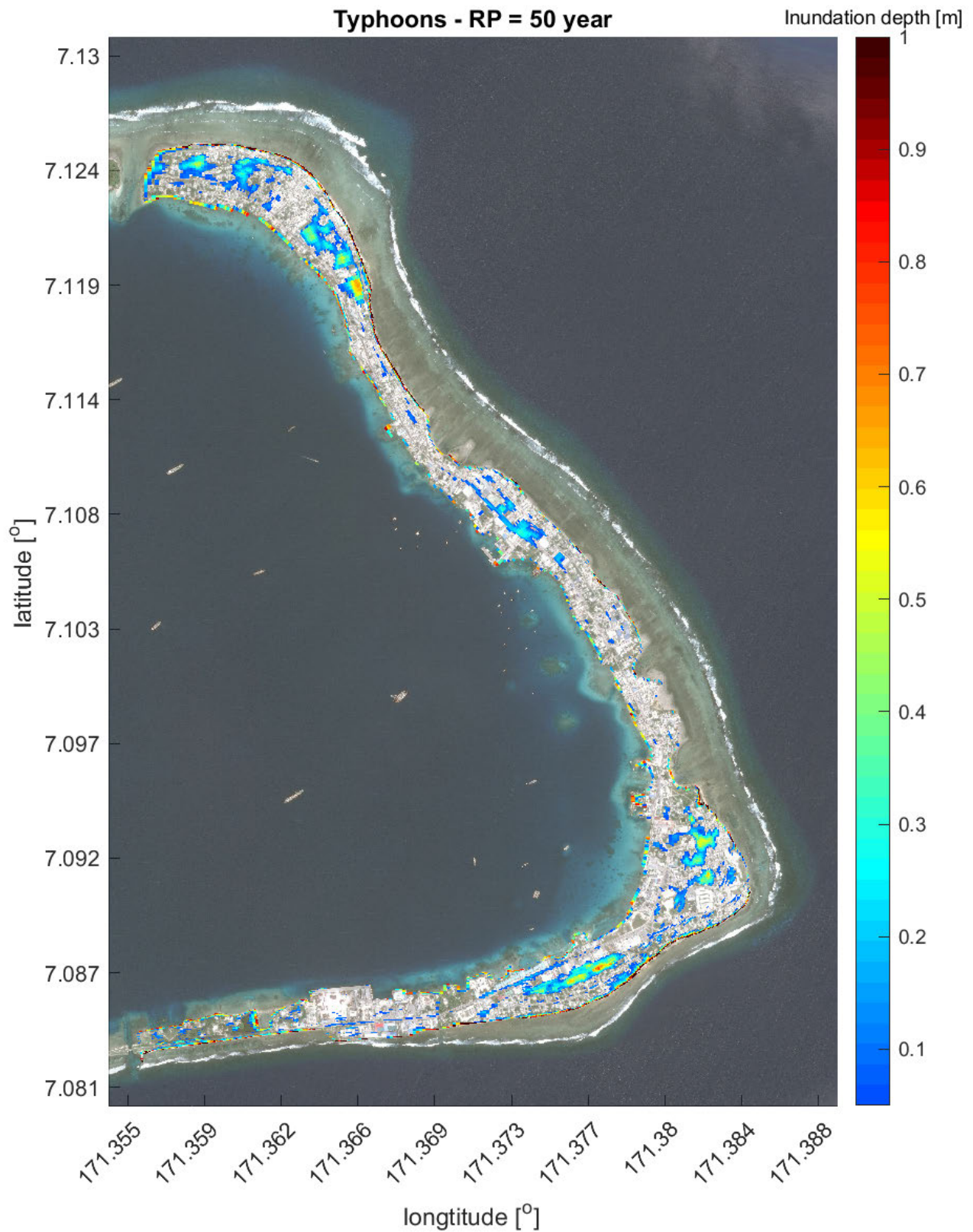
Figure 5.3: *Estimated inundation depths due to typhoons with a return period of 50 year. Underlying satellite image: ©2019 CNES/Airbus, 17-3-2017 via Google Maps.*

5.2. Non-typhoon related flood hazard

In this Section, the flood maps for the non-typhoon conditions are presented for different return periods. Subsequently, the contributions of coastal flooding and precipitation to non-typhoon related flooding are elaborated.

5.2.1. Non-typhoon related flood hazard for different return periods

The inundation depths of the previous section are combined into flood maps for non-typhoon conditions by taking the maximum inundation depth for each grid cell. These are shown for 5 and 50 year return periods in Figures 5.4 and 5.5 respectively.

Flooded locations do partially coincide with those for typhoons, but for non-typhoon conditions flooded areas are in general closer to the coastline. Especially areas in the north (around 7.124°N; 171.357°E) seem to face significant flood hazard. Furthermore, the areas around 7.119°N; 171.366°E and 7.093°N; 171.382°E seem to be regularly flooded. Al these areas are relatively low-lying and near the shoreline. Compared to the flood extents for a 5 year return period, flood extents increase only slightly for a 50 year return period.

5.2.2. Non-typhoon related flood hazard per category

To gain more insight in the relevant flood drivers for different areas, additional flood maps for non-typhoon conditions were made for the scenarios with only precipitation and only coastal flooding respectively. The compound flooding scenarios were completely excluded here. These 3 categories of flooding for non-typhoon conditions are in correspondence with Section 4.2.4.

The flood map presented in Figure 5.6 below is based on all events where *only* coastal flooding (i.e. waves and water levels) may potentially lead to flooding. The flood map presented in Figure 5.7 below is based on all events where *only* precipitation may potentially lead to flooding. Only the maps for a 50 year return period are presented here. The flood maps for a return period of 5 years can be found in Appendix D.2. Inundation depths are approximate, as the compound events are excluded for both.

Coastal flooding occurs mainly at locations close to the shoreline while precipitation related flooding mainly occurs at the more central areas with lower elevation. For the non-typhoon conditions, flood extents for coastal flooding are significantly larger than those for precipitation related flooding. Besides an increase in flood extents, some increase in inundation depths for areas can be observed as well when comparing the maps for 5 and 50 year return periods.

Areas flooded due to precipitation are similar to those for typhoon Paka, but slightly smaller. Table 5.1 provides an overview of the flooded area as fraction of the total DUD area due to coastal flooding and precipitation. Flood extents of Figure 5.1 for typhoon Paka are included here as well.

Table 5.1: Comparison of the flooded area due to precipitation related flooding, coastal flooding and compound flooding. The shown percentages are the fraction of the total land area inundated by at least 5 cm.

Type	Typhoon Paka (1997)	Non-typhoon - RP 5	Non-typhoon - RP 50
Coastal	30.9%	16.2%	18.3%
Precipitation	9.2%	3.8%	6.2%
Compound	34.8%	-	-
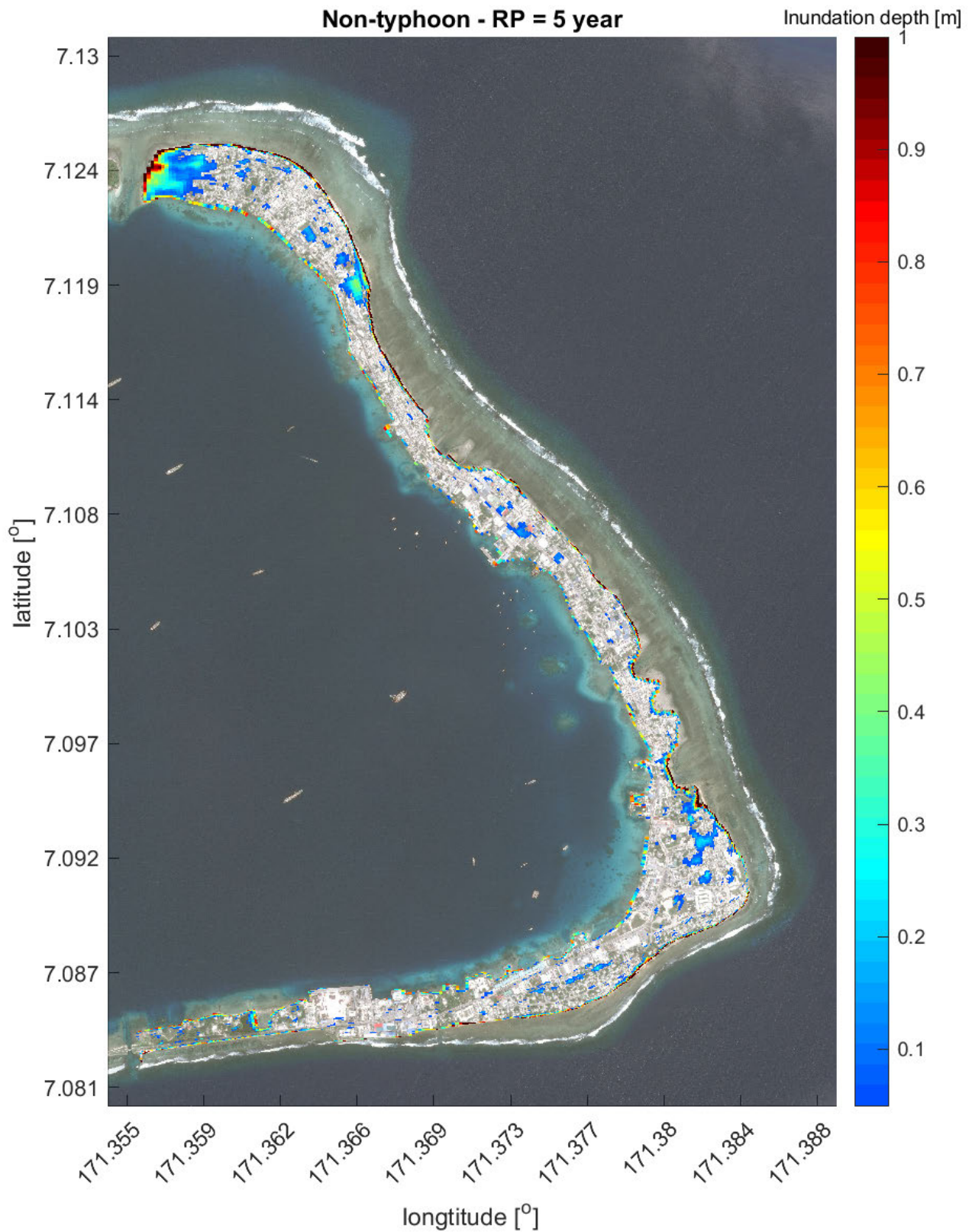
Figure 5.4: *Estimated inundation depths for non-typhoon conditions with a return period of 5 year. Underlying satellite image: ©2019 CNES/Airbus, 17-3-2017 via Google Maps.*
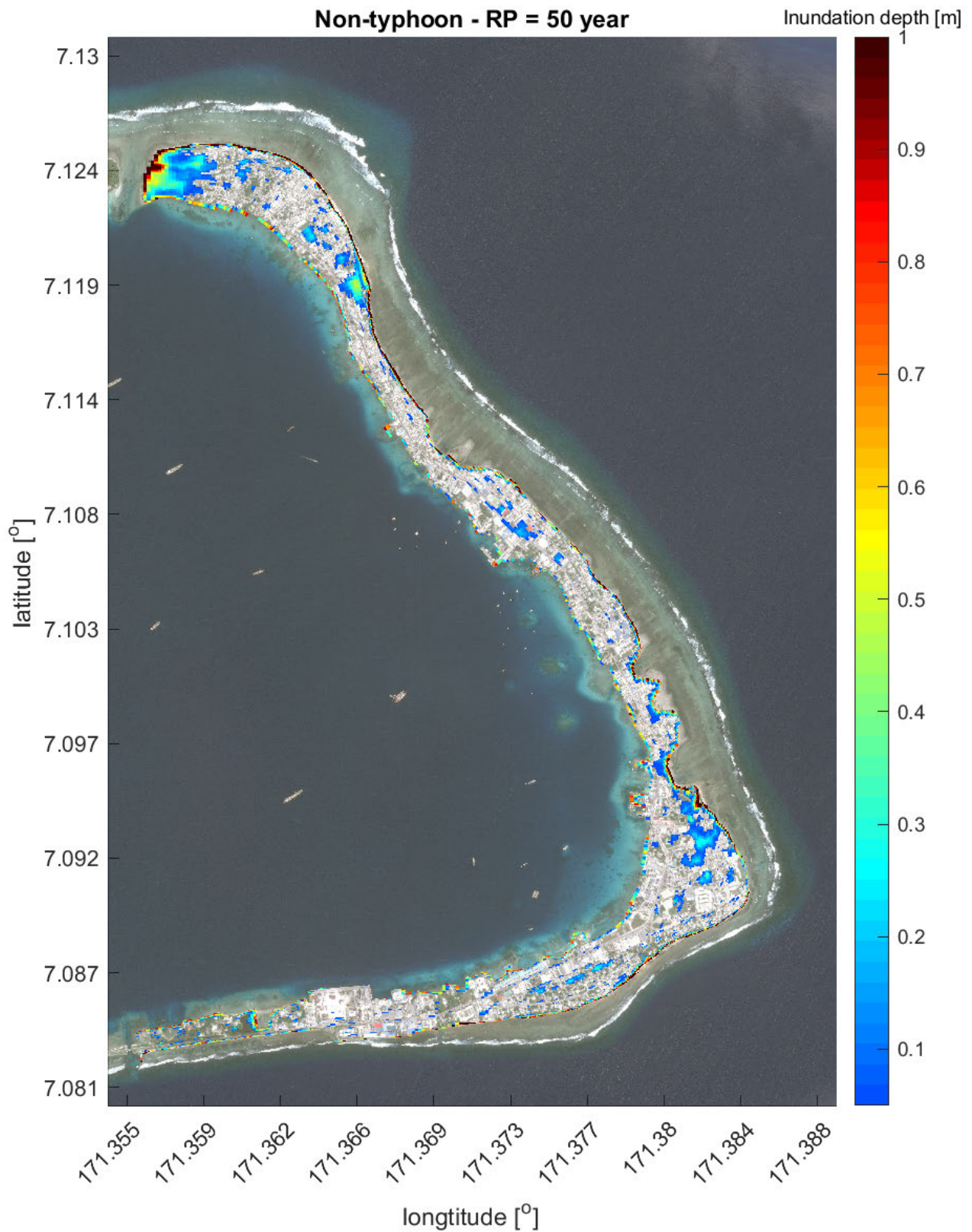
Figure 5.5: *Estimated inundation depths for non-typhoon conditions with a return period of 50 year. Underlying satellite image: ©2019 CNES/Airbus, 17-3-2017 via Google Maps.*
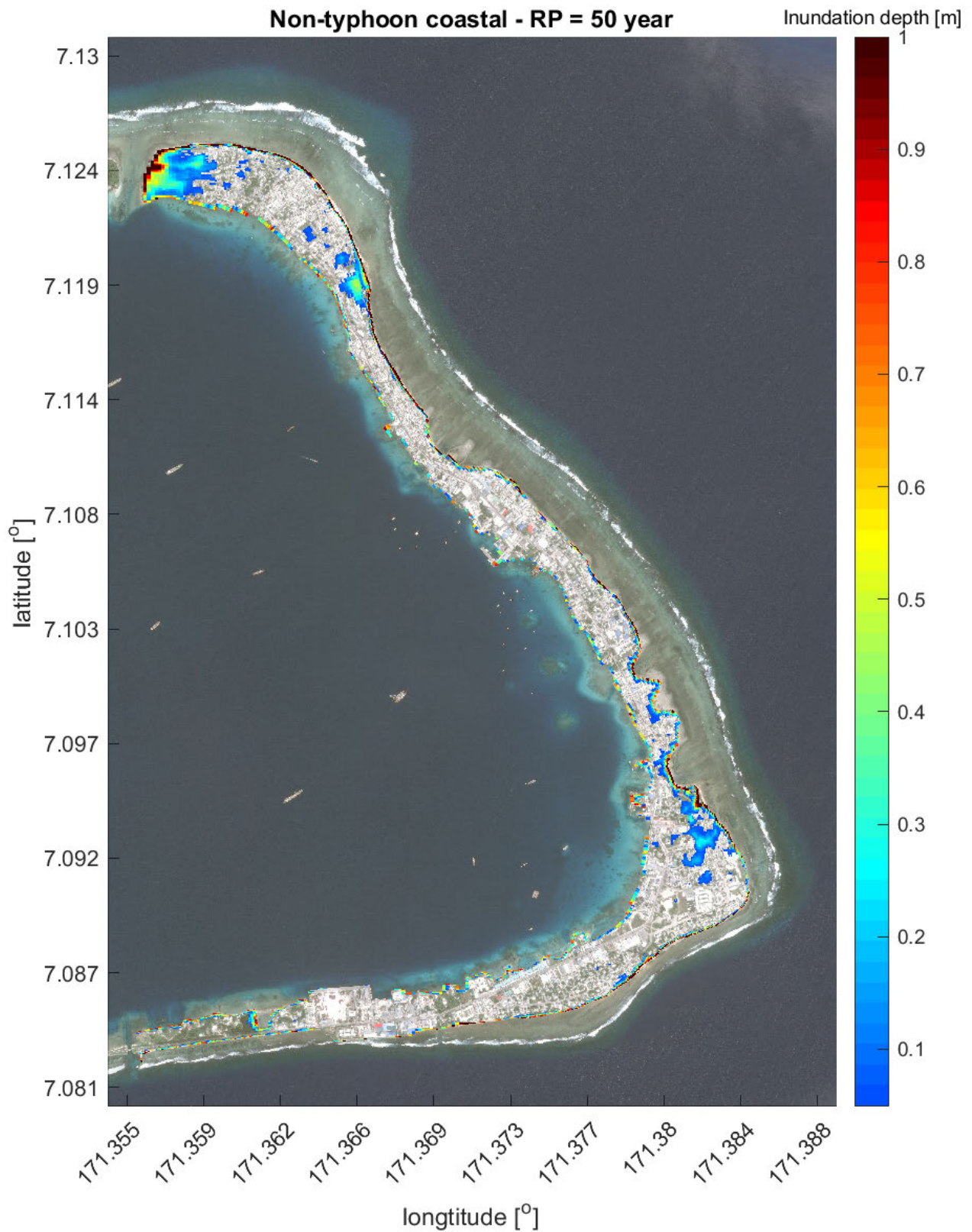
Figure 5.6: *Estimated inundation depths for coastal flooding during non-typhoon conditions with a return period of 50 year. Underlying satellite image: ©2019 CNES/Airbus, 17-3-2017 via Google Maps.*
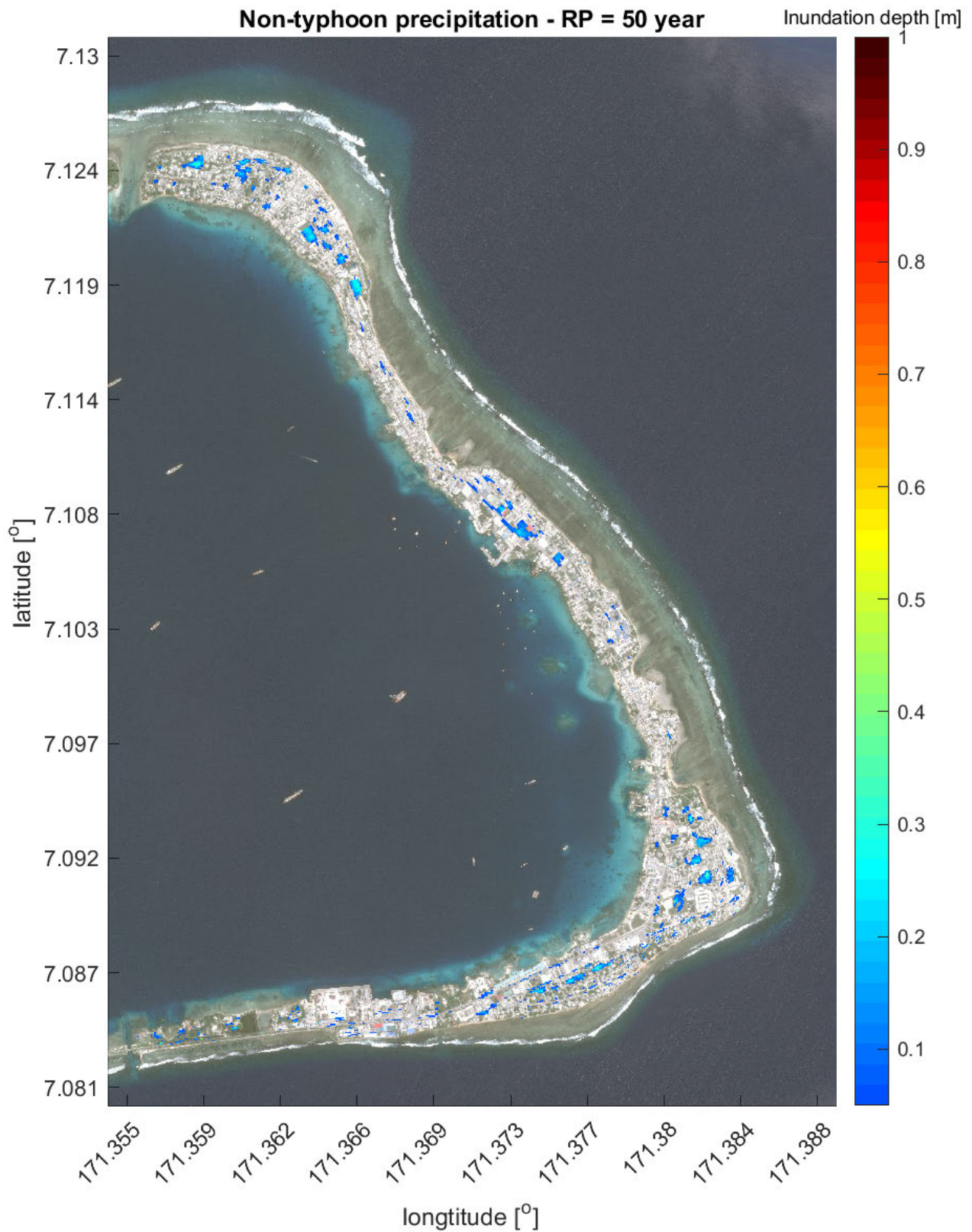
Figure 5.7: *Estimated inundation depths for precipitation related flooding during non-typhoon conditions with a return period of 50 year. Underlying satellite image: ©2019 CNES/Airbus, 17-3-2017 via Google Maps.*

5.3. Combined flood hazard

The flood maps below show the total flood hazard for the DUD region – here the maximum inundation depths for typhoon and non-typhoon conditions are combined. In Section 3.1 typhoon and non-typhoon conditions were defined as mutually exclusive in time. Hence, the combined flood maps could just simply be derived by taking the maximum inundation depth per grid cell of the flood maps for typhoons and non-typhoon conditions with the same return period.

Flood maps for 5 and 50 year return periods are presented in Figures 5.8 and 5.9 respectively. Flood maps for return periods of 20 and 100 years can be found in Appendix D.3. Here, also the maximum simulated inundation depths can be found, which correspond to a return period of 1000 years as inundation depths for 1000 years of events were determined. However, for reasons explained in the next chapter the estimated inundation depths for larger return periods come with large uncertainty.

Table 5.2 below provides an overview of the flood extents as fraction of the DUD region for different return periods. Areas prone to flooding due to typhoons and non-typhoon conditions clearly overlap but are not exactly the same, as the percentage for the combined flood extent is higher than those for typhoons and non-typhoon conditions individually. For return periods below 5 years and above ±100 years, uncertainty in the shown percentages is larger and those should be interpreted with caution.

Table 5.2: *Flooded area at the DUD region for different return periods, for typhoons, non-typhoon conditions and the combination. The shown percentages are the fraction of the total land area inundated by at least 5 cm.*

Return period [years]	Typhoons	Non-typhoon conditions	Combined
1	8.9%	17.5%	18.7%
2	16.7%	18.3%	23.6%
5	21.0%	19.2%	26.5%
10	22.2%	19.9%	27.4%
20	22.9%	20.6%	28.0%
50	24.3%	22.4%	29.4%
100	25.7%	24.1%	31.0%
200	27.0%	26.3%	32.8%
500	28.4%	29.1%	35.0%
Maximum (1000)	33.8%	35.4%	40.3%
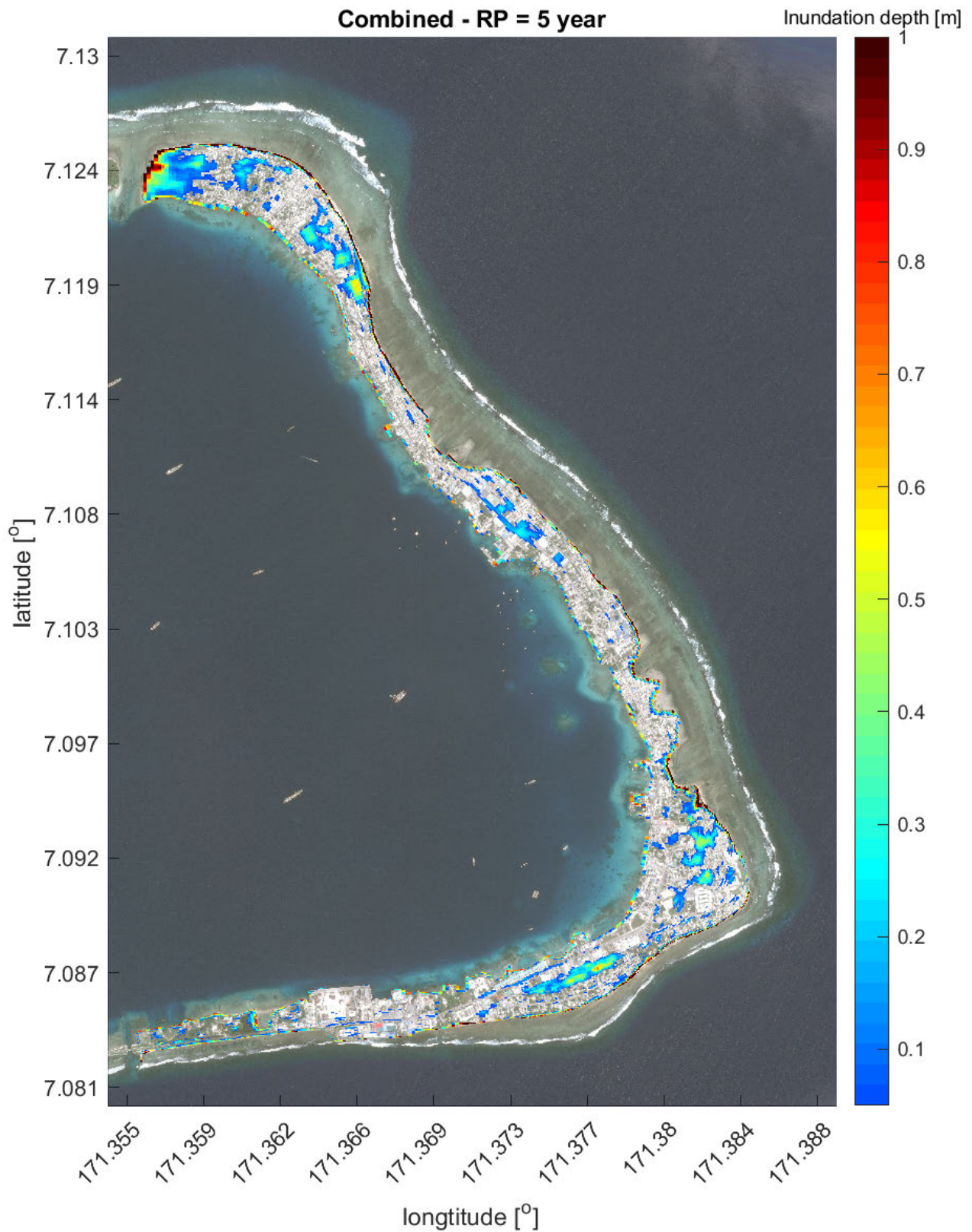
Figure 5.8: *Estimated inundation depths for a return period of 5 year. Underlying satellite image: ©2019 CNES/Airbus, 17-3-2017 via Google Maps.*
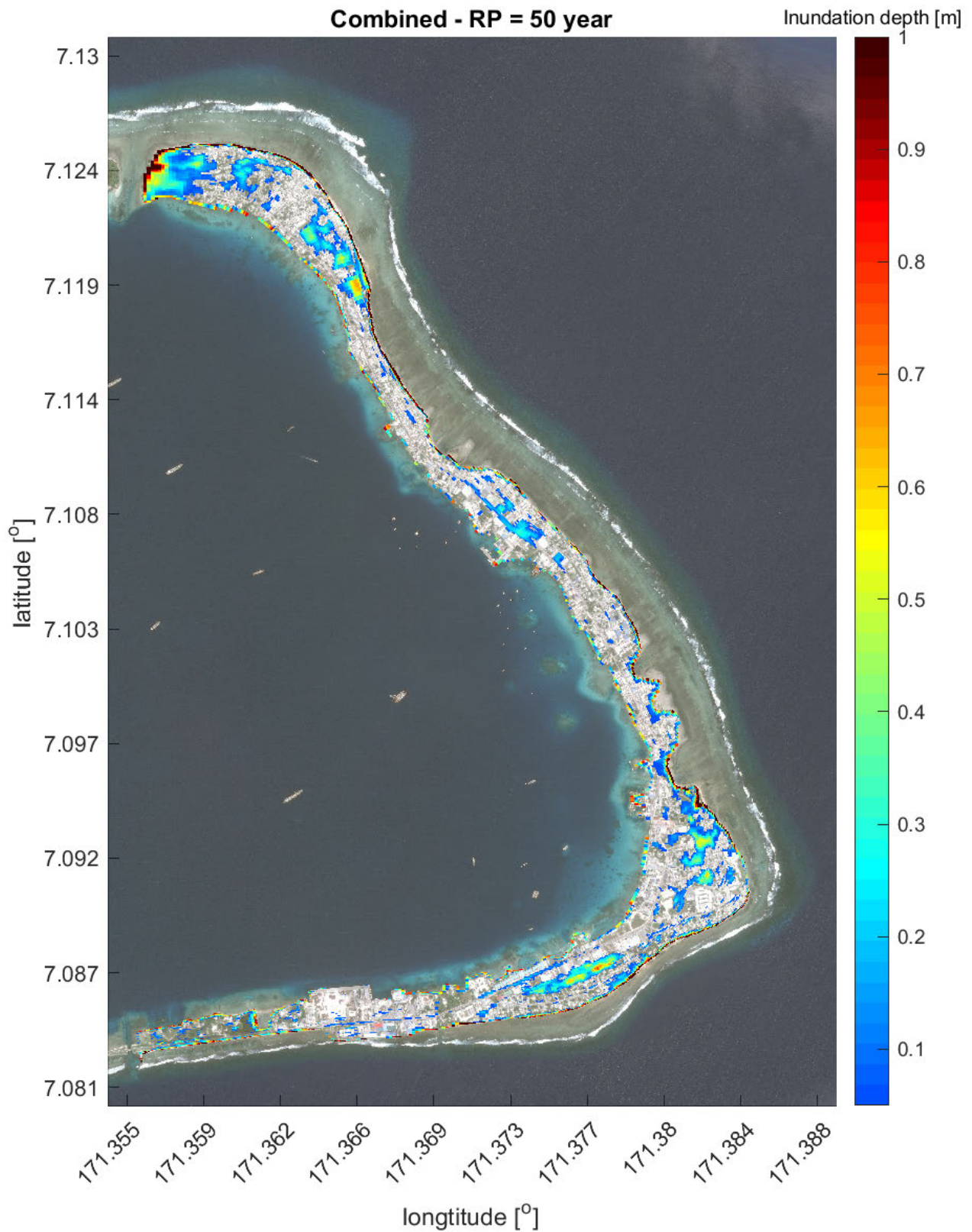
Figure 5.9: *Estimated inundation depths for a return period of 50 year. Underlying satellite image: ©2019 CNES/Airbus, 17-3-2017 via Google Maps.*

6

Discussion

Chapter summary

- In Section 6.1, the different parts of the flood hazard assessment approach, and the scenarios derived in Chapter 4 are discussed. By distinguishing typhoons and non-typhoon conditions and the generation of synthetic data, the different interdependencies seem to be reasonably well included. Subsequently, a three step approach was successfully applied to make simulation of inundation depths computationally feasible: (1) Scenario selection by MDA, (2) compound flood modelling with XBeach and (3) interpolation with Softmax. For each step, important limitations and implications for the flood hazard assessment of the DUD region are discussed.

- The flood maps for the DUD region of Chapter 5 – for different flood drivers and return periods – are discussed and compared in Section 6.2. For a return period of 5 years, flooding related to non-typhoon events seem to be more important than typhoon related flooding. For a return period of 50 years, flood extents and inundation depths for both seem to be more similar, although this varies significantly per location. The specific characteristics of atoll islands (i.e. narrow island with lowest elevation in the middle) seem to have important consequences for the inundation depths; these are maximum near the coastline, but also significant for the more central low-elevation areas. Here, inundation depths seem to be limited to some maximum, whereafter excess water flows into the lagoon. Inclusion of precipitation was shown to be important for flooding, but an important limitation here is the absence of infiltration in the used XBeach model. In any case, further validation of the models used – especially the XBeach model – is necessary.

- Suggestions for improvement and future work are summarized in Section 6.3. First those related to the flood hazard assessment approach and scenario derivation are discussed, whereafter some suggestions more specific for the DUD region are elaborated.

6.1. Flood hazard assessment approach and scenarios

Key to the inclusion of compound events in a flood hazard assessment is to capture the full range of possible scenarios with correct probability of occurrence in a computationally feasible approach. The approach in this study was tailored to the specific characteristics of atoll islands (i.e. narrow and low-lying) and the flood drivers for Majuro, although parts seem applicable to many other study areas where a high number of scenarios is needed to include all (combinations of) drivers.

By distinguishing typhoon and non-typhoon conditions and the generation of large synthetic data sets, a much wider range of scenarios with seemingly realistic interdependencies of the different types of flood drivers could be generated. The combination of Maximum Dissimilarity Algorithm (MDA), simulation of representative events, and interpolation could be used to obtain a significant reduction in the number of scenarios that has to be simulated. Hereby simulation with the computationally expensive XBeach model was made feasible, which was needed to properly include waves.

In spite of that, many parts of the approach in this case study can be seen as a first application. Hence, there are many possibilities for improvements in future cases. The key elements of the approach are discussed step by step below, together with their limitations and suggestions for future improvements (discussed in Section 6.3). The results for Majuro and the DUD region specifically are discussed in Section 6.2.

6.1.1. Synthetic data generation
First, the distinction between typhoon and non-typhoon scenarios is briefly elaborated, after which the synthetic data generation for each is discussed.

Distinguishing typhoon and non-typhoon scenarios
Distinguishing typhoon and non-typhoon scenarios (Section 3.1) proved to be a useful method for including the different interdependencies between precipitation and coastal flooding. A major disadvantage is the rather arbitrary distinction between the two. The conditions at Majuro for part of the historical time frames that were marked as *'typhoon conditions'*, were most likely not dominated by the typhoon. This mainly had important implications for the selection of representative typhoons, as discussed in Section 6.1.2 below.

Although the derived synthetic data sets contain many more different scenarios, the influence of individual events can sometimes still be distinguished. For example, in the maps for the maximum wind speed (Figure 4.5) the contributions of individual typhoon tracks can be clearly distinguished. By generating a synthetic data set for an even longer period (e.g. 10 000 years) this might be solved relatively easily. Hereby, the uncertainty in derived inundation depths for low return periods could be reduced. However, one should keep in mind that the data is still based on the same historical data set, and thereby comes with larger uncertainty for higher return periods.

Synthetic typhoons
The 1000 years of synthetic typhoons derived with TCWiSE were presented in Section 4.1.1. Based on comparison with historical typhoons, these were concluded to be generally realistic, although a few tracks were located closer to the equator than can be expected based on historical events and from a physical point of view. This is expected to be of limited importance for the flood hazard assessment of Majuro, as (a) this applies to only a few of the 2135 typhoons and (b) those only pass Majuro at such distance that they have limited impact.

Synthetic non-typhoon events
The 1000 years of synthetic non-typhoon events derived by use of a Bayesian Network (BN) in Uninet (Section 4.2) were reasonably well in correspondence with the historical events, although not all interdependencies were completely realistic. This is mainly because (a) the fitted distributions for the marginals deviate from the historical data, and (b) the joint normal copulas used here are not necessarily a good model for the dependencies (but were the only available option). Especially at the southern side of the DUD region (location G), reason (a) may have led to some underestimation

of the wave conditions and thereby flooding.

Threshold values for the minimum runup (by BEWARE, Section 4.2.3) and cumulative precipitation on a day were used to select only those events that may potentially lead to flooding. Based on BEWARE, relatively more synthetic events than historical events were concluded to potentially lead to flooding. Especially for the infrequent compound events, this difference was large. Most likely this is caused by reasons (a) and (b) of the previous paragraph. Additionally, the binned character of the BEWARE output could play a role, as the estimated runup of an event could just fall in a higher bin and be concluded to potentially cause flooding or vice versa.

Another consequence of the binned output of BEWARE was that the threshold value of the runup had to be set relatively high. Besides, the threshold was set to MSL +3.5 m for all locations, while different threshold values for different locations may actually be more realistic. A consequence may be that for some locations, especially location G in the south, some excluded events with wave conditions below the threshold value may actually lead to flooding. A sensitivity analysis of BEWARE may provide more insight in the effects of the binned character of the output.

6.1.2. Scenario selection

First some general remarks on the Maximum Dissimilarity Algorithm (MDA) are discussed, whereafter some specific points for the typhoon and non-typhoon scenarios are elaborated.

Maximum Dissimilarity Algorithm (MDA)

MDA proved to be quite well capable of selecting a set of representative events out of a larger set of (synthetic) events. The method was successfully applied to both the typhoon and non-typhoon scenarios. In both cases, selected representative events are well spread over the synthetic events and most of the extremes are included. Nevertheless, this case study contains only some first applications, and many parts could be further developed and optimized.

The sets of parameters and weight factors used here were based on physical insights and seem to work well. All combinations of 2 parameters were assessed and in general, the selected scenarios showed to be well spread over the 2 parameter space. Although it can thereby be expected that the spread in events over the full parameter space is reasonable as well, this is difficult to assess.

One of the complications in using MDA in high dimensional problems is the assessment of the quality of the obtained set of scenarios. The algorithm used for MDA calculates the distance between different events based on all normalized parameters combined (see Section 2.4.4). Hence, the number of parameters should be limited, to prevent that the influence of the individual parameters on the combined distance between events becomes insignificant.

On the other hand, the specific characteristics of an event can be better described by more parameters. In addition, the actual values of the parameters do matter and weight factors further complicate things. Hence it is impossible to obtain one optimal set of parameters or weight factors, and other combinations may lead to better results. Nevertheless, for both the typhoons and non-typhoon conditions, MDA proved to be a useful and promising tool in selecting representative scenarios.

Typhoon scenarios

In general the representative typhoon scenarios selected for this study in Section 4.1.2 were concluded to be a good representation of all synthetic events. Already with 50 representative scenarios, reasonable results were obtained. With 200 scenarios the results for the higher return periods improved considerably (see Section 4.1.4). However, some of the synthetic typhoons in the Delft3D model domain (or area of interest) were actually irrelevant for flooding. Therefore a part of the selected representative events also became irrelevant. One way to improve this is to make a better selection of events *before* selecting the representative events.

After simulation in Delft3D, 17 out of 50 representative typhoons appeared to have such low significant wave heights at the boundary of the XBeach model and such low precipitation rates, that they

were considered irrelevant for flooding. These scenarios where not further simulated in XBeach, and no flooding was assumed. From the perspective of computational efficiency, it is unfavourable that so many irrelevant scenarios are simulated. On the other hand, the range of the events should be chosen large enough to make sure that all events that can potentially lead to flooding are included.

In Figure 6.1 the maximum simulated offshore surge levels of Figure 4.13 are plotted against the minimum distance of the corresponding typhoon track to Majuro. Typhoons that passed at distances larger than roughly 700 km did not lead to noticeable surge, while the majority of the representative events was selected from these. This suggests that the area could be substantially decreased without excluding relevant typhoons.

However, for flooding at Majuro, waves are much more important than surge. As waves can propagate over large distances, it can be expected that also typhoons passing at distances larger than 700 km may lead to waves at Majuro. Based on the simulated wave conditions for the representative typhoons this indeed seems to be the case, although waves from the more distant typhoons are in general small. For computational time reasons, wave conditions could not be simulated for all synthetic typhoons at this location. A compromise could be to decrease the domain of the FLOW module of the Delft3D model, while keeping the same domain WAVE module. Similar figures for the water levels and wave heights at Charchenga Station (Bangladesh) can be found in Appendix C.2.1.
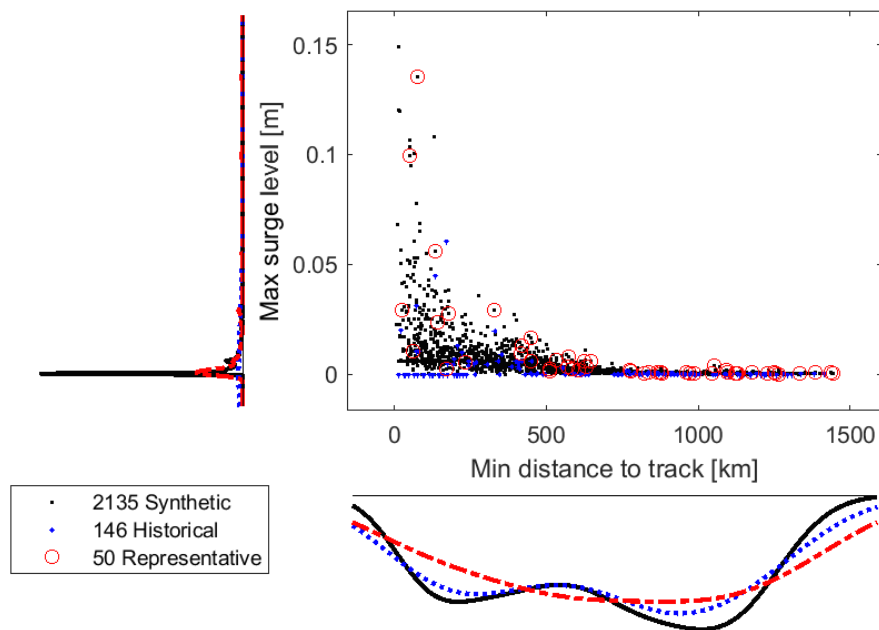
Figure 6.1: Maximum offshore surge level versus the minimum distance of the typhoon track to Majuro. Surge levels are simulated with the Delft3D-FLOW model (see Section 3.3.2) and presented for the location north of Majuro (see Figure 3.1).

Following from the flood maps for typhoon conditions in Section 5.1, precipitation can considerably contribute to the inundation depths. Although the precipitation rates are linked to the maximum wind speed by the relations of Bader (2019), inclusion of the variation in this could be improved by adding precipitation related parameters to the MDA (e.g. maximum or cumulative precipitation rate in the area of interest). Similarly, inclusion of parameters related to the total water level could further improve the method to select representative scenarios. In any case, it seems advisable to base such selection of parameters as much as possible on physical insights.

Non-typhoon scenarios
In Section 4.2.4, selected representative events for non-typhoon conditions were concluded to be a good representation of all synthetic non-typhoon events that may potentially lead to flooding.

Extremes were well included and the scenarios are well spread over the parameter space for all shown combinations of parameters.

Some of the suggestions for improvement of the typhoon scenario selection described above were already implemented in the selection of representative non-typhoon events. For example, the total water level was used in the MDA, and BEWARE was used to decrease the number of simulated events that was actually irrelevant. For the non-typhoon conditions, the main improvements can be made in the synthetic data generation and interpolation method.

6.1.3. Compound flood modelling with XBeach

Inundation depths for all representative scenarios were simulated by use of the XBeach model described in Section 3.3.3. Although some checks of simulated water levels, wave heights and inundation depths were done, validation of the XBeach model was not possible. Comparison of different grid sizes showed that inundation depths may actually be somewhat underestimated by the grid used (Appendix B.2.3). The grid used is also coarser than recommended (Hoonhout, 2015). Unfortunately, a finer grid was computationally unfeasible (Section 3.3.4).

Waves from the lagoon side were not included in the model. Especially during typhoon events, these can be expected to cause compound flooding. During non-typhoon conditions these may also be relevant. Waves generated locally in the lagoon can lead to flooding on atoll islands (Giardino et al., 2018). Furthermore, swell waves breaking on the reef can lead to great water influx into the lagoon and high water levels; this phenomenon has led to major flood events at other atoll islands (Canavesio, 2019). Inclusion of wave impact from the lagoon side in the XBeach model was not possible, as the boundary conditions could only be applied at one side of the domain. A possible solution could be the carrying out of additional simulations with only boundary conditions applied at the lagoon side.

The newly developed rainfall function in XBeach was validated by use of a simple case study (see Appendix B.2.1). In addition, typhoon Paka was used to assess the influence of inclusion of rainfall (Section 5.1.1). The results seem to be in line with expectations, but due to the bathymetry applied for the DUD region model, validation of the simulated inundation depths by comparison with the applied rainfall rates is not feasible.

Infiltration, possible drainage systems, seawalls (if not present in the bathymetry data) and erosion processes were not included. Inclusion of infiltration seems especially important when precipitation is included, although this should be confirmed by future research. Inclusion of these would most likely lead to lower inundation depths. Erosion seems especially important for longer and more extreme storms, when higher elevation areas near the shoreline may (partially) erode and allow for more water to flow to lower elevation areas. When the needed data for validation becomes available in the future, it is strongly recommended to perform an comprehensive validation of the model.

Boundary conditions

Wave conditions and surge levels were derived using Delft3D and SWAN models. Although some checks were done and a similar setup for the Delft3D model was used by Giardino et al. (2018), further validation of the results is advisable.

For computational time reasons, only the peak of the typhoon events was simulated. These time frames were selected manually and varied per typhoon; the most extreme conditions for all were included. This may lead to underestimation of the inundation depths, especially for precipitation related flooding, as the cumulative precipitation rates are important. For example, only one third of the total precipitation of the typhoon in Figure 4.16 was included in the XBeach simulation. On the other hand, Bader (2019) mentions that precipitation rates may be somewhat overestimated for larger distances from the typhoon eye. Hence, precipitation rates for some typhoons may actually be slightly overestimated, especially when the typhoon passes at larger distance. For the non-typhoon conditions, some variation may be included in the standard event.

For both typhoon and non-typhoon scenarios, the tidal water level was randomly selected and ±24 hours were simulated to include a semi-diurnal tidal cycle. Nevertheless, for both typhoon and non-typhoon scenarios, the timing of the high tide in relation to the other B.C. (e.g. the peak wave height and peak precipitation) is random. The timing of these peaks may actually significantly influence the observed inundation depths per event. By taking 50 events it can be expected that this effect is partially averaged out, although especially via the most extreme events it may influence the maximum simulated inundation depths.

For non-typhoon conditions, wave conditions were assumed to be constant at their maximum value while in fact they will most likely vary over the day (see Section 4.1.5 and especially Figure 4.23). Hereby, the highest water levels and peak wave conditions always coincide, so that inundation depths are overestimated. Although variations in wave conditions over the day are not expected to be as large as for precipitation, this could be improved e.g. by using a standard event.

6.1.4. Interpolation

In order to make flood maps for different return periods, the inundation depths for *all* synthetic events have to be known – not just those of the simulated representative events. These were derived by interpolation with Softmax according to the method explained in Section 3.4.3.

Although Softmax was used for both typhoon and non-typhoon conditions, validation was only done for typhoon conditions. For typhoon conditions, simulated offshore water levels and significant wave heights for different return periods could be reasonably well approximated as shown by the Charchenga station (Bangladesh) case study in Section 4.1.3. 90 representative typhoons were shown to cover a broader range of typhoon events than 90 historical events. This was confirmed by comparison of simulated and approximated offshore water levels near Majuro (see Figure 4.13). Performance for water levels offshore at Majuro was better compared to Charchenga station, which is most likely related to (a) the size of the area used to select relevant typhoons and (b) the fact that part of the typhoons near Charchenga station passes at the land side.

When looking at the approximated inundation depths for individual synthetic typhoons, larger errors can be found especially for the more extreme events (see Appendix C). Apparently these errors for the individual typhoons are partially averaged out when going to the return periods, but for return periods larger than ±100 years, this is not necessarily true and uncertainties become larger. It can be expected that improvements to the parameters and size of the area of interest (as discussed in Section 6.1.2) will improve this. Possibly other interpolation techniques (e.g. radial basis functions as applied by Rueda et al., 2019) are actually more suitable and lead to further improvement.

For non-typhoon events it was not possible to validate the results after interpolation. The approach is similar as for the non-typhoon conditions, and for reasons explained in Section 4.2.4 it can be expected that the applied β factor is in the right order of magnitude. In any case, it is highly recommended to validate this in the future. One way to do this could be the simulation of part of the synthetic non-typhoon events (e.g. 1000 randomly selected events) and compare the simulated and approximated inundation depths – these should be similar just as for the typhoon conditions.

6.2. Flood hazard for the DUD region

The flood maps of Chapter 5 provide insight into which areas are most prone to flooding and to some extent, what the main drivers of flooding are. Relative importance of different flood drivers for different return periods, and implications for the DUD region are discussed below. Flood maps were derived for different return periods for typhoon conditions (Section 5.1.2) and non-typhoon conditions (Section 5.2.1). In addition, some flood maps were made to assess the relative importance of precipitation and coastal flooding. For typhoon conditions, this was only done by comparison of the flood extents for typhoon Paka (Section 5.1.1). For non-typhoon conditions, again flood maps for different return periods were made (Section 5.2.2).

When comparing the flood maps for typhoon and non-typhoon conditions, it seems that flooding

related to non-typhoon conditions is for most locations more important than typhoon-related flooding. This is especially the case for low return periods; non-typhoon related flood events seem to be more frequent at Majuro, although the most extreme events are typhoons. For the southern part of the DUD region, occasional flooding during typhoons seems more important than coastal flooding, but flood depths during non-typhoon conditions may be somewhat underestimated there for reasons explained in Section 6.1.1.

Both coastal flooding and precipitation may lead to flooding, and following from Section 5.1.1 flood extents are underestimated when both are assessed independently. The relative importance of precipitation and coastal flooding differs per location. Especially areas that are more in the middle of the island are prone to precipitation related flooding. These are surrounded by higher elevation, hence the so called *'bathtub'* (Section 2.1). As infiltration is not included in the XBeach model, water can not escape from these areas in the model.

Areas at the ocean side often have higher elevation, and when the topographic slope allows, precipitation can run off; these areas are more prone to coastal flooding. On the other hand, when these higher elevation areas are over topped by oceanic water, the lower elevation areas in the middle of the island get flooded as well. Hence, the areas most frequently flooded by oceanic water may be found near the coastline (for low return periods), but for higher return periods, the areas with the highest inundation depths can be found in more central lower elevation areas.

For many areas, the inundation depth seems to be limited to some maximum, whereafter inundation depths do not significantly increase for higher return periods. This can be explained again by the *'bathtub'* shape of a cross section; at some point *'the bathtub is full'* and excess water flows of to other areas – often the lagoon. This idea seems to be confirmed by Figure 6.2 below. Here inundation depths over time (left) for all grid cells in an area at Majuro (right, marked in red), are presented for the simulation of precipitation during typhoon Paka. For many grid cells the inundation depth remains constant after some time, while the cumulative precipitation still increases. Hence, excess precipitation should run off to other lower lying areas.
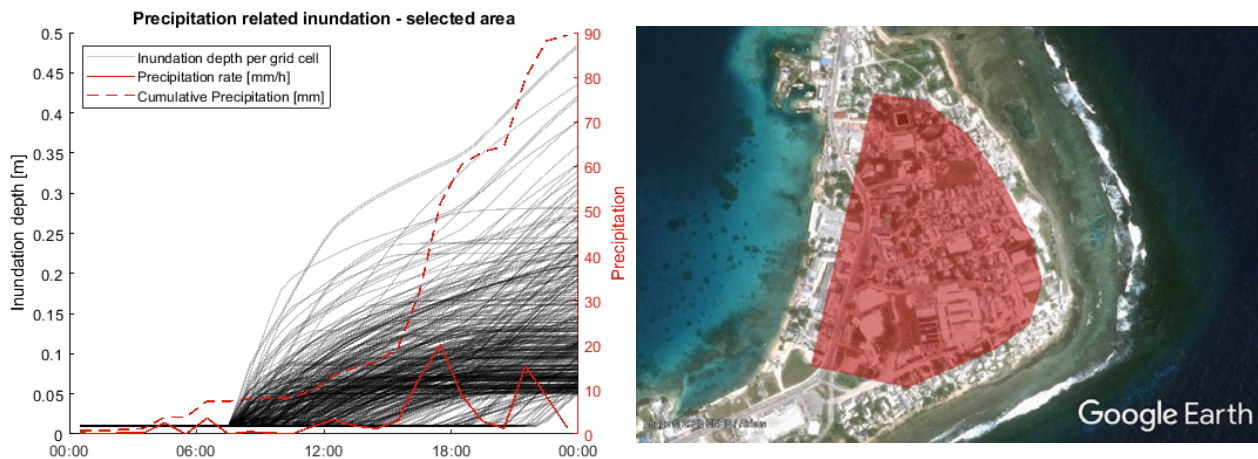
Figure 6.2: Inundation depths over time (left) for all grid cells in the area of the DUD region marked in red (right). While cumulative precipitation increases, for many locations (i.e. grid cells) the inundation depth does not. Hence there seems to be a maximum inundation depth.

Based on the Section 4.1.4, the method seems to be reasonably capable of approximating (offshore) water levels with a return period up to ±100 years based on 50 representative scenarios. For higher return periods, the uncertainties become larger. Several limitations and uncertainties were identified in Section 6.1. Hence the derived flood maps, especially those for the higher return periods, should only be used with those limitations and uncertainties in mind.

Inundation depths and flood extents derived for the DUD region seem to be lower than those derived in a case study for the relatively nearby Ebeye (Giardino et al., 2017, 2018), although it is

unclear to what extent these islands can be compared. As no precipitation nor compound flooding were included in that case study, actually more flooding may be expected. On the other hand, typhoons are somewhat more frequent around Ebeye, which seems less sheltered compared to the DUD region behind Arno Atoll. Hence given all the uncertainties in both studies, the results are reasonably well in agreement.

6.3. Next steps

Suggestions for improvements and future work following from the above Sections are summarized below. In line with the above Sections, first the recommendations related to the compound flood hazard assessment approach are discussed, whereafter those for the flood hazard at the DUD region are elaborated.

6.3.1. Flood hazard assessment approach and scenarios

As discussed in Section 6.1, many parts of the approach seem useful and promising for future case studies, and in many perspectives this study should only be seen as a first case study. Some suggestions for further improvement of the approach in future case studies are summarized below. Lastly, some suggestions for additional validation of the XBeach model are briefly discussed.

Following from Section 6.1.2, it seems that reducing the size of the area used to distinguish typhoon and non-typhoon conditions will lead to a set of synthetic typhoons that is more relevant for flooding. Based on Figure 6.1 the suggested area could be a circle with a radius of ±700 km. For atoll islands surrounded by the deep ocean, the model domain for the FLOW part of the coupled Delft3D model could be significantly reduced to save computational time.

Although MDA performed well in selecting representative scenarios, the selection could be improved by including parameters related to precipitation and to the tide for typhoon conditions. Possibly as replacement of other parameters, such as the median forward velocity and the median of the maximum wind speed. Inclusion of a larger number of representative events (e.g. 200 instead of 50) seems advisable, as results improved – especially for the high return periods. For the non-typhoon conditions it seems advisable to perform a more in-depth study into the different interdependencies as represented by the BN. As the optimal β factor in Softmax does depend on the total and the representative number of scenarios, possibly a more advanced interpolation method such as radial base functions could further improve reliability of the results.

Application of the method in more case studies is needed before generalization. Although the approach was tailored to atoll islands, parts of this approach may also be very useful for other coastal areas – especially the selection of representative scenarios by MDA. In such case studies, preferably the results of all scenarios can be compared with those based on the representative scenarios in combination with interpolation. In this study, offshore water levels (for the Majuro and Bangladesh cases) and wave heights (for the Bangladesh case) were compared, but in the end interpolation was used to obtain the inundation depths on land. Hence, validation of the inundation depths seems preferable.

Compound flood modelling with XBeach

Although some checks of the XBeach model results were done, thorough validation was impossible due to limited availability of data. Hence, it is strongly advisable to perform a detailed validation of the XBeach model, based on field measurements. For example, this could be done by comparing measured and simulated water levels on the reef flat, for different offshore wave conditions and water levels. Some checks of the bathymetry seem useful as well, as deviations here can have very large consequences for the simulated inundation depths.

A more detailed study into the influence of the grid size seems useful, given the fact that a finer (computationally unfeasible) grid led to more flooding in simulations for typhoon Paka (Appendix B.2.3). The same applies to possible boundary effects – especially in the northern part of the DUD region. Further validation of the rainfall function and especially the inclusion of infiltration in the

XBeach model may further improve the model. Additional validation of the Delft3D and SWAN models used to derive the boundary conditions for the XBeach model is advisable as well.

Application to other study areas
The general concept of (a) synthetic data generation based on historical events to include a wider range of (combinations of) events, and (b) downscaling of the number of scenarios that has to be simulated in models use of by MDA and interpolation, seems applicable to many other study areas.

Part (b) of the approach has been proposed in similar form by (Camus et al., 2011) for downscaling of wave climates, as for example applied by (Antolínez et al., 2018) in relation to morphological changes. In that perspective, this study can be seen as two more applications (i.e. the downscaling of scenarios for typhoon and non-typhoon scenarios). The inclusion of part (a) seems especially useful when data scarcity is an issue, or when extremer events have to be included. This is often the case in hazard and risk assessments.

On the other hand, some parts of the approach are tailored to atoll islands specifically, such as the used configuration of models. Other parts of the approach seem partially applicable to other areas as well, but validation – or possibly adaptation – for the specific characteristics of other areas is needed. Examples are the sets of parameters and weight factors, used for the selection of representative events by MDA and interpolation. Many areas prone to typhoon related flood hazard are not surrounded by the deep ocean, but located on the continent and have areas with large continental shelf. Therefore, typhoons can have significantly more impact from one side, and wind induced setup can be much more important. This effect can be seen in the selected events for the Charchenga Station case, as described in Section 4.1.2.

6.3.2. Flood hazard for the DUD region
With the above limitations in mind, the derived flood maps could be used to develop measures to improve resilience, or as a base for a flood risk assessment. Besides, they can be used as a starting point for future research into various related aspects that fell outside the scope of this thesis. Examples are climate change and freshwater availability. Furthermore, inclusion of wind related damage will lead to a more complete assessment of typhoon related risks. Boundary conditions were for a large part derived for the full Majuro Atoll. Hence, extension to other parts of the atoll is relatively easy and a similar approach could be followed.

Extension to flood risk assessment
Following from Section 2.3 a logical additional step would be the translation of the obtained flood hazard maps to flood risk maps. Flood risk maps provide more insight in the human consequences of flooding, as the inundation depths would be combined with information about the exposure (land use maps) and vulnerability (depth-damage curves); see Section 2.3.1. This could be done by use of the Delft-FIAT model for example. Figure 6.3 provides a schematic overview of the additional steps when the approach for the flood hazard assessment of Figure 1.6 would be extended to a flood risk assessment.
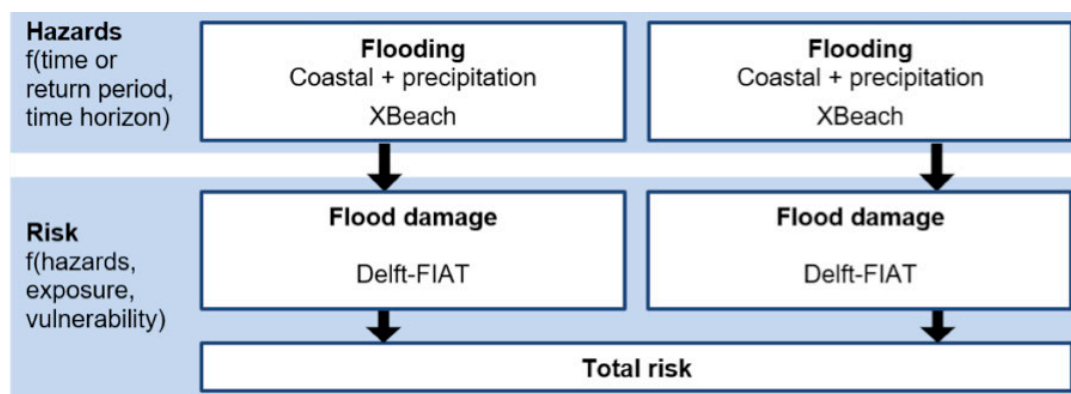

Figure 6.3: Schematic overview of the additional steps to extend the flood hazard assessment of Figure 1.6 to a flood risk assessment.

Assessment of related risks and the impacts of climate change
In this thesis, only flood hazard is assessed for typhoons, while direct damage due to wind may be important as well. Damage due to high wind speeds can be even more important in some cases, as shown by Richards (2019) in a Saint Martin case study for tropical cyclone Irma. Here, 98% of the total damage was associated to wind and only 2% flooding related. However, most parts of Saint Martin have a higher elevation and for low lying coastal areas, damage due to flooding was relatively more important. As the characteristics of atoll islands are more similar to low lying coastal areas it can be expected that flooding is more important during typhoons. Nevertheless, wind damage may significantly contribute to the typhoon related damage.

Climate change is expected to let flood risks for atoll islands increase significantly (e.g. Giardino et al., 2018; Storlazzi et al., 2018). Impacts on the DUD region of expected sea level rise, possibly more frequent typhoons, and more extreme precipitation events (IPCC, 2018), could be assessed based on the hazard assessment of the current situation, as presented in this study. In such assessments, the methods, models and processed data from this study could be reused. Such a study would preferably include the long term impacts of coastal flooding on freshwater availability, especially as the effects on ground water are expected to have large impact on the possibilities for human habitation (Storlazzi et al., 2018). In Sections 1.1.3 and 2.1 the relation between flooding and freshwater scarcity was briefly elaborated.

Improving resilience for the DUD region
Both coastal flooding and precipitation are important for the flood hazard at the DUD region, but may lead to different approaches for disaster risk reduction and risk management. In any case, improving resilience locally seems very much preferable for Majuro. Even when relocation would appear to be unavoidable in the future, that would preferably be on the atoll. For example Spennemann (1996) already mentioned that based on traditional settlement patterns, relocation of inhabitants of Majuro from the DUD region to the less vulnerable Laura could be considered. In all cases, policies should be based on well-founded insight in the risks involved.

Examples of measures could locally be sea walls or drainage systems, but such measures should not only prevent flooding but also take into account the effects on (underground) freshwater availability. Although both types lead to damage, flooding by precipitation (freshwater) will in general lead to less damage compared to oceanic water. This is especially true in relation to freshwater availability in underground freshwater lenses, where precipitation is actually favourable while oceanic water may lead to salinization. Hence, preferably a set of measures would lead to a system without coastal flooding, while as much as possible precipitation infiltrates into the groundwater instead of being drained towards the ocean.

Speculating on possible solutions for the long term that may contribute to such a system, measures to promote infiltration at locations where flooding is mainly due to precipitation might be more useful than drainage systems. If inundation depths are indeed limited to some maximum, elevated houses could for example be a solution. While making the atoll islands vulnerable to flooding, the limited width and low elevation of the atoll island may potentially be used as an advantage as well.

As coastal flooding is mainly related to wave-induced setup over the reef flat, water levels at the lagoon side can be expected to be often lower. Hence, instead of letting the water rise until flooding occurs, one could think of measures that make controlled flooding of designated areas (or even channels) possible. Hereby, water could flow controlled towards the lagoon and water levels on the reef flat might be reduced. In any case, further research into the design and feasibility of measures is needed, as well as into the contributions of precipitation and coastal flooding to the total inundation depths.

7

Conclusion and recommendations

Chapter summary

Conclusions

- By distinguishing typhoons and non-typhoon conditions, and generating a large synthetic data set for both, it is possible to account for the different interdependencies in the flood drivers.

- Synthetic events for typhoon conditions can be generated with TCWiSE and a Global Tide and Surge Model (GTSM). Relevant synthetic events for non-typhoon conditions can be generated by use of a combination of extreme value analysis, a Bayesian Network, GTSM and BEWARE.

- Inundation depths of all synthetic events can be reasonably well approximated by a 3 step approach: (1) Selection of representative events by Maximum Dissimilarity Algorithm (MDA); (2) Simulation of the inundation depths for each of the representative events. (3) Interpolation to obtain the maximum inundation depths for each of the synthetic events. Hereby a significant reduction in simulated events can be obtained.

- During both typhoons and non-typhoon conditions, both coastal flooding and precipitation related flooding contribute to the flood hazard for Majuro, although their relative importance varies significantly per area.

- Combined assessment of precipitation and coastal flooding into compound flooding is necessary as otherwise flood extents are underestimated.

- Analysis of inundation depths suggests that for many areas at the DUD region there is a maximum inundation depth, whereafter excess water drains to the ocean – mainly the lagoon.

Recommendations

- Validate the hydrodynamic models and simulated inundation depths.

- Further develop the method to reduce the number of simulated scenarios.

- Perform a more in-depth study into the boundary conditions for the DUD region.

- Assess flood hazard from the lagoon side and extend to other regions at Majuro

- Extend to a flood risk assessment and future time horizons including climate change.

- Perform an in-depth study into the influence of precipitation and coastal flooding on freshwater availability – also in relation to measures.

7.1. **Conclusions**

In this Majuro Atoll case study, an attempt was made to developed a method whereby all relevant flood drivers can be included in a compound flood hazard assessment. Representative scenarios and interpolation were used to make numerical modelling of scenarios with all relevant processes computationally feasible. Key findings, more general advances and the main limitations of this study are summarized below.

7.1.1. **Key findings**

In the Introduction of this thesis, 4 research questions were stated (Section 1.3). The key findings of this study are summarized by answering these questions.

How can the different interdependencies of flood drivers relevant for compound flooding on atoll islands be accounted for in a flood hazard assessment?

Main flood drivers for the DUD region were identified to be waves, high water levels (dominated by the tide) and precipitation from different sources. During typhoon conditions, waves and precipitation are both driven by the typhoon. During all other moments (non-typhoon conditions) these are only weakly related. Distinguishing (a) typhoon conditions, and (b) non-typhoon conditions, makes inclusion of the different interdependencies in flood drivers possible. Hereby flood hazard could be assessed independently for both types in terms of inundation depths for different return periods, whereafter the results could be combined to obtain the total flood hazard.

Within both the typhoon conditions and non-typhoon conditions, the variation in events and interdependencies could be accounted for by generating a large synthetic data set (i.e. 1000 years) based on historical data. By obtaining the inundation depths for 1000 years of flood drivers, many more different combinations of flood drivers are included whereby the interdependencies are much better represented.

How can the variation in typhoon events be described by a computationally feasible set of scenarios that combined give a full statistical description?

For the typhoon conditions, a synthetic data set of 1000 years of typhoons was generated with TCWiSE. This contained 2135 typhoon events within a defined area of influence around Majuro. Combined these seem to give a good description of all possible typhoons that could potentially impact Majuro. To accurately simulate inundation depths due to typhoons, a combination of the computationally expensive coupled Delft3D-FLOW + WAVE and XBeach models seemed the best (available) approach. Especially inclusion of wave transformation over the reef was important. However, simulation of inundation depths for all 2135 typhoons individually was computationally unfeasible and only for 50 scenarios inundation depths could be derived in sufficient detail.

A 3 step approach proved to be useful to reduce the number of scenarios while preserving the information on the probability of occurrence per event:

1. *Selection of representative typhoons* – Maximum Dissimilarity Algorithm (MDA) was used successfully to select 50 representative scenarios based on typhoon characteristics in 4 categories: (a) typhoon track, (b) maximum wind speed, (c) maximum forward velocity and (d) distance to the location of interest (e.g. Majuro).

2. *Simulation of the inundation depths for each of the representative typhoon tracks* – Offshore water levels were derived by use of the Delft3D-FLOW + WAVE model for each typhoon. The XBeach model – with the newly build in function to apply rainfall as a boundary condition – was used to simulate inundation depths for each representative typhoon.

3. *Interpolation to obtain the maximum inundation depths for each of the synthetic typhoons* – Interpolation with Softmax was used based on the same typhoon characteristics as in step (1) to approximate the inundation depths for all 2135 synthetic typhoons.

The selected representative typhoons seem to be a good representation of all synthetic typhoons. The method was validated and optimized by comparison of simulated and approximated water lev-

els and wave heights in a second case study. The optimized method was verified by comparison of simulated and approximated water levels for all synthetic typhoons offshore at Majuro.

By following this approach, inundation depths for 1000 years of typhoons could be approximated in a computationally feasible way, while a reduction in number of simulated typhoon scenarios of a factor ±40 was obtained (i.e 50 versus 2135 simulated typhoons). The use of more representative typhoons (e.g. 200), would lead to more reliable results.

How can compound flooding due to combinations of multiple flood drivers during non-typhoon conditions be described by a computationally feasible set of scenarios that combined give a full statistical description?

For the non-typhoon conditions, a synthetic data set of 1000 years of events that could potentially lead to flooding was created based on historical data. The data set contains 19619 events with specified precipitation rates (based on Extreme Value Analysis), wave conditions at different nearshore locations and surge levels (based on a Bayesian Network in Uninet), and tidal water levels (by use of a Global Tide and Surge Model). By comparison with historical data, it was concluded that the synthetic data provide a reasonably good expansion of the historical data set. However, especially the Bayesian Network, and the used setup of BEWARE have their limitations. Events that could potentially lead to compound flooding are much better included in the synthetic data set.

To obtain the inundation depths for all 19619 events in a computationally feasible way, the same 3 step approach as for the typhoon conditions proved to be useful. Again 50 scenarios were selected, but now based on characteristics of the non-typhoon event. Parameter in the following categories were used: (a) cumulative precipitation per day, (b) offshore water levels and (c) nearshore wave conditions. The selected representative events seem to be a good representation of all events, but validation of the results including the interpolation step was not possible. With this approach, inundation depths for 1000 years of non-typhoon conditions could be approximated in a computationally feasible way. The non-typhoon events are more similar than the typhoon events and seem to be even better represented. A reduction in number of simulated scenarios of a factor ±400 (i.e 50 versus 19619 simulated events) was obtained.

What are the key drivers of flooding for the DUD region at Majuro Atoll and what is their relative importance for different return periods?

During both typhoon and non-typhoon conditions, waves and precipitation cause flooding, where high (offshore) water levels further amplify wave induced flooding. Waves are in general higher at the northern and northeastern side compared to the southerns side of the DUD region. Offshore water levels are almost completely dominated by the tide as surge levels are minimal. Inclusion of both precipitation and coastal flooding into compound flooding was shown to be important; if both are assessed individually, flood extents are underestimated. The relative importance of the precipitation and coastal flooding varies significantly per location on the DUD region.

Flood maps were derived for typhoon conditions, non-typhoon conditions and their combination. For a return period of 5 years, flood hazard related to non-typhoon events seems to be more important than typhoon related flooding, especially in more northern parts of the DUD region. For a return period of 50 years, flood hazard due to both seems to be more similar, although this again varies significantly per location. Typhoons are the most extreme events in terms of wave conditions and precipitation rates and lead to the most severe flooding. Nevertheless, severe typhoon impact is infrequent and for the lower return periods typhoon related flooding was mainly related to precipitation and may be slightly overestimated. Precipitation can significantly contribute to the flood depths, especially for low-lying areas in the middle of the DUD region.

In addition some flood maps were derived for only precipitation and only coastal flooding during non-typhoon conditions. Coastal flooding was found to be more important for most areas during non-typhoon conditions. Precipitation causes flooding as well, but less severe, as precipitation rates are lower in comparison to typhoon conditions. Compound flooding during non-typhoon conditions seems to be infrequent.

Analysis of inundation depths for different return periods suggests that for many areas at the DUD region there is a maximum inundation depth, whereafter excess water drains to the ocean – mainly into the lagoon. This might be explained by looking into the specific bathymetry of narrow atoll islands: piling up of water against higher elevation areas is not possible and a cross section gives a bathtub like bathymetry. In other words: *'the bathtub can be full'*. Further research should be done to confirm this.

7.1.2. Advances
In Section 1.3 three main objectives were defined. The main advances in relation to these objectives are elaborated below.

Assessment of flood hazard for the DUD region at Majuro Atoll
Flood maps for different return periods were derived, for coastal flooding, flooding due to precipitation and compound flooding, during both typhoons and non-typhoon conditions. It was shown that already within the DUD region the importance of different flood drivers varies significantly per location and may be limited for certain areas. The flood maps provide direct insight in the flood hazard per location and can be used to improve resilience or for example as a base for assessment of flood risk, climate change impacts and freshwater availability.

Inclusion of compound events (i.e. coastal flooding and precipitation) in a methodology for flood hazard assessment of atoll islands
Key to the inclusion of compound events in a flood hazard assessment is to capture the full range of possible scenarios with correct probability of occurrence. By distinguishing between typhoon and non-typhoon conditions, the different relations between precipitation and coastal flooding for both can be better captured. By using a large data set of synthetic events instead of historical data, all possible combinations of precipitation and coastal flooding can be included. Furthermore, the results suggest that inundation depths for atoll islands may be limited to some maximum, although further research is needed to confirm this.

Selection of a computationally feasible set of scenarios that combined give a full statistical description of all conditions that can lead to compound flooding.
One of the main problems in compound flood hazard assessments is that the number of scenarios often increases dramatically while resulting inundation depths have to be determined within sufficient detail. The proposed 3 step method was shown to be a useful and promising tool to overcome this, as significant reduction in computation time can be obtained while information about the probability of occurrence per event can be preserved.

7.1.3. Limitations
The limitations and assumptions of the proposed approach to select the scenarios and the flood hazard assessment have been described in the Discussion (Chapter 6). Key points are summarized below:

- Limited validation of the hydrodynamic models was possible. This is especially relevant for the XBeach model, as comparison of various grid sizes showed that flood hazard may actually be underestimated and the new option to include rainfall has only been tested to a limited extent.

- Infiltration, possible drainage systems, sea walls (if not present in the bathymetry) and erosion processes were not included in the models and no additional checks of the available bathymetry were done.

- The timing of the different boundary conditions *within* an event is now partially random, most importantly that of the tide. For the non-typhoon conditions a standard precipitation event is used in combination with constant maximum wave conditions.

- Limited validation of the generated synthetic data. Especially for non-typhoon conditions, the synthetic data sampled from the Bayesian Network was not completely in agreement with historical data.

- Simulation of only 50 representative scenarios for typhoons and 50 for non-typhoon conditions was computationally feasible. The results showed that when using only 50 instead of 200, the uncertainty is larger – especially for higher return period events.

- Validation of the results after interpolation was not possible for the non-typhoon conditions. Only a check of the selected non-typhoon scenarios was possible and estimation of the parameter in the Softmax interpolation.

- Precipitation and tidal water level were not included for selection of typhoon conditions.

- The scenario selection is a high dimensional problem (i.e. with many parameters). When applying Softmax interpolation or MDA to scenarios that are described by many parameters, the effect of individual parameters may become to small to get a good selection or interpolation.

In spite of these limitations, the obtained inundation depths give useful insights in the flood hazard for the DUD region due to different flood drivers. The developed approach – to assess compound flood hazard for atoll islands by use of representative scenarios – should be seen as a first case study, but the concept seems promising for many more applications where the number of scenarios is constrained by computational feasibility.

7.2. Recommendations

Based on the findings and limitations of this study, suggestions for future research and applications are summarized below.

1. **Validate the hydrodynamic models and simulated inundation depths**

   One of the main uncertainties in this study is in the limited validation of the hydrodynamic models. Especially for the XBeach model additional validation is strongly needed, as many different processes play a role here and comparison of simulations with different grid resolutions showed that the used model may underestimate the flood extents. Recommended steps are:

   - Check the simulated inundation depths for even finer grids, as the recommended grid resolution was even lower than the finest grid tested in this study.
   - Validate the XBeach model with measurements. For exapmle, this could be done by obtaining measurements of water levels and wave heights on the reef flat, for different conditions at the location of the XBeach model domain boundary. Subsequently, the measured conditions at the boundary could be applied to the XBeach model, and simulated and measured water levels and wave heights on the reef could be compared.
   - Validate the flood maps. This could be done by use of measurements for a flood event, but potentially interviews with local residents or analysis of online sources (e.g. videos, photos, news articles, twitter) may provide such insights as well.

   Other aspects of the XBeach model that may require additional checks are the applied bathymetry, the bottom roughness and the potential presence of protective measures such as sea walls. Additional validation of the rainfall function seems advisable as well, as for the DUD region it was complicated to assess the performance of this new function. Validation of the Delft3D and SWAN models with measurements is required as well, but seems less urgent than for the XBeach model. Here a similar approach as for the XBeach model could be used.

2. **Further develop the method to reduce the number of simulated scenarios**

   The used three step method was shown to be a useful and promising tool to reduce the number of scenarios, but for many aspects this case study should only be seen as a first step. Improvements on almost all aspects seem possible, some suggestions are summarized below:

   - Reduce the area used to distinguish typhoon and non-typhoon conditions (e.g. to a circle with a radius of ±700 km). Hereby a more relevant set of scenarios will be obtained and thereby the selected representative scenarios will be more relevant for flooding.

- Add precipitation and water levels to the set of parameters to select the typhoon scenarios, possibly replacing other parameters. It is expected that this will lead to an even more representative set of scenarios.
- Try different (more advanced) interpolation methods. Although the interpolation method worked reasonably well, other methods (e.g. radial base functions) may potentially be more suitable.

To improve the method and gain more confidence in the results, especially the performance of more case studies is strongly needed. These could be for other atoll islands in the Northwestern Pacific or other basins. Furthermore, the approach seems useful for other areas prone to flood hazard – especially typhoon related – as was shown by the Charchenga (Bangladesh) case study. When computationally feasible, it is strongly advised to use more representative events (e.g. 200) as it was shown to lead to better results, especially for the high return periods.

3. **Perform a more in-depth study into the boundary conditions for the DUD region**

In this study, it was shown that interdependencies of the boundary conditions are important. For example, wave conditions at the DUD region vary significantly per location. Synthetic data was generated to account for this. The synthetic typhoons as generated with TCWiSE in general seemed reasonable, but some deviations were observed. For example, some synthetic typhoons crossed the equator – which seems unlikely from a physical point of view. Adaptation of the TCWiSE to prevent this is recommended. As suggested by Bader (2019), precipitation rates at large distance of the typhoon eye seem to be on the high side, whereby typhoon related inundation depths for low return periods may be slightly overestimated. Hence, it is recommended to investigate the possible radial limit on the TC rainfall as already suggested by Bader (2019).

The generated synthetic data for the non-typhoon conditions deviates slightly from the historical data. Most importantly, compound events were relatively more frequent, wave conditions at the southern side of Majuro are slightly underestimated and the dependencies of wave conditions for different locations as represented by the Bayesian Network (BN) partially deviate from historical data. To improve the synthetic data, a more in-depth study into the interdependencies and their schematization – especially in the BN – could be useful.

4. **Assess flood hazard from the lagoon side and extend to other regions at Majuro**

Flooding at Majuro is also by water from the lagoon, and assessment of flood hazard due to waves and high water levels from this side is needed. Such study should preferably also look into possible compound events. Flood hazard assessment of other parts of Majuro is strongly recommended. This especially applies to the inhabited areas of Laura in the west and large parts of the southern rim. For these areas, the boundary conditions were already partially derived and a similar approach can be used.

In such additional studies, the hypothesis of a maximum inundation depth for many areas on atoll islands (or at least Majuro) could also be tested. The water level at the shoreline at the lagoon side during flooding can be expected to be important in relation to this.

5. **Extend to a flood risk assessment and future time horizons including climate change**

Flood maps for the DUD region provide insight in which areas are most prone to flooding. Risk maps provide additional insights, that can be especially useful when efficient mitigation measures have to be taken. Translation of the flood hazard to flood risk could be done by combining the flood maps with exposure data (e.g. land use maps), and vulnerability information (e.g. depth damage curves). This seems a relatively easy additional step.

Although flood hazard was shown to be significant already in the current situations, climate change is expected to further amplify this in the future. This was one of main reasons to assess the flood hazard at Majuro. Hence, it is strongly recommended to assess the impacts of climate change on Majuro. In any case sea level rise should be included in such study, but for example also potentially stronger typhoons and more extreme precipitation events during non-typhoon conditions should be investigated. In addition, it is recommended to especially include the influence of flooding on the freshwater availability, as salinization of underground freshwater lenses may make atoll islands uninhabitable before flooding itself does (Storlazzi et al., 2018).

6. **Perform an in-depth study into the influence of precipitation and coastal flooding on freshwater availability – also in relation to measures**

In this study, it was shown that precipitation may lead or contribute significantly to flooding. In the perspective of climate change and corresponding impacts on freshwater availability for atoll islands, the relative importance of precipitation related flooding and coastal flooding is crucial. Both coastal flooding and flooding by precipitation are unwanted, but recharge of the underground freshwater lenses by precipitation seems favourable above drainage to the ocean. Flooding by coastal water seems in any case unfavourable, as it has additional negative effects on the groundwater.

Part of the precipitation may infiltrate into the ground, whereby flood hazard may be overestimated now. The influence of this on the derived flood maps is unknown, and also depends on the local infiltration rates at the DUD area. Hence, a study into the infiltration rates for the DUD region is recommended and depending on the outcomes possible inclusion of infiltration into the XBeach model is recommended.

If measures would have to be designed, it is strongly advised to follow a more integral approach that also includes the effects on freshwater – especially on the long term. Measures such as drainage systems might reduce the flood hazard, for example for some of the low-lying and more central areas at the DUD region, but on the long term such measures may potentially have important negative effects on the underground freshwater lenses as well. Although this study provides some useful insights in the relative importance of the flood drivers for different areas, a more in-depth study that includes effects on underground freshwater lenses seems justified.

Bibliography

Alves, J.-H. G. M. (2006). Numerical modeling of ocean swell contributions to the global wind-wave climate. *Ocean Modelling 11*(1-2), 98–122.

Anderson, D., A. Rueda, L. Cagigal, J. A. A. Antolínez, F. J. Méndez, and P. Ruggiero (2019). Time-varying Emulator for Short and Long-Term Analysis of Coastal Flood Hazard Potential. *Journal of Geophysical Research: Oceans 124*(12), 9209–9234.

Anthony, S. S., F. L. Peterson, F. T. Mackenzie, and S. N. Hamlin (1989). Geohydrology of the Laura fresh-water lens, Majuro atoll: a hydrogeochemical approach. *Geological Society of America Bulletin 101*(8), 1066–1075.

Antolínez, J. A. A., A. B. Murray, F. J. Méndez, L. J. Moore, G. Farley, and J. Wood (2018). Down-scaling changing coastlines in a changing climate: The hybrid approach. *Journal of Geophysical Research: Earth Surface 123*(2), 229–251.

Australian Government Bureau of Meteorology (2010). SOPAC Member Countries National Capacity Assessment: Tsunami Warning and Mitigation Systems, Republic of Marshall Islands, 25-28 May 2009. Research report, compiled by C. Stitz-O'Brien, Australian Government Bureau of Meteorology, Melbourne.

Bader, D. (2019). Including Stochastic Rainfall Distributions in a Probabilistic Modelling Approach for Compound Flooding due to Tropical Cyclones. Master's thesis, TU Delft.

Bailey, R., J. Jenson, and A. Olsen (2010). Estimating the ground water resources of atoll islands. *Water 2*(1), 1–27.

Bailey, R. T., J. W. Jenson, and A. E. Olsen (2009). Numerical modeling of atoll island hydrogeology. *Groundwater 47*(2), 184–196.

Barkey, B. and R. Bailey (2017). Estimating the impact of drought on groundwater resources of the Marshall Islands. *Water 9*(1), 41.

Bevacqua, E., D. Maraun, I. Hobæk Haff, M. Widmann, and M. Vrac (2017). Multivariate statistical modelling of compound events via pair-copula constructions: analysis of floods in Ravenna (Italy). *Hydrology and Earth System Sciences 21*(6), 2701–2723.

Booij, N., L. H. Holthuijsen, and R. C. Ris (1997). The "SWAN" wave model for shallow water. In *Coastal Engineering 1996*, pp. 668–676.

C3S (2017). ERA5: Fifth generation of ECMWF atmospheric reanalyses of the global climate. Copernicus Climate Change Service (CS3), Climate Data Store (CDS), https://cds.climate.copernicus.eu/cdsapp#!/home.

Camus, P., F. J. Méndez, and R. Medina (2011). A hybrid efficient method to downscale wave climate to coastal areas. *Coastal Engineering 58*(9), 851–862.

Camus, P., F. J. Méndez, R. Medina, and A. S. Cofiño (2011). Analysis of clustering and selection algorithms for the study of multivariate wave climate. *Coastal Engineering 58*(6), 453–462.

Canavesio, R. (2019). Distant swells and their impacts on atolls and tropical coastlines. the example of submersions produced by lagoon water filling and flushing currents in french polynesia during 1996 and 2011 mega swells. *Global and planetary change 177*, 116–126.

Couasnon, A., A. Sebastian, and O. Morales-Nápoles (2018). A Copula-based Bayesian Network for modeling compound flood hazard from riverine and coastal interactions at the catchment scale: an application to the Houston Ship Channel, Texas. *Water 10*(9), 1190.

Cox, A. T., V. J. Cardone, and V. R. Swail (2011). On the use of the climate forecast system reanalysis wind forcing in ocean response modeling. In *Proceedings, 12th int. Workshop wave, hindcasting, forecasting, Hawaii, USA*.

CRED and UNISDR (2015). The Human Cost of Weather Related Disasters 1995-2015. Technical report, CRED and UNISDR.

Darwin, C. (1842). *The Structure and Distribution of Coral Reefs*. London: Smith, Elder & co., 214 pp.

de Moel, H., B. Jongman, H. Kreibich, B. Merz, E. Penning-Rowsell, and P. J. Ward (2015). Flood risk assessments at different spatial scales. *Mitigation and Adaptation Strategies for Global Change 20*(6), 865–890.

Deltares (2019). Wes - wind enhance scheme for cyclone modelling - user manual.

Ford, M., J. M. Becker, M. A. Merrifield, and Y. T. Song (2014). Marshall Islands fringing reef and atoll lagoon observations of the Tohoku tsunami. *Pure and Applied Geophysics 171*(12), 3351–3363.

Ford, M., M. A. Merrifield, and J. M. Becker (2018). Inundation of a low-lying urban atoll island: Majuro, marshall islands. *Natural Hazards 91*(3), 1273–1297.

Ford, M. R., J. M. Becker, and M. A. Merrifield (2013). Reef flat wave processes and excavation pits: Observations and implications for Majuro Atoll, Marshall Islands. *Journal of Coastal Research 29*(3), 545–554.

Ford, M. R. and P. S. Kench (2015). Multi-decadal shoreline changes in response to sea level rise in the Marshall Islands. *Anthropocene 11*, 14–24.

Gallina, V., S. Torresan, A. Critto, A. Sperotto, T. Glade, and A. Marcomini (2015, 12). A review of multi-risk methodologies for natural hazards: Consequences and challenges for a climate change impact assessment. *Journal of environmental management 168*, 123–132.

Gariel, M., A. N. Srivastava, and E. Feron (2011). Trajectory clustering and an application to airspace monitoring. *IEEE Transactions on Intelligent Transportation Systems 12*(4), 1511–1524.

Genest, C. and A. Favre (2007). Everything you always wanted to know about copula modeling but were afraid to ask. *Journal of hydrologic engineering 12*(4), 347–368.

Giardino, A., C. M. Nederhoff, M. Gawehn, E. Quataert, and A. Capel (2017). Coastal risk assessments for Ebeye. Technical report, Deltares, Delft, The Netherlands.

Giardino, A., K. Nederhoff, and M. Vousdoukas (2018). Coastal hazard risk assessment for small islands: assessing the impact of climate change and disaster reduction measures on Ebeye (Marshall Islands). *Regional Environmental Change 18*(8), 2237–2248.

Goodfellow, I., Y. Bengio, and A. Courville (2016). *Deep Learning*. MIT Press. http://www.deeplearningbook.org, Chap. Numerical Computation.

Greene, J. S., M. Klatt, M. Morrissey, and S. Postawko (2008). The comprehensive Pacific rainfall database. *Journal of Atmospheric and Oceanic Technology 25*(1), 71–82.

Hanea, A., O. M. Napoles, and D. Ababei (2015). Non-parametric bayesian networks: Improving theory and reviewing applications. *Reliability Engineering & System Safety 144*, 265–284.

Hegermiller, C. A., J. A. A. Antolínez, A. Rueda, P. Camus, J. Perez, L. H. Erikson, P. L. Barnard, and F. J. Méndez (2017). A multimodal wave spectrum–based approach for statistical downscaling of local wave climate. *Journal of Physical Oceanography 47*(2), 375–386.

Hein, J. R., F. L. Wong, and D. L. Mosier (2007). Bathymetry of the Republic of the Marshall Islands and Vicinity. US Geological Survey, Miscellaneous Field Studies Map MF 2324, Version 1.3.

Hoek, J. (2017). Tropical Cyclone Statistical Wind Estimation: In Regions with Rare Cyclone Occurrence. Master's thesis, TU Delft.

Hoeke, R. K., K. L. McInnes, J. C. Kruger, R. J. McNaught, J. R. Hunter, and S. G. Smithers (2013). Widespread inundation of Pacific islands triggered by distant-source wind-waves. *Global and Planetary Change 108*, 128–138.

Holland, G. J. (1980). An analytic model of the wind and pressure profiles in hurricanes. *Monthly weather review 108*(8), 1212–1218.

Holland, G. J., J. I. Belanger, and A. Fritz (2010). A revised model for radial profiles of hurricane winds. *Monthly Weather Review 138*(12), 4393–4401.

Holthuijsen, L. H. (2010). *Waves in oceanic and coastal waters*. Cambridge university press.

Hoonhout, B. (2015). XBeach User Manual. https://xbeach.readthedocs.io/en/latest/user_manual.html. Accessed: 2019-10-30.

IPCC (2012). Managing the Risks of Extreme Events and Disasters to Advance Climate Change Adaptation. A Special Report of Working Groups I and II of the Intergovernmental Panel on Climate Change [Field, C.B., V. Barros, T.F. Stocker, D. Qin, D.J. Dokken, K.L. Ebi, M.D. Mastrandrea, K.J. Mach, G.-K. Plattner, S.K. Allen, M. Tignor, and P.M. Midgley (eds.)]. Cambridge University Press, Cambridge, UK, and New York, USA, 582 pp.

IPCC (2018). Global Warming of 1.5°C. An IPCC Special Report on the impacts of global warming of 1.5°C above pre-industrial levels and related global greenhouse gas emission pathways, in the context of strengthening the global response to the threat of climate change, sustainable development, and efforts to eradicate poverty. [Masson-Delmotte, V., P. Zhai, H.-O. Pörtner, D. Roberts, J. Skea, P.R. Shukla, A. Pirani, W. Moufouma-Okia, C. Péan, R. Pidcock, S. Connors, J.B.R. Matthews, Y. Chen, X. Zhou, M.I. Gomis, E. Lonnoy, T. Maycock, M. Tignor, and T. Waterfield (eds.)], World Meteorological Organization, Geneva, Switzerland, 32 pp.

Jiang, H., J. B. Halverson, and J. Sim (2006). Difference of rainfall distribution for tropical cyclones over land and ocean and rainfall potential derived from satellite observations and its implication on hurricane landfall flooding prediction. In *27th Conference on Hurricanes and Tropical Meteorology, Monterey, CA, American Meteorology Society*.

Kendall, M., T. Battista, and C. Menza (2012). Majuro Atoll, Republic of the Marshall Islands coral reef ecosystems mapping report. NOAA/National Centers for Coastal Ocean Science.

Kernkamp, H. W. J., A. Van Dam, G. S. Stelling, and E. D. de Goede (2011). Efficient scheme for the shallow water equations on unstructured grids with application to the Continental Shelf. *Ocean Dynamics 61*(8), 1175–1188.

Klaver, S. (2018). Modelling the effects of excavation pits on fringing reefs. Master's thesis, TU Delft.

Knapp, K. R., H. J. Diamond, J. P. Kossin, M. C. Kruk, and C. J. Schreck (2018). International best track archive for climate stewardship (ibtracs) project, version 4, jtwc-wp. NOAA National Centers for Environmental Information. Accessed: 3-6-2019.

Knapp, K. R., M. C. Kruk, D. H. Levinson, H. J. Diamond, and C. J. Neumann (2010). The international best track archive for climate stewardship (IBTrACS) unifying tropical cyclone data. *Bulletin of the American Meteorological Society 91*(3), 363–376.

Konrad, C. E. and L. Baker Perry (2010). Relationships between tropical cyclones and heavy rainfall in the Carolina region of the USA. *International Journal of Climatology: A Journal of the Royal Meteorological Society 30*(4), 522–534.

Kottermair, M. and A. Jalandoni (2016). Majuro atoll coastline. Photo credit: University of Guam (UOG). Retrieved 14-10-2019, from https://www.usgs.gov/media/images/majuro-atoll-coastline.

Kron, W. (2005). Flood risk= hazard• values• vulnerability. *Water International 30*(1), 58–68.

Leijnse, T., A. Giardino, and K. Nederhoff (2019). Assessing present and future coastal hazards due to tropical cyclones in the Bay of Bengal using synthetic tracks. Manuscript in preparation.

Leonard, M., S. Westra, A. Phatak, M. Lambert, B. van den Hurk, K. McInnes, J. Risbey, S. Schuster, D. Jakob, and M. Stafford-Smith (2014). A compound event framework for understanding extreme impacts. *Wiley Interdisciplinary Reviews: Climate Change 5*(1), 113–128.

Lesser, G. R., J. A. Roelvink, J. A. T. M. Van Kester, and G. S. Stelling (2004). Development and validation of a three-dimensional morphological model. *Coastal engineering 51*(8-9), 883–915.

Lian, J. J., K. Xu, and C. Ma (2013). Joint impact of rainfall and tidal level on flood risk in a coastal city with a complex river network: a case study of Fuzhou City, China. *Hydrology and Earth System Sciences 17*(2), 679.

Marzocchi, W., A. Garcia-Aristizabal, P. Gasparini, M. L. Mastellone, and A. Di Ruocco (2012). Basic principles of multi-risk assessment: a case study in Italy. *Natural hazards 62*(2), 551–573.

McLean, R. and P. Kench (2015). Destruction or persistence of coral atoll islands in the face of 20th and 21st century sea-level rise? *Wiley Interdisciplinary Reviews: Climate Change 6*(5), 445–463.

Merz, B. and A. H. Thieken (2009). Flood risk curves and uncertainty bounds. *Natural hazards 51*(3), 437–458.

Moftakhari, H. R., G. Salvadori, A. AghaKouchak, B. F. Sanders, and R. A. Matthew (2017). Compounding effects of sea level rise and fluvial flooding. *Proceedings of the National Academy of Sciences 114*(37), 9785–9790.

Montaggioni, L. F. (2005). History of Indo-Pacific coral reef systems since the last glaciation: development patterns and controlling factors. *Earth-Science Reviews 71*(1-2), 1–75.

Muis, S., M. Verlaan, H. C. Winsemius, J. C. J. H. Aerts, and P. J. Ward (2016). A global reanalysis of storm surges and extreme sea levels. *Nature communications 7*(1), 1–12.

Nederhoff, K., A. Giardino, M. van Ormondt, and D. Vatvani (2019). Estimates of tropical cyclone geometry parameters based on best track data. *Natural Hazards and Earth System Sciences Discussions 2019*, 1–26.

NOAA (2019). Saffir-simpson hurricane wind scale. National Hurricane Center and Central Pacific Hurricane Center, https://www.nhc.noaa.gov/aboutsshws.php. Accessed: 3-11-2019.

OECD, World Bank (2016). Climate and Disaster Resilience Financing in Small Island Developing States. Technical report, A report jointly authored by the Organization for Economic Co-operation and Development (OECD) and the Small Island States Resilience Initiative (SISRI) team in the Climate Change Group of the World Bank. Washington, DC: World Bank.

Palaseanu-Lovejoy, M., S. K. Poppenga, J. J. Danielson, D. J. Tyler, D. B. Gesch, M. Kottermair, A. Jalandoni, E. Carlson, C. Thatcher, and M. Barbee (2017). One Meter Topobathymetric Digital Elevation Model for Majuro Atoll, Republic of the Marshall Islands, 1944 to 2016. U.S. Geological Survey data release.

Parodi, M. U. (2019). Investigating Uncertainty in Coastal Flood Risk Assessment in Small Island Developing States. Master's thesis, TU Delft.

PCRAFI (2011). The Marshall Islands – Country risk profile (English). Pacific Catastrophe Risk Assessment and Financing Initiative (PCRAFI), World Bank Group, Washington, DC.

PCRAFI (2015). The Marshall Islands - Country note (English). Disaster Risk Financing and Insurance; PCRAFI Country Note, prepared by B.J. Bailey, S.J. Cook, and O. Mahul, World Bank Group, Washington, DC.

Pearson, S. G. (2016). Predicting Wave Induced Flooding On Low Lying Tropical Islands. Master's thesis, TU Delft.

Pearson, S. G., C. D. Storlazzi, A. R. van Dongeren, M. F. S. Tissier, and A. J. H. M. Reniers (2017). A Bayesian-based system to assess wave-driven flooding hazards on coral reef-lined coasts. *Journal of Geophysical Research: Oceans 122*(12), 10099–10117.

Petzold, J. and B. M. W. Ratter (2015). Climate change adaptation under a social capital approach – An analytical framework for small islands. *Ocean & Coastal Management 112*, 36–43.

Quataert, E., C. Storlazzi, A. Rooijen, O. Cheriton, and A. Dongeren (2015). The influence of coral reefs and climate change on wave-driven flooding of tropical coastlines. *Geophysical Research Letters 42*(15), 6407–6415.

Richards, H. L. (2019). Multi-Hazard Risk Assessment due to Hurricane Activity: Case Study of St. Martin, the Caribbean. Master's thesis, TU Delft.

Roelvink, D., A. Reniers, A. Van Dongeren, J. van Thiel de Vries, R. McCall, and J. Lescinski (2009). Modelling storm impacts on beaches, dunes and barrier islands. *Coastal engineering 56*(11-12), 1133–1152.

Roelvink, F. E. (2019). Coral restoration for coastal hazard risk reduction: the effect of coral restoration on wave transformation over various reef morphologies and the resulting runup. Master's thesis, TU Delft.

Rueda, A., L. Cagigal, S. G. Pearson, J. A. A. Antolínez, C. Storlazzi, A. van Dongeren, P. Camus, and F. J. Mendez (2019). HyCReWW: A Hybrid Coral Reef Wave and Water level metamodel. *Computers & geosciences 127*, 85–90.

Salvadori, G., G. Tomasicchio, and F. D'Alessandro (2014). Practical guidelines for multivariate analysis and design in coastal and offshore engineering. *Coastal Engineering 88*, 1–14.

Sato, D. and H. Yokoki (2011). Numerical calculation on shoreline conservation in Majuro atoll, the Marshall Islands. *Coastal Engineering Proceedings 1*(32), 94.

Schölzel, C. and P. Friederichs (2008). Multivariate non-normally distributed random variables in climate research– introduction to the copula approach. *Nonlinear Processes in Geophysics 15*(5), 761–772.

Scott, F. (2019). Data Reduction Techniques of Coral Reef Morphology and Hydrodynamics for use in Wave Runup Prediction. Master's thesis, TU Delft.

Sebastian, A., E. Dupuits, and O. Morales-Nápoles (2017, 3). Applying a Bayesian network based on Gaussian copulas to model the hydraulic boundary conditions for hurricane flood risk analysis in a coastal watershed. *Coastal engineering 125*, 42–50.

Sklar, A. (1959). Fonctions de répartition à n dimensions et leurs marges. *Publ. Inst. Stat. Univ. Paris 8*, 229–231.

Slangen, A. B. A., M. Carson, C. A. Katsman, R. S. W. Van de Wal, A. Köhl, L. L. A. Vermeersen, and D. Stammer (2014). Projecting twenty-first century regional sea-level changes. *Climatic Change 124*, 317–332.

Smith, G. and N. Juria (2019). Diagnosis of historical inundation events in the Marshall Islands to assist early warning systems. *Natural Hazards 99*(1), 189–216.

Snaiki, R. and T. Wu (2018). An analytical framework for rapid estimate of rain rate during tropical cyclones. *Journal of Wind Engineering and Industrial Aerodynamics 174*, 50–60.

SPC (2012). Republic of the Marshall Islands 2011 Census report. Census of population and housing, by the Economic Policy, Planning and Statistics Office, Republic of the Marshall Islands, and the SPC Statistics for Development Programme, Noumea, New Caledonia.

SPC (2017). Climate and Abstraction Impacts in Atoll Environments (CAIA) – Assessment of the 2015–2016 drought impacts on the fresh groundwater lens at Laura, Majuro Atoll, Republic of the Marshall Islands. SPC Technical Report SPC00055), SPC, Geoscience Division of the Pacific Community, by P. Sinclair, S. Galvis-Rodriguez, A. Loco, and A. Kuma, Suva, Fiji.

SPC-SOPAC (2012). Republic of the Marshall Islands Investment in Disaster Risk Management. Economic Report (PR107), Secretariat of the Pacific Community (SOPAC), Applied Geoscience and Technology Division, prepared by S. Cook, Suva, Fiji.

Spennemann, D. H. R. (1996). Nontraditional settlement patterns and typhoon hazard on contemporary Majuro Atoll, Republic of the Marshall Islands. *Environmental Management 20*(3), 337–348.

Sperotto, A., J.-L. Molina, S. Torresan, A. Critto, and A. Marcomini (2017). Reviewing Bayesian Networks potentials for climate change impacts assessment and management: A multi-risk perspective. *Journal of environmental management 202*, 320–331.

Storlazzi, C. D., S. B. Gingerich, A. van Dongeren, O. M. Cheriton, P. W. Swarzenski, E. Quataert, C. I. Voss, D. W. Field, H. Annamalai, G. A. Piniak, and R. McCall (2018). Most atolls will be uninhabitable by the mid-21st century because of sea-level rise exacerbating wave-driven flooding. *Science Advances 4*(4), eaap9741.

Takeuchi, K. (1984). Annual maximum series and partial-duration series—Evaluation of Langbein's formula and Chow's discussion. *Journal of hydrology 68*(1-4), 275–284.

The Guardian (2015). Losing paradise: the people displaced by atomic bombs, and now climate change. https://www.theguardian.com/environment/2015/mar/09/losing-paradise-the-people-displaced-by-atomic-bombs-and-now-climate-change. By K. Mathiesen. Accessed: 22-7-2019.

The Marshall Islands Journal (2016a). Lagoon flooding in Majuro. https://marshallislandsjournal.com/lagoon-flooding-majuro/. Accessed: 26-8-2019.

The Marshall Islands Journal (2016b). Storm-driven tide cause flooding. https://marshallislandsjournal.com/storm-driven-tides-cause-flooding/. Article by G. Johnson, photo by K. Earnshaw. Accessed: 26-8-2019.

The New York Times (2015). The Marshall Islands Are Disappearing. https://www.nytimes.com/interactive/2015/12/02/world/The-Marshall-Islands-Are-Disappearing.html. By C. Davenport. Accessed: 22-7-2019.

Torres Dueñas, L. F. (2018). Flood Risk Assessment of the Clear Creek Watershed considering compound events. Master's thesis, TU Delft.

UN-Habitat (2015). Urbanization and Climate Change in Small Island Developing States. Technical report, United Nations Human Settlements Programme (UNHabitat), Nairobi.

UN-OHRLLS (2015). Small Island Developing States in Numbers – Climate Change Edition 2015. Technical report, United Nations Office of the High Representative for the Least Developed Countries, Landlocked Developing Countries and Small Island Developing States (UN-OHRLLS).

UNINET Help (n.d.). Manual for uninet, available in Uninet Software. Chief programmer Dan Ababei, vice programmer is Daniel Lewandowski. Mathematical support is provided by Daniel Lewandowski, Anca Hanea, Oswaldo Morales, Dorota Kurowicka and Roger Cooke.

UNISDR (2015). Sendai framework for disaster risk reduction 2015–2030. Technical report, United Nations Office for Disaster Risk Reduction (UNISDR), Sendai, Japan.

Van Dongeren, A., R. Lowe, A. Pomeroy, D. M. Trang, D. Roelvink, G. Symonds, and R. Ranasinghe (2013). Numerical modeling of low-frequency wave dynamics over a fringing coral reef. *Coastal Engineering 73*, 178–190.

Veldt, T. (2019). The effect of wave directional spread on coastal hazards at coastlines fronted by a coral reef. Master's thesis, TU Delft.

Vousdoukas, M. I., D. Bouziotas, A. Giardino, L. M. Bouwer, L. Mentaschi, E. Voukouvalas, and L. Feyen (2018). Understanding epistemic uncertainty in large-scale coastal flood risk assessment for present and future climates. *Natural Hazards and Earth System Sciences 18*(8), 2127–2142.

Werner, A. D., H. K. Sharp, S. C. Galvis, V. E. A. Post, and P. Sinclair (2017). Hydrogeology and management of freshwater lenses on atoll islands: Review of current knowledge and research needs. *Journal of hydrology 551*, 819–844.

World Bank and CDIAC (2019). CO2 emissions (metric tons per capita) data for Marshall Islands and World. Carbon Dioxide Information Analysis Center (CDIAC), Environmental Sciences Division, Oak Ridge National Laboratory, United States. Data available via website of The World Bank, https://data.worldbank.org/?locations=MH-1W. Retrieved: 7-5-2019.

WSO Majuro (2013). Weather Station Office Inundation Report. Weather Station Office (WSO). Prepared by R. White, Meteorologist in charge, Majuro.

Xue, C. (2001). Coastal erosion and management of Majuro atoll, Marshall Islands. *Journal of Coastal Research 17*(4), 909–918.

Yamano, H., H. Shimazaki, T. Matsunaga, A. Ishoda, C. Mcclennen, H. Yokoki, K. Fujita, Y. Osawa, and H. Kayanne (2006). Evaluation of various satellite sensors for waterline extraction in a coral reef environment: Majuro Atoll, Marshall Islands. *Geomorphology 82*, 398–411.

Young, I. (2003, 05). A review of the sea state generated by hurricanes. *Marine Structures 16*, 201–218.

A
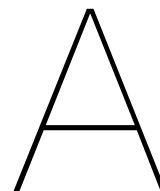
Data processing

Chapter summary

- This Appendix elaborates some important aspects of the data processing in more detail. First a flowchart of all main elements in the methodology is presented in Section A.1. The flowchart includes all used tools together with their input and output.

- The transformation of ERA5 wave data from offshore to nearshore is briefly elaborated in Section A.2. Subsequently, various distributions were fitted to the data for the nearshore significant wave height at different locations and the surge levels. These distributions were used for the generation of synthetic data for non-typhoon conditions in Uninet.

- In Section A.3, some steps in the processing of precipitation data are elaborated in more detail. First, the extreme value analysis based on monthly maximum rates is presented and compared with the peak over threshold approach. Subsequently, data of different stations is compared to get insight in the spatial variation in precipitation rates. Lastly, the derivation of a standard event based on hourly data is discussed.

A.1. **Flowchart of the methodology**

A flowchart including all main elements of the approach can be found in Figure A.1 below.
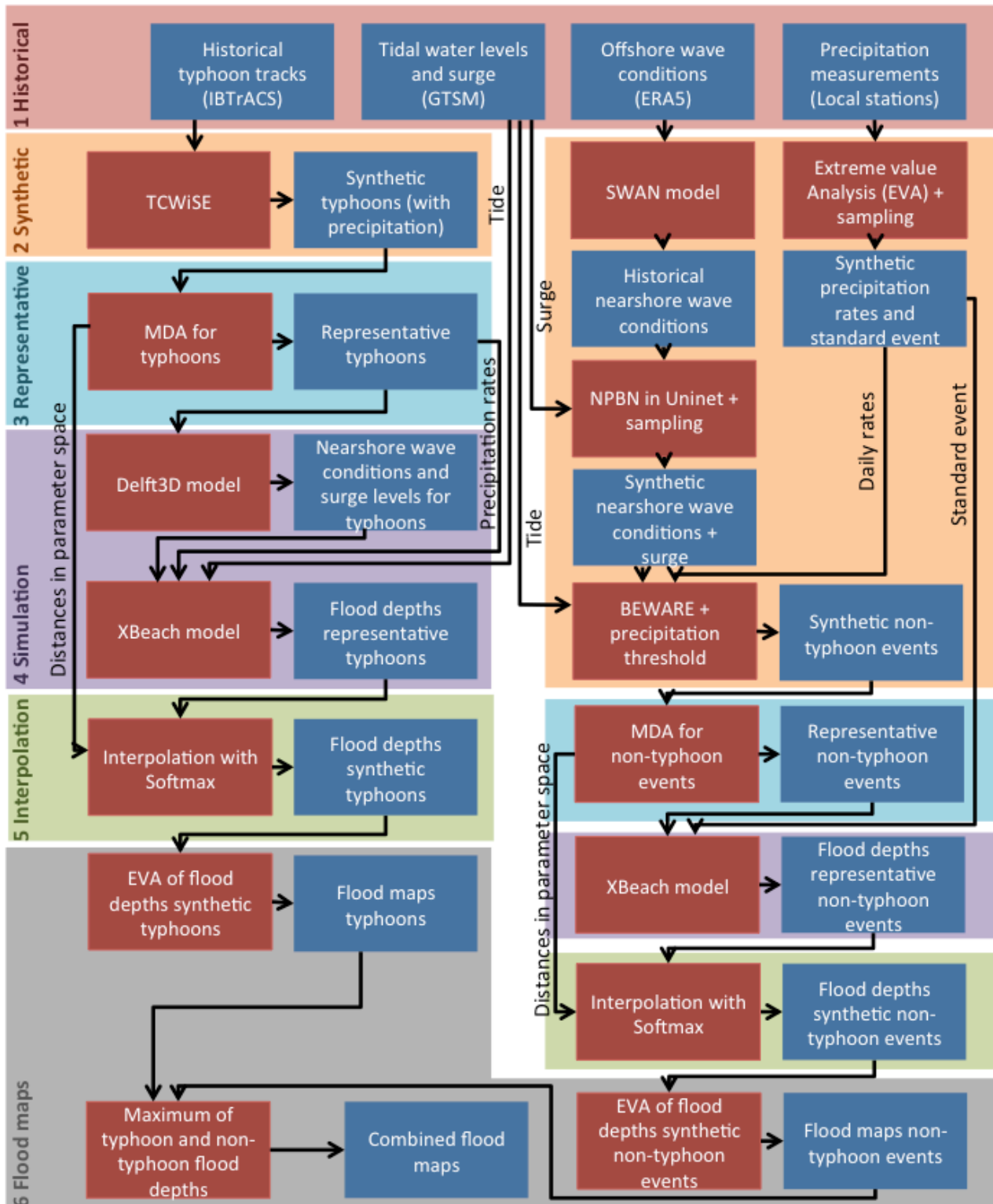
Figure A.1: *Flowchart of the methodology, including the main tools together with their input and output. The approach for typhoons can be found at the left side, the approach for non-typhoon events at the right side. All tools are shown in red; data (i.e. input and output of the tools) is shown in blue. 6 main steps can be distinguished when going from historical data to flood maps, these steps are described in Section 1.4.2.*

A.2. **Wave conditions**

This Section provides additional information about the data for offshore wave conditions and the transformation to nearshore conditions, done by a SWAN model. Furthermore, the fits of extreme value distributions to the non-typhoon part of the wave conditions and surge are discussed.

A.2.1. **Wave transformation to nearshore conditions**

A comparison wave roses of the wave buoy and ERA5 data for the nearest point is shown in Figure A.2 below. There is a clear difference in wave conditions according to the buoy data and the nearest point ERA5 data point. The buoy data consists of actual measurements, but only for one location and insufficiently long time series. Hence, to obtain the nearshore wave conditions for different locations, the ERA5 data was used.
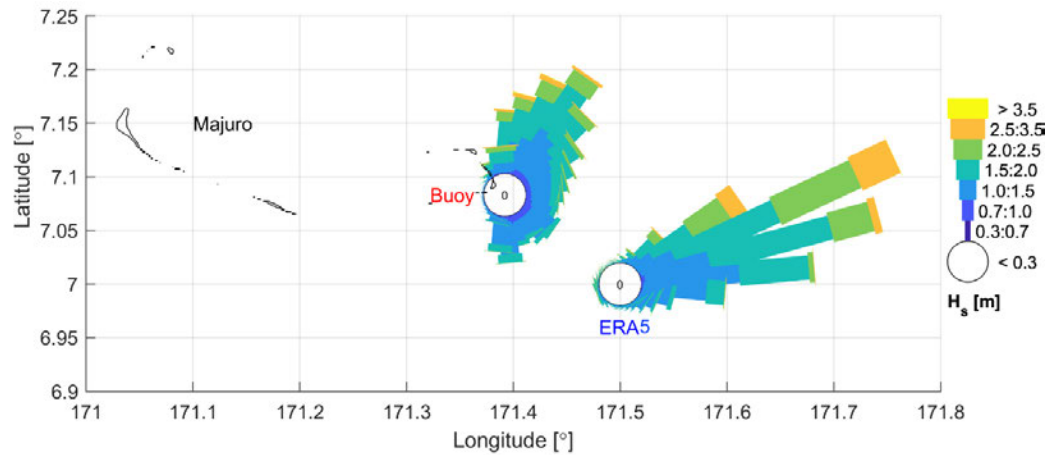
Figure A.2: *Comparison of the waves roses of buoy data and the nearest ERA5 point. Wave directions are presented in nautical convention.*

The transformation to nearshore conditions was done by use of a SWAN model. The ERA5 data of the outer locations in Figure A.3 was used for the boundary conditions of the SWAN model. The boundaries of SWAN grid (0.02°x 0.02°cells) with the nested grid for Majuro (0.002°x 0.002°cells) can also be found in Figure A.3.
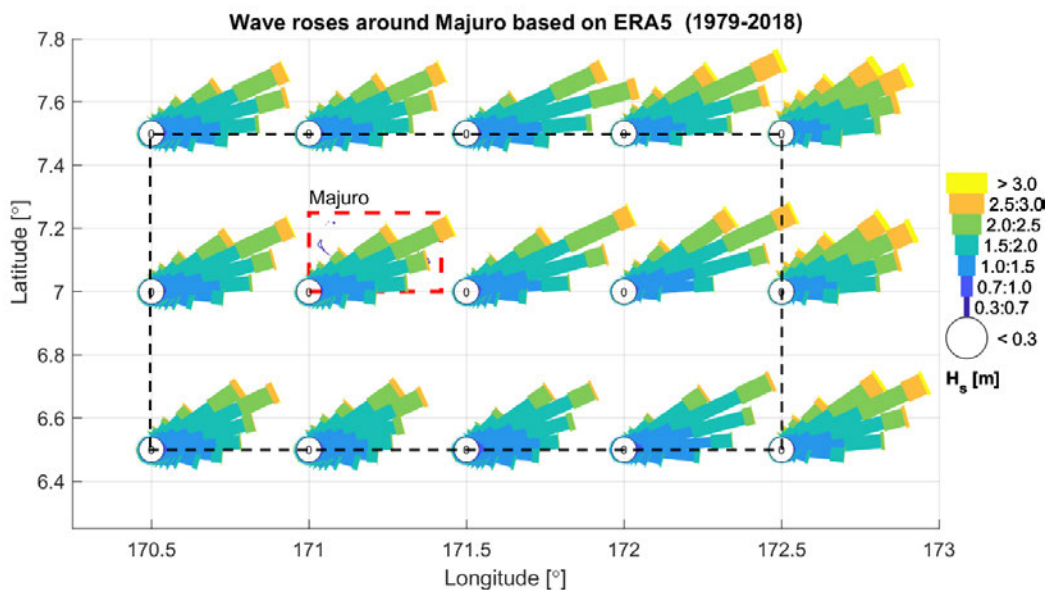
Figure A.3: *ERA5 offshore wave roses and the boundaries of the used SWAN model (black) with nested grid for Majuro (red). Wave directions are presented in nautical convention.*

A.2.2. Extreme value analysis for non-typhoon conditions

To allow synthetic data generation in Uninet, different extreme value distributions were fitted to the data and compared. This was done for the significant wave height (H_s) at the 5 different nearshore locations (C-G) where the wave conditions were specified, and for the offshore surge levels. See the results in Figure A.4 below.

For the significant wave height in cross sections C-F, the Weibull distribution gives the best fit. Only in Cross section G, the fit differs significantly and the Log-normal distribution would be a better model. In spite of that, the Weibull distribution was used for the significant wave height at all locations – including G – to be consistent. For the surge (lower right in Figure A.4) the Normal distribution gives the best fit.
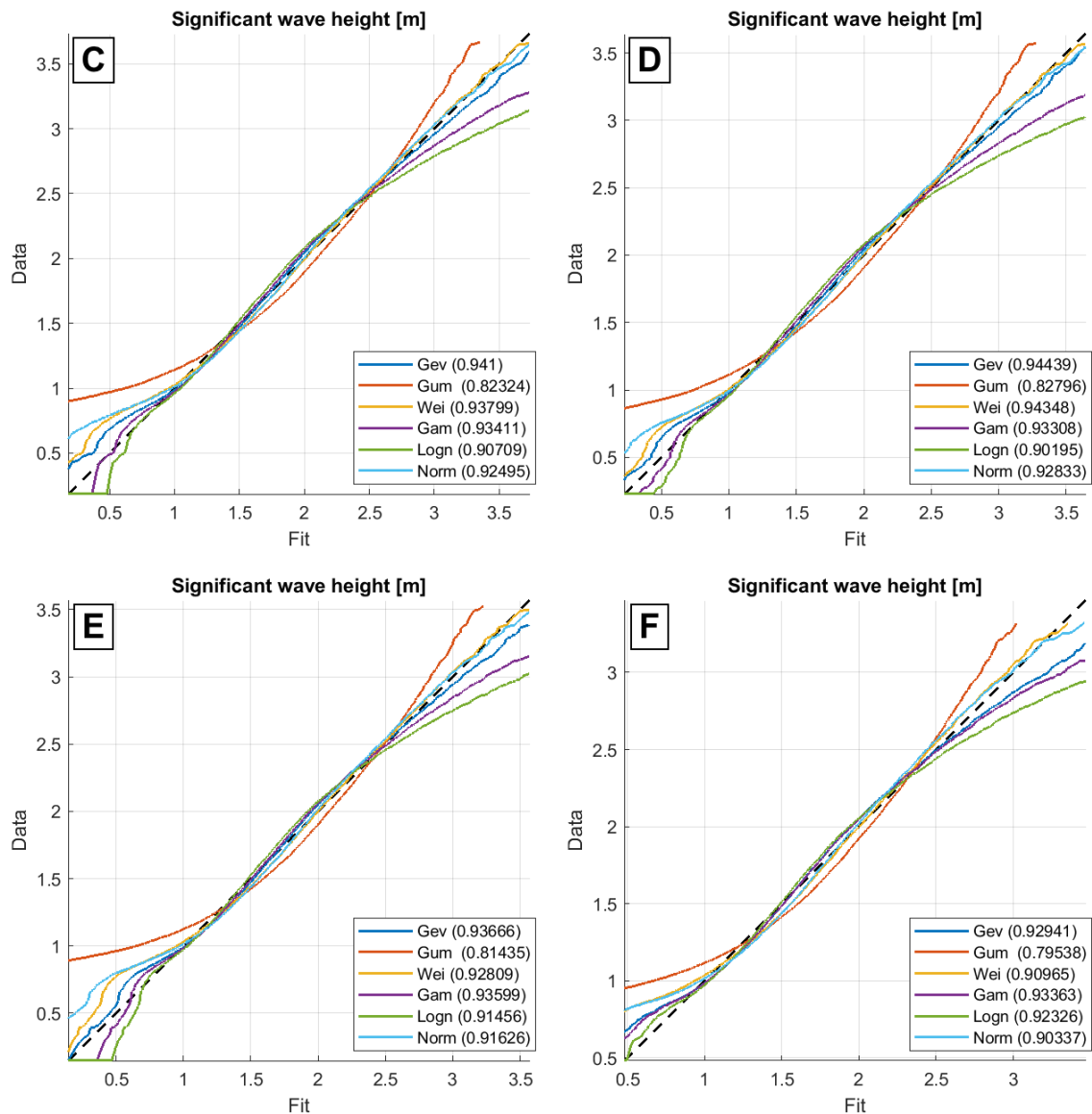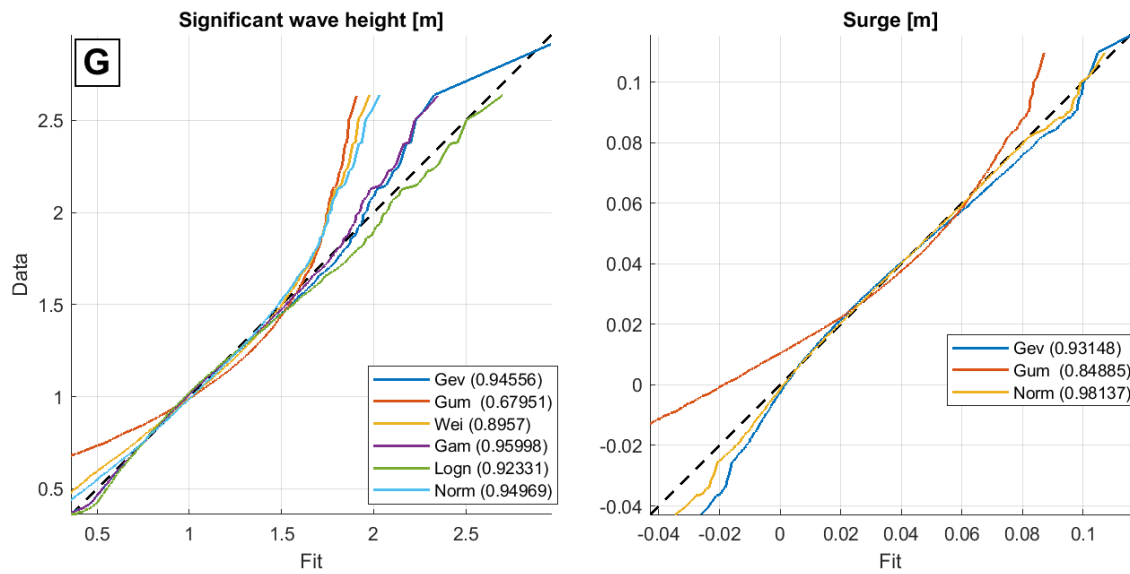
Figure A.4: Different fits of extreme value distributions compared with the data. The root mean square error of each of the fitted distributions compared to the data is shown in parentheses.

A.3. Precipitation

In this Section, steps in the processing of the precipitation data are elaborated. First, the results of the extreme value analysis based on monthly maximum rates are presented. Secondly, the spatial variation in precipitation and derivation of a standard event based on hourly precipitation rates are briefly elaborated.

A.3.1. Extreme value analysis based on monthly maximum rates

For the extreme value analysis of the daily precipitation rates, data of Majuro WBAS Airport station was used. After exclusion of data for typhoon conditions monthly maximum rates were selected, see Section 3.2.2. Subsequently, Generalized Extreme Value (GEV) Gamma (GAM) and Log-normal (LOGN) distributions were fitted to the data. See the resulting fits in Figure A.5 below.

The Log-normal distribution gives a poor fit, while both Gamma and GEV distributions give reasonable fits. Nevertheless, precipitation rates are underestimated as a number of events are included that should actually not be seen as extreme events (i.e. for some months, the maximum rates are in the order of a few millimeters). This could have been solved partially by using only the yearly maximum rates for example. However, this would mean that a large part of the events that may actually lead to flooding would be excluded as well. Hence, as a compromise, a peak over threshold approach was chosen, with a such a threshold that on average one event per month was selected. The results can be found in Section 4.2.2.

A.3.2. Spatial variation in precipitation rates

To check if precipitation rates on Majuro are comparable or higher than those on Kwajalein and to get some insight in the spatial variation in precipitation events around Majuro, data of different stations was compared. Data with daily precipitation rates of 4 different measuring stations was used, as described in Section 3.2.2. Figure 3.1 shows the locations of the Majuro WBAS Airport, Laura and Arno stations. Kwajalein Station is located about 430 km northwest of Majuro station.

Extreme precipitation rates were selected and compared based on a peak over threshold approach. For each of the stations, the threshold was chosen such that on average one event per month was included. The time series do not coincide and vary in length. For Majuro and Kwajalein (Ebeye), much longer time series were available than for Laura and Arno Stations. See the results in Figure A.6 below.
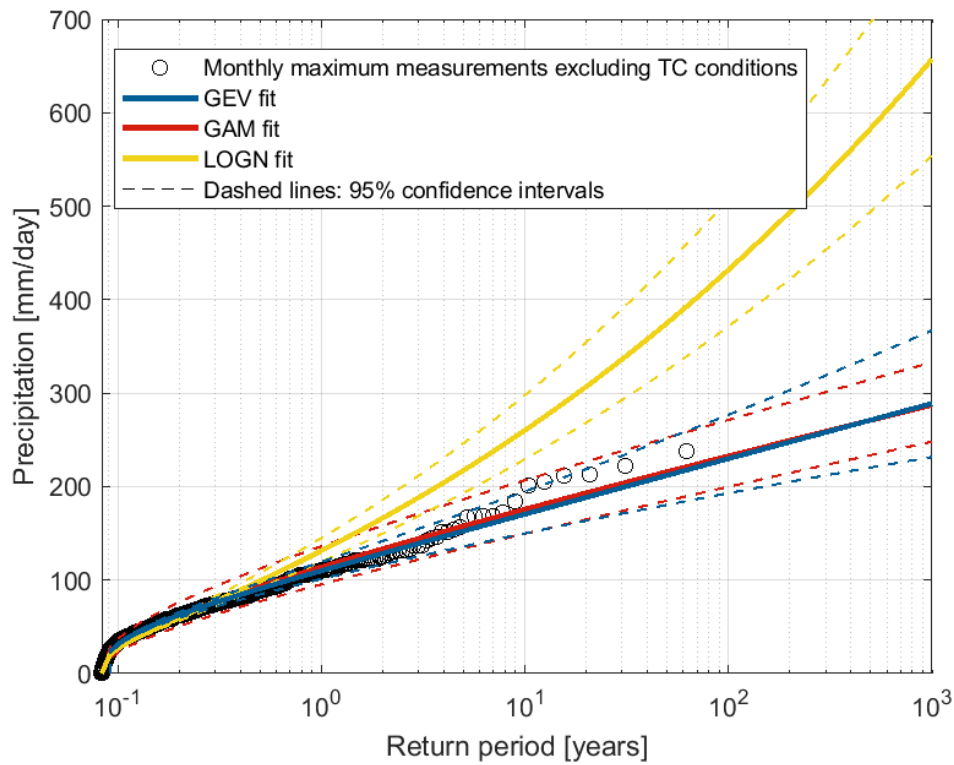
Figure A.5: *Comparison of the Generalized Extreme Value (GEV), Gamma and Log-normal distributions fitted to the monthly maxima of the daily precipitation rates.*
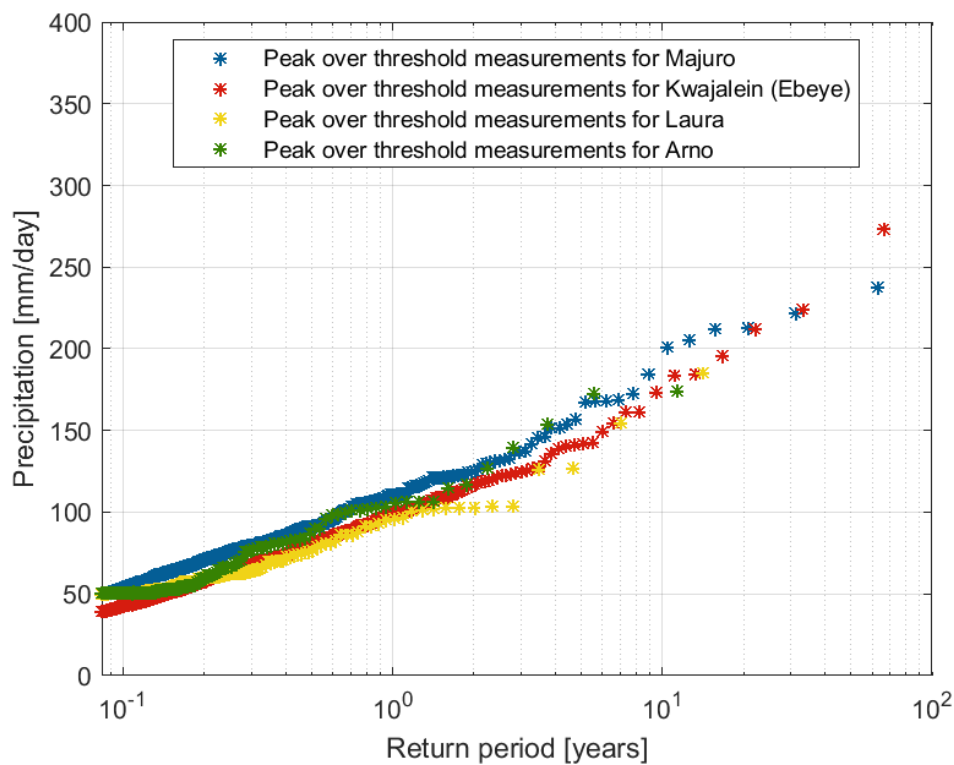

Figure A.6: *Comparison of Precipitation rates for different stations, based on a peak over threshold approach. Mark the difference in maximum return period and number of data points per station. For Majuro and Kwajalein (Ebeye), much longer time series were available than for Laura and Arno Stations.*

A.3.3. Derivation of a standard event

A standard event for precipitation during non-typhoon conditions was constructed by use of hourly measurements, as described in Section 3.2.2. An overview of the available hourly precipitation rates is provided in Figure A.7 below. Only the data for non-typhoon conditions was used to construct the standard event, as the standard event is only used for precipitation during non-typhoon conditions.
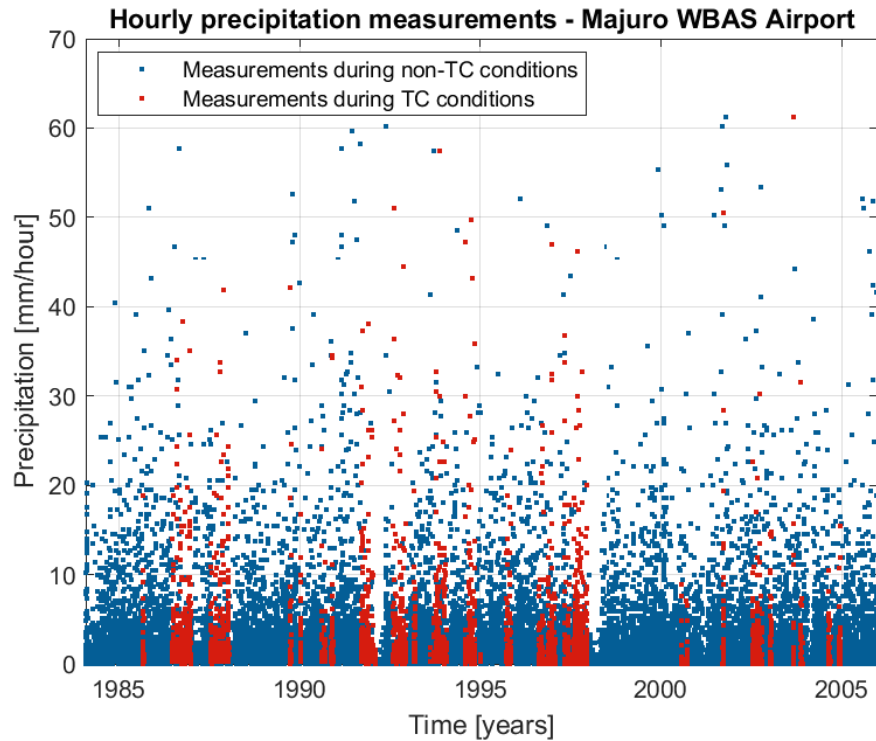
Figure A.7: All hourly measurements for Majuro WBAS Airport station. Measurements during typhoon conditions are filtered out of the data set.

As especially the events with high precipitation rates are important for flooding, those should be well represented by the standard event. To prevent a disproportional influence of days with little precipitation, a threshold value is chosen for the cumulative precipitation on a day. Hence, data for days with a cumulative precipitation above 49.5 mm/day was selected, in consistency with the daily precipitation rates. By doing so, sufficient data was included to get a good average, while the most extreme events are good represented as well.

Peak precipitation is not always in the same hour of the day. Hence, for each day the hour with the highest precipitation rate [mm/hour] is selected as hour zero, and all other hours of that day are added before and after. All events were normalized with the precipitation rate of the peak hour, and for each hour the mean value of all events was chosen. Subsequently, only the middle 24 hours were selected for the standard event, see Figure A.8. Lastly, the percentage of the total precipitation for each hour was calculated. The resulting standard event with the precipitation distribution over a day for non-typhoon conditions can be found in section 4.2.2.

To get some insight in the influence of the threshold value, different values were compared, see Figure A.9 below. Clearly, a lower threshold leads to a more peaked standard event. For events with a threshold of 100 mm, such limited number of events is available that the influence of individual events becomes visible in the standard event (i.e. a bump around 8 hours after the peak).

The problem with taking a lower or even a 0 mm threshold, is that most days with very peaked events are those with for example only one hour with 1 mm precipitation. As all days have an equal weight when taking the average of the (normalized) events, these will have disproportional

influence on the standard event. Hence such standard event would not well represent days with higher precipitation rates, while these are most relevant for flooding.
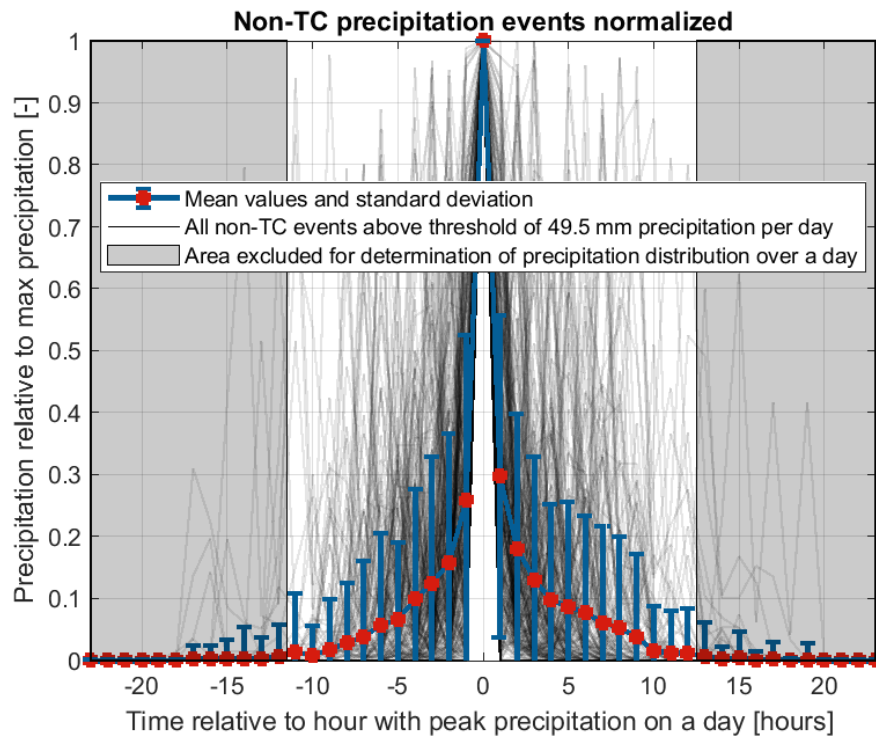
Figure A.8: *Normalized precipitation distribution over the days with a cumulative precipitation above the threshold value of 49.5 mm/day. For each event, the precipitation rates are normalized to the hour with peak precipitation.*
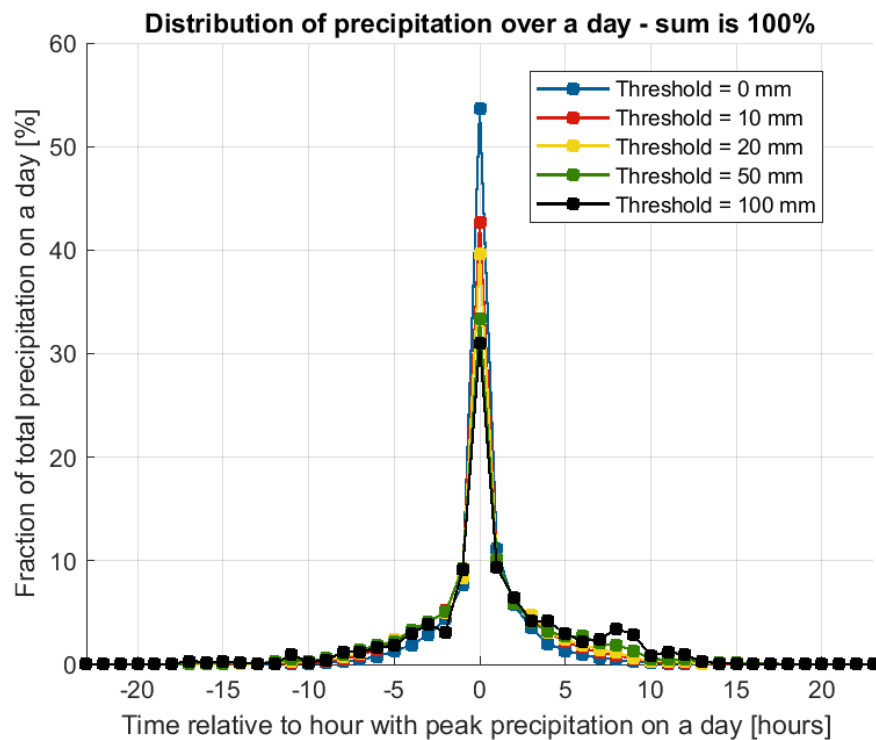
Figure A.9: *The influence of the threshold value of the cumulative precipitation on a day on the distribution over a day. A lower threshold value leads to a more peaked events*

B

Model setup and validation

Chapter summary

- In this Appendix some aspects of the setup and validation of the different numerical models are described in more detail. The simulation of water levels and wave conditions for Typhoon Paka in Delft3D is elaborated in Section B.1.

- For the XBeach model, first the boundary conditions as used for Typhoon Paka (1997) are presented, whereafter the influence of the grid size is discussed. The flood extents and inundation depths increase significantly when a finer grid is used, see Section B.2.

- Section B.3 describes the setup of the Delft3D-FM model used in the Charchenga Station (Bangladesh) case to simulate water levels and wave conditions, provided by Leijnse et al. (2019).

B.1. Typhoon Paka in Delft3D

As described in Section 3.3.4, validation by comparison of simulated water level or wave heights with measurements was impossible, only a simple check of the water levels and a qualitative assessment of the wave conditions was done for Typhoon Paka. In this Section the results are presented and discussed.

B.1.1. Validation of simulated water levels

Offshore of Majuro, where waves are not influenced by the bottom, an increase in water level (surge) is expected due to the pressure drop during the passage of the typhoon. For a comparison of the water levels and air pressure, the location of the wave buoy was chosen (see Figure 3.1 for this location) where the water depth is 553 m.

Only air pressure and wind fields were applied as boundary conditions, but as a location with large depth is chosen, no wind or wave induced setup is expected. Hence, the magnitude of this pressure drop should be approximately inversely proportional to the air pressure. After conversion of the pressure drop in hPa to meters water column, a comparison can be made.

Following from Figure B.1, the water level is indeed approximately the inverse of the air pressure. Only during peak pressure drop, the water level is slightly lower than expected and there is a pressure difference of about 1.5 cm. This can possibly be explained by the fact that adaptation of the water level to the air pressure may take some time (i.e. water has to flow to this location). Hence, this small deviation actually seems realistic, and it was concluded that the model is well capable of simulating offshore water levels based on the applied boundary conditions.
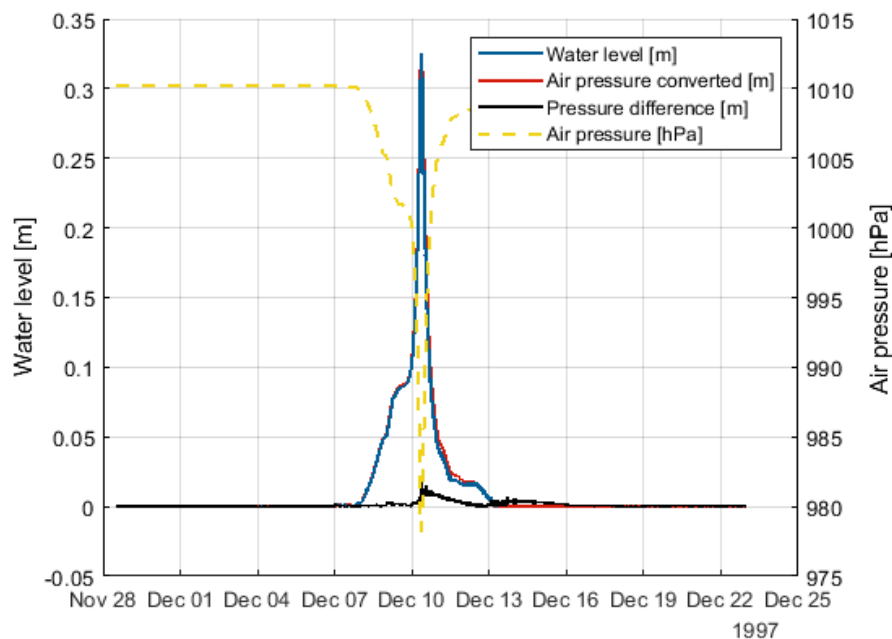
Figure B.1: Simulated water levels during Typhoon Paka in 1997 compared with the air pressure applied as boundary condition at the location of the wave buoy (water depth of 553 m).

B.1.2. Check of wave conditions

As the coupled model was used for simulation of Typhoon Paka, wave conditions were also included and could be assessed qualitatively. Again, this is done for the location of the wave buoy in deep water conditions. Based on Ford et al. (2018), it is expected that the maximum significant wave height is at least above 4.11 m (see Section 3.3.4). This is indeed the case, as the maximum simulated significant wave height is approximately 6.9 m. Estimated significant wave heights by Giardino et al. (2018) for Paka were in the same order of magnitude.

Validation with actual measurements would be much more favourable, but as no data was available this was not feasible within this thesis. Nevertheless, the simulated wave heights for typhoon Paka seem to be at least in the right order of magnitude. Hence, the model seems capable of simulating waves around Majuro, although future validation is strongly recommended when data would become available.

B.2. XBeach model

Two different aspects of the XBeach model were tested in more detail: the inclusion of precipitation and the required grid resolution to accurately model inundation. These are discussed below.

B.2.1. Simple model with precipitation in XBeach

To validate the new function to include rainfall in XBeach, 3 simple tests were done. A small XBeach model of 10 by 10 grid cells of 1 by 1 m each was used, without any waves or water levels applied at the boundaries. For all the model boundaries, the type *'Wall'* was selected, whereby water could not flow out of the domain. Precipitation rates were kept uniform over the domain. 3 types of boundary conditions were applied:

- Constant rainfall rate

- Increasing rainfall rate

- Rainfall peak

The applied rainfall rates over time can be found in Figure B.2 - left. For all simulations the cumulative precipitation after 1 hour was 100 mm. The resulting water levels can be found in Figure B.2 - right. For all 3 tests, the water level in the domain was 100 mm after one hour. Besides, the rise of the water levels over time was in correspondence with the applied boundary condition. Hence the rainfall function was concluded to work as expected.
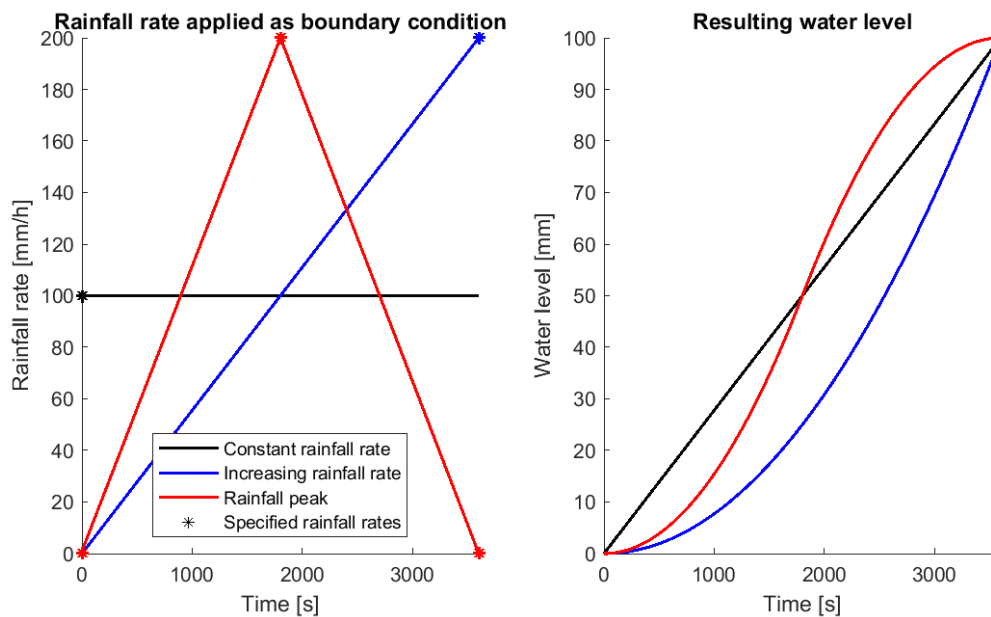
Figure B.2: Simple test of the rainfall function with applied B.C. (left) and resulting water levels (right).

B.2.2. Boundary conditions for Typhoon Paka

Figure B.3 gives an overview of all boundary conditions as applied in the XBeach model for Typhoon Paka; the comparison of flooding due to precipitation, coastal flooding and compound flooding in Figure 5.1 in Section 5.1.1 is based on these boundary conditions. Wave conditions and surge were obtained from the Delft3D model. Precipitation is based on measurements from Majuro WBAS

Airport station and the tide is obtained from the GTSM and added to the surge to obtain the total water level.
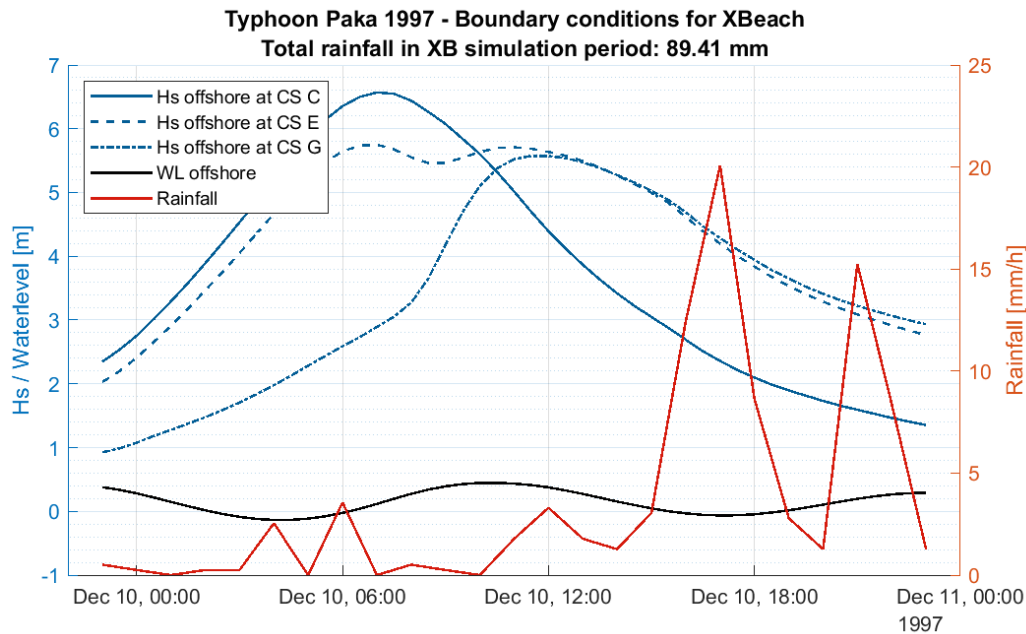
Figure B.3: Boundary conditions as applied in XBeach for typhoon Paka. For the comparison of the grids, only the December 10, 01:00 - 13:00 period was simulated and no precipitation was included.

B.2.3. Grid size of the XBeach model

As described in Section 3.3.3, 4 different grid sizes were tested and compared. This was done by simulation of typhoon Paka with the different grids, while applying the same boundary conditions. Here, only wave conditions and water levels were applied as boundary conditions. No precipitation rate was applied, as the grid size is mainly relevant wave transformation and precipitation would disturb the results. Hence, only the December 10, 01:00 - 13:00 period in Figure B.3 was simulated. Comparison of the grids was done in 2 ways:

- By comparing the maximum water level and Root Mean Squared Wave Height (H_{rms}) across the reef. The comparison was done for cross section C and G, in the northern and southern side of the DUD region respectively. H_{rms} was calculated based on the 30 minutes around the moment with the peak of the significant wave height at the location of the wave buoy. See Figure B.4 for the results.

- By comparing the maximum inundation depths and flood extents for the DUD region, see Figure B.5 below. Inundation was only compared for the 8, 4 and 2 m grids.

Following from figure B.4, the difference in maximum water level and wave height of the two coarser grids differ significantly from the two finer grids. The difference between the 4 and 2 m grid is much smaller. The 8 m grid with the 2x finer grid in the longshore direction does not perform significantly better than the 8 m grid. This was also concluded based on the figures for inundation depth (not shown for the 8 m grid with the 2x finer grid in the longshore direction).

The flood extents and inundation depths for the grid resolutions of 8, 4 and 2 m are presented in Figure B.5 below. Clearly, the finer grid leads to significantly more flooding in most areas, especially in the northeastern parts of the DUD region. However, in the northwestern side of the DUD region, slightly less flooding is observed. Possibly, some boundary effects play a role here, as the boundary f the XBeach model is relatively close here and in shallow water (see Figure 3.14).
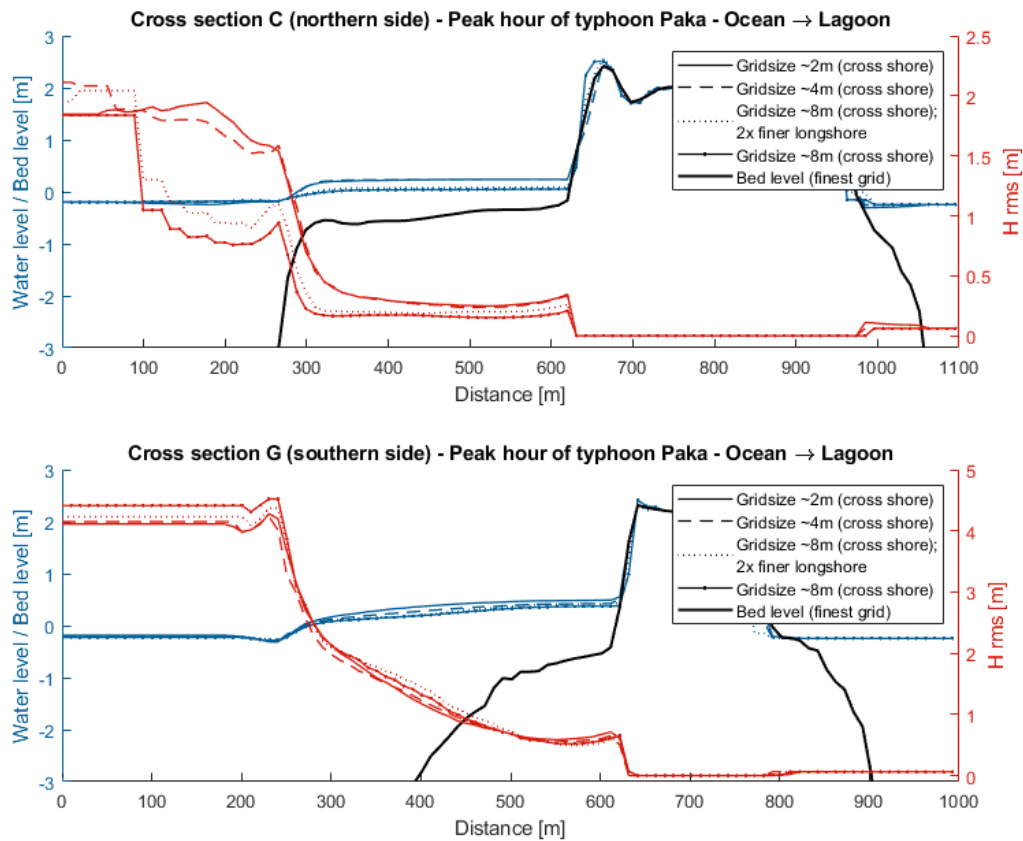
Figure B.4: *Maximum water level and Root Mean Squared Wave Height (H_{rms}) in cross sections C and G, from Ocean (left) to lagoon (right). The bed level is only shown for the grid of 2m, hence for the other grids, the elevation of the bed level is not exact.*

It can be expected that the XBeach model with the finer grid gives more realistic results. Following from the Matlab toolbox for XBeach (Hoonhout, 2015), the advised grid size based on the wave length is even smaller than 2 m; possibly only 1 m in cross shore direction. Unfortunately, using the 2m grid for all simulations in this thesis was already computationally unfeasible. Hence, the 4 m grid is used, but validation of the inundation depths for different boundary conditions and tests with higher grid resolution are recommended.
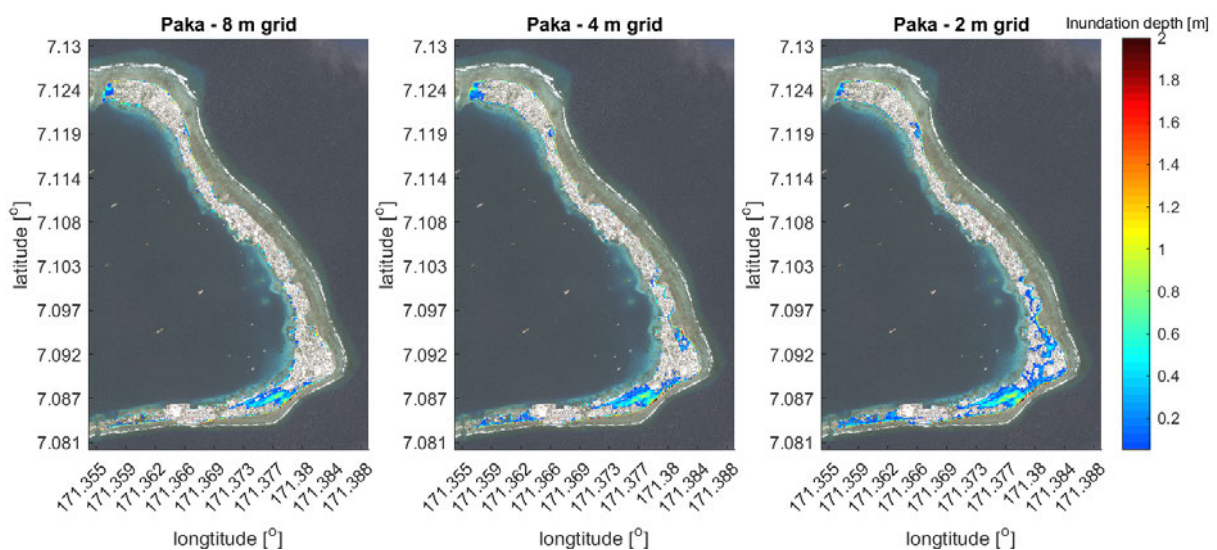
Figure B.5: *Comparison of the inundation depths for different grid sizes. The same boundary conditions are applied for all simulations. Underlying satellite image: ©2019 CNES/Airbus, 17-3-2017 via Google Maps.*

B.3. Delft3D model for Bangladesh case

To validate the method for the selection of representative tropical cyclones and to optimize the β parameter in the Softmax interpolation (see Section 4.1.3), simulated water levels and wave conditions for a large set of synthetic TC were required. This was not available nor computationally feasible for the Majuro case, while for Charchenga Station, Bangladesh, this data was already available. The data was provided by Leijnse et al. (2019), who assessed present and future coastal hazards due to tropical cyclones in the Bay of Bengal using synthetic tracks.

Charchenga Station is located at 22.2167°N; 91.0500°E, see Figure B.6 below. Although data for more locations around the Bay of Bengal was available, Charchenga station was chosen because a measuring station is available at this location and simulated water levels were validated by measurements. Wave output was obtained at the nearest SWAN model grid cell in water deeper than 30 m, as waves in shallower water were not resolved by the SWAN model.

Model setup

Similarly to the Majuro case, the water levels and wave conditions were simulated for each individual tropical cyclone. This was done by use of coupled hydrodynamic and wave models. Water levels resulting from tropical cyclones were computed using a Delft3D-FM (Flexible Mesh; Kernkamp et al., 2011) model. The Delft3D-FM model is based on the grid of the Global Tide and Surge Model (GTSM; Muis et al., 2016), with the coarsest resolution of 25 km on the ocean and the finest resolution equal to 1 km. Waves were simulated using the Delft3D-WAVE (based on SWAN) with an rectilinear grid with an approximate resolution of 0.02 degrees (±2 km). The non-stationary mode with a time step of 10 minutes was used. Water levels and flow velocities are coupled with Delft3D-FM and updated every 30 minutes. See Figure B.6 for the used grids.

The Delft3D-FM (Flexible Mesh) model and Delft3D-FLOW model (used for Majuro) are slightly different, both are able to accurately model a whole range of hydrodynamic situations, including storm surge during tropical cyclones. The same setup as for the Majuro was used; wind and air pressure field were applied as boundary conditions. Tidal forcing is excluded from the model to be able to compare the impact of TCs directly, without the timing of the tidal water levels playing a role. For the southern boundary at the open ocean, no information is applied, and therefore waves are only generated by the forcing related to the tropical cyclones.
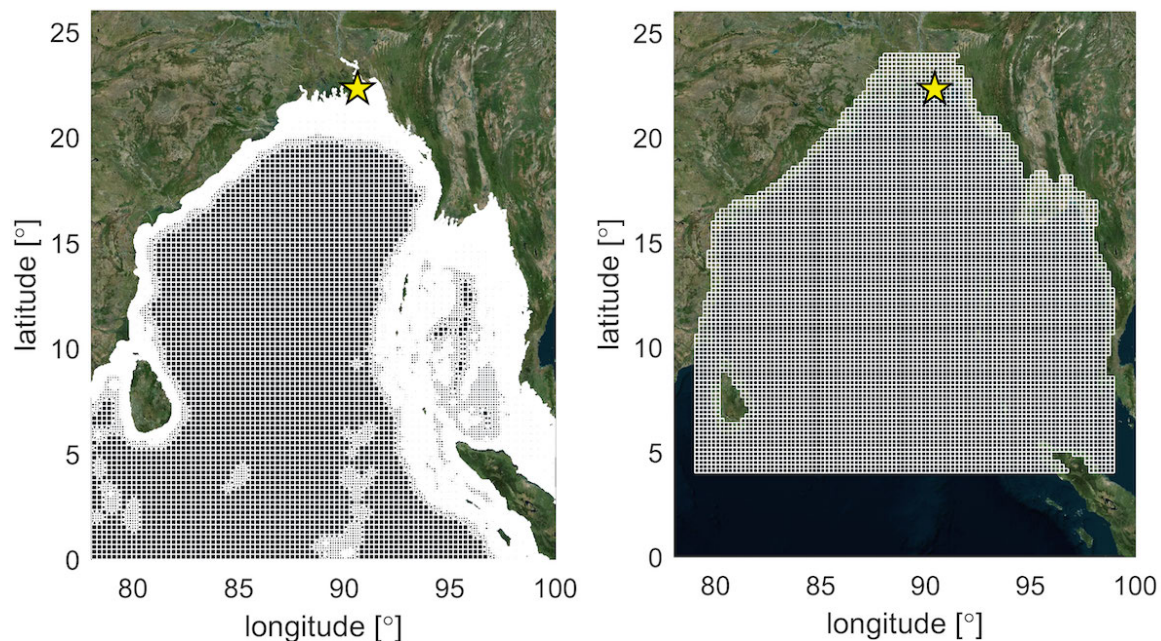
Figure B.6: *Used grids for the coupled Delft3D-FM (left) and SWAN (right) for the Bangladesh case study by Leijnse et al. (2019). Charchenga Station is located at 22.2167° N; 91.0500° E (marked with a yellow star).*

C
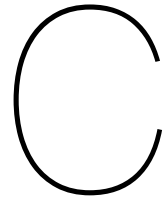
Scenario selection

Chapter summary

This Appendix provides some additional figures with results of the scenario selection. First, some additional figures for combinations of parameters as used in MDA are presented. For all combinations the selected representative typhoons seem to be a good representation of all synthetic typhoons. Subsequently, the approximated and simulated water levels and wave heights are compared for Charchenga Station (Bangladesh). The influence of the minimum distance of the typhoon track to the location of interest is also briefly assessed.

C.1. Typhoon scenario selection for Majuro

To get more insight in the spread of the representative typhoons over the synthetic typhoons for all used parameters, some additional figures for various combinations of parameters are presented in this Section. Each of the Figures below shows the distribution for two parameters and only a selection of 10 combinations is shown. In total there are 231 possible combinations of 22 parameters. However, it was not possible to show all combinations. All presented figures are for the final set of weight factors (C. More weight to local parameters). These weight factors and an overview of the used parameters can be found in Table 3.2.

Just as for the Figures in Section 4.1.2, the distributions of synthetic typhoons should be similar to those for historical typhoons, while those for representative typhoons should be more uniformly spread over the parameter space. Concluding from the Figures below, this generally seems to be the case.
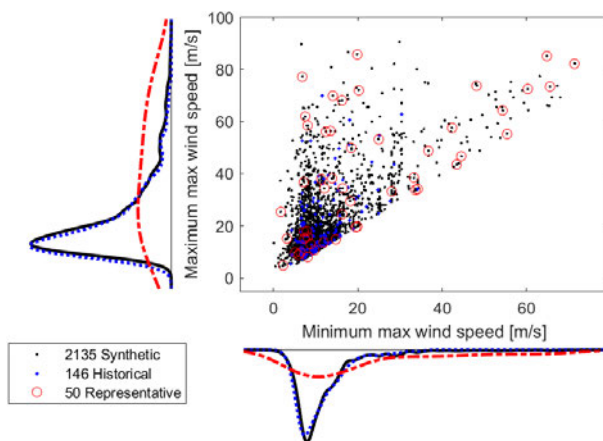
Figure C.1: Maximum (in time) of the maximum (in space) wind speed in the area of interest versus the minimum (in time) of the maximum (in space) wind speed in the area of interest.
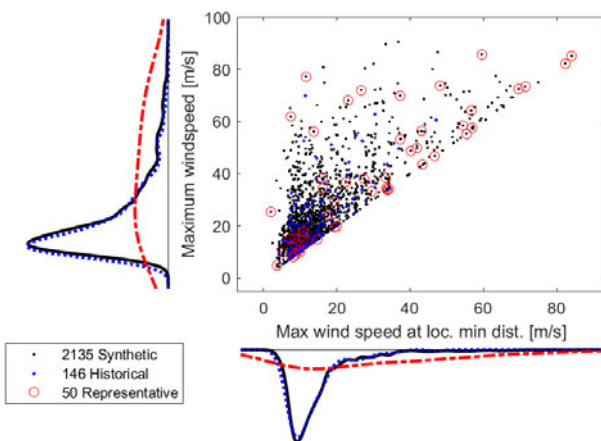
Figure C.2: Maximum wind speed in the area of interest versus the maximum wind speed at the location of minimum distance of the typhoon track to Majuro.
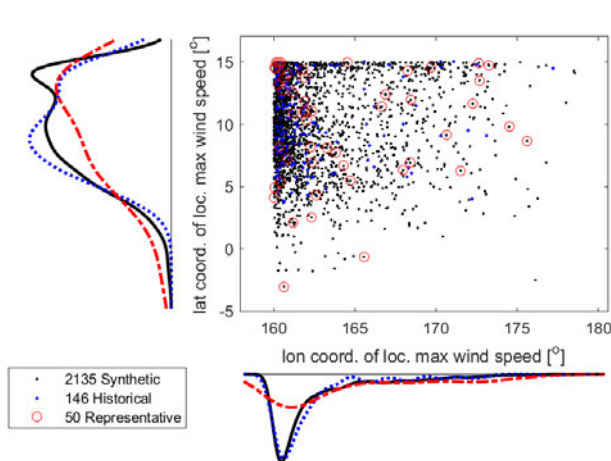
Figure C.3: Location of the typhoon in the area of interest with maximum wind speed. Clearly, typhoons have the highest wind speeds in the northwestern part of the area of interest.
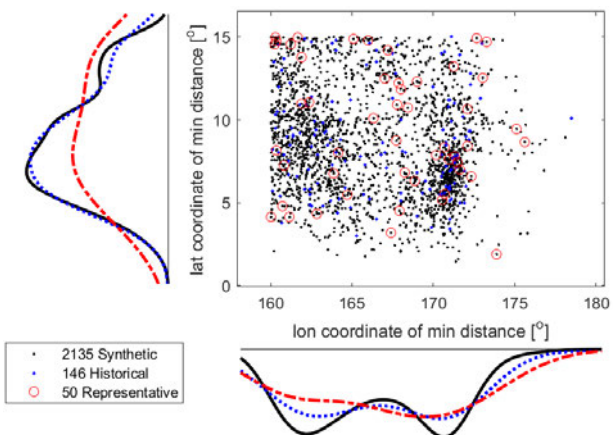
Figure C.4: Locations of the minimum distance of the track to Majuro. Typhoons in general move towards roughly the northwest. Therefore, typhoons with genesis locations in the southeast of the area of interest pass Majuro, while those with genesis locations northwest of the area of interest do not pass Majuro.
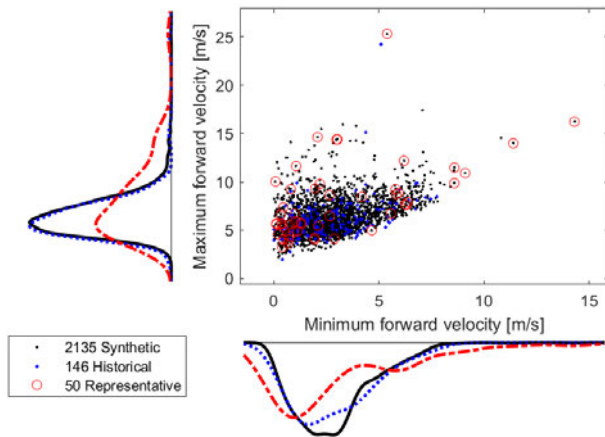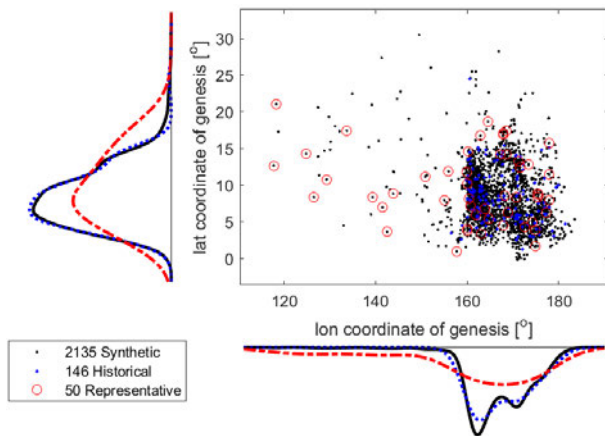
Figure C.5: *Maximum versus minimum forward velocity in the area of interest. Relatively many typhoons with low minimum forward velocity were selected.*
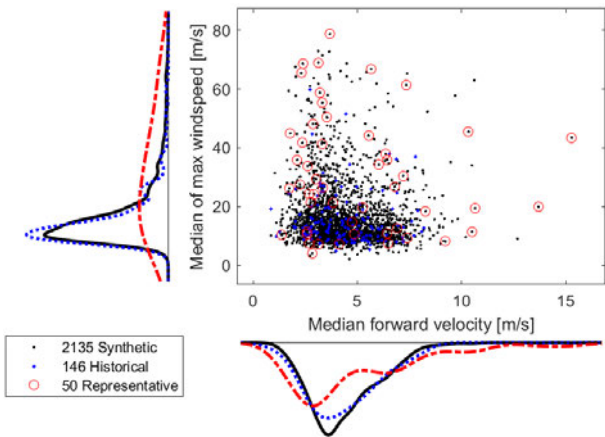
Figure C.6: *Median of the max. wind speed versus the median forward velocity in the area of interest. The forward velocity and maximum wind speed seem to be unrelated.*


Figure C.7: *Genesis locations of the typhoons that pass through the area of interest. Most typhoons also have their genesis location in this area, which can be expected as in general typhoons move into northwestern direction here.*
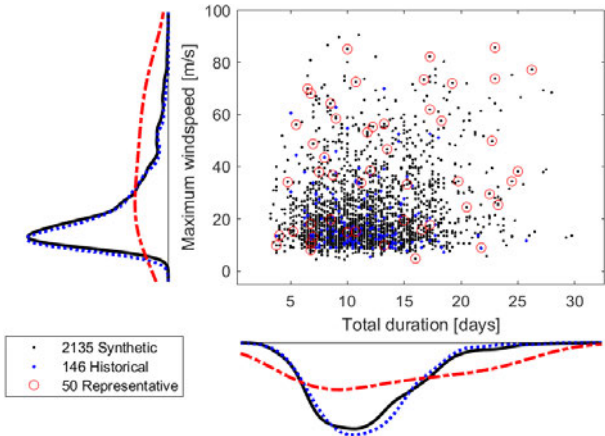
Figure C.8: *Total duration of the typhoon versus the maximum wind speed in the area of interest. Typhoons with the highest total duration often seem to have already high wind speeds in the area of interest.*
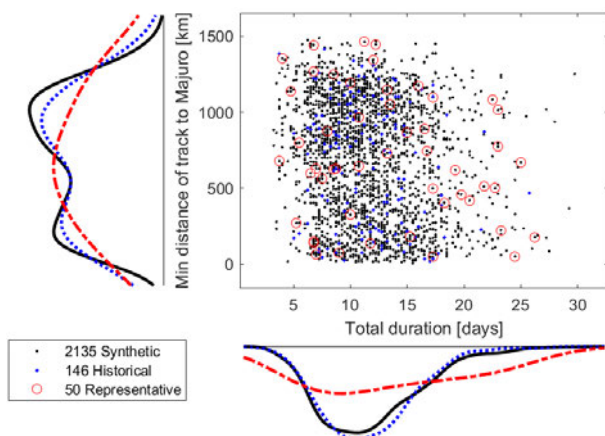
Figure C.9: *Total duration of the typhoon versus the minimum distance of the typhoon track to Majuro.*
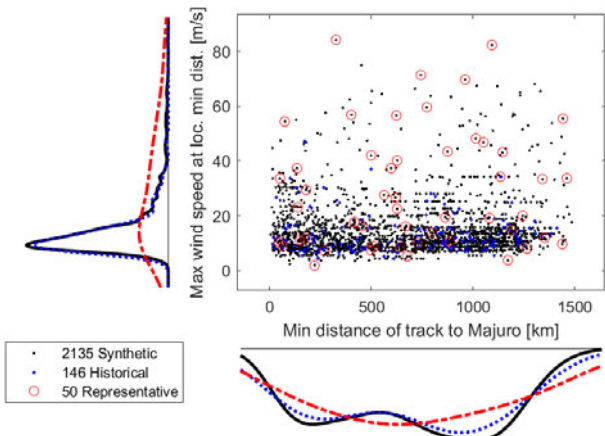
Figure C.10: *Minimum distance of the typhoon track to Majuro versus the maximum wind speed of the typhoon at that location.*

C.2. Water levels and wave heights at Charchenga Station

In Figures C.11 and C.12 the maximum simulated water levels and significant wave heights for all historical typhoons, synthetic typhoons, and approximated synthetic typhoons based on 50 representative typhoons and interpolation, are compared for the location of Charchenga station (Bangladesh).
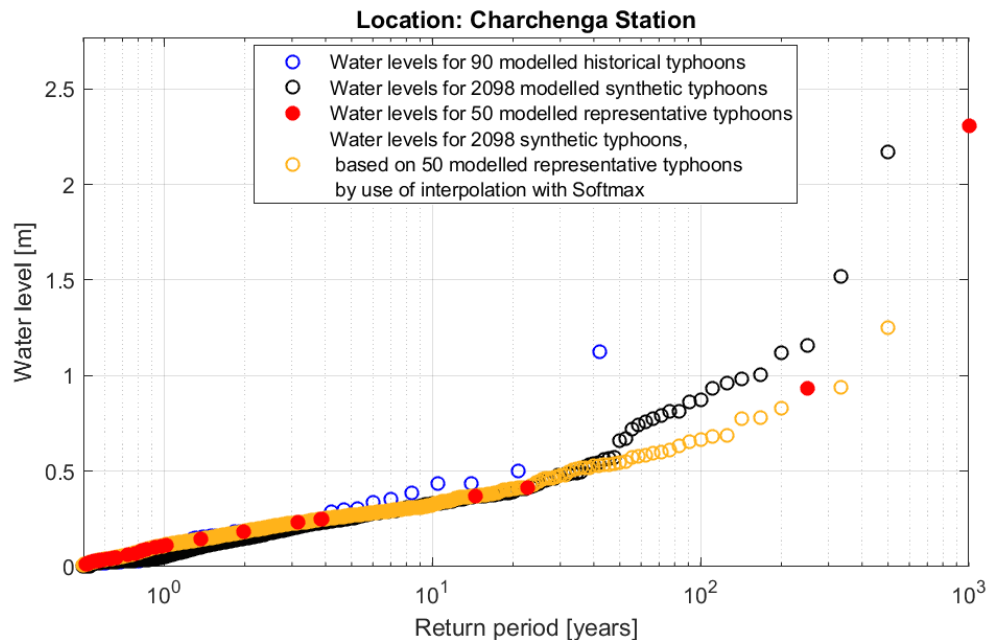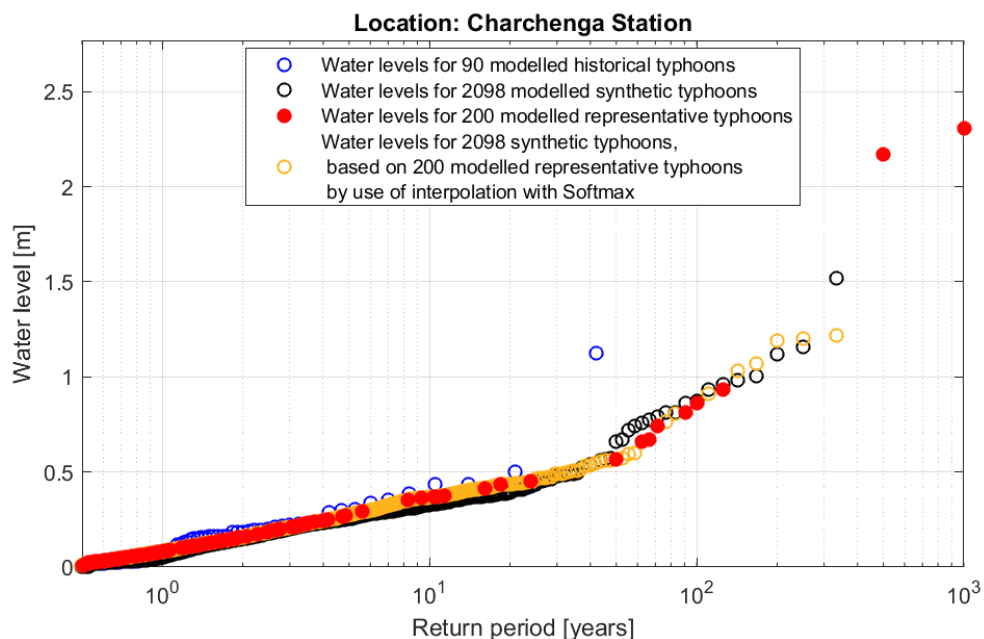

Figure C.11: *Comparison of maximum water levels for all historical typhoons, synthetic typhoons and approximated synthetic typhoons based on 50 representative typhoons and interpolation for Charchenga station.*
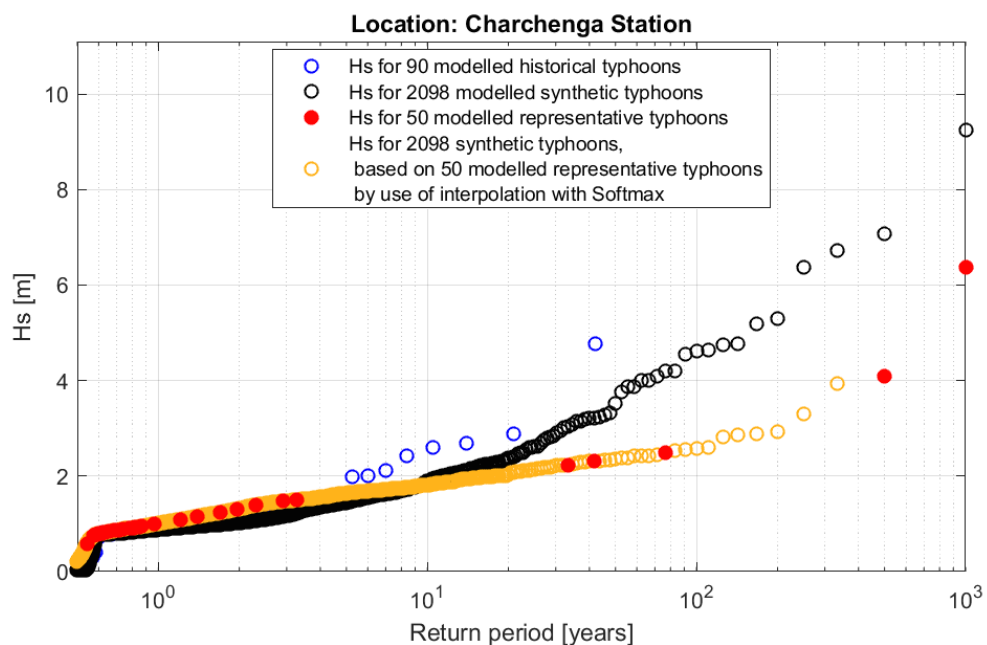
Figure C.12: *Comparison of maximum significant wave height (H_s) for all historical typhoons, synthetic typhoons and approximated synthetic typhoons based on 50 representative typhoons and interpolation for Charchenga station.*

Similarly to Figure 4.13 for the maximum water levels around Majuro, the maximum water levels

around Charchenga station were reasonably well approximated, although just a few of the more extreme typhoons were selected. For the maximum significant wave height however, the most extreme typhoon was not selected as representative. As interpolation is used, the wave conditions for the most extreme events could not be approximated correctly based on the other representative typhoons. Hence, the wave heights for the highest return periods are significantly underestimated.

When the number of representative typhoons is again increased to 200 (similarly to Figure 4.14 for Majuro), the above mentioned issues are largely solved and the water levels and wave heights can be well approximated, see Figures C.13 and C.14 below.


Figure C.13: *Comparison of maximum water levels for all historical typhoons, synthetic typhoons and approximated synthetic typhoons based on 200 representative typhoons and interpolation for Charchenga station.*
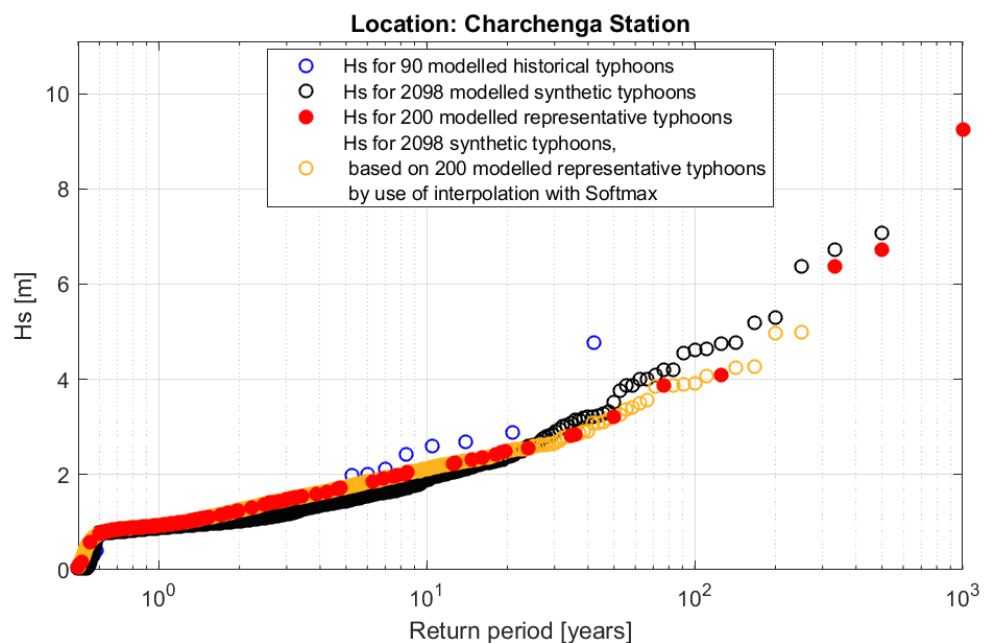

Figure C.14: *Comparison of maximum significant wave height (H$_s$) for all historical typhoons, synthetic typhoons and approximated synthetic typhoons based on 200 representative typhoons and interpolation for Charchenga station.*

C.2.1. Influence of the area of interest in Bangladesh case

Following from Figures C.11 and C.12, the most extreme events in terms of maximum water level and wave height are not those typhoons that get closest to Charchenga station. However, in the weight factors for MDA and in the selection of the first event for MDA the minimum distance to the tracks an the maximum wind speed of that location are the most important. This is confirmed by Figure C.15 below, and could partially be explained by looking at the location of Charchenga station. Some of the selected representative typhoons do pass very close to Charchenga Station, but at the northern side and thus over land. Hence, these do most likely not lead to very high waves.
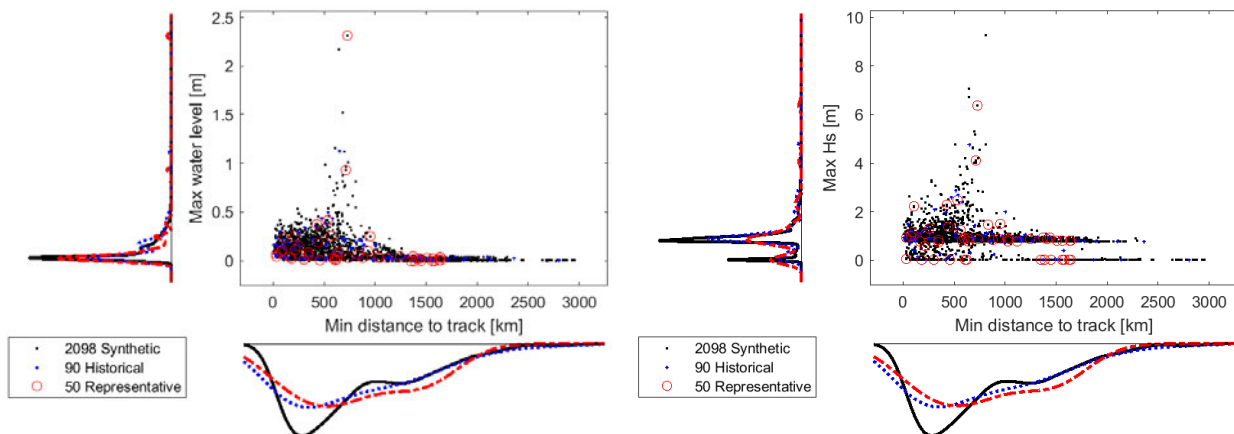
Figure C.15: *Overview of the minimum distance of the typhoon track to Charchenga station versus the maximum water level (left) and significant wave height (right).*

The effect of the land on one side of Charchenga station can also explain the *'two layers'* in the right side of Figure C.15. Part of the typhoons does not cause only very low waves (below ±1 m) although passing very close to Charchenga Station. Most likely, these typhoons do pass on the land side. On the other hand, a large part of the typhoons causes waves of at least 2 m, even at large distance. These are most likely related to typhoons passing on the ocean side. For Majuro this does not apply as it is completely surrounded by the ocean. Hence it can be expected that the typhoon that has the highest wind speeds near Majuro will also cause the highest waves and water levels at Majuro (although just on one side of the island). This is indeed the case for water levels, as can be seen in Figure 6.1.

D
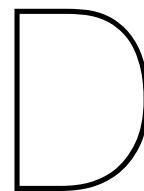
Additional flood maps

Chapter summary

In this Appendix some additional flood maps are presented that provide more detailed insights in the flood hazard for the DUD region. First the simulated inundation depths for typhoon Paka (1997) are presented (Section D.1). Additional flood maps for coastal flooding and precipitation related to non-typhoon conditions with a return period of 5 year are presented in Section D.2. Additional flood maps for the combined flood hazard for the DUD region are presented in Section D.3.

D.1. Inundation depths for typhoon Paka

The inundation depths of typhoon Paka, corresponding to the flood extents of compound flooding of Figure 5.1. Compared with other simulated (synthetic) typhoons, Paka was one of the most extreme in terms of inundation.
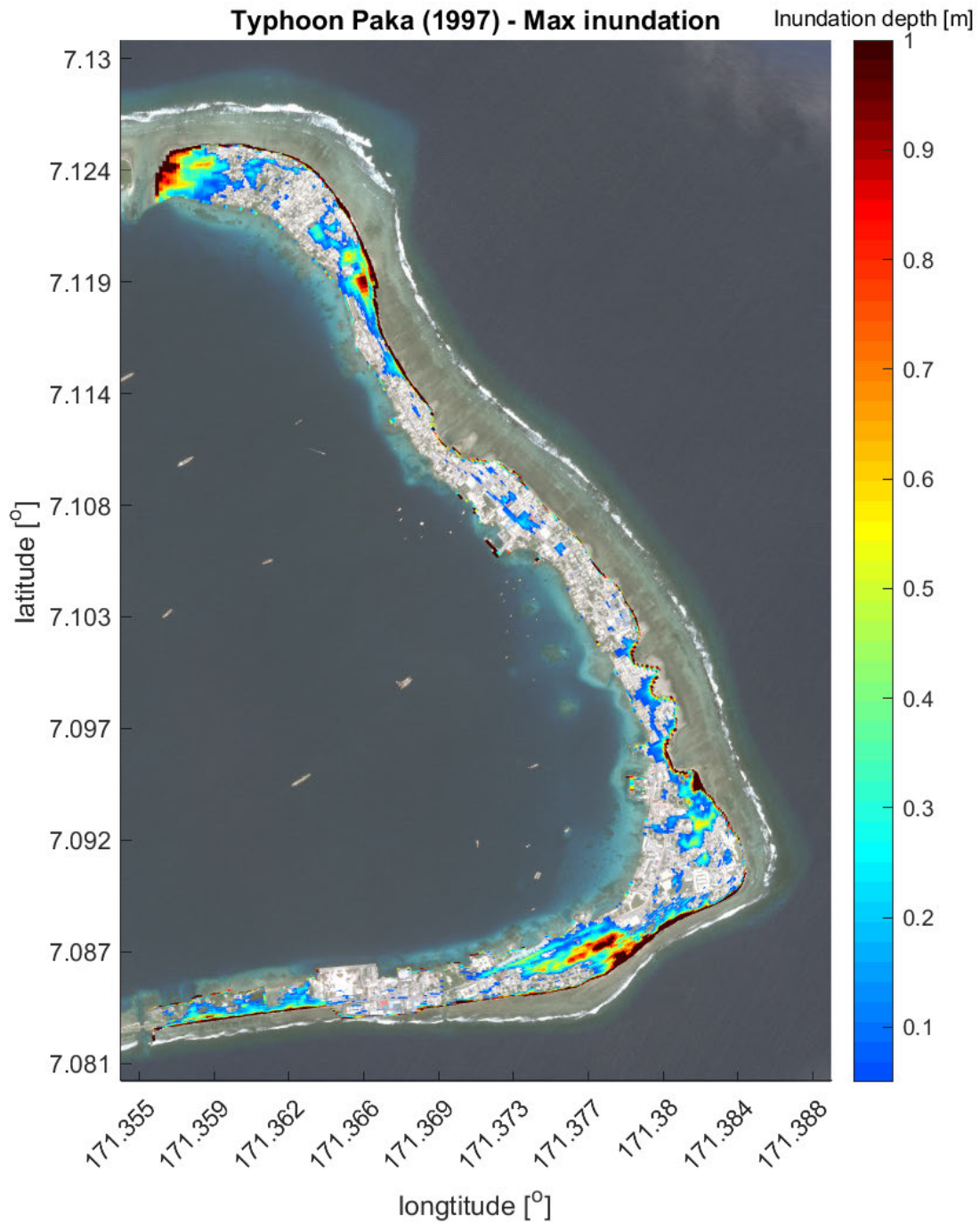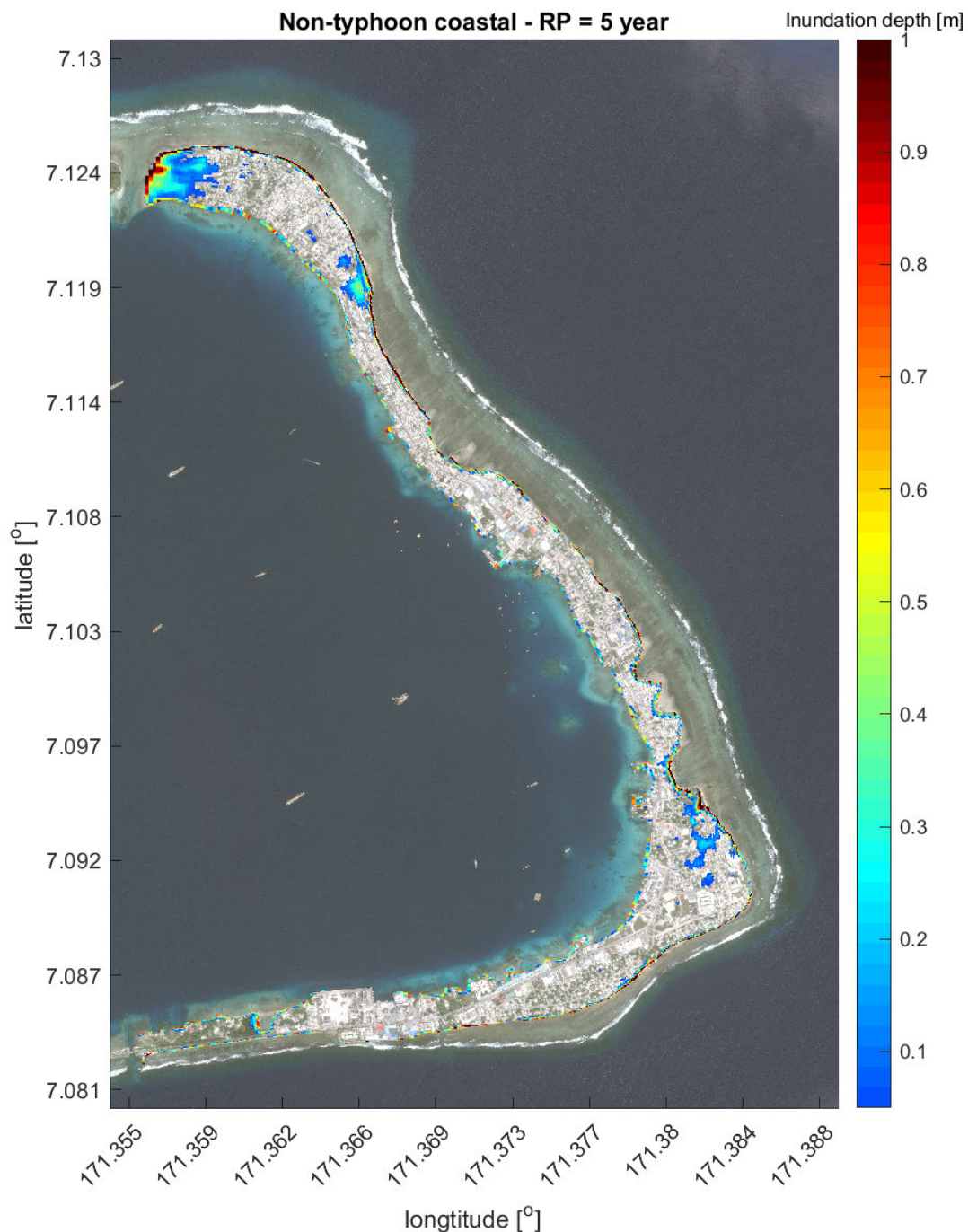

Figure D.1: *Simulated inundation depths for typhoon Paka (1997) for compound flooding (i.e. coastal flooding and precipitation combined). Underlying satellite image: ©2019 CNES/Airbus, 17-3-2017 via Google Maps.*
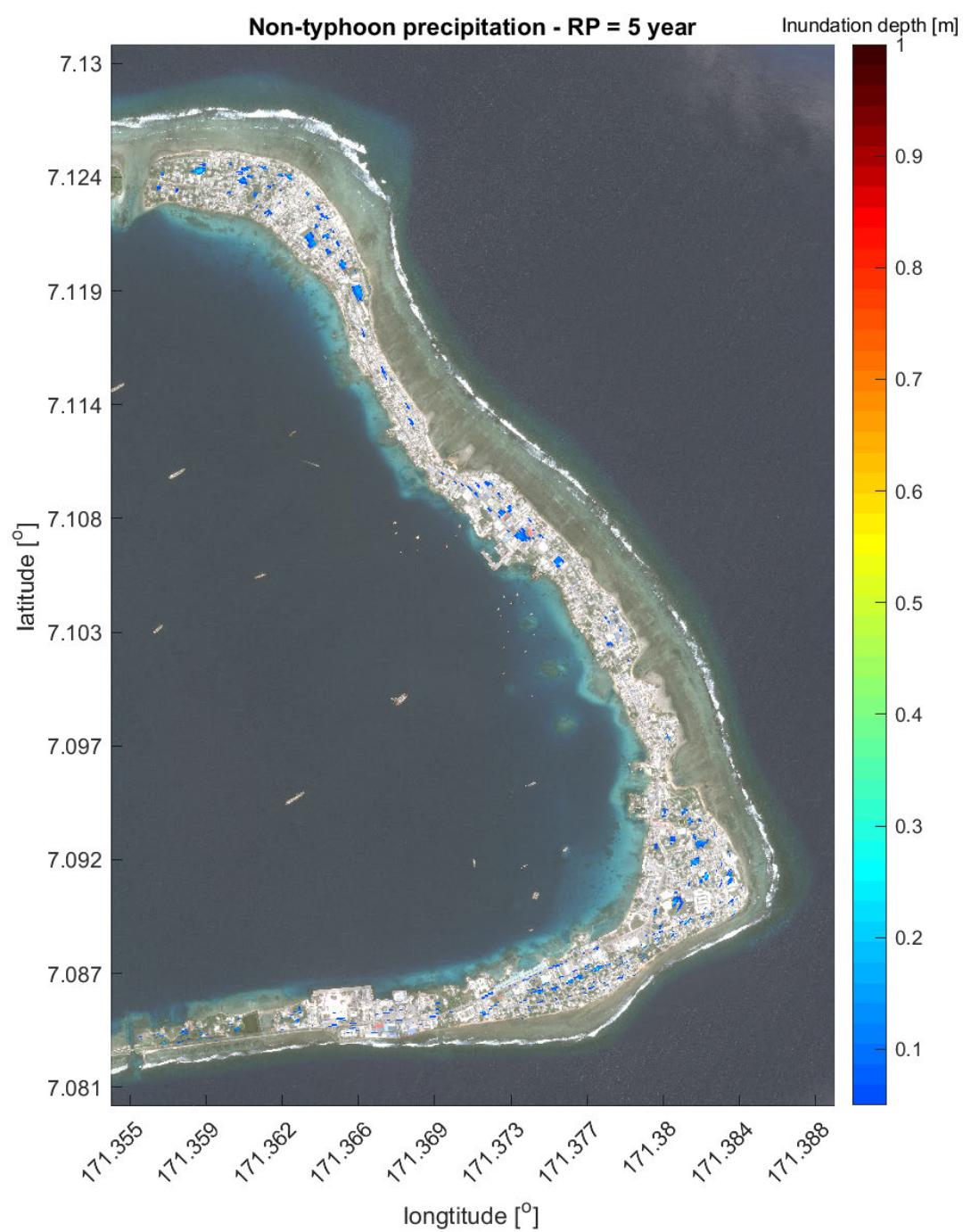
D.2. Additional flood maps for non-typhoon conditions

In this Section the flood maps for non-typhoon related coastal flooding (Figure D.2) and precipitation related flooding (Figure D.3) with a return period of approximately 5 years are presented. By comparison with the same maps for a 50 year return period in Section 5.2.2, these provide additional insights in the importance of different flood drivers. The inundation depths are approximate, as the compound events are excluded for both.

Coastal flooding with 5 year return period – non-typhoon

Figure D.2: *Estimated inundation depths for coastal flooding during non-typhoon conditions with a return period of 5 year. Underlying satellite image: ©2019 CNES/Airbus, 17-3-2017 via Google Maps.*

**Precipitation related flooding with 5 year return period – non-typhoon**

Figure D.3: *Estimated inundation depths for precipitation related flooding during non-typhoon conditions with a return period of 5 year. Underlying satellite image: ©2019 CNES/Airbus, 17-3-2017 via Google Maps.*

D.3. Combined flood maps for other return periods

Additional flood maps for the combined typhoon and non-typhoon flood hazard are presented for return periods of 20 and 100 years in Figures D.4 and D.5. In Figure D.6, the maximum simulated inundation depth for all 100 simulated scenarios (i.e. 50 typhoon and 50 non-typhoon) is presented. This should correspond to flood map with return period of 1000 years, although with significantly larger uncertainty than those derived for lower return periods.
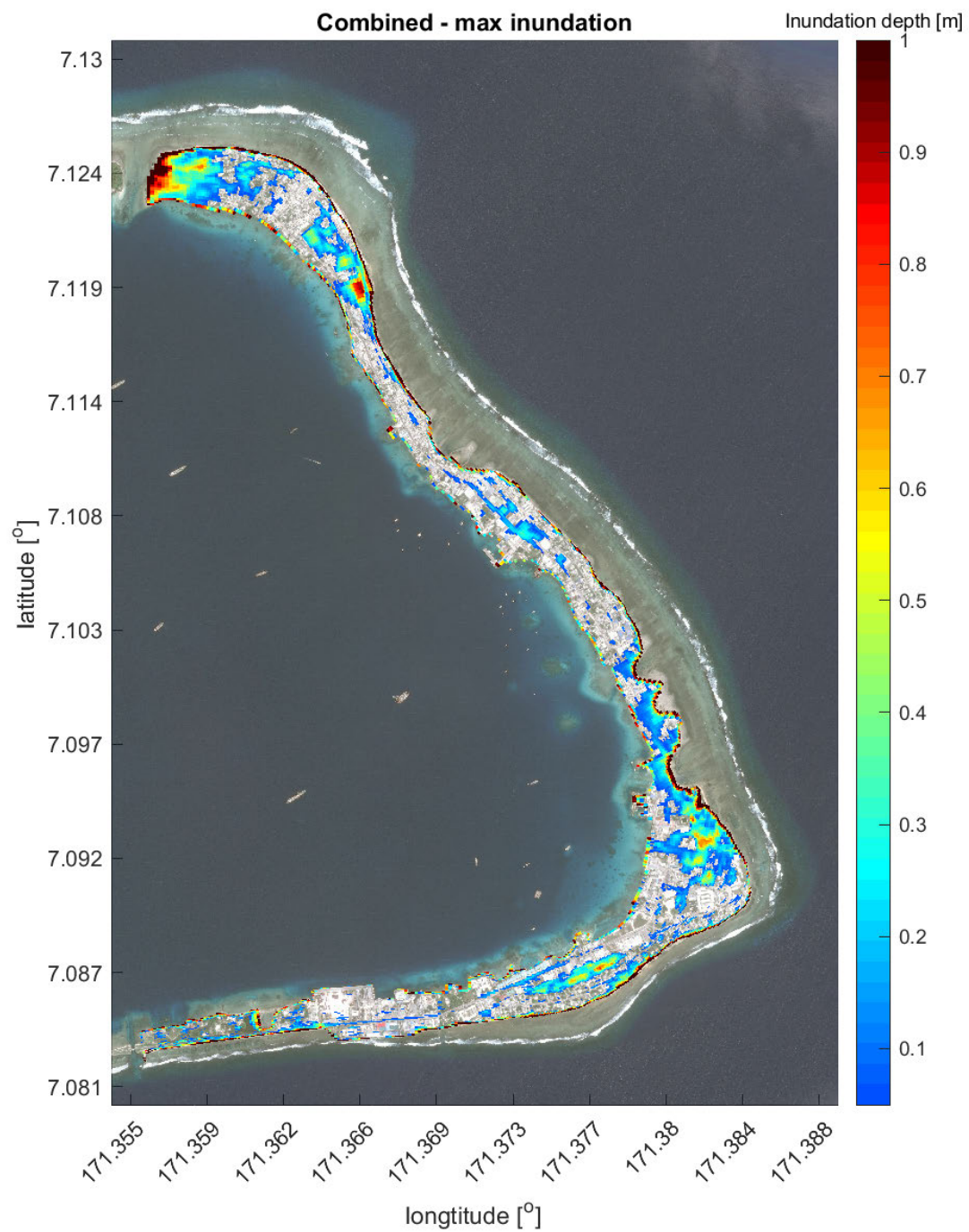
Flood map for return period of 20 years
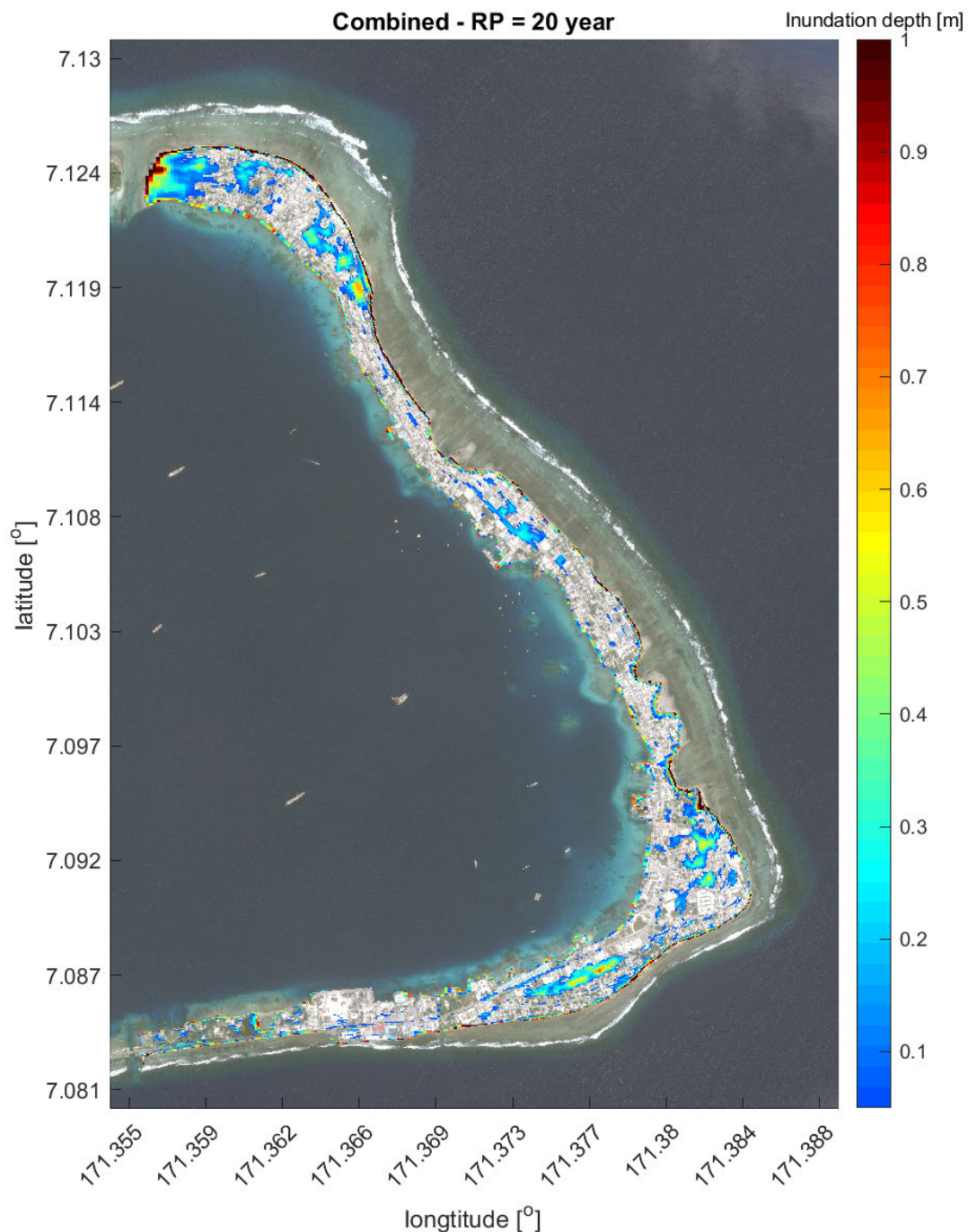
Figure D.4: *Estimated inundation depths for a return period of 20 year. Underlying satellite image: ©2019 CNES/Airbus, 17-3-2017 via Google Maps.*

Flood map for return period of 100 years
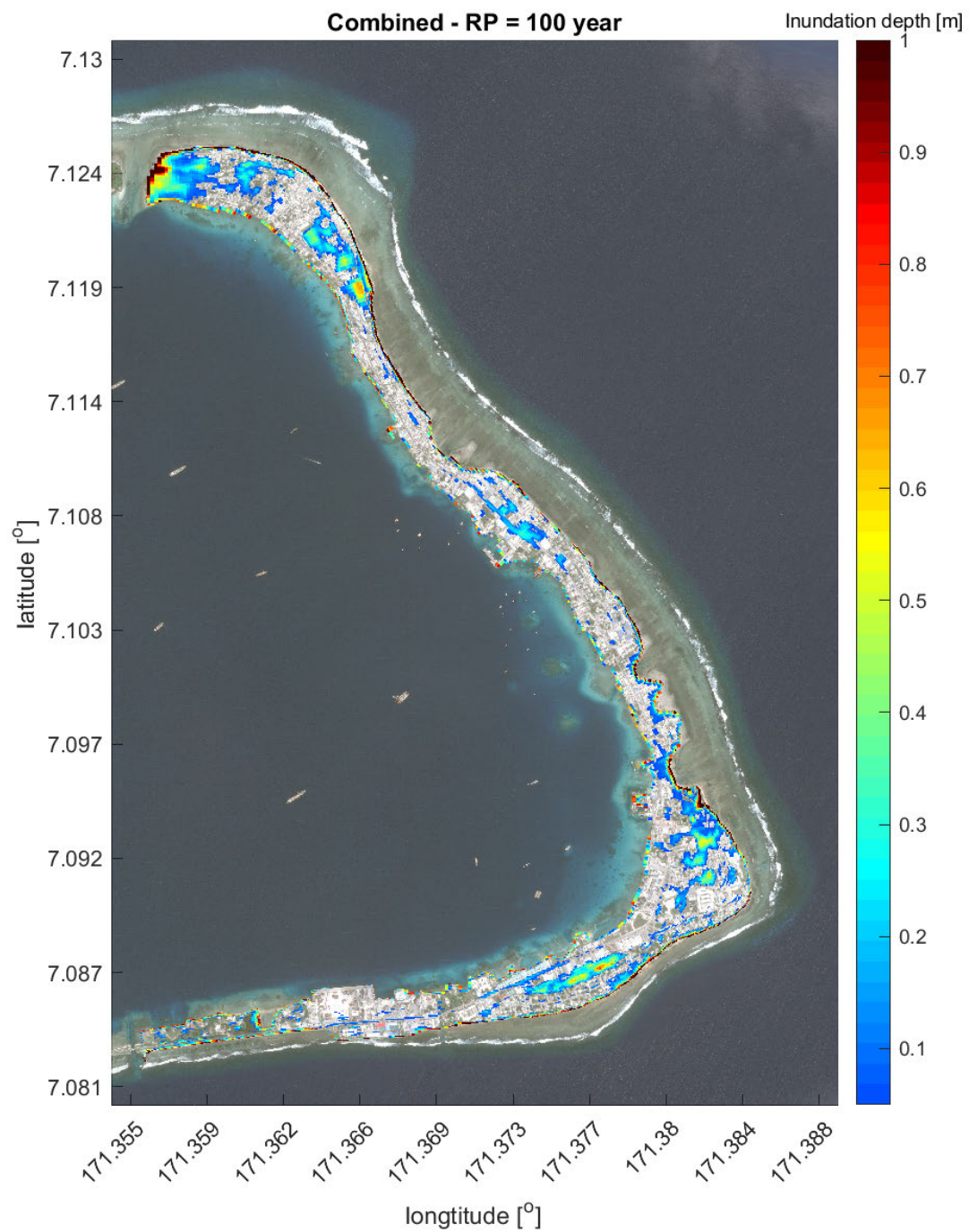
Figure D.5: *Estimated inundation depths for a return period of 100 year. Underlying satellite image: ©2019 CNES/Airbus, 17-3-2017 via Google Maps.*

Maximum simulated flood depths

Figure D.6: Maximum simulated inundation depths corresponding to a return period of 1000 years, although with with significant uncertainties. Underlying satellite image: ©2019 CNES/Airbus, 17-3-2017 via Google Maps.